UNIVERSITÉ PARIS-EST

Thèse présentée pour obtenir le grade de

Docteur de l'Université Paris-Est

Spécialité : Géotechnique

par

Simona Saba

Ecole Doctorale : SCIENCES, INGENIERIE ET ENVIRONNEMENT

Comportement hydromécanique différé des barrières ouvragées argileuses gonflantes

JURY

Tom Schanz	*Rapporteur*
Enrique Romero	*Rapporteur*
Gioacchino Viggiani	*Examinateur*
Anh Minh Tang	*Examinateur*
Jean-Dominique Barnichon	*Examinateur*
Pierre Delage	*Invité*
Nicolas Lenoir	*Invité*
Yu-Jun Cui	*Directeur de thèse*

UNIVERSITÉ PARIS-EST

Dissertation presented for the degree of

Doctor of Paris-Est University

Specialty : Geotechnics

by

Simona Saba

Doctoral school: SCIENCE, ENGINEERING AND ENVIRONMENT

Hydro-mechanical behaviour of bentonite-sand mixture used as sealing materials in radioactive waste disposal galleries

REVIEWERS

Tom Schanz
Enrique Romero

Gioacchino Viggiani
Anh Minh Tang
Jean-Dominique Barnichon

Pierre Delage
Nicolas Lenoir

Yu-Jun Cui

To the memory of Madona
To my parents

AKNOWLEDGEMENT

I would like to take this opportunity to acknowledge all the persons who contributed in the accomplishment of this work and without whom this PhD experience wouldn't have been one of the best experiences in my life.

I would start by thanking the professors Cino Viggiani, Tom Schanz and Enrique Romero who carefully reviewed this dissertation and whose remarks induced further reflections on different aspects of this work.

I am very thankful to my advisors Yu-Jun Cui and Jean-Dominique Barnichon who trusted my capacity to carry this PhD and offered me all the scientific and human support that I needed. The rich scientific discussions we had together with Anh Minh Tang and Pierre Delage were of great interest to me. I hereby greet their high expertise in the geotechnical field and their professionalism in the management of this research project. I also like to thank Nicolas Lenoir for his collaboration in this work and the help he offered me.

I thank the French Institute for Radiation Protection and Nuclear Safety (IRSN) for the financial support. I also want to express my pleasure to work on a part of the "SEALEX Project" for its added practical value to this PhD. I would like to thank the people working on the "SEALEX Project", the PhD students I had the chance to meet and the scientific direction for their continuous support.

The experimental tests executed during this PhD could not have been possible without the great help of Emmanuel Delaure and his technical team. I am very thankful for their efforts, advices and good humour.

I spent these three years of PhD studies at the geotechnical team "CERMES" of Navier Laboratory at Ecole des Ponts and I am grateful for the nice working environment. I thank all the people I met in these three institutions and who helped in a way or another. I specially thank the amazing friends I made and with whom I shared laughter, excitement, disappointment, stress and finally success. I extend my gratitude to the administration members of University Paris-Est who offered me the possibility to take very interesting non-scientific courses. Thanks to the Doctoriales, the DPM at ENPC MBA PARIS and the NCT "Nouveau Chapitre de la Thèse" I learned how to combine between my scientific and professional skills which helped me finding my current job.

Many thanks to "the one" I met during this PhD for making me feel confident, happy and loved.

At the end, I am grateful to the endless support of my big family including my old friends. A big THANK YOU from the heart to my courageous, endlessly loving and caring parents.

Le travail de thèse ici présenté a été effectué au sein de l'Equipe Géotechnique (CERMES) du Laboratoire Navier à l'Ecole des Ponts ParisTech. Il a été financé par l'Institut de Radioprotection et de Sûreté Nucléaire (IRSN).

The presented PhD work was carried out in the Geotechnical division (CERMES) of "Laboratoire Navier" at "Ecole des Ponts ParisTech". It was financed by the French Institute for Radiation Protection and Nuclear Safety (IRSN).

RESUME

Dans le but de vérifier l'efficacité des dispositifs de scellement ou des barrières ouvragées dans le stockage géologique des déchets radioactifs, l'Institut de Radioprotection et de Sûreté Nucléaire (IRSN) a mis en œuvre le projet expérimental SEALEX (SEALing performance EXperiments) auquel ce travail est étroitement lié. Dans le cadre de ce projet, des essais in-situ sont effectués à l'échelle représentative et dans des conditions naturelles sur un mélange compacté de bentonite et de sable. Ce matériau de mélange a été choisi pour sa faible perméabilité et surtout pour sa capacité de gonflement qui permet de colmater les vides existant dans le système, notamment le vide technologique correspondant au vide radial entre le noyau de scellement et la roche hôte et qui est inévitable au cours de l'installation du noyau dans le forage. Une fois les vides scellés, le gonflement à volume constant engendre une pression de gonflement aussi bien sur la roche hôte (radiale) que sur les structures de confinement en béton (axiale). Le comportement de ce matériau dans ces conditions de couplages hydromécaniques est alors étudié dans ce travail. La microstructure du matériau à son état initial a été premièrement examinée par micro-tomographie rayons-X. Ceci a permis de caractériser la distribution des grains de bentonite et de sable ainsi que le réseau de pores dans l'échantillon. Des macro-pores se sont retrouvés concentrés à la périphérie de l'échantillon ainsi qu'entre les grains de sable, ce qui pourra affecter à court terme la perméabilité. L'hydratation du même matériau en condition de gonflement limité a été ensuite observée par photographie 2D et par micro-tomographie aux rayons-X. Le mécanisme de gonflement par production de gel de bentonite, la cinétique de gonflement, la diminution de densité et l'homogénéisation du matériau final ont été analysés. L'hydratation en conditions de gonflement empêché a été aussi étudiée par des essais où la pression de gonflement a été mesurée dans deux directions : radialement et axialement. La différence retrouvée entre les pressions de gonflement axiales et radiales indique la présence d'une anisotropie de microstructure qui a été analysée en fonction de la masse volumique sèche de bentonite dans le mélange. Des essais en modèle réduit reproduisant à une échelle 1/10ème les essais in situ (SEALEX) ont été également effectués afin d'étudier le comportement du noyau compacté après rupture des structures de confinement. Des mesures locales de pression de gonflement le long des échantillons ont permis de mettre en évidence l'évolution du gradient de densité durant le gonflement axial. Finalement une comparaison entre les résultats obtenus dans ce travail et ceux d'un essai in situ (SEALEX) a été faite. Une bonne correspondance entre les valeurs d'humidités relatives a été retrouvée pour les mêmes longueurs d'hydratation tout en prenant en compte la saturation par le vide technologique radial. Un facteur de temps égal à 100 a été retrouvé en comparant les pressions de gonflement entre les essais à échelle réduite (1/10) et les essais in situ.

Mots clés : Mélange bentonite/sable ; stockage des déchets radioactifs ; gonflement ; microstructure ; anisotropie ; essais à échelle réduite ; comportement hydromécanique.

ABSTRACT

In order to verify the effectiveness of the geological high-level radioactive waste disposal, the French Institute for Radiation protection and Nuclear Safety (IRSN) has implemented the SEALEX project to control the long-term performance of swelling clay-based sealing systems, and to which this work is closely related. Within this project, In-situ tests are carried out on compacted bentonite-sand mixture in natural conditions and in a representative scale. This material is one of the most appropriate sealing materials because of its low permeability and good swelling capacity. Once installed, this material will be hydrated by water from the host-rock and start swelling to close all gaps in the system, in particular the internal pores, rock fractures and technological voids. Afterwards, swelling pressure will develop. In the present work, laboratory experiments were performed to investigate the sealing properties under these complex hydro-mechanical conditions taking into consideration the effect of technological voids. The microstructure of the material in its initial state was first examined by microfocus X-ray computed tomography (µCT). This allowed identification of the distribution of grains of sand and bentonite as well as the pores in the sample. Macro-pores are found concentrated at the periphery of the sample and between the grains of sand, which could affect in the short term the permeability. The hydration of the same material in limited swelling conditions was then observed by 2D photography and 3D µCT. The swelling mechanism with bentonite gel production, the swelling kinetics, the density decrease and the homogenisation of the material were analyzed. The hydration in the conditions of prevented swelling was also studied by swelling pressure tests with radial and axial measurements of swelling pressure. The difference found between the axial and radial swelling pressures suggested the presence of an anisotropic microstructure. Mock-up tests at a 1/10 scale of the in situ SEALEX tests were carried out for the study of the recovery capacity of the mixture in case of the failure of the confining structures. Local measurements of swelling pressures along the sample allowed analysis of the density gradient evolution during axial swelling. Finally, a comparison between the laboratory results and those from an in-situ test was done, showing a good fitting in the relative humidity curves for the same infiltration length while considering the saturation effect from the technological void. The swelling pressure comparison resulted in a time factor of 100 between the laboratory (1/10) and in situ tests.

Keywords: Bentonite/sand mixture; radioactive waste disposal; microstructure; swelling; anisotropy; mock-up tests; hydro-mechanical behaviour.

PUBLICATIONS

Journal Papers

1. **Saba, S.**, Delage, P., Cui, Y.J, Tang, A.M., Lenoir, N. and Barnichon, J.D. 2014. Further insight into the microstructure of compacted bentonite/sand mixture**.** Engineering Geology Volume 168, Pages 141–148.
2. **Saba, S.**, Barnichon, J.D., Cui, Y.J., Tang, A.M. and Delage, P. 2013. Microstructure and anisotropic swelling behaviour of compacted bentonite/sand mixture. Accepted to be published in Journal of Rock Mechanics and Geotechnical Engineering.
3. **Saba, S.**, Cui, Y.J, Tang, A.M., Tran, T.P.H. and Barnichon, J.D. 2013. Anisotropic swelling of compacted bentonite/sand mixture. Submitted to Soils and Foundations.
4. **Saba, S.**, Barnichon, J.D., Cui, Y.J. and Tang, A.M. 2013. On the hydro-mechanical behaviour of compacted bentonite/sand mixture: comparison between laboratory and in situ experiments. Submitted to Engineering Geology.
5. **Saba, S.**, Barnichon, J.D., Cui, Y.J. and Tang, A.M. 2013. On the hydro-mechanical behaviour of compacted bentonite/sand mixture by small scale infiltration tests. Submitted to Canadian Geotechnical Journal.
6. **Saba, S.**, Cui, Y.J., Barnichon, J.D. and Tang, A.M. 2013. Small scale infiltration column with local measurements of swelling pressure: cell validation. Submitted to Geotechnical Testing Journal.
7. **Saba, S.**, Cui, Y.J, Delage, P., Lenoir, N., Tang, A.M. and Barnichon, J.D. 2013. Limited swelling and homogenisation of compacted bentonite/sand mixture: a 3D investigation using X-ray computed tomography (μCT). Ssubmitted to Applied Clay Science.
8. Wang, Q., Cui, Y.J., Tang, A.M., Barnichon, J.D., **Saba, S.** and Ye, W.M. 2013b. Hydraulic conductivity and microstructure changes of compacted bentonite/sand mixture during hydration. Engineering Geology 164, 67-76.

Conference communications

1. **Saba, S.**, Cui, Y.J., Barnichon, J.D. and Tang, A.M. 2012. Swelling of highly compacted bentonite-sand mixtures used as sealing materials in radioactive waste disposal. In proceedings of E-Unsat 2012, Unsaturated soils: Reasearch and Applications. pp 241-247 June 20-22, Naples, Italy. (Oral presentation).
2. **Saba, S.**, Delage, P., Cui, Y.J, Tang, A.M., Lenoir, N. and Barnichon, J.D. 2013. Further insight into the microstructure of compacted bentonite/sand mixture**.** Clays in natural and Engineered Barriers for Radioactive Waste Confinement, 5th International Meeting, Oct. 22-25 2012, Montpellier, France. (Oral presentation).
3. **Saba, S.**, Cui, Y.J., Tang, A.M. and Barnichon, J.D. 2012. Anisotropic swelling of compacted bentonite/sand mixture. Clays in natural and Engineered Barriers for Radioactive Waste Confinement, 5th International Meeting, Oct. 22-25 2012, Montpellier, France. (Poster).
4. **Saba, S.**, Barnichon, J.D., Cui, Y.J., Tang, A.M. and Delage, P. 2013. Microstructure and anisotropic swelling behaviour of compacted bentonite/sand mixture. UNSAT-WASTE 2013, July 7-10, Shanghai, China. (Oral presentation).

5. **Saba, S.**, Wang, Q., Tang, A.M., Cui, Y.J. and Barnichon, J.D. 2011. Hydro-mechanical behaviour of compacted bentonite-sand mixture used as sealing materials in radioactive waste disposal. Mechanics and Physics of Porous Solids (MPPS) Symposium. Apr. 11-20 2011 Paris, France.(Poster).

CONTENTS

RESUME I
ABSTRACT III
PUBLICATIONS V

INTRODUCTION 1

Chapter 1 Microstructure of the material at its initial state 7
INTRODUCTION 9
Further insight into the microstructure of compacted bentonite/sand mixture 11
1 Introduction 11
2 Material and methods 12
3 Results 15
4 Discussion 23
5 Conclusion 25
References 25

Chapter 2 Free/limited swelling upon direct contact with water 29
INTRODUCTION 31
Swelling of highly compacted bentonite-sand mixtures used as sealing materials in radioactive waste disposal 33
1 Introduction 33
2 Materials and methods 34
3 Results and discussion 35
4 Conclusion 37
References 38
Limited swelling and homogenisation of compacted bentonite/sand mixture: a 3D investigation using X-ray computed tomography (µCT) 39
1 Introduction 39
2 Materials and methods 41
3 Results 43
4 Discussion 51
5 Conclusion 53
References 54

Chapter 3 Swelling pressure anisotropy investigation 57
INTRODUCTION 59
Anisotropic swelling of compacted bentonite/sand mixture 61
1 Introduction 61
2 Materials and methods 63
3 Experimental results 66
4 Discussion 70
5 Conclusion 73
References 74
Microstructure and anisotropic swelling behaviour of compacted bentonite/sand mixture. 77
1 Introduction 77
2 Material and methods 79
3 Results and discussions 83
4 Conclusions 88
References 89

Chapter 4 Hydro-mechanical response of mock-up tests 93
INTRODUCTION 95
Small scale infiltration column with local measurements of swelling pressure: cell validation 97
1 Introduction 97
2 Materials 98
3 Experimental set-up 99
4 Test procedure 107
5 Results and discussion 109
6 Conclusion 113
References 114
Investigation of the swelling behaviour of compacted bentonite/sand mixture by mock-up tests 117
1 Introduction 117
2 Materials 119
3 Experimental methods 119
4 Mock-up tests 121
5 Swelling pressure versus suction 132
6 Simulation of confinement failure in Mock-up 2 135
7 Conclusion 139
References 141

Chapter 5 Link between laboratory experiments and in situ tests 143
INTRODUCTION 145
On the hydro-mechanical behaviour of compacted bentonite/sand mixture: comparison between laboratory and in situ experiments 147
1 Introduction: 147
2 Materials studied 149
3 SEALEX in situ test 149
4 Laboratory tests 153
5 Experimental results and comparison 156
6 Conclusion 163
References 164

CONCLUSION 167
REFERENCES 171

Introduction

INTRODUCTION

The management of radioactive waste is a major concern for the countries that produce or use nuclear energy like China, Belgium and France among others. These wastes are treated differently depending on their activity and their period (i.e. half-life). In France, High Level and Intermediate Level Long-Lived (HL/IL-LL) wastes are temporarily stored at surface by the respective producers awaiting a long-term sustainable management solution. Deep geological disposal has been considered as a possible solution to successfully isolate these wastes from the biosphere for a very long period. This involves placing the waste in an underground facility, located several hundreds of meters in a relatively impermeable rock, in order to isolate them over periods allowing for the radioactive decay of isotopes they contain. Such storage is based on the concept of multi-barrier: the natural or geological barrier (host rock) and engineered barriers (waste container, buffer and sealing elements). In the French concept, once the wastes containers will be installed, galleries and access shafts are closed and sealed by swelling clay based cores. Compacted mixture of bentonite and sand is one of the candidate sealing materials in this system thanks to their low permeability, high swelling and high radionuclide retardation capacities (Pusch, 1979; Yong et al., 1986; Villar et al., 2008). Moreover, addition of 30% sand has a negligible effect on the hydraulic conductivity of the mixture (Cho et al., 2000) but was found to be advantageous with respect to ease of handling, manufacturing and cost (Agus, 2005).

Once installed in the repository, these sealing materials will be subject to coupled hydro-mechanical loadings: hydration due to the infiltration of pore water from the natural barrier and mechanical confinement resulting from the relatively prevented swelling of the engineered barriers. It is therefore essential to understand well their behaviour under such loadings when assessing the overall repository safety.

In this context, a number of laboratory studies has been conducted to investigate the performance of buffer/sealing materials (e.g. Delage et al., 1998; Lloret et al., 2003; Agus and Schanz, 2005; Romero et al., 2005; Lloret & Villar, 2007). Various experiments were also performed in underground research laboratories (URL) such as FEBEX at Grimsel (Switzerland), RESEAL at Mol (Belgium), KEY at Bure (France) and SEALEX at Tournemire (France), to which this work is closely related.

In order to identify the key factors related to the long-term performance of bentonite-based sealing systems, the French institute IRSN (Institut de Radioprotection et de Sûreté Nucléaire) has launched the SEALEX project. This project consists of a series of in situ experiments

performed in natural conditions and at a representative scale in the Tournemire URL. The tests program was specially built in order to provide useful information about the effect of technical specifications, design, construction, defects, etc. (Barnichon et al. 2009, 2010). Clay cores made of pre-compacted disks of MX80 bentonite/sand mixture were considered. The cores were introduced in boreholes excavated in claystone where they undergo the saturation process. During this process, the injected water volume, total pressure and relative humidity changes are monitored at several positions. The impact of the technical specification and design of the sealing plug will also be investigated by changing the intra-core geometry (jointed vs. monolithic disks), core composition (MX80/sand ratio) and core conditions (pre-compacted vs. in situ compacted). Furthermore, the effect of altered conditions will be also studied by simulating the decrease of swelling pressure caused by a failure of the concrete confining structure. Considering the complexity of the in-situ conditions, it appears important to identify the hydro-mechanical behaviour of compacted mixture in laboratory conditions in order to obtain useful information for interpreting the results obtained in the field conditions.

Problematics and objective of the study:

Once the initially unsaturated bentonite/sand core is in place, it undergoes a process of saturation by infiltration of pore water. The present work specially focuses on the interface between the seal and the host-rock while considering the presence of radial technological void. This void is the annular gap that is technically needed for the installation of the seal in the gallery (Barnichon et al., 2010, 2012). Once in contact with water, a first mechanism of bentonite free swelling by gel formation starts to fill the void (Cui et al, 2002; Cui et al, 2008). A density gradient is then present between the compacted centre and loose gel at the interface with the host-rock. This gel will consolidate over time being blocked between the continuously swelling compacted centre and the relatively stiff host-rock. Meanwhile, the swelling of the compacted centre to the rear of this gel induces a reduction of their density which can approach that of the consolidated gel. Theoretically, the density gradient is expected to decrease over time and to reach a final state of uniform density. In reality, as a result of the complex interface and microstructure of compacted materials, this ideal case of uniform final density may never be reached. If the density gradient persists in the clay core in the final state, it must be taken into account in the assessment of overall safety of the storage system, for instance by considering the hydro-mechanical properties as a function of density. The objective of this work is to study the long term evolution of the density gradient and that in terms of microstructure, swelling stress and density measurements.

The testing program consists of different types of experimental laboratory tests that were performed in order to study several phenomena. The initial microstructure was investigated by microfocus X-ray computed tomography (µCT) and Mercury Intrusion Porosimetry (MIP); the limited swelling and homogenisation were studied by time lapse photography and µCT; the anisotropy of swelling pressure was studied by constant volume elementary tests and finally the hydro-mechanical behaviour was investigated by 1/10 mock-up tests and by comparing with the results from in-situ experiments.

Organisation of the dissertation:

The results of this work are subjected to 8 published, submitted and to-be-submitted papers. One of them was published in the proceedings of E-Unsat 2012 Conference; two other papers were accepted with moderate modifications in Engineering Geology journal and Journal of Rock Mechanics and Geotechnical Engineering. The other papers were submitted to Soils and Foundations, Applied Clay Science, Engineering Geology, Canadian Geotechnical Engineering and Geotechnical Testing journal. The dissertation includes 5 chapters composed each by an introduction and the corresponding papers/manuscripts, in their original form.

The first chapter presents the microstructure of the compacted material at its initial compacted state before hydration. The study was done by microfocus X-ray computed tomography (µCT) in addition to Mercury Intrusion Porosimetry (MIP). µCT is a non-destructive 3D imaging technique increasingly used in the field of geosciences. The bentonite and sand grains organisation in the sample was examined; the pores distribution in the sample was further investigated using image analysis. A qualitative and quantitative study of the 3D sample is shown in this chapter as well as an analysis of the complementary features of the two techniques (MIP and µCT).

The second chapter involves the limited swelling of the material after being immersed in water. A 2D examination by time lapse photography constitutes the first part of the chapter and a 3D investigation using µCT constitutes the second part. In the first part, the swelling mechanism was observed and analysed especially in terms of gel production and swelling kinetics. By µCT, the 3D limited swelling was observed; the gel formation and the sample homogenisation due to swelling was further studied by image analysis.

Constant volume swelling and anisotropy were studied in the third chapter. In a first part, the swelling stress was measured in two different directions (radial and axial). Emphasis was put on the anisotropy of swelling pressure knowing that the swelling pressure of compacted

bentonite/sand mixture was studied in the past but only by considering a single global swelling pressure (axial) for the clay core. On the other hand, in practice, the seal swells in both directions, axially towards the confining elements and radially towards the host-rock. The swelling pressure kinetics, final swelling pressure values and the anisotropy was further studied. In a second part of this chapter, an investigation of the microstructure features was conducted to complete the analysis of the results on the anisotropy of swelling pressure. The microstructure observation was made using µCT on unsaturated compacted sample and a saturated sample after swelling pressure test.

In connection with the SEALEX project, 1/10 mock-up tests were performed to study the saturation of the compacted sample with local measurements of swelling pressure. In the first part of the fourth chapter, the cell specially designed for this purpose is described in details. The obtained measurements like the swelling pressures, the volume of infiltrated water, and the axial displacement were compared to other results in literature in order to validate the cell. In the second part of this chapter, the hydro-mechanical behaviour of compacted bentonite/sand mixture was studied by combining the swelling pressure measurements with the previous suction measurements by Wang et al. (2013b). In this same part, the failure of confining elements was experimentally simulated and the sealing of the created void was investigated. The density gradient was also studied from the radial swelling pressure measurements along the sample.

Finally, the results obtained from the laboratory tests were compared with the in situ results. A SEALEX test was chosen for this comparison where the same material was tested with measurements of swelling pressure and relative humidity. Despite the significant differences in the scale of tests and the technical complications, some interesting comparison factors were defined.

Chapter 1

Microstructure of the material at its initial state

INTRODUCTION

The main role of the sealing materials is to limit fluxes of underground waters around the galleries, by their low permeability and high swelling capacity that help in closing all gaps. These two characteristics are then the most important and consequently the most investigated in the past. Very often, bentonite-based materials are considered as the most appropriate sealing materials. As the macroscopic behaviour of bentonite-based materials is closely related to their microstructure features, it is important to well characterise the microstructure of the studied material in its initial state.

The traditional microstructure observation techniques are the Mercury Intrusion Porosimetry (MIP) and the Scanning Electron Microscopy (SEM) and they have been successfully applied to bentonite-based materials (Agus and Schanz, 2005; Delage et al., 2006). However, these techniques require preliminary sample treatment and the volume of the sample is limited to about 1 cm^3 in the case of MX80/sand mixture. In addition, both techniques are destructive and the tested sample cannot be reused. The MIP technique provides the pore size distribution and the porosity of the tested sample but it cannot tell about the pores distribution in the whole as-compacted sample unless several tests are performed at small samples taken at different locations. This technique also cannot tell about pores connectivity. The SEM method gives a 2D observation at microscopic scale and cannot provide an overall look at the macroscopic scale of the sample.

In this first chapter, microfocus X-ray computed tomography (µCT) observations were used in parallel to the MIP measurements to further investigate the microstructure of a compacted bentonite/sand sample. µCT is a non-destructive 3D imaging technique that does not impose a preliminary sample treatment. It has been recently successfully applied on bentonite-based materials. The overall grains and pores distribution in the "as-compacted sample", their connectivity was further investigated by qualitative observation completed by image analysis.

The results are presented in the form of a paper tentatively accepted for publication in "Engineering Geology".

Further insight into the microstructure of compacted bentonite/sand mixture

Simona Saba[1,2], Pierre Delage[1], Yu-Jun Cui[1], Anh Minh Tang[1], Nicolas Lenoir[1] and Jean-Dominique Barnichon[2]

Abstract: Compacted bricks of bentonite/sand mixture are planned to be used as sealing plugs in deep radioactive waste disposal repositories because of their low permeability, high swelling capacity and favourable properties with respect to radionuclide retention. The isolating capacity of compacted bentonite/sand mixture is closely related to microstructure features that have been often investigated, in particular by using scanning electron microscope (SEM or ESEM) and mercury intrusion porosimetry (MIP). In this work, μCT observations were used in parallel to MIP measurements to further investigate, at larger scale, the microstructure of a laboratory compacted bentonite/sand disk (65/35% in mass). Qualitative observation of μCT images showed that sand grains were inter-connected with some large pores between them that were clearly identified in the bimodal pore distribution obtained from MIP measurements. Due to the gravitational and frictional effects along the specimen periphery, a higher density was observed at the centre of the specimen with bentonite grains closely aggregated together. This porosity heterogeneity was qualitatively estimated by means of image analysis that also allowed the definition of the representative elementary volume. Image analysis also provided an estimate of the large porosity, in good agreement with MIP measurements.

Keywords: compacted sand-bentonite mixture; sealing plug; radioactive waste disposal; microstructure; mercury intrusion porosimetry; X ray micro tomography.

1 Introduction

In deep radioactive waste disposal concepts, sealing plugs made of compacted bentonite/sand blocks are planned to be used to close the galleries and to limit water transfers. Compacted bentonite/sand plugs are used for their low permeability, high radionuclides retention capability and sealing/swelling abilities when infiltrated by water (e.g. Pusch, 1979; Yong et al., 1986). Once the disposal galleries are closed, plugs will be progressively infiltrated by the pore water of the host rock. They will swell and seal the so-called technological voids of the system, i.e. the voids remaining between blocks and at the interfaces with the rock. These technological voids are estimated at 14% of the total volume of the plugs by IRSN (Institut de Radioprotection et de Sûreté Nucléaire, the French expert Institution in the field of nuclear safety).

Various investigations of the microstructure of compacted bentonites and sand bentonite mixture have been carried out by using mercury intrusion porosimetry (MIP) and scanning electron microscopy (SEM, ESEM, Komine and Ogata, 1999; Villar and Lloret, 2001;

[1] Ecole des Ponts ParisTech, Laboratoire Navier, Marne La Vallée, France
[2] Institut de Radioprotection et de Sûreté Nucléaire (IRSN), Fontenay-aux-Roses, France

Montes-H, 2002; Cui et al., 2002; Lloret et al., 2003; Agus and Schanz, 2005; Delage et al., 2006). These techniques require a cautious preliminary dehydration of the samples, often by freeze-drying. They provide local observations on a small part of millimetric samples. They are hence interestingly completed at a larger scale by microfocus X-ray computed tomography (µCT), a high-resolution non destructive 3D observation technique that does not need any sample pre-treatment and that gives further 3D information on the whole sample (including grain size distribution as well as pores size distribution and pores inter-connectivity).

Previous applications of µCT have been devoted to the monitoring of hydro-chemo-mechanical processes (Comina et al., 2008), to the detection of desiccation cracks (Gerbrenegus et al., 2006; Mukunoki et al., 2006), to the visualisation of diffusion/hydration phenomena, to the study of fluid movements (Rolland et al., 2003; Rolland et al., 2005; Carminati et al., 2006; Koliji et al., 2006) and to the investigation of the microstructure of compacted bentonite based materials (Kozaki et al., 2001, Van Geet et al., 2005 and Kawaragi et al., 2009). In this work, µCT was coupled to MIP for further microscopic investigation of a compacted bentonite/sand sample.

2 Material and methods

2.1 Material

The studied material is a compacted mixture of Wyoming MX-80 bentonite (65% in dry mass, commercial name Gelclay WH2) and sand (35%). The MX80 bentonite contains 92% of montmorillonite with several other minerals including quartz, alumina, and hematite (Tang et al., 2008). The sand is of pure quartz nature (commercial name TH1000).

The mixture was provided in boxes containing a powder with an initial water content of 10.2% and a suction of 73.3 MPa measured with a chilled mirror dew point tensiometer (Decagon WP4). The grain size distribution of the bentonite powder obtained by dry sieving is presented in Figure 1 together with that of the deflocculated bentonite obtained by sedimentation. The grain size distribution of the sand is also plotted in Figure 1. The grain size distribution curves show that the bentonite powder grains are larger than the sand grains with D_{50} values of 1.2 and 0.6 mm, respectively. Both curves are representative of well sorted materials. The unit mass of bentonite particles was measured using a pycnometer and found equal to 2.77 Mg/m^3 in agreement with the published data (Madsen, 1998; Karnland et al., 2006). The density of bentonite grains was also measured using a pycnometer with a

desaromatised immiscible oil (commercial name Kerdane) having a density of 0.791 at 20°C. It was found equal to 2.00 Mg/m^3. The value for sand grains was found equal to 2.65 Mg/m^3. Compacted samples were prepared by uniaxial static compaction (strain rate of 0.1 mm/min) in a cylindrical mould in order to obtain a disk (diameter 50 mm, height 10 mm) at the target dry density (1.8 Mg/m^3 obtained at a maximum compaction stress of 25.5 MPa).

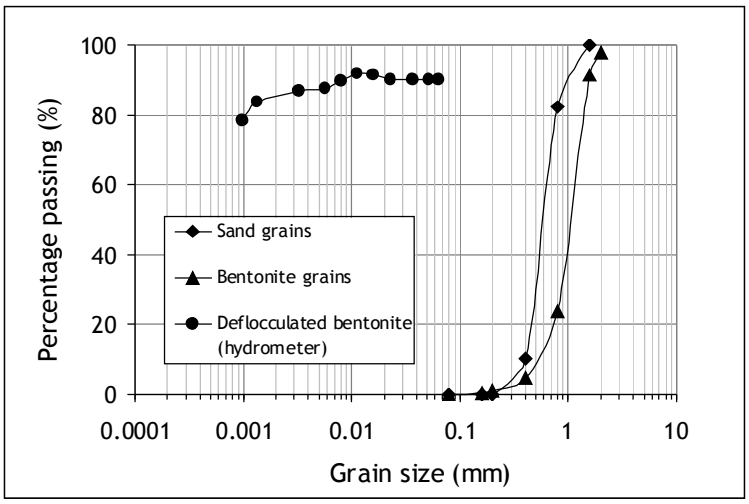


Figure 1. Grain size distribution curves.

The sample water content was 10%, resulting in a degree of saturation of 55 % and a suction of 76.3 MPa. Note that this value is close to that of the powder prior to compaction (73.3 MPa). The slightly higher value may be due to some effects of evaporation during the process of compaction. In any case, these small changes in suction after compaction are compatible with the observations of Li (1995), Gens et al. (1995) and Tarantino and De Col (2008) on soils compacted on the dry side of Proctor optimum. It confirms that suction is governed by aggregates that are not much affected by the compaction. As a consequence, there is little dependency of the water retention properties on the sample density in compacted bentonite based materials.

2.2 Mercury intrusion porosimetry

The pore size distribution of the compacted samples was measured on freeze dried samples using an Autopore IV 9500 mercury intrusion porosimeter (Micromeritics) that operates at a maximum pressure of 230 MPa. Instantaneous freezing was carried out by plunging small samples (volume 0.40 cm^3) in slush nitrogen (-210°C) obtained by previously submitting it to vacuum (Delage et al., 2006). In such conditions, there is no nitrogen boiling around the samples when plunging them into nitrogen, resulting in an optimized quick freezing and good microstructure preservation. The intruded porosity was determined from the total volume of mercury intruded into the sample and the pore size distribution was obtained, in a standard

fashion, assuming parallel, cylindrical nonintersecting pores of different radii, using the Autopore IV 9500 V1.09 standard software package. The intruded porosity was systematically compared to the total porosity obtained by standard methods so as to detect the smaller porosity (entrance equivalent diameter smaller than 5.5 nm) not intruded by mercury at the highest applied pressure (200 MPa).

2.3 Microfocus X-ray tomography and image analysis

Microfocus x-ray computed tomography (µ-CT) was used to examine, in three dimensions, the internal microstructure of the compacted bentonite/sand mixtures. µ-CT is a non destructive observation technique that has proven to be useful in the investigation of various geological porous media including compacted bentonite (Kozaki et al., 2001), bentonite pellet/powder mixture (Van Geet et al., 2005) and compacted bentonite/quartz mixture (Kawaragi et al., 2009). µ-CT consists firstly in recording a set of two-dimensional X-ray radiographs of an object at several angles (typically at 180° or 360°) and secondly in reconstructing the 3D slices from the radiographs using a mathematical algorithm. The final 3D image of the internal structure is obtained by stacking the slices. The final measurement is the attenuation coefficient to x-ray which depends on the mass density and the atomic number of the object (Ketcham and Carlson, 2001; Van Geet et al., 2005).

The µCT scans presented here were carried out with the device of the Navier laboratory (Ecole des Ponts ParisTech), an "Ultratom" device specifically designed and manufactured by RXsolutions (France). Images were reconstructed using the software Xact-reconstruction developed by RXsolutions. The system is a dual-head and dual-imager scanner; two sources [a nano-focus xs-160hpnf/GE-Phoenix (160 kV, 15W, 0.9 µm min spot size) and a micro-focus xs-225d/GE-Phoenix (225 kV, 320W, 5 µm min spot size)], two interchangeable imagers: [HD camera PhotonicScience VHR (4008x2672 pixels, 9µm pixel size) and a flat-panel-CsI scintillator-Varian 2520V/Paxscan (14 bit, 1920x1526 pixels, 127µm pixel size)].

The couple micro-focus source/flat panel was used in this study. The X-ray source parameters were a voltage of 140 kV with an intensity of 210 µA, a source power resulting in a spot size below or equal to the spatial resolution, here a voxel size of 30 µm. The sample was scanned using 1440 projections on 360° with an exposure time of 0.2 s. Each projection was integrated on 4 s (average of 20 frames) in order to obtain a good signal-to-noise ratio. The total scanning time was about one hour and a half. The final 3D image is a 16 bit type with a size of 1840x1840x386 voxels. The image analysis and treatment was then carried out using ImageJ, a public domain Java image processing program (Rasband, 1997-2012). Note that the

image was first converted to 8 bit for size reasons.

3 Results

3.1 Pore size distribution

The pore size distribution determined at a dry density of 1.8 Mg/m^3, a water content of 10% and a suction of 76.6 MPa is presented in terms of cumulative and density functions curves in Figure 2. The bimodal curve obtained is comparable to that of samples compacted dry of optimum (Ahmed et al., 1974; Delage et al., 1996; Romero et al., 1999 among others) and also with the results of Cui et al. (2002), Lloret et al. (2003), Agus and Schanz, (2005) on compacted bentonite materials.

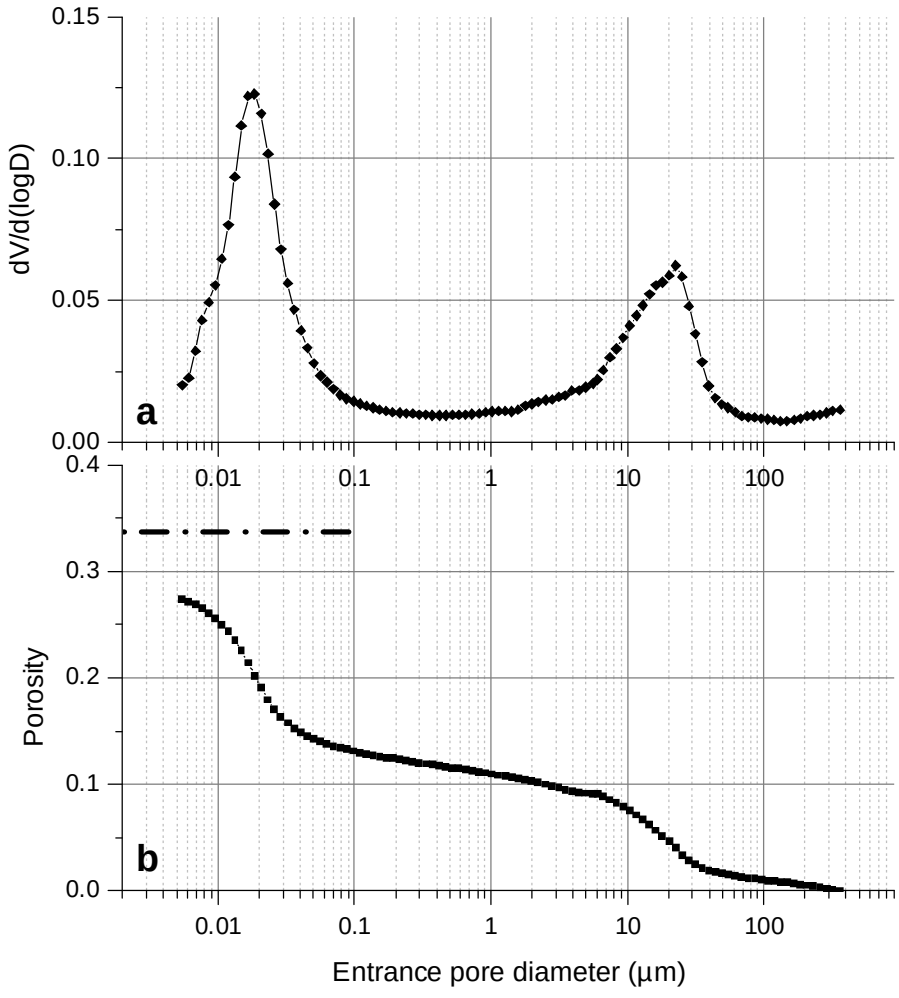


Figure 2. (a) Pore size distribution curve and (b) Cumulative porosity curve.

The PSD curve indicates that the smaller pores population (micro-pores) has a mean entrance diameter of 0.019 µm and the larger pore population (macro-pores) has a mean entrance diameter of 22 µm. Note that the intrusion of mercury into the specimen starts at quite a low

pressure, evidencing a largest diameter of 360 µm, the upper limit of the method. The total porosity (0.337) calculated in a standard fashion by macroscopic volume measurements are also plotted in Figure 2.

The smaller value of the porosity intruded by mercury (0.273) confirms that pores with an entrance diameter smaller than 5.5 nm (the lower limit of MIP) could not be intruded by mercury. This feature is typical of compacted bentonites and strongly depends on the water content (the higher the water content, the higher the smallest porosity, see Delage et al., 2006).

3.2 Microfocus X-ray computed tomography (µ-CT)

The reconstructed 3D volume of a compacted sample of bentonite/sand mixture at a dry density of 1.8 Mg/m^3 and a water content of 10% is presented in Figure 3.

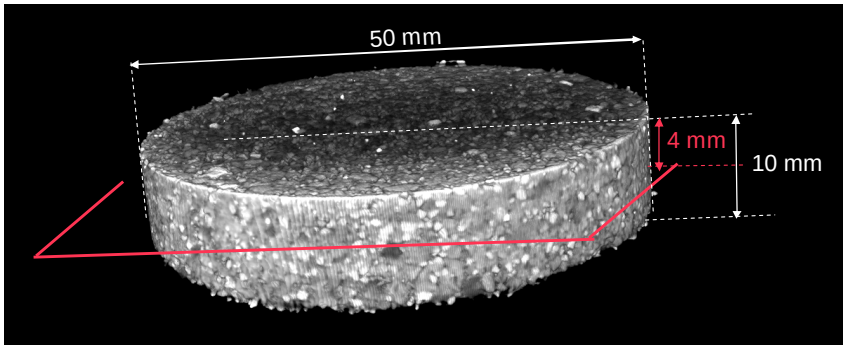


Figure 3. The 3D reconstructed image of the sample with the position of the cross section considered.

The position of the plane where the cross section has been done is indicated. The horizontal cross section at 4 mm from the top of the sample is provided in Figure 4. The µCT technique is able to distinguish the various components according to their density and atomic composition (the grey level range goes from white representing high attenuating material to black representing void). A clear distinction can be made between the clearer sand grains (density of 2.65 Mg/m^3) and the less clear larger bentonite powder grains (hydrated at a gravimetric water content of 13% and with a density of 2.00 Mg/m^3). This is due to their density and atomic composition difference. One can also observe in Figure 4 that the sample density is not strictly homogeneous with more voids observed around the sample and a larger density with less voids in the centre. This shows that, unsurprisingly, compaction was less effective around the sample along the ring against which friction effects resulted in less compaction. Detailed observation made on a zoom taken close to the sample perimeter also shows that the bentonite powder grains remain clearly apparent around the sample and that they are apparently more frequent than at the centre where powder grains appear to be more compacted one against another, resulting in a denser structure. Inspection of Figure 4 also

shows that the bentonite/sand mixture is not really homogeneous and that sand grains and powder grains appear to be somewhat segregated. As indicated in the figure, aggregations of powder grains are observed in some locations and sand grains packings with inter-grains pores in other locations. This segregation, probably resulting from the difference in density between the bentonite powder and the sand grains, is not compatible with the common statement that, in a 35-65% sand/bentonite mixture, sand grains should be homogeneously scattered among a (supposedly finer) clay matrix.

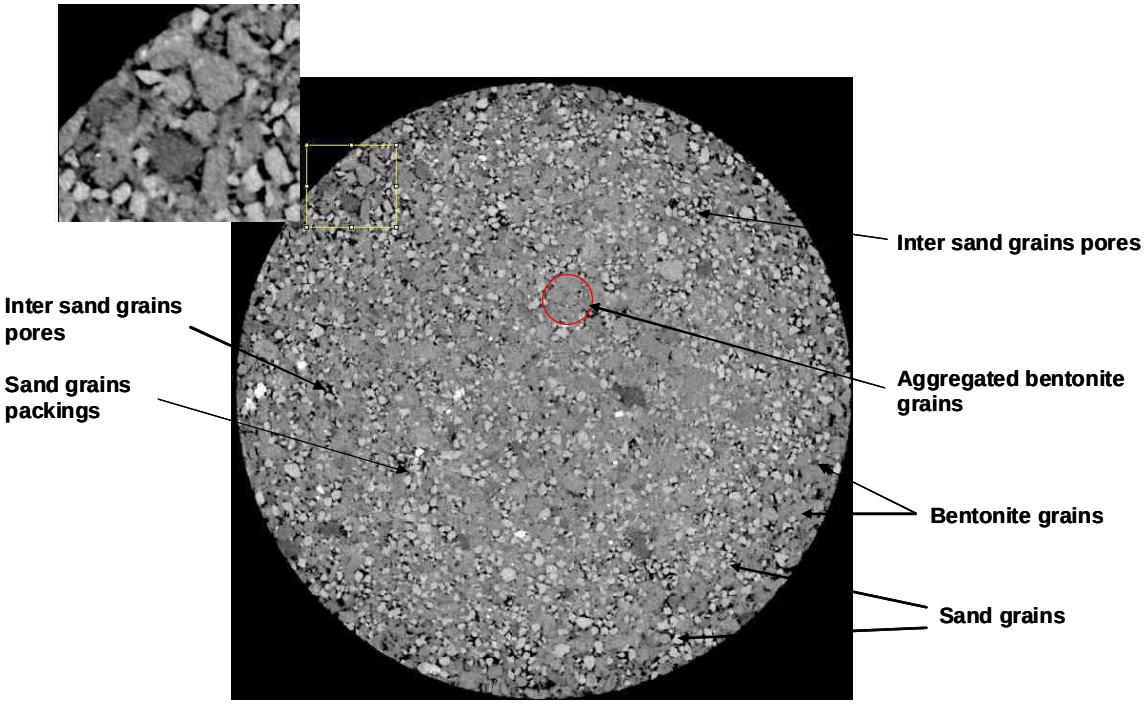


Figure 4. A typical horizontal µCT cross section of the compacted bentonite/sand mixture sample (dry density: 1.8 Mg/m^3, water content: 10%. disk diameter is 50 mm).

Conversely, it seems that, due to segregation, some continuity between the sand grains is observed with the bentonite powder grains located inside a loose grain "skeleton". As a consequence, there could be some continuity and interconnection of the pores located between sand grains.

Further examination of the voids configuration shows that many voids are located between sand grains. Around the sample, some voids are also located between powder grains but this is less true at the denser centre in which bentonite grains appear to be aggregated together. This suggests that the maximum compression stress, in spite of being as high as 25.5 MPa, is not high enough to allow the intrusion of clay particles (hydrated at a water content of 13 % with 73.3 MPa suction) into the pores located between the sand grains. This high compression stress only allows some aggregation of bentonite grains as observed at the centre (around 8

grains of various diameters are aggregated in the circle indicated). This slight deformability of dry grains under high stresses is compatible with the observation made above about the small suction variations observed when compacting samples in dry conditions: compaction affects the assembly of bentonite grains but not significantly the bentonite grains themselves, the microstructure of which is governing suction.

Visual observation of two cross sections close to the bottom and to the top of the sample also showed that the pore distribution was not homogeneous along the axial direction, with more large pores and large particles observed in the bottom of the sample. This is related to segregation effects during sample preparation. When pouring the powder into the compaction mould, the largest grains first tumble resulting in more macro-pores at the bottom.

Observation of Figure 4 provides further information about the interpretation of the PSD curves of Figure 2, in which one observes that mercury intrusion started in macro-pores with an entrance diameter of 330 µm and an average diameter of 22 µm. This size is compatible with the inter-grain pores observed in µCT in Figure 3. Given that the sample tested in MIP was extracted from the centre in which bentonite grains are more closely aggregated together, this pore population is mainly related to the pores located between the sand grains. The clear presence of the pore inter-grains population in the PSD curve confirms the interconnection of inter-grains pores along the grain skeleton that was suspected from the µCT image and commented above. Hence, the bimodal porosity that is generally related to inter-aggregate and intra-aggregate pores in soils compacted dry of optimum (Ahmed et al 1974, Delage et al. 1996, Romero et al. 1999) is here due to the nature of the mutual arrangement of sand and bentonite powder grains. Indeed, the inter-aggregate average entrance pore diameter observed by Delage et al. (1996) in a compacted low plasticity Jossigny silt is 8 µm whereas Romero et al. (1999) detected inter-aggregates pores close to 2 µm in compacted Boom clay. The significantly larger average entrance pore diameter detected here is too large to be representative of inter-aggregate pores as in the case of standard compacted soils, it is linked to the connected inter-grains pores observed along the sand skeleton in µCT.

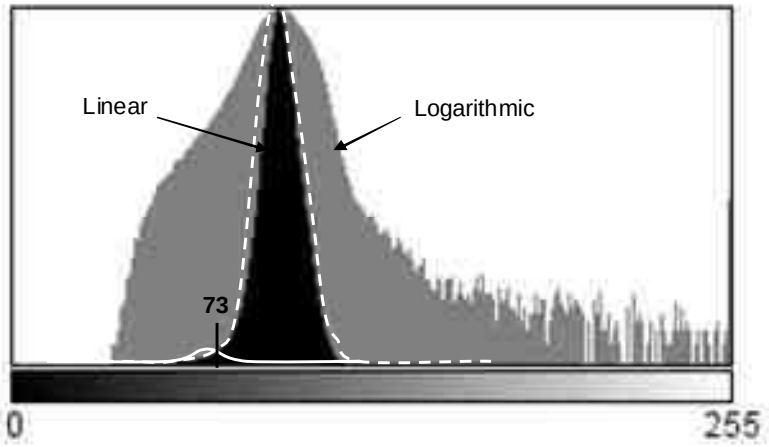
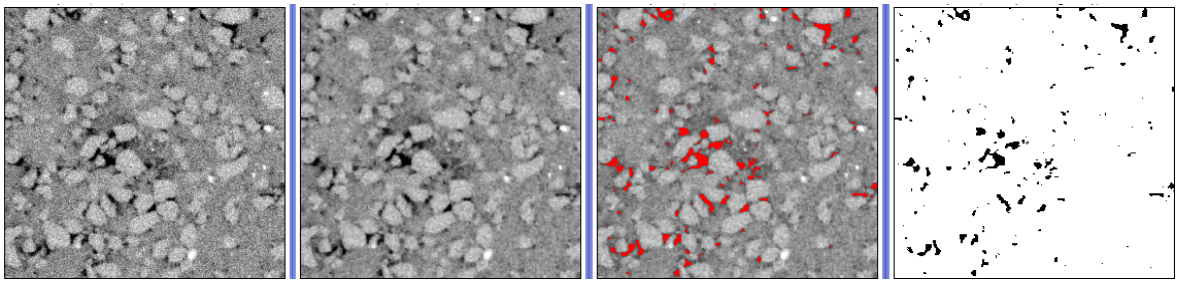


Figure 5. Histogram of the image (linear and logarithmic scale) with the fitted Gaussians and the obtained threshold value.

Further investigation of the microstructure was carried out using the ImageJ image analysis software. The first step was to reduce noise by applying a 3D median filter with a 1 pixel radius. Then, a segmentation of the image is needed in order to isolate pores from the other existing phases. The choice of the threshold value is made using the "mixture modelling" plugin. The mixture modelling technique is a histogram based technique that assumes that the histogram distribution is represented by two Gaussian curves. The histogram is then separated in two classes using a Gaussian model and a threshold value of 73 is then calculated as the intersection of the two Gaussians. Figure 5 shows the histogram of the image on a linear (black) and logarithmic (grey) scale. The linear graph does not exhibit two clearly distinct peaks because the number of pore voxels is too small compared to that of the grains. However the logarithmic graph evidences a non-symmetrical shape indicating the presence of the smaller pore population. The two Gaussians are then fitted using the "mixture modelling" plugin as seen in the Figure 5 represented by the white (continuous and dashed) curves.

Figure 6 shows an image at different stages before segmentation: a) initial state; b) after applying a 3D median filter; c) after applying a 73 threshold value (Figure 5) and d) the segmented image. An investigation on the effect of the size of the studied volume on the calculated porosity was conducted. To this end, the porosity was calculated using the histogram of the segmented image and by dividing the number of black voxels by the total number of voxels. Starting from the middle horizontal cross section of the sample at different positions (see Figure 7a), cubic volumes were selected with sides starting from 21 to 271 pixels.



a) **b)** **c)** **d)**

Figure 6. Images at different stages before segmentation: a) non-treated, b) after applying 3D median filter, c) during threshold and d) final segmented image.

The side on the *z* direction is limited by the height of the sample (10 mm) that corresponds to a maximum thickness of 271 pixels. *x* and *y* were afterwards increased until 700 resulting in a parallelepiped volume. The porosity values calculated with respect to the considered volumes are plotted in Figure 7. The curves start with some irregularities and then stabilise. Some curves continuously and slowly increase (bottom and right in Figure 7a). These increases suggest a spatial heterogeneity of the porosity. Indeed, when the studied volume increases, porosity increases because some zones located on the side of the specimen with higher porosity are more and more included into the volume. Stabilization is observed for volumes greater than 20 x 10^6 voxels. This volume corresponds to a cube with a side approximately equal to the height specimen i.e. 271 pixels. It can hence be considered as a Representative Elementary Volume (REV).

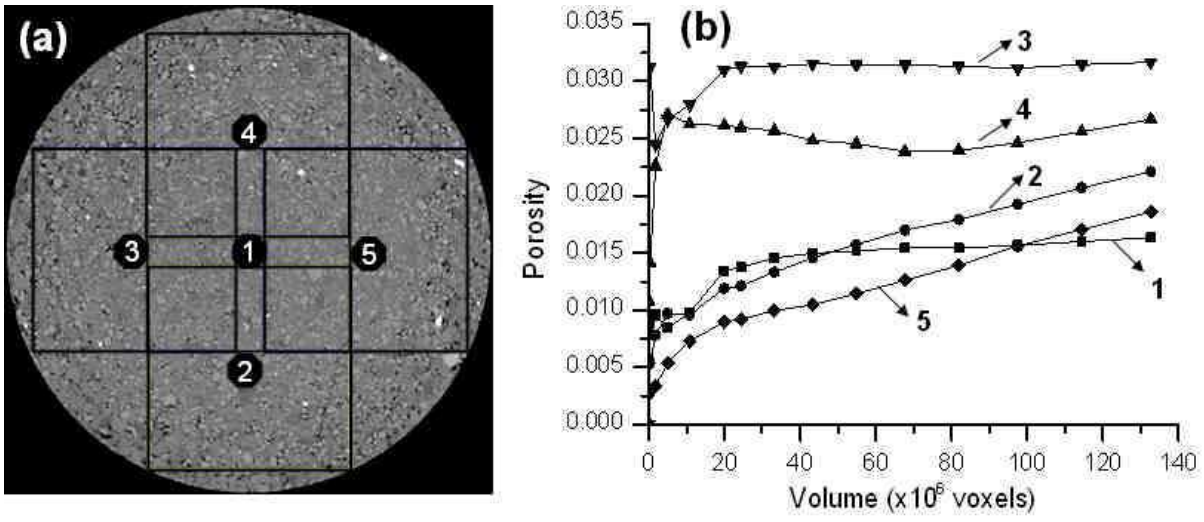


Figure 7. Calculated porosity for different volumes and at different locations in the sample.

This side size corresponds to 9 adjacent grains (D_{50} mixture = 0.9 mm = 30 voxels), which is compatible with previous studies (e.g. Razavi et al., 2007).

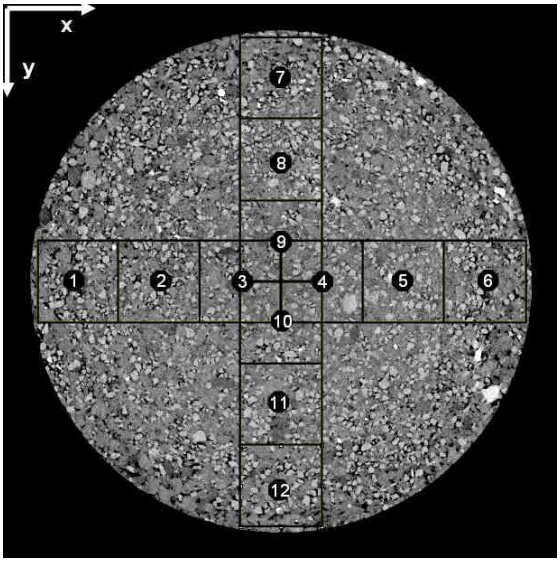


Figure 8. Sections of the volumes investigated in the sample (thickness 271 voxels).

The spatial distribution of the porosity is now investigated at different locations along the *x* and *y* directions by using volumes with heights equal to 271 pixels. The locations of the volumes sections investigated are presented in Figure 8. Figure 9 shows the variation of porosity with respect to *x* and *y* (volumes 1 to 12 in Figure 8). A clear difference is observed in the porosity values between the border (*x*, *y* = 160 and 1515) and the centre. A significant difference in porosities is also noticed for *x* (or *y*) varying between 1244 and 1515 while *y* (or *x*) equals 925. It corresponds to cubes 5 and 6, 11 and 12 in Figure 8. The porosity variation at these points is not smooth like in the others but the slope is steep showing a sudden change in porosity.

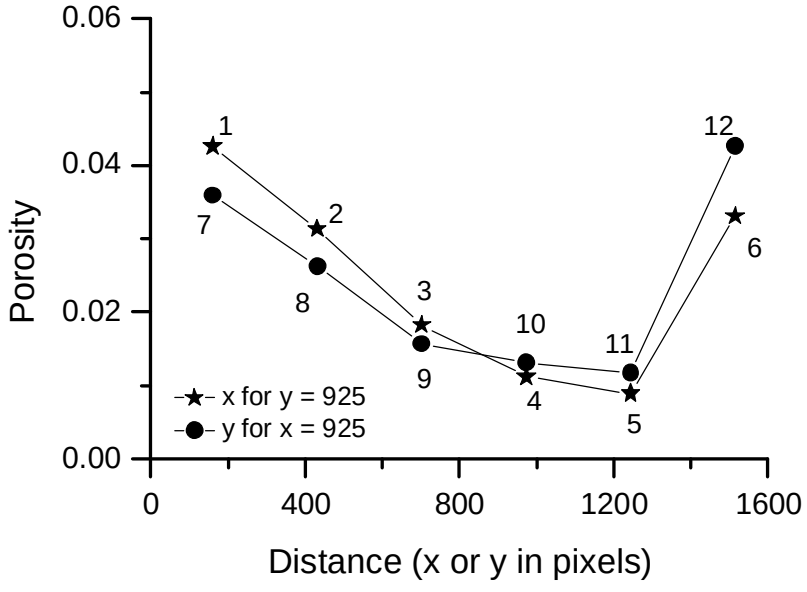


Figure 9. Porosity changes with respect to the position of the studied volume in the sample (x and y).

It confirms the slow increase observed in the REV study (Figure 7b), since it corresponds to the same positions (right for cubes 5 and 6 and bottom for cubes 11 and 12). The same study is now made on concentric rings having a height of 271 pixels and a width of 167 pixels starting from the centre (radius from 0 to 167) to the contour (radius from 501 to 835, see Figure 10).

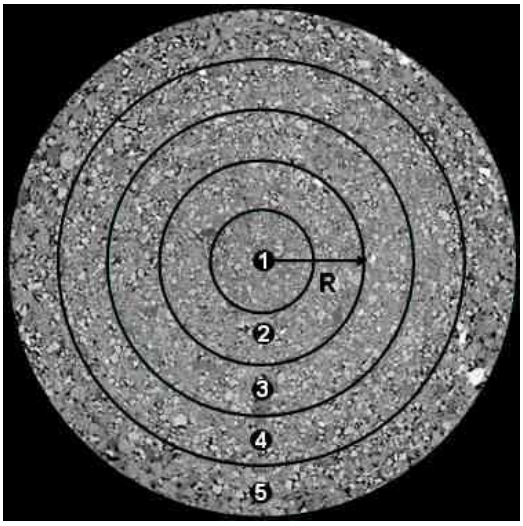


Figure 10. Concentric rings studied.

The porosities obtained with respect to the radius are presented in Figure 11. The smallest detail that can be identified in the µ-CT images is defined by the size of the voxel (30 µm). The porosity estimated by image analysis only involves pores with a diameter larger than 3 voxels (partial volume effect).

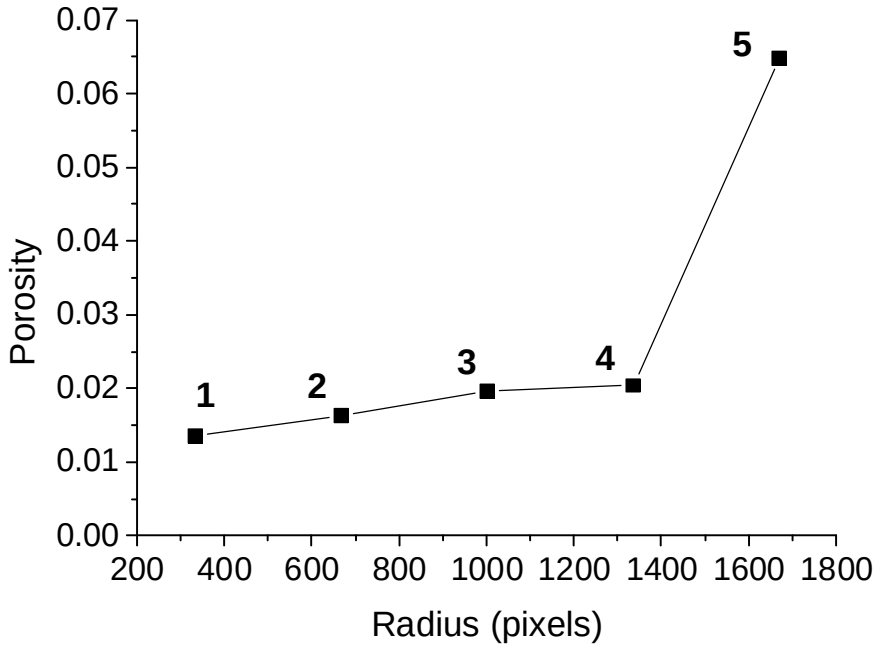


Figure 11. Changes in macro porosity with respect to the radius of the ring selected.

The value of the cumulated porosity of pores larger than 90 µm from the PSD curves (Figure 2) is 0.0108. This value is in the same range as that obtained by image analysis in the central part of the sample where MIP was performed (0.0135 porosity for radius smaller or equal to 334 voxels). This confirms that, in spite of some limitation related to the voxel size, µCT is an interesting complementary method to MIP for estimating the macro-pores and giving additional information on the spatial distribution of the porosity.

4 Discussion

Most of the investigations carried out up to now on compacted soils in laboratory have been obtained from the combined use of MIP and SEM on freeze dried samples. It is commonly admitted that the bimodal pore distribution observed in fine-grained soils compacted dry of optimum is due to the aggregate microstructure of compacted soils, with macro-pores being inter-aggregate pores and micro-pores being intra-aggregate pores. In such soils, it has also been demonstrated that compaction has little effect on the sample's suction (Li et al., 1995, Gens et al., 1995, Tarantino and De Col, 2009), given that suction is governed by intra-aggregate phenomena (mainly the adsorption of water along the clay fraction, Romero et al., 1999) whereas the change in density are due to the compression of larger inter-aggregate pores with little effect on the aggregates (Delage, 2009).

Compacted bentonites and sand-bentonite mixtures are a special case of compacted soils. They are obtained by compacting powder grains that may have, as observed here, a size significantly larger than the aggregates in laboratory compacted soils. Compacted bentonites and sand-bentonite mixtures also have quite large values of suction (76.6 MPa here). In the mixture studied here, the powder grains of bentonite (1.2 mm average diameter) are larger than the sand grains (0.6 mm average diameter). As in standard compacted soils, suction appeared here not to change significantly before and after compaction (73.3 MPa in the powder before and 76.6 MPa after compaction), confirming a well known trend in compacted soils.

Compared to MIP and SEM, µCT provided further infomation on a larger scale going from the size of the grains (sand and bentonite, 1 mm order of magnitude) to the size of the sample (50 mm), i.e. on a scale much larger and representative than both MIP and SEM. Interestingly, µCT has been able to distinguish clearly enough the bentonite from the sand grains within the compacted mixture, in spite of small difference in density. Thus, µCT provided interesting complements to MIP and SEM observations, including grains

connectivity and distribution through the sample.

An important point is that µCT observation confirmed that the bentonite grains seem to have not been crushed during compression. They still have an average size compatible with macroscopic grain size measurements and an angular shape with no clear appearance of local grain breakage. This finding is in agreement with the small variation of suction before and after compaction, as suspected from studies in laboratory compacted soils. Suction didn't change because the grains have not been significantly affected by compression, even under 25.5 MPa. µCT also provides clear information about the mutual arrangement between sand and bentonite grains within the mixture, showing that it is not really homogeneous with some continuity observed between sand grains with the bentonite grains (65% in mass) located within the sand grains assembly (35% in mass). The common hypothesis of having sand grains isolated within a clay matrix is not confirmed and some continuity of the inter-grains porosity is suspected. In the looser zone around the sample, some large pores with a size comparable to that of the inter-grains pores have also been observed between the bentonite grains. These pores, that are likely to exist in less densely compacted sand-bentonite samples, are no longer observed in the denser central zone in which the compaction stress appear to be high enough to aggregate the bentonite grains together.

In spite of the precautions taken during sample preparation, µCT clearly evidenced that the compacted sand-bentonite mixture was heterogeneous with looser zones all around the sample close to the ring in which compaction was made. This difference could have been better estimated by running MIP tests at different distances from the centre to compare them with the data of Figure 2 obtained in the denser central area. Some segregation probably resulting from the difference in density between the bentonite and the sand grains was also detected by µCT. The hydro-mechanical response of the sample should be somewhat influenced by this heterogeneity, with mechanical parameters affected by the stronger central area and the hydraulic conductivity affected by the smaller permeability around the sample.

In this regard, it would be interesting to perform µCT observations on industrially processed compacted bricks to check their degree of heterogeneity, either due to change in density or to particle segregation during the process (that might be more severe than in the laboratory). Compared to the 2D friction effects observed here along the ring walls, 3D friction effects should be more pronounced close to the corners of the bricks. The question as to whether this heterogeneity affects the global response of the material arises, particularly with respect to water transfer during infiltration, arises. Indeed, the looser zones observed around the sample

could facilitate water transfer and reduce the infiltration time, a serious concern in mock-up tests (e.g. Dixon et al., 2002). In this regard, it appears that the direct determination of the hydro-mechanical parameters of the industrially compacted bricks becomes necessary to confirm the measurements carried out on samples of different shapes and sizes compacted in the laboratory. It would also be interesting to have an estimation of the global permeability of an assemblage of bricks, accounting for the effects of the technical voids.

5 Conclusion

The µCT investigation of the microstructure of compacted bentonite/sand mixture samples (65/35%) provided interesting complementary features at larger scale that could not have been identified by using MIP. µCT allowed further observation of the mutual arrangement of bentonite and sand grains. The commonly admitted hypothesis of having isolated sand grains among a clay matrix has not been confirmed. Conversely, sand grains appeared to be scattered along a loose granular skeleton with interconnected inter-grains large pores that were also detected by MIP.

A study on the effect of the size of the REV demonstrated that it was necessary to consider a cubic volume with a size of 271 voxels (around 9 grains). The sample heterogeneity due to compaction with a larger porosity around the sample was quantified by carrying a 3D estimation of porosity by using image analysis.

The interconnection of inter-grains pores evidenced here could have some effects during the hydration of the bentonite/sand mixture, at least in the vapour phase, since it could facilitate the propagation of vapour within the mixture through connected inter-grains pores. The question as to whether this porosity remains interconnected and not clogged when bentonite grains start being hydrated remains. It could be examined by conducting a similar investigation at various degrees of hydration.

References

Agus S.S. and Schanz T. 2005. Effect of shrinking and swelling on microstructures and fabric of a compacted bentonite-sand mixture. Proceedings of the International Conference on Problematic Soils, Cyprus, 32, 543 – 550.

Ahmed S., Lovell C. W. and Diamond S. 1974. Pore sizes and strength of compacted clay. J. Geotech. Eng. Div. Am. Soc. Civ. Eng., GT4, 407– 425.

Carminati A., Kaestner A., Hassanein R. and Koliji A. 2006. Hydraulic properties of aggregate-aggregate contacts. In: Desrues J, Viggiani G, Bésuelle P (eds.) Advances in Xray tomography for geomaterials. ISTE Ltd, London, UK, 325–331

Comina C., Foti S., Musso G. and Romero E. 2008. EIT oedometer: an advanced cell to

monitor spatial and time variability in soil. Geotech Test J. ASTM 31, No. 5, 404–412.

Cui Y.J., Loiseau C. and Delage P. 2002.. Microstructure changes of a confined swelling soil due to suction controlled hydration. In Unsaturated soils: proceedings of the Third International Conference on Unsaturated Soils, UNSAT 2002, 10-13 March 2002, Recife, Brazil, volume 2, 593-598.

Delage P. 2009. Compaction behaviour of clay: discussion. Géotechnique 59 (1), 75-76.

Delage P., Marcial D., Cui Y.J. and Ruiz X. 2006. Ageing effects in a compacted bentonite: a microstructure approach, Géotechnique 56(5):291–304.

Delage P., Audiguier M., Cui Y.J., and Howat M. 1996. The microstructure of a compacted silt. Canadian Geotechnical Journal, 33: 150-158.

Dixon D., Chandler N., Graham J. and Gray M. 2002. Two large-scale sealing tests conducted at Atomic Energy of Canada's underground research laboratory: the buffer container experiment and the isothermal test. Canadian Geotechnical Journal 39 (3): 503-518.

Gens A., Alonso E.E., Suriol J. and Lloret A. 1995. Effect of structure on the volumetric behaviour of a compacted soil. Proc. 1st Int. Conf on Unsaturated Soils UNSAT' 95 1, 83-88.

Gebrenegus T., Tuller M. and Muhuthan B. 2006. The application of X-ray computed tomography for characterisation of surface crack networks in bentonite-sand mixtures. In: Desrues J, Viggiani G, Bésuelle P (eds) Advances in X-ray tomography for geomaterials. ISTE Ltd, London, UK: 207–212

Karnland O., Olsson S. and Nilsson U. 2006. Mineralogy and sealing properties of various bentonites and smectite-rich clay material. SKB.

Kawaragi C., Yoneda T., Sato T. and Kaneko K. 2009. Microstructure of saturated bentonites characterized by X-ray CT observations. Engineering. Geology., 106, 51–57

Ketcham R. A. and Carlson W. D. 2001. Acquisition, optimization and interpretation of X-ray computed tomographic imagery : applications to the geosciences. Computers&Geosciences Vol. 27, 381-400.

Koliji A., Carminati A., Kaestner A., Vulliet L., Laloui L., Fluehler H., Vontobel P. and Hassanein R. 2006. Experimental study of flow and deformation in aggregated soils using neutron tomography. In: Desrues J, Viggiani G, Bésuelle P (eds). Advances in X-ray tomography for geomaterials. ISTE Ltd, London, UK: 341–348

Komine H. and Ogata N. 1999. Experimental study on swelling characteristics of sand-bentonite mixture for nuclear waste disposal. Soils and Foundations 39(2): 83-97.

Kozaki T., Suzuki S., Kozai N., Sato S. and Ohashi H. 2001. Observation of microstructures of compacted bentonite by microfocus X-ray computerized tomography (Micro-CT). J. Nucl. Sci. Technol., 38 (8), pp. 697–699

Li Z.M. 1995. Compressibility and collapsibility of compacted unsaturated loessial soils. Proc. 1st Int. Conf on Unsaturated Soils UNSAT' 95 1, 139-144, Paris, Balkema, Rotterdam.

Lloret, A., Villar, M. V., Sanchez, M., Gens, A., Pintado, X. & Alonso, E. E. 2003. Mechanical behaviour of heavily compacted bentonite under high suction changes. Géotechnique 53, No. 1, 27-40.

Madsen FT. 1998. Clay mineralogical investigations related to nuclear waste disposal. Clay Minerals, 33(1):109–129.

Montes-H G. 2002. Etude expérimentale de la sorption d'eau et du gonflement des argiles par microscopie électronique à balayage environnementale (ESEM) et analyse digitale d'images. PhD Thesis. Louis Pasteur University, Strasbourg I, France.

Mukunoki T., Otani J., Maekawa A., Camp S., Gourc J.P. 2006. Investigation of crack behaviour on cover soils at landfill using X-ray CT. In: Desrues J, Viggiani G, Bésuelle P(eds) Advances in X-ray tomography for geomaterials. ISTE Ltd, London, UK: 213–219.

Pusch, R. 1979. Highly compacted sodium bentonite for isolating rock-deposited radioactive waste products. Nucl. Technol, United States. 45(2):153-157.

Rasband W.S. 1997-2012. ImageJ, U. S. National Institutes of Health, Bethesda, Maryland, USA, http://imagej.nih.gov/ij/.

Razavi M.R., Muhunthan B. and Al Hattamleh O. 2007. Representative elementary volume analysis using X-ray computed tomography, Geotechnical Testing Journal 30 (3) doi:10.1520/GTJ100164.

Rolland S., Stemmelen D., Moyne C. and Masrouri F. 2003. Transfert hydrique dans un sol argileux gonflant non sature´: influence du confinement. Revue Française Géotech 104:21–35

Rolland S., Stemmelen D., Moyne C. and Masrouri F. 2005. Experimental hydraulic measurements in an unsaturated swelling soil using the dual-energy gamma-ray technique. Proceedings of International Symposium on Advanced Experimental Unsaturated Soil Mechanics, Trento, Italy. In: Tarantino A, Romero E, Cui YJ (eds) Advanced experimental unsaturated soil mechanics. Taylor, Francis Group, London, 305–310.

Romero E., Gens A., and Lloret A. 1999. Water permeability, water retention and microstructure of unsaturated compacted Boom clay. Engineering Geology, 54: 117-127.

Tang A.M., Cui Y.J. and Le T.T. 2008. A study on the thermal conductivity of compacted bentonites. Appl Clay Sci; 41:181-189.

Tarantino A. and De Col E. 2008. Compaction behaviour of clay. Géotechnique 58(3): 199-213.

Van Geet M., Volckaert G. and Roels S. 2005. The use of microfocus x-ray computed tomography in characterising the hydration of a clay pellet/powder mixture. Applied Clay Science, 29(2):73–87, 2005.

Villar M.V. and Lloret A. 2001. Variation in the intrinsic permeability of expansive clays upon saturation. In: Adachi K., Fukue M. (eds) Clay Science for Engineering. A.A. Balkema, Rotterdam, 259-266.

Yong R.N., Boonsinsuk P. and Wong G. 1986. Formulation of backfill material for a nuclear fuel waste disposal vault. Canadian Geotechnical Journal, 23(2):216–228.

Chapter 2

Free/limited swelling upon direct contact with water

INTRODUCTION

The geometry of the sealing plugs considered in this work is cylindrical and formed by a succession of pre-compacted bentonite/sand disks. When they are emplaced in the galleries, they are in an unsaturated state. They will then start being saturated by water infiltration from the host rock starting from their outer boundary. This will result in radial swelling allowing the closure of the radial technological void between the sealing plug and the host-rock. The plug starts to swell freely by forming a gel until it touches the host-rock. Then, the gel is consolidated between the host-rock and the continuously swelling core. The densification of the gel and the homogenisation of the seal are essential in preventing any leakage. In a first part of this chapter, the radial free swelling (before touching the rock) is reproduced at the laboratory scale for a compacted disk of bentonite/sand mixture immersed in water, allowing observation of the gel development and study of the swelling kinetics and magnitude. Observation was made by 2D images taken by a camera at a fixed time interval. The images were then analysed using an image analysis software and the results have been published in the proceedings of the E-UNSAT 2012 conference. The published paper constitutes the first part of this chapter.

The second part of this chapter involves the limited swelling of a similar sample that was also in radial contact with water. The observation of swelling was made in 3D using microfocus computed tomography (µCT). The density degradation that accompanies the free swelling was observed and estimated using digital image analysis. The long term homogenisation was also examined and the results are presented in the second part of this chapter in the form of a paper to be submitted to "Applied clay science".

Swelling of highly compacted bentonite-sand mixtures used as sealing materials in radioactive waste disposal

Simona Saba, Anh Minh Tang, Yu-Jun Cui, Jean-Dominique Barnichon

Abstract. In the radioactive waste disposal concepts, highly pre-compacted bentonite-sand mixtures are considered as appropriate sealing materials to fill the galleries. Compacted elements of bentonite-sand mixtures are placed adjacent to each other, forming a plug that should limit the transfer of radionuclide. The bentonite has proven to have the capability of retaining radionuclides and the capability of swelling when getting in contact with water and then closing all the voids in the system especially the radial technological void being the gap between the bentonite-sand elements and the host rock. Indeed, when the bentonite-sand elements is emplaced in the gallery, they are first in an unsaturated state and they will start being saturated by the host-rock pore water. They will then start swelling, forming a gel that will close the gap. In this work, such hydration process is experimentally analysed on a small scale. The swelling is analysed by time-lapse photography, its kinetic is also studied by image processing. We can see that the swelling of this material is fast and large, and we can distinguish different states of the material during swelling, starting from the dry centre to the outer boundary. On the other hand, the presence and behaviour of sand grains in the gel formation is evidenced by images as well. The sand grains are found to be covered by bentonite particles and being carried with the bentonite swelling.

Keywords: Radioactive waste disposal; bentonite-sand mixture; swelling; digital image analysis.

1 Introduction

In the high-level radioactive waste repository concepts, pre-compacted elements of bentonite-sand mixture could be used as sealing material thanks to its low permeability, high swelling and high radionuclide retardation capacities (Pusch, 1979; Yong et al., 1986). When emplaced in the gallery, such bentonite-based seals are first in an unsaturated state. Once the repository is closed and local groundwater conditions are re-established, water in the host rock formation will flow toward the repository and start saturating the seals from their extremity. When absorbing water, bentonite swells and forms a gel which should fill the radial technological void as the gap between the seal and the host rock. After filling all the technological voids, the gel will be consolidated between the host rock and the swelling core.

In this study, the radial swelling and gel formation are investigated. Small compacted bentonite-sand disks were immerged in distilled water and time-lapse photography coupled with digital image analysis was performed to study their swelling kinetics for different dry densities. Swelling was defined as the variation of the disk surface over time. The growth of the total surface and the reduction of the dry central surface were monitored. The movement of sand grains was also investigated. It was found that the sand grains were firstly pushed

radially by the swelling of the bentonite aggregates until the surrounding material becomes too loose to support them: the grains finally dropped down by gravity.

2 Materials and methods

2.1 Materials

The soil studied is a mixture of MX-80 bentonite (Gelclay WH2) and quartz sand with a bentonite content of 70% in dry mass. The bentonite has a montmorillonite content of 92%; it has an average specific gravity of 2.76, a liquid limit of 520%, and a plastic limit of 42%. The grain size distribution curve determined by sedimentation shows that 84% grains are smaller than 2 μm (clay-size fraction).

2.2 Methods

The prepared disks have been compacted statically using a mechanical press, and have a diameter of 35 mm and a thickness of 10 mm. Several disks were prepared by compaction at different dry densities. They were then placed between two transparent Plexiglas plates to avoid the axial swelling of the disk when the whole frame was immerged in distilled water. A computer controlled camera was fixed on a special holder above the container at a defined height and was able to take photos automatically at a given time interval. Artificial lighting was used and the system was covered with a black fabric to isolate it from external lights in order to avoid changes in lights between day and night (see Figure 1).

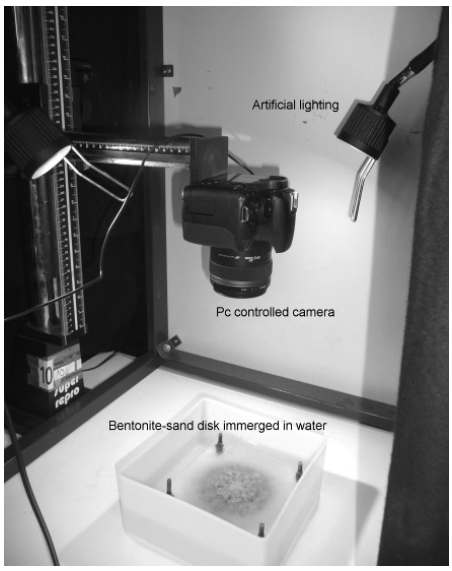


Figure 1 The experimental system: A computer controlled camera is fixed above a bentonite-sand sample immerged in distilled water to follow its swelling with time.

Photos were then analysed using an image processing program (*Fiji of ImageJ*) to help estimate the surface and tracking object movements. For the estimation of surface, an automatic method can be used: photos were first treated (contrast enhancing, illumination,

background removal), then a threshold value was applied to isolate the surface of interest. This is a delicate operation especially as the interface gel/water is not sharp since the bentonite gel is transparent. Therefore, for the estimation of the surface evolution over time, a manual selection of the surface was used. Finally, to avoid confusion in units, photos are calibrated with the original object units (in mm).

3 Results and discussion

3.1 General observation

The swelling of bentonite-sand disks was studied using time lapse photography coupled with digital image analysis. The swelling of the disk is due to the swelling of bentonite present in the mixture.

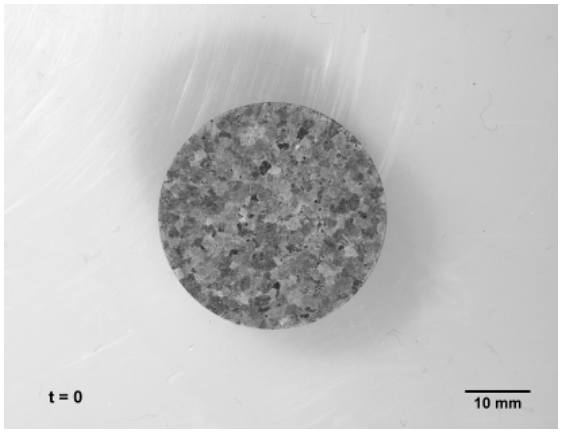


Figure 2 Initial state of a bentonite-sand disk with a dry density of 1.97 Mg/m^3.

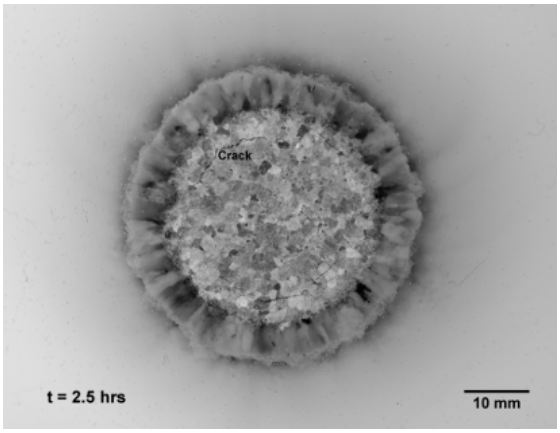


Figure 3 Same disk after 2.5 hours (swelling = 60%).

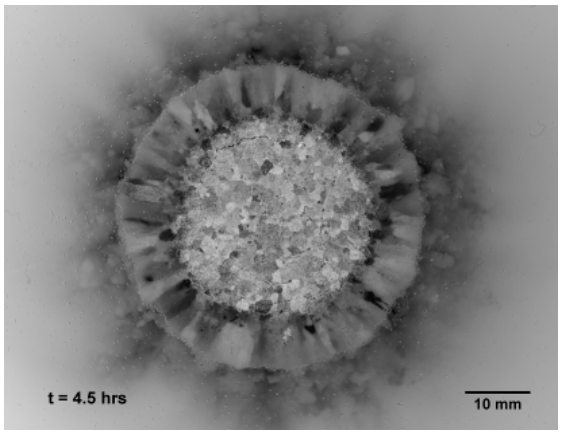


Figure 4 Same disk after 4.5 hours (swelling = 70%).

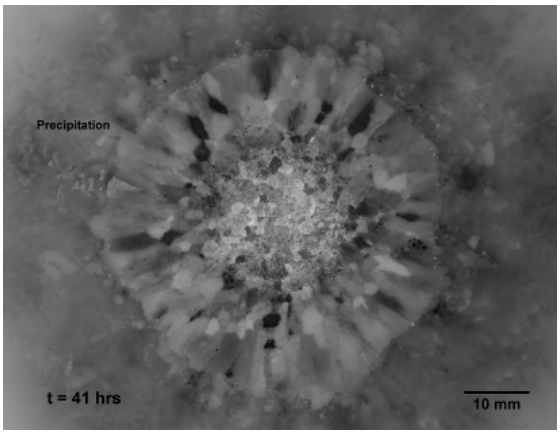


Figure 5 Same disk after 41 hours (swelling = 125%)

Figures 2, 3, 4 and 5 show a bentonite-sand disk compacted to a dry density of 1.97 Mg/m^3 at different times during swelling starting from its initial state (Figure 2). In Figure 3, it is noted

that there are some cracks in the dry centre during the first hours of swelling, and they are closing with time (see Figure 4) to disappear at the end. This is explained by the rearrangement of the aggregates. The last three figures show three different states of the material in the disk viewed from its upper face: an external ring of loose gel, a ring of saturated material that has not turned into gel yet and a dry centre. In fact, water was absorbed by the disk starting from its boundary; the bentonite aggregates on the boundary started swelling first as they have enough free space to produce a gel. Actually, knowing the microstructure of the bentonite aggregates we understand the way they swell when in contact with water (Mitchell, 1993). As water continued infiltrating to the disk, internal bentonite aggregates did not have enough space to swell freely and then did not turn into a gel, while in the dry centre water still did not arrive. Over time, the gel on the extremity became very loose due to the exfoliation of the bentonite aggregates and their precipitation to form a bentonite suspension (see Figure 5). This phenomenon of water over-saturation of aggregates was also evidenced by Montes (2002). It is explained by the existence of a certain amount of water causing the exfoliation of aggregates into small particles (Ye et al. 2009). Consequently, the internal bentonite started swelling freely following the same mechanism. As an overall result, the gel surface became larger and the dry surface became smaller due to water infiltration.

3.2 Swelling kinetics

Experimental results on the swelling of bentonite-sand disks are obtained after digital image analysis (i.e. a two-dimensional analysis). In Figure 6, three curves are illustrated: one for the variation of the external total surface of the disk, one for the variation of the dry central surface and the difference between the two curves that represents the surface of the gel ring.

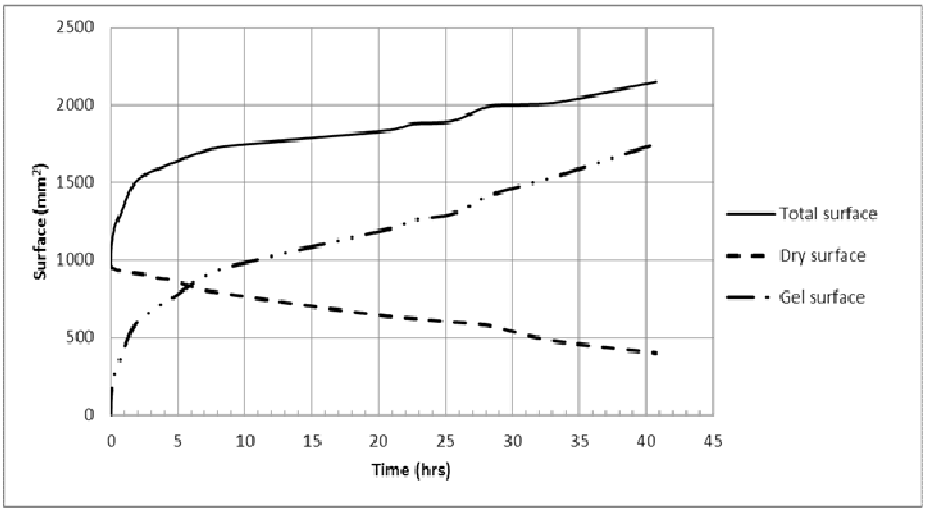


Figure 6 Variation of the total surface, dry surface and gel surface with time for a bentonite-sand disk having a density of 1.97 Mg/m^3.

The shape of the total surface curve shows a rapid swelling for the first three hours, after that it becomes slightly slower and exhibits a constant rate. The test was stopped after 2 days when the swelling reached 300%. The variation of the dry surface is almost linear, which makes the shape of the gel surface curve similar to that of total surface but with a sharper slope. The gel surface curve is moving toward the total surface curve, which indicates that at a certain time the curves will superimpose and this corresponds to the state where the disk becomes saturated and the maximum swelling is reached.

3.3 Presence of sand grains

Figure 7 shows the trajectory of a sand grain during the disk swelling; the grain apparently disappears after six and a half hours (Figure 8). In fact, when the disk was in contact with water and the bentonite aggregates started to swell radially, the sand grains were covered by swelled bentonite and were pushed outwards by the pressure from the radial swelling. When the swelled bentonite around the sand grain exfoliated and became loose (similar to a bentonite suspension), the sand grains fell down.

On the other hand, the proportion of sand in the compacted disk is about 30% in dry mass. When the swelled bentonite formed an external ring containing transported sand grains, the volume fraction of sand grains became lower. The concentration in sand grains was lower on the outer boundary of the disk and is mainly located at the bottom.

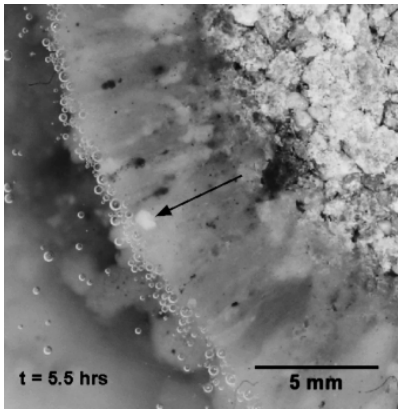


Figure 7 A sand grain pushed radially in the gel formation.

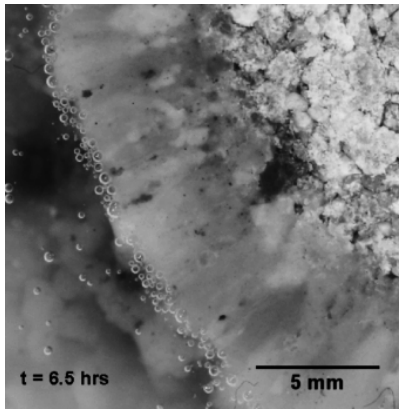


Figure 8 Precipitation of the sand grain (not visible anymore).

4 Conclusion

The swelling of a compacted bentonite-sand disk is experimentally studied using time-lapse photography coupled with digital image processing. The main advantage of this method is the rapidity for obtaining qualitative and quantitative results. However, it was difficult to analyse the images automatically due to lack of contrast.

Thanks to the observations of the photos it was possible to identify different states of the material during swelling: the dry centre, the gel extremity and a saturated un-swelled surface in between.

The image analysis allows drawing swelling kinetic curves and tracking the trajectory of a sand grain during swelling. It was found that the swelling started rapidly and then became slower. The sand grains were found to be covered with swelled bentonite and pushed outward until they dropped down and precipitated under gravity when the swelled bentonite became very loose similar to a bentonite suspension.

References

Mitchell, J.K. 1993. Fundamentals of soil behaviour. John Wiley and Sons, Inc., New York, ISBN: 0-471-85640-1

Montes-Hernandez, G. 2002. Etude expérimentale de la sorption d'eau et du gonflement des argiles par microscopie électronique à balayage environnementale (ESEM) et analyse digitale d'images. PhD thesis, Louis Pasteur University, Strasbourg I, France.

Pusch, R. 1979. Highly compacted sodium bentonite for isolating rock-deposited radioactive waste products. Nucl. Technol, United States. 45(2):153-157.

Ye W.M., Cui Y.J., Qian L.X., Chen B. 2009. An experimental study of the water transfer through compacted GMZ bentonite. Engineering Geology 108, 169 – 176.

Yong R N, Boonsinsuk, P, and Wong, G. 1986. Formulation of backfill material for a nuclear fuel waste disposal vault. Canadian Geotechnical Journal, 23(2):216–228.

Limited swelling and homogenisation of compacted bentonite/sand mixture: a 3D investigation using X-ray computed tomography (µCT)

Simona Saba[1,2], Yu-Jun Cui[1], Pierre Delage[1], Nicolas Lenoir[1], Jean-Dominique Barnichon[2] and Anh Minh Tang[1]

Abstract: Cylindrical sealing plugs made of compacted bentonite/sand mixture will be used to seal radioactive waste disposal galleries and limit water transfer in the disposal. Upon contact with water, these seals will swell and hence fill all the so-called technological voids created during the setting of the system. In this work, a laboratory test designed to mimic the filling of technical voids by the swelling of the compacted sand-bentonite mixture is presented. A 50 mm diameter compacted sample (70/30 bentonite/sand mixture) was placed in a 80 mm diameter PMMA cylindrical cell, resulting in a radial peripheral void allowing a 60% radial swelling. The changes in density resulting from the swelling and filling of the radial void by the samples were monitored using microfocus X-ray computed tomography (µCT). The cell was scanned at different hydration times, enabling the analysis of the material at initial state, during swelling and subsequent homogenisation once the swelled sample reached the cell wall. At initial state, the 3D image showed that the mixture constituents (bentonite and sand grains) were heterogeneously organised in the sample, with a fracture observed along the sample diameter in the upper 5 mm. This fracture disappeared after 3 days of hydration, confirming the self-sealing capacity of the material. The qualitative monitoring of swelling over time revealed that swelling took place by clay exfoliation from the bentonite grains around the sample and by creation of a gel. Swelling started quickly and slowed down over time. Sand grains were found to be transported by the swelling of bentonite grains. Once touching the cell, the gel started consolidating under the swelling pressure generated by hydration of the denser centre. The homogenisation was studied using image analysis by plotting grey level profiles at different hydration times along a given diameter. A gradient was observed between the denser centre and the looser periphery and it progressively decreased, i.e. the density of the central part decreased whereas that of the periphery increased.

Keywords: bentonite/sand mixture, sealing, X-ray tomography, swelling, density gradient, homogenisation.

1 Introduction

In high-level radioactive waste repository concepts, pre-compacted bentonite/sand mixtures are often foreseen to be used as sealing materials to limit fluxes (water, and radionuclides) around storage galleries thanks to their low permeability, high radionuclide retardation capacities and high swelling potential (Pusch, 1979; Yong et al., 1986). Swelling of compacted mixtures helps in closing all gaps existing within the disposal system, especially the so-called radial technological voids between the seal and the host-rock (Barnichon et al., 2010, 2012). When initially placed in the gallery, bentonite-based seals are unsaturated. Their hydration by the host-rock pore-water starts once the repository is closed, when local groundwater conditions are progressively recovered. When absorbing water, bentonite swells

[1] Ecole des Ponts ParisTech, Laboratoire Navier, Marne La Vallée, France
[2] Institut de Radioprotection et de Sûreté Nucléaire (IRSN), Fontenay-aux-Roses, France

and forms a gel that fills the radial technological void around the plugs. Axial swelling is also prevented by concrete retaining structures placed in the gallery.

The swelling behaviour of bentonite has been largely studied in the past, especially in the context of geological radioactive waste disposal. Particular attention has been paid to the swelling pressure. Pusch (1980), Komine and Ogata (1999), and Wang et al. (2012), among others, studied the swelling pressure of bentonite either through laboratory tests or numerical modelling. In the studies of bentonite erosion and hydrated bentonite extrusion into fractures of granitic host-rocks, the free swelling of bentonite and its transformation into a gel upon contact with water have also been investigated (see Pusch, 1999; Jansson, 2009; Neretnieks et al., 2009; and Moreno et al., 2009). Based on the swelling mechanism identified, a model was developed allowing the description of the clay colloid formation. Dvinskikh et al. (2009) studied the bentonite swelling and homogenisation by immersing a bentonite pellet in water. They used Magnetic Resonance Imaging (MRI) and Nuclear Magnetic Resonance (NMR) to estimate the evolution of the clay volume fraction profiles over time. This experiment was then used to validate a dynamic force balance model developed by Liu et al. (2009) to further study the colloid expansion. It was found that the bentonite pellet at an initial density of 1.8 Mg/m^3 swelled over time and almost reached homogenisation within 26 days.

The hydration of bentonite was also studied by Van Geet et al. (2005) by using microfocus X-ray computed tomography (µCT). They studied the density homogenisation of a FoCa clay pellet/powder mixture hydrated under a water pressure of 0.5 MPa and found that homogenisation was achieved at the end of the test (after five and a half months). Moreover, they observed that the initial macro-porosity present in the powder and the fractures in the pellet disappeared after one and a half month.

Dueck et al. (2012) studied the limited swelling of compacted bentonite blocks after full saturation (maximum radial void of 31%) in order to predict the final state of the block after swelling and homogenisation. They performed several tests to study the radial swelling of an initially saturated compacted bentonite block. At the end of their tests, they measured the densities at different positions and evidenced a difference in dry density of about 0.1 to 0.2 Mg/m^3 between the centre and the border of the sample after about one week hydration.

The long-term homogenisation of sealing plugs is an important issue in the context of radioactive waste disposal. It is hence important to be able to further investigate the long-term sample homogenisation by a non-destructive monitoring of the density gradient during

swelling and by observing the gel formation.

In this study, a disk of compacted bentonite/sand mixture placed in a PMMA (polymethyl methacrylate) cylinder having a larger diameter was saturated while continuously observing hydration by means of microfocus X-ray tomography (µCT). Qualitative observation and image analysis were conducted to observe the initial state and further changes of the sample during swelling.

2 Materials and methods

2.1 Materials

The studied material is a compacted mixture of Wyoming MX-80 bentonite (commercial name Gelclay WH2, 70% in dry mass) and sand (30%). The MX-80 bentonite contains 92% montmorillonite with several other minerals such as quartz, alumina, and hematite (Tang et al., 2008). The sand is a pure quartz one (commercial name TH1000).

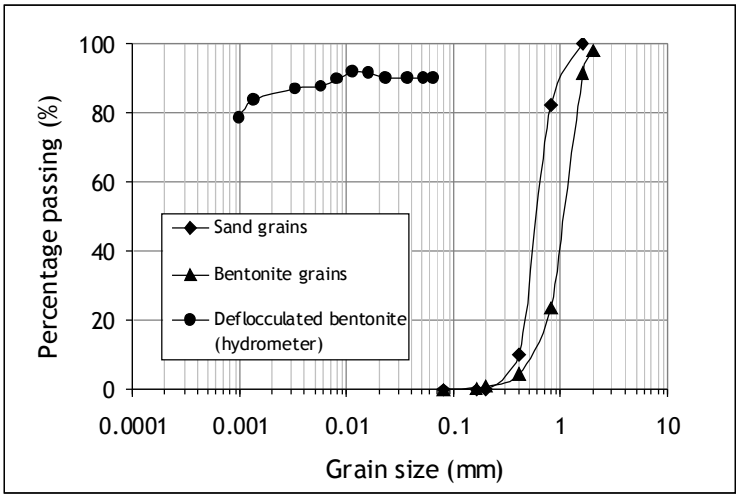


Figure 1. Grain size distribution curves.

The mixture was manually prepared by mixing a given mass of bentonite powder at an initial water content of 13.3% with dry sand. The grain size distribution curve of the bentonite powder obtained by dry sieving is presented in Figure 1 along with that of the deflocculated bentonite obtained by hydrometer test. The grain size distribution curve of the sand is also plotted in Figure 1. It is observed that bentonite powder grains are larger than sand grains, with a D_{50} value of 1.2 mm against 0.6 mm. Both curves are representative of well sorted materials. The unit masses of bentonite particles and sand were measured (using a pycnometer), and found equal to 2.77 Mg/m^3 and 2.65 Mg/m^3, respectively. The density of bentonite grains was also measured using a pycnometer with a desaromatised immiscible oil (commercial name Kerdane) having a density of 0.791 at 20°C. It was found to be equal to

2.00 Mg/m^3.

The compacted sample was prepared by uniaxial static compaction at a rate of 0.1 mm/min in a cylindrical mould. A maximum compaction stress of 25.5 MPa was applied, resulting in a final dry density of 1.8 Mg/m^3 corresponding to a bulk density of 1.98 Mg/m^3 at 11% water content. The final dimensions of the sample were 50 mm in diameter and 10 mm in height.

2.2 Microfocus X-ray computed tomography (µCT)

The Microfocus X-ray computed tomography (µCT) is able to distinguish various components of a material according to their density and atomic composition. The grey level range observed in µCT goes from white (representing high attenuating dense material) to black (representing void). µCT is a non destructive observation technique used in the investigation of various geological porous media like compacted bentonite (Kozaki et al., 2001), bentonite pellet/powder mixture (Van Geet et al., 2005) and compacted bentonite/quartz mixture (Kawaragi et al., 2009). The technique uses a set of two-dimensional X-ray projections of an object at several angles and consists in reconstructing the 3D slices of the object using a mathematical algorithm, resulting in a 3D image of the internal structure. The parameter of interest is the attenuation coefficient to X-rays (μ) that depends on the mass density and on the atomic number of the object (Ketcham and Carlson, 2001; Van Geet et al., 2005).

The µCT used in this study is an "Ultratom" device provided by RXsolutions (France). Images were reconstructed using the software Xact-reconstruction developed by RXsolutions. The micro-focus source is an xs-225d/GE-Phoenix (225 kV, 320W, 5 µm min spot size) and the imager is a flat-panel-CsI scintillator-Varian 2520V/Paxscan (14 bit, 1920 × 1526 pixels, 127 µm pixel size). The voxel size varies between 32 µm and 48 µm depending on the scanned area. The size of the 3D images is 1840 × 1840 × 1180 voxels. The image analysis and treatment are conducted using ImageJ, a public domain Java image processing program (Rasband, 1997-2012).

2.3 Experimental set-up and test program

The test cell is made of Polymethyl Methacrylate (PMMA), a material transparent to X-rays. A vertical cross-section of the cell is presented in Figure 2. It consists of a cylinder (80 mm inner diameter) fixed on a base. A circular plate of 80 mm diameter is placed at the top of the sample and is glued to the internal surface of the cylinder to prevent axial swelling. The used glue is removable to facilitate releasing the sample after test. The upper plate is perforated along its periphery (11 holes) to let water flow through, fill the peripheral volume and hydrate

radially the sample from its external perimeter.

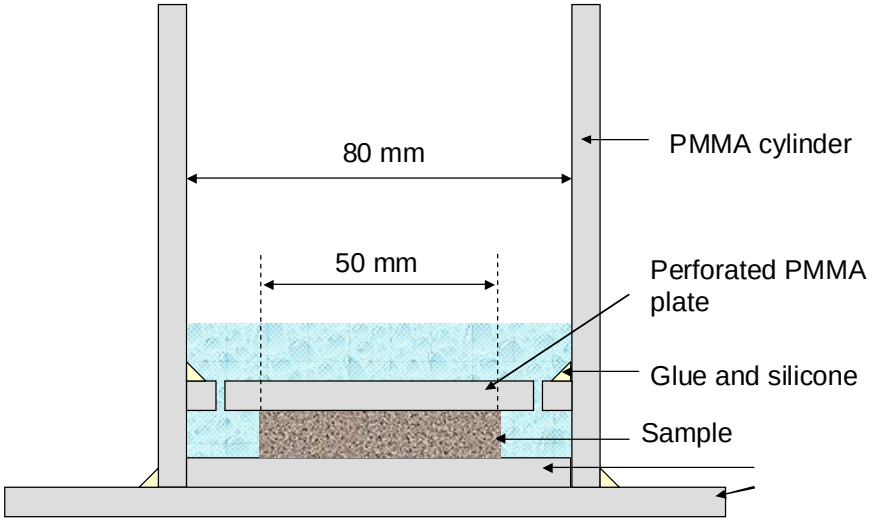


Figure 2. Outline of the PMMA test cell.

A first scan was performed at the initial (as compacted) state of the sample prior to filling the peripheral volume with water. Five scans were then performed at different hydration times: 15 min, 3 h, 1 day, 3 days and 52 days with a scan duration around 2 hours. All along the experiment, the cell was covered by a plastic film and preserved in an ambient environment at a constant temperature of 20°C to avoid evaporation.

3 Results

3.1 Dry state observation

The µCT horizontal cross-section at 5 ± 0.1 mm from the top of the sample is shown in Figure 3. At the adopted scan resolution (32.5 µm), one can distinguish the different constituents of the sample: clear sand grains, less clear larger bentonite grains (hydrated at a gravimetric water content of 13.3%) and dark voids. The grey level difference between sand and bentonite grains is due to the larger unit mass of sand (2.65 Mg/m^3) compared to that of bentonite grains (2.00 Mg/m^3). Inspection of Figure 3 also shows that the bentonite/sand mixture is not really homogeneous, a segregation being observed between sand grains and bentonite grains as illustrated by some clustering of sand grains. This heterogeneity probably results from the effect of the difference in size and mass between the bentonite and the sand grains during sample preparation.

In Figure 3, the grey level is not homogeneous with a darker centre. Such an artefact, typical of X-ray µCT, is called beam hardening effect and is not representative of a real change in density.

Observation of the upper cross-sections of the sample (Figure 4) shows the occurrence of a

fracture along the diameter of the sample. The fracture has a depth of about 5 mm, i.e. 50% of sample thickness. It probably appeared during the placement of the upper plate at the top of the sample.

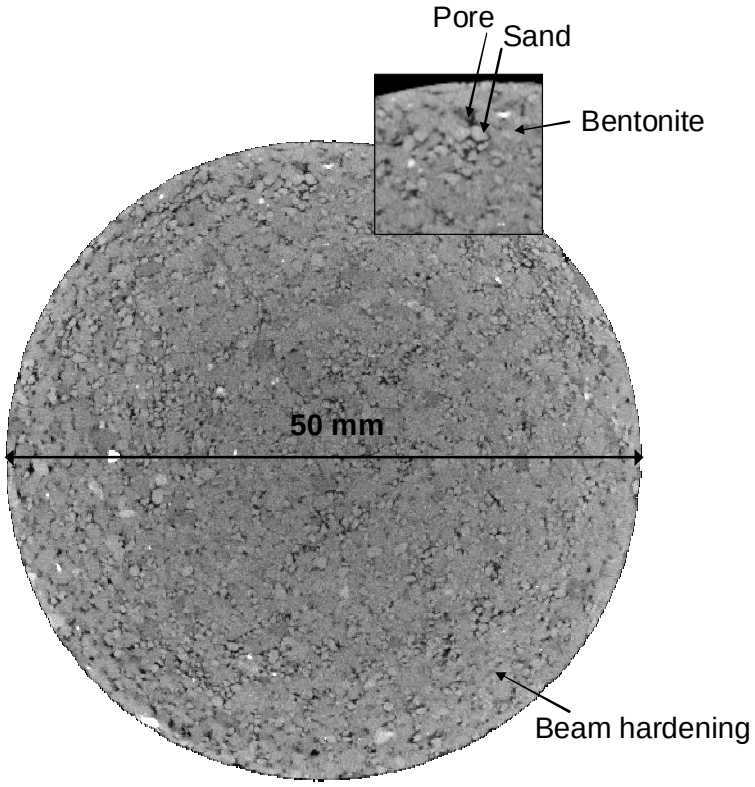


Figure 3. Horizontal cross section at a distance of 5 mm from the top of the sample.

3.2 Swelling observation

Figure 5 shows the evolution of the same horizontal cross-section of the sample during hydration from the initial compacted state. The images are obtained after eliminating the external void by fixing a grey level threshold of 55 that separates gel from air or water.

After the first 15 min of hydration, curved cracks parallel and close to the perimeter of the sample appear all around and the sample diameter increased from 50 to 52.8 mm. The bentonite separated by the cracks along the perimeter swelled first and was quickly transformed into gel, with a sharp contrast observed between the gel ring and the denser compacted area. The cracks result from the effect of the extremely high suction gradient and differential radial swelling strains resulting from the sudden contact imposed between liquid water (zero suction) and the compacted mixture with an initial suction of 76 MPa.

After about 3 hours of hydration, water infiltrated more the sample with a further increase in diameter to 55.3 mm and a comparable pattern of cracks.

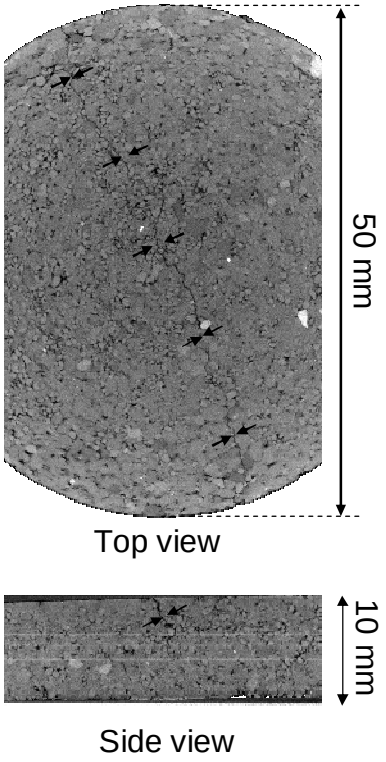


Figure 4. Top view and side view of the sample at the position of the crack.

After 1 day, the clear separation observed in the previous scans around the sample is no longer apparent. Some cracks are still observed around the sample, but their opening is smaller than previously. This crack network separates the central zone in which the effects of compaction is still apparent from a zone appearing much more homogeneous, which is representative of the gel. Closer to the sample periphery, the gel zone progressively darkens. The diameter of the hydrated sample is estimated at 75 mm. Interestingly, one can observe that sand grains transported by the hydrated and swelled bentonite are clearly apparent in the gel around the sample, with a small concentration. The structure of the newly produced gel close to the crack pattern is denser (clearer) than that was previously produced, which is now located at larger radius. This difference in density is due to the difference in boundary conditions: while the first bentonite grains at the initial sample periphery swelled freely in water, the subsequent bentonite grains (i.e. located behind) swelled in contact with the already swelled mixture. We can also observe that after 1 day the fracture that was observed at the initial state almost disappeared (see Figure 6).

After 3 days, swelling continued and the gel almost filled the 15 mm radial void between the sample and the cell. The whole sample was not completely saturated as the central dryer part was still identified. Until this time, the sample swelling was still free. By means of image analysis, we can estimate the surface increase over time. By considering the sample's

diameter evolution obtained as explained earlier after fixing a grey level threshold, one can estimate the surface increase with respect to time.

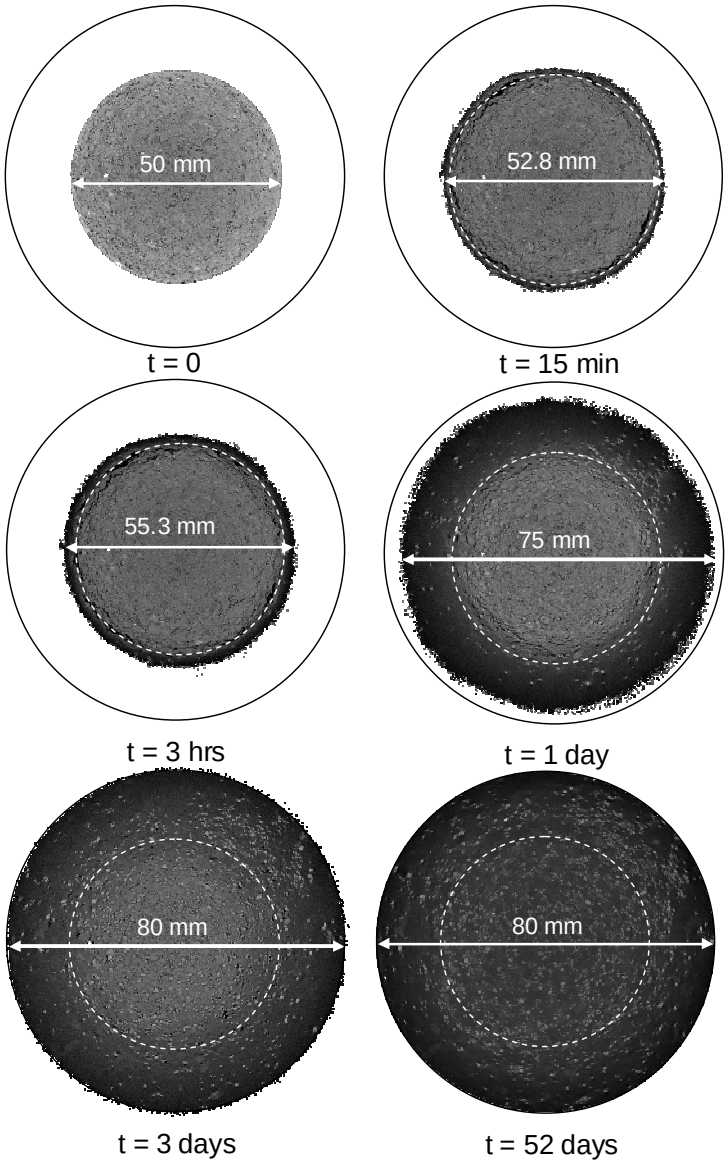


Figure 5. A cross section of the sample at the middle of the sample at different hydration times (time of the start of the scan).

Figure 7 shows the evolution of swelling defined as the ratio of the increase of surface with respect to the initial surface. Results obtained in a previous work in which no limit to radial swelling was imposed (Saba et al., 2012) are also reported in this figure. The difference between the two tests relies in the sample diameter (50 mm in this work and 35 mm in the previous work) and in the sample initial unit mass (1.8 Mg/m^3 in this work and 1.97 Mg/m^3 in the previous work). Similar changes are observed with a fast increase in the beginning and a rate decreasing over time. However, the swelling magnitudes are not comparable, with here lower values at the beginning and higher values at the end. This may be the result of the lack of data in this work for the first period due to the different time scale.

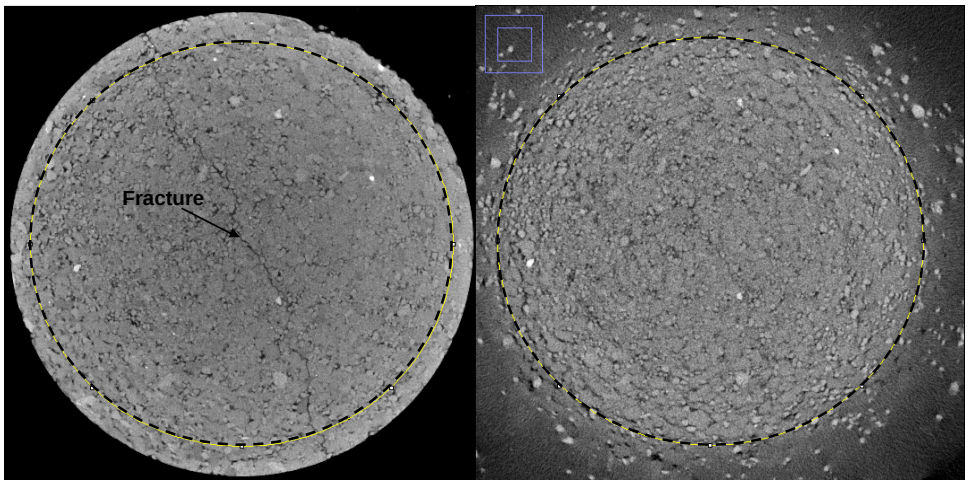


Figure 6. Fracture closure after 1 day of hydration. The circular line outlines the unsaturated part after 1 day and its position is reported in the initial state.

After 52 days, the sample was completely hydrated, touched the cell and could no longer increase in surface even though the swelling of the bentonite grains closer to the centre still occurred. From this moment on, swelling occurred under constant volume conditions. The internal parts of the sample that continued to swell consolidated the peripheral gel. The homogenisation of the sample started, characterised by the progressive disappearance of the dryer dense central part and of the sharp contrast previously observed. A radial swelling pressure was simultaneously mobilized along the ring together with an axial swelling pressure that resulted in an axial displacement of about 1.5 mm, as shown in Figure 8 in which the initial and final cross-sections are presented. The change in grey level between both sections is clear.

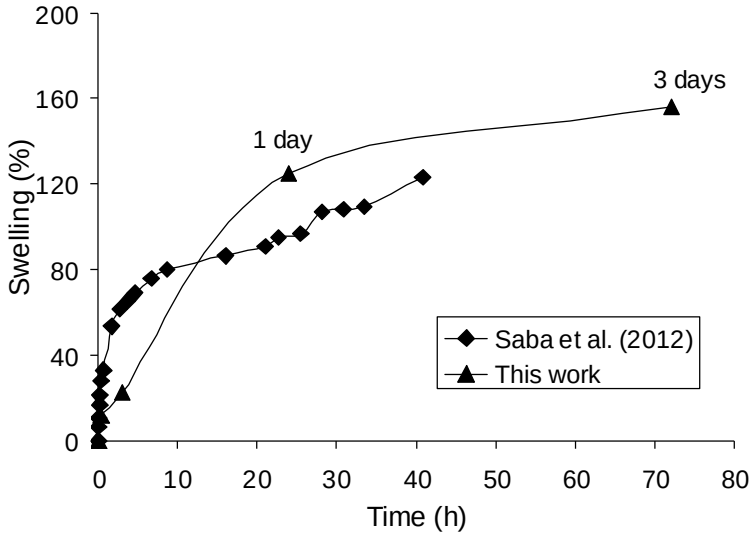


Figure 7. Free swelling kinetics and comparison with previous results.

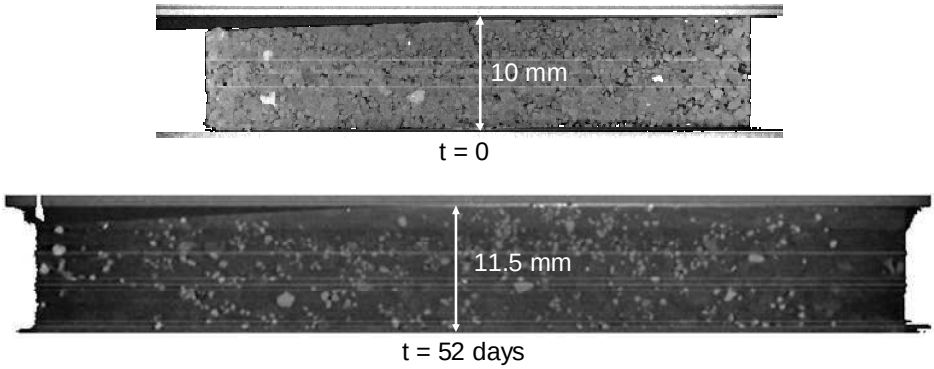


Figure 8. The axial swelling occurring between the initial state and after 52 days.

During the sample swelling, sand grains were found to be transported by the swelling of bentonite and radially moved toward the cell wall. Closer inspection of Figure 5 shows however that full homogeneity is not achieved, as evidenced by a darker periphery containing less sand grains. Note also that the sand grain concentration is not fully constant at the same distance from the centre, more grains being observed on the top right section. Due to hydration, the volume of bentonite grains became 10.5 times larger than that of sand grains and sand grains were finally dispersed in a bentonite gel matrix.

3.3 Profiles evolution

Figure 9 shows the grey level profile along the diameter of the sample in the initial dry state at a cross-section located in the middle at a depth of 5 mm. The profile shows a significant fluctuation of values corresponding to the grey levels of the different constituents of the sample. Highest peaks correspond to the denser sand grains whereas smallest peaks correspond to pores full of air.

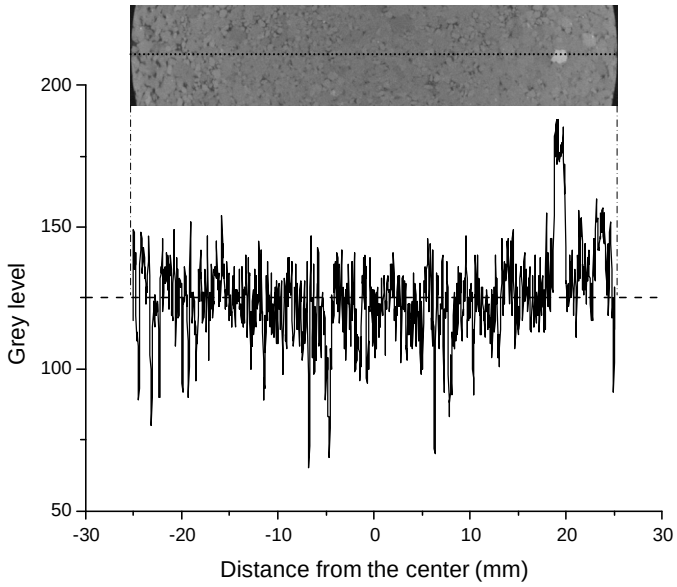


Figure 9. The grey level profile along a diameter on only one slice at t = 0.

The profile along the whole thickness of the sample, obtained by averaging the grey intensity along the whole stack of slices forming the sample, is presented in Figure 10. A reduction in fluctuation due to averaging is observed. The general form of the profile evidences the cupped effect due to the beam hardening artefact that was presented in Figure 3. Ignoring this artefact, the mean grey level along the diameter can be determined and a value of 119.47 was obtained. This mean grey level value is represented by the dashed line in Figure 10, it was obtained on a sample with an the initial density of 1.98 Mg/m^3.

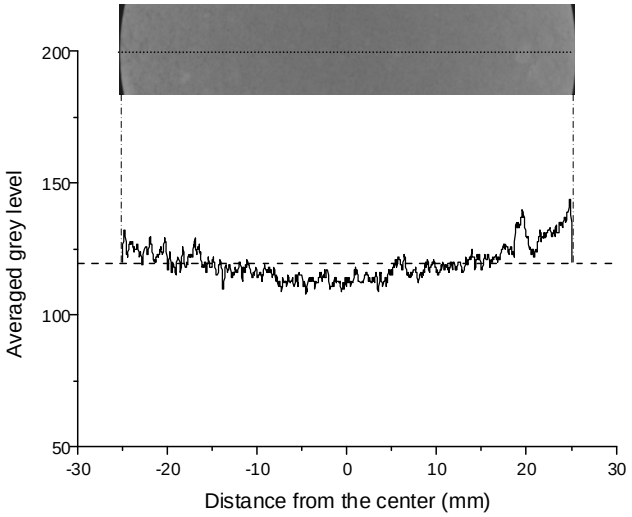


Figure 10. Averaged gray level profile of the central 8 mm thickness along the diameter at t = 0.

Figure 11 shows the averaged grey level profiles along a given diameter of the sample at different hydration times along with the mean grey level value in dashed line. For simplicity, the presented curves represent the 50 points average of the original data. The profile corresponding to the initial state is the same as that in Figure 10, but here in terms of moving average values; it serves as a reference in the analysis. The curve corresponding to 15 minutes hydration is characterised by a sharp decrease of grey level on the extremity, indicating the production of loose gel.

In the central part of the sample (along a diameter of 20 mm), the grey levels are not ordered with respect to the progression of hydration. The points after 1 day are mostly located above those after 3 hours, which is not satisfactory. There are also some cases in which the points after 3 days are close to that after 3 hours. It seems then that it appears difficult, in this feasibility test, to affect a given density to a given grey level. Also, the sudden decrease observed in the central part between the start of the test (t = 0) and the state at 3 hours appears too strong, compared to the change afterwards observed between 3 hours and 3 days. It seems then reasonable to consider that the density changes in the central part are not significant

during the first 3 days, as deduced from the qualitative observation previously conducted. Note however that the global decrease in grey level observed after 52 days is significant of a global decrease in density, as commented earlier.

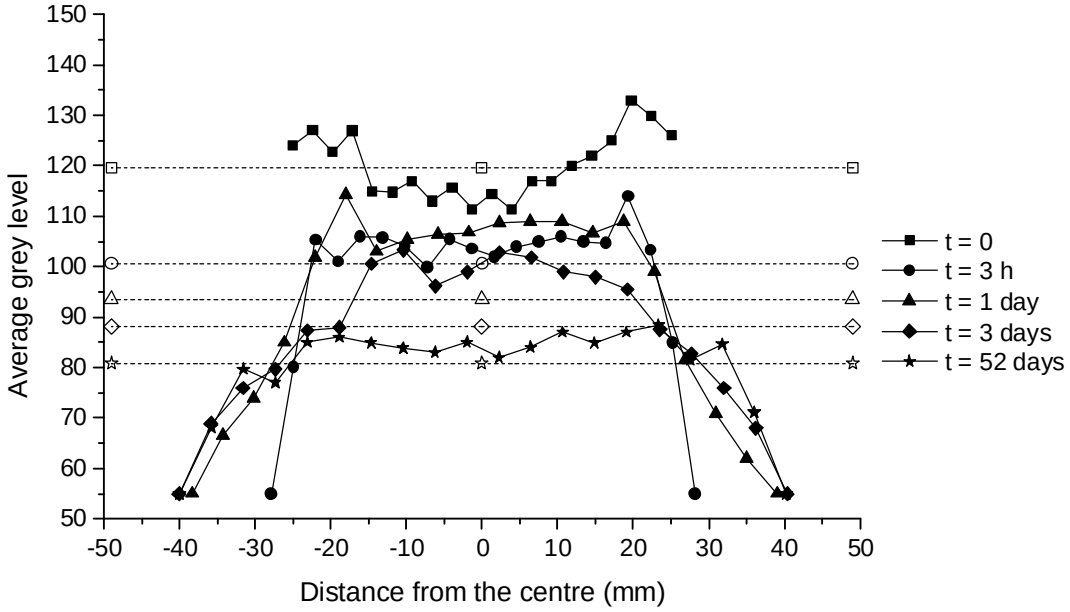


Figure 11. Grey level profiles along the same diameter at different hydration times. The mean values corresponding to the different hydration times are also plotted in dashed line.

For a given profile at a given time, more significance is given to differential changes in grey level and by the change in the slopes of grey level at the extremities. The decrease in slope between 1 hour and 1 day illustrates the progressive water infiltration and coupled swelling that result in an increase in diameter and a decrease in the diameter of the central part corresponding to the zone still unaffected by hydration. Note that the averaged slopes of the curves on each side are comparable at 1 day, 3 days and 52 days. Simultaneously, the steady grey level values in the central area indicate that there is no significant density gradient in this area. The significantly lower grey level in the central part after 52 days seems to indicate a decrease in density compared to the situation between 1 and 3 days.

In order to make a quantitative study in terms of density, calibration (as in Van Geet et al., 2005) should be first conducted on various samples of different well controlled densities in the relevant range, along with a global enhancement of the scan quality (same scanned area, beam hardening correction, etc.).

An estimation of the final average density value can be obtained considering the final volume of the sample supposed saturated and using the unit mass of bentonite particles (2.77 Mg/m^3) and sand grains (2.65 Mg/m^3), giving a value of 1.40 Mg/m^3. Hence, the decrease in grey

level in central areas level observed in the Figure between the first hydration stages in which the sample central area was not affected (between 0 and 3 days) and the final stages (52 days) can be somehow related to the decrease in unit mass from 1.8 to 1.40 Mg/m^3. Again, a satisfactory correlation would require further calibration tests.

4 Discussion

The homogenisation of seals is of high importance in limiting fluxes in the context of geological nuclear waste disposal. The test carried out in this study reproduced the conditions to which the seal will undergo in disposal galleries. Only radial swelling was allowed before the sample touched the cell (corresponding to the host-rock in situ); the axial swelling was prevented by the upper plate (corresponding to the boundary conditions applied by the concrete retaining structures). Note however that during the test, the axial boundary conditions were not perfectly reproduced as an axial swell of 1.5 mm occurred, showing that the axial swelling pressure developed was higher than the adhesion stress of the glue. Despite this phenomenon, the main objective of this study, i.e. investigating the radial swelling, is thought to have been reasonably achieved.

The percentage of the radial void adopted in the present laboratory test is considerably larger than the one considered in situ (60% against 14% in the in-situ experiments performed by the French Institute for Radiation Protection and Nuclear Safety - IRSN). This on-purpose test was designed to study the radial swelling phenomenon more clearly.

The µCT technique is a non destructive technique that allows continuous monitoring of grey level (i.e. of density) gradient between the centre and the periphery of the sample during hydration. It avoided making several tests with different samples at different hydration times. It was observed that µCT was successfully used on the bentonite/sand mixture. With this technique, we can distinguish the different constituents of the sample as shown in Figure 3. This figure also shows a heterogeneous dispersion of these constituents in the sample that indicates the difficulty in preparing the bentonite/sand mixture due to the difference in grains in size and density. The same phenomenon was previously observed by Saba et al. (2013) who also observed a concentration of larger pores (resulting in a lower density) along the periphery of the cylindrical sample that they used. This can only be visually observed in Figure 3 because beam hardening artefact affected the grey level profile along the diameter (Figure 10).

The 3D image at initial state also showed the presence of a fracture along the diameter,

starting from the upper face of the sample. This fracture was mostly the result of pushing the upper plate to ensure good contact with the upper surface of the sample. Indeed, since the sample's upper and lower surfaces were not exactly horizontal with a non uniform thickness, the pushing of the upper the plate resulted in a non-uniform force leading to traction at the middle of sample that created the fracture. One also observed that this fracture disappeared after one day hydration, indicating the effect of soil swelling and confirming good self-sealing performances.

During the first 15 minutes of hydration, a rough and rapid swelling took place, affecting the bentonite grains located at sample periphery, as they were first in contact with water. This rough swelling and exfoliation of bentonite grains were previously investigated in Saba et al. (2012). Cracks parallel to the perimeter of the sample were observed in both studies as the result of differential swelling between the grains at the border and those closer to the centre. As water continued to infiltrate into the sample in the radial direction, swelling of the bentonite grains continued with a concentric pattern. Swelling progressively slowed down over time as it became conditioned by the already swelled parts that applied a certain resistance.

Density gradients could be observed during hydration thanks to the differential changes in grey level observed in Figure 10. The decrease in density was not homogeneous over the sample as it started at the sample periphery where the gel was produced. A density gradient developed between the loose gel at the border and the denser soil of the central part. Over time, this gradient became smoother for the same reason as explained previously: the swelling of the inner parts was conditioned by the resistance of the already swollen parts. The density of the gel produced by the inside hydrated bentonite grains was consequently higher. As swelling continued, the volume of the denser central part decreased to finally reached a value close to the final average value of 1.4 Mg/m^3 determined at the end on the saturated sample. From Figure 10, we can also notice the increase in volume that can be detected by the increase in length of the density profiles.

After filling the radial void, the gel started to be consolidated under the effect of swelling pressure developed by the inner bentonite grains. This consolidation was characterised by an increase of gel density over time observed in the density profiles. The grey level or density gradient decreased as the profiles became more flat and steady. Full homogenisation can be expected to be reached at long-term with a homogeneous final unit mass of 1.4 Mg/m^3.

As mentioned before, the initial radial void was about 60% of the total volume in the experiment carried-out in this work whereas the percentage of initial void in the in situ experiment is 14%. Basically, it is not the percentage of void that conditions the time required to fill the void, but the void dimensions. If we consider in situ conditions, the void dimensions are similar to those in the test conducted in the laboratory, but the seal dimensions are 10 times larger. As a result, it will take the same time for filling the void by gel, but a much longer time for full homogenisation. Moreover, the different void percentages did not affect the kinetics of swelling because the process involved occurred at the grain level, and the grain level was the same both in the laboratory and in situ.

5 Conclusion

The limited swelling and homogenisation of compacted MX-80 bentonite/sand mixture were investigated experimentally using µCT scans coupled to digital image analysis. A specific testing cell in PMMA was designed for this purpose. A 70/30 bentonite/sand mixture was prepared and uniaxially compacted to obtain a sample having a diameter of 50 mm and a height of 10 mm, corresponding to an initial dry density of 1.8 Mg/m^3. This sample was placed in the cell (80 mm diameter) and hydrated under the conditions of limited radial swelling and prevented axial swelling. The cell was scanned in µCT at different hydration times, enabling the analysis of the material at initial state, during swelling and homogenisation.

At the initial state, the 3D data showed that the constituents were heterogeneously organised in the sample. In addition, a fracture was observed along the diameter of the sample and in the upper 5-mm thickness of the sample. This fracture disappeared after 3 days of hydration, confirming the self-sealing capacity of the material. The qualitative monitoring of swelling over time revealed that swelling took place at the scale of bentonite grains. It started quickly at the beginning and became slower over time. The sand grains were found to be carried along by the swelling of bentonite grains. Some cracks parallel to the perimeter were produced during the first hours and they disappeared with time as hydration proceeded. Swelling continued with an increase in gel production and a decrease in the volume of the unsaturated central part. When the gel touched the cell, it consolidated due to the subsequent swelling pressure resulting by the confinement exerted by the cell. Visually, the material became more homogeneous with sand grains more homogeneously distributed in the bentonite gel matrix. This homogenisation was further studied by image analysis by plotting grey level profiles along the same diameter of the sample at different hydration times. A density gradient was

found between the dense centre and the loose border of sample. This density gradient became smoother over time as the density of the central part decreased and that of the border increased.

The considered radial void percentage considered here was much larger than in the in-situ case: 60% against 14%. However, as the void dimensions were similar, the time required for filling the void should be similar as in both cases swelling takes place at the level of bentonite grains. The time needed to reach homogenisation should be longer in the case of larger seal, and a higher final density can be expected in this case. More accurate µCT characterization based on careful preliminary calibration of grey levels carried out with samples at various known densities should be carried out next to refine the results presented here and provide values of densities from the grey level as done in Van Geet et al. (2005). Also, the density gradients in seals and their effects on their hydro-mechanical behaviour should be further investigated.

References

Barnichon, J.D., Dick. P., & Deleruyelle, F. 2010. A sealing performance in situ experiments project (SEALEX): main objectives and expected outcomes, Clays in natural & Engineered Barriers for Radioactive Waste Confinement, 4th international meeting, march 2010, Nantes, France 261-262

Barnichon, J. D., Dick P. & Bauer C. 2012. The SEALEX in situ experiments: performance test of repository seals. Harmonising Rock Engineering and the Environment – Qian & Zhou (eds) Taylor & Francis Group, London, ISBN 978-0-415-80444-8, pages 1391-1394.

Dueck, A., Goudarzi, R. and Börgesson, L. 2012. Buffer homogenisation, status report. SKB technical report TR-12-02.

Dvinskikh, S.V., Szutkowski, K. and Furó, I. 2009. MRI profiles over very wide concentration ranges: Application to swelling of a bentonite clay. Journal of Magnetic Resonance 198 (2009) 146–150.

Kawaragi C., Yoneda T., Sato T. and Kaneko K. 2009. Microstructure of saturated bentonites characterized by X-ray CT observations. Engineering Geology 106, 51–57

Ketcham R. A. and Carlson W. D. 2001. Acquisition, optimization and interpretation of X-ray computed tomographic imagery: applications to the geosciences. Computers & Geosciences Vol. 27, 381-400.

Komine H. and Ogata N. 1999. Experimental study on swelling characteristics of sand-bentonite mixture for nuclear waste disposal. Soils and Foundations 39 (2): 83-97.

Kozaki T., Suzuki S., Kozai N., Sato S. and Ohashi H. 2001. Observation of microstructures of compacted bentonite by microfocus X-ray computerized tomography (Micro-CT). Journal of Nuclear Science Technology 38 (8), pp. 697–699

Liu, L., Moreno, L. and Neretnieks, I. 2009. A Dynamic Force Balance Model for Colloidal Expansion and Its DLVO-Based Application. Langmuir 25, 679-687.

Moreno, L., Neretnieks, I. and Liu, L. 2010. Modelling of erosion of bentonite gel by gel/sol flow. SKB Technical report TR-10-64.

Neretnieks, I., Liu, L. and Moreno, L. 2009. Mechanisms and models for bentonite erosion. SKB technical report TR-09-35.

Pusch, R. 1979. Highly compacted sodium bentonite for isolating rock-deposited radioactive waste products. Nucl. Technol, United States. 45(2):153-157.

Pusch, R. 1980. Swelling pressure of highly compacted bentonite. SKB technical report TR-80-13.

Pusch, R. 1999. Clay colloid formation and release from MX-80 buffer. SKB technical report TR-99-31.

Jansson, M. 2009. Bentonite erosion, laboratory studies. SKB technical report TR-09-33.

Rasband W.S. (1997-2012). ImageJ, U. S. National Institutes of Health, Bethesda, Maryland, USA, http://imagej.nih.gov/ij/

Saba, S., Cui, Y.J., Tang, A.M. and Barnichon, J.D. 2012. Swelling of highly compacted bentonite/sand mixture used as sealing material in radioactive waste disposal concepts. In proceeding of E-UNSAT 2012, Naples.

Saba, S., Delage, P., Lenoir, N., Cui, Y.J., Tang, A.M. and Barnichon, J.D. 2013. Further insight into the microstructure of compacted bentonite/sand mixture. Submitted to Engineering Geology.

Tang, A.M., Cui, Y.J. and Le, T.T. 2008. A study on the thermal conductivity of compacted bentonites. Applied Clay Science; 41 (3-4):181-189.

Van Geet, M., Volckaert, G. and Roels, S. 2005. The use of microfocus X-ray computed tomography in characterising the hydration of a clay pellet/powder mixture. Applied Clay Science, 29 (2):73–87, 2005.

Wang, Q., Tang, A. M., Cui, Y.J., Delage, P., & Gatmiri, B. 2012. Experimental study on the swelling behaviour of bentonite/claystone mixture, Engineering Geology, Vol. 124, 59–66.

Yong, R.N., Boonsinsuk, P. and Wong, G. 1986. Formulation of backfill material for a nuclear fuel waste disposal vault. Canadian Geotechnical Journal, 23(2):216–228.

Chapter 3

Swelling pressure anisotropy investigation

INTRODUCTION

Once emplaced in the galleries, the compacted elements constituting the sealing plugs (disks, torus) will start being saturated by the water from the host-rock and swell. Once all voids are sealed, constant volume swelling will result in the development of swelling pressure radially in the direction of the host-rock and axially in the direction of the confinement elements. The study of the swelling pressure is important as it should be high enough to ensure a good sealing and at the same time it should not exceed the yield stress of the rock and of the confinement elements. This explains the numerous studies conducted on the swelling pressure of compacted bentonite-based materials. However, in most cases, a unique isotropic swelling pressure was considered. Some authors tried to measure the radial swelling pressure (Börgesson et al., 1996; Cho et al., 2000 and Lee et al., 2012) and a difference between the radial and axial swelling pressures was found.

In the first part of this chapter, an experimental study on the radial and axial swelling pressures was undertaken on samples compacted at different dry densities. Emphasis was put on the swelling pressure kinetics, the stabilisation value of swelling pressure and the anisotropy coefficient defined as the ratio of radial pressure to vertical swelling pressure. The results are presented hereafter in the original form of a paper submitted to “Soils and Foundations” journal.

In the second part of this chapter, microstructure observation of two samples by microfocus X-ray Computed Tomography (µCT) was presented: one in its as-compacted state and another after a swelling pressure test. The bentonite grains swelling and the pores clogging were examined. These observations helped in further analysing the results obtained in the first part of this chapter. The results are presented in a paper accepted in Journal of Rock mechanics and Geotechnical Engineering.

Anisotropic swelling of compacted bentonite/sand mixture

Simona SABA[1,2], Yu-Jun CUI[1], Anh Minh TANG[1], Thi Phuong Huyen TRAN[1], Jean-Dominique BARNICHON[2]

Abstract: In the conception of deep radioactive waste disposal, the use of sealing materials is needed to limit water transfer in the vicinity of waste canisters. Compacted disks of bentonite/sand mixture are often considered as possible sealing plugs for their low permeability, good radionuclide retention capacity and high swelling ability. In the design of such sealing plugs, the swelling pressure is an important parameter to be taken into account. Nowadays, a unique isotropic swelling pressure has been usually considered. However, this consideration can be far from the reality as the sealing plug can swell in both radial direction against the host rock and axial direction against the retaining concrete structures. Thus, the swelling involved is anisotropic by nature, depending on the microstructure of the sealing plugs. In the present work, this anisotropic swelling is experimentally investigated by performing infiltration tests under constant volume conditions in a cell with both axial and radial swelling pressure measurements. Results obtained confirm the anisotropy of swelling pressure. Furthermore, the initial anisotropic structure caused by the sample compaction disappears after hydration for a certain range of dry densities, beyond this range the anisotropy being well preserved. Different kinetics of swelling pressure is also observed at different dry densities and along different directions. An exponential relationship is identified between the final swelling pressure and the dry density.

Keywords: bentonite/sand mixture; infiltration test; dry density; swelling pressure; anisotropy; kinetics.

1 Introduction

Compacted bentonite/sand mixtures are often considered as possible sealing materials for geological radioactive waste disposal due to their low permeability, high radionuclides retention capacity and swelling ability (Pusch, 1979; Yong et al., 1986). A possible configuration is the use of sealing plugs made of pre-compacted bentonite/sand mixture. Upon water infiltration, these plugs absorb water and swell, filling all existing voids (technological voids, pores and fractures in the rock). Afterwards, swelling pressure will progressively develop in both radial and axial directions, on the host-rock and on the retaining concrete structures, respectively. In the design of such sealing plugs, the swelling pressure is an important parameter to be controlled. Indeed, it must be high enough to ensure a good sealing performance and at the same time it must be lower than both the in situ minor stress of the host rock and the retaining capacity of the concrete structures.

Up to now, for designing sealing plugs or engineered barriers and assessing their swelling behaviour, a unique swelling pressure, usually the axial one, is usually considered. The

[1] Ecole des Ponts ParisTech, Laboratoire Navier, Marne La Vallée, France
[2] Institut de Radioprotection et de Sûreté Nucléaire, Fontenay-aux-Roses, France

swelling pressure can be determined in the laboratory by different methods: constant volume, swell-load, zero swell and adjusted constant volume method (Tang et al., 2011b). It has been found that different methods give different values of swelling pressure. Number of studies on the swelling properties of compacted bentonite-based materials was reported (Pusch, 1982; Komine and Ogata 1994, 2003, 2004; Delage et al., 1998; Agus and Schanz, 2005; Komine et al., 2009; Wang et al., 2012). The effect of mineralogical composition was studied by Komine and Ogata (1994) and they found that the swelling potential is higher when the fraction of expansive minerals (montmorillonite) is larger. They also found that the swelling pressure increases exponentially with the increase of initial dry density and that the initial water content of the soil specimen has insignificant effect on the swelling pressure. The increase in salinity of the saturating water was found to reduce the swelling capacity, although this influence becomes less significant at higher densities (Karnland et al., 2005; Castellanos et al., 2008; Siddiqua et al., 2011).

As mentioned previously, in most cases the swelling pressure was measured in one direction (usually the axial one). Some authors also tried to measure the radial swelling pressure (Cho et al., 2000; Lee et al., 2012 and Börgesson et al.; 1996). Börgesson et al. (1996) carried out several tests such as swelling/compression tests in an oedometer with measurement of axial and radial swelling pressure, tri-axial tests and constant volume infiltration tests to measure the swelling pressure. They found that the values of radial pressure (oedometer), isotropic pressure (tri-axial) and axial swelling pressure (constant volume cell) measured agree well: the radial pressure from swelling compression tests is similar to the swelling pressure at constant volume. Nevertheless, experimental results show a difference of 2 MPa between the radial and the axial swelling pressure at a void ratio of 0.6. Cho et al. (2000) and Lee et al. (2012) measured the radial and axial swelling pressures in a constant volume cell using pressure sensors mounted in the two directions. They also found a difference between the two directions, the larger difference being at higher dry densities. This was explained by the effect of uni-axial compaction for the preparation of samples.

In the present work, the anisotropy of swelling pressure was evaluated in the laboratory on a bentonite/sand mixture compacted at various densities. A special constant volume cell was used with a total pressure sensor to measure the radial pressure and a force transducer to measure the axial force. The results obtained are analysed in terms of kinetics, stabilisation value and anisotropy coefficient.

2 Materials and methods

The material studied is a compacted mixture of Wyoming MX-80 bentonite (commercial name Gelclay WH2) and quartz sand (commercial name TH1000) with a proportion of sand of 30% (in mass). Note that the mixture was provided in boxes and the sand proportion of 30% is a global one. Further examination of the sand proportion (*S*) in the samples tested showed that the real proportion varies from 32 to 40% (see Table 2). The initial water content of the mixture is 10.2% corresponding to a suction of 73.3 MPa (measured using a chilled mirror dew point tensiometer). Note that this mixture is the same as that used in the in-situ SEALEX experiments carried out by IRSN (Institut de Radioprotection et de Sûreté Nucléaire, the French expert national organisation in nuclear safety) in the underground laboratory in Tournemire (Barnichon et al., 2012). The grain size distribution of the bentonite powder determined by dry sieving is presented in Figure 1 together with the grain size distribution of pure bentonite determined by the hydrometer method. The grain size distribution of the sand is also shown in Figure 1.

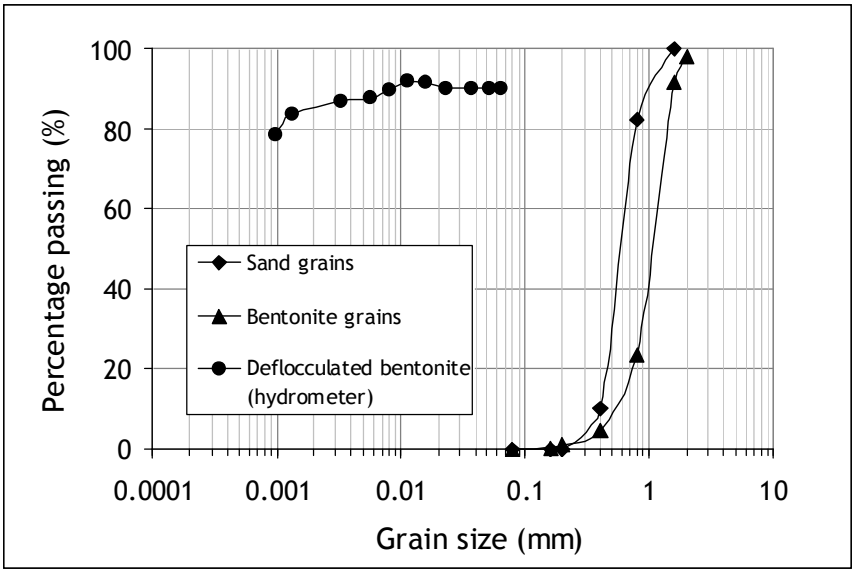


Figure 1. Size distribution curves of bentonite grains, sand grains and bentonite particles

The grain size distribution curves show well sorted materials having a mean grain diameter D_{50} of 1.2 mm and 0.6 mm for bentonite and sand, respectively. The unit mass of bentonite particles measured using a pycnometer is 2.77 Mg/m^3, in agreement with the corresponding literature data (Karnland et al., 2006; Madsen, 1998). The unit mass of sand is 2.65 Mg/m^3. The main clay mineral of the MX80 bentonite is montmorillonite (92%), other minerals being quartz, alumina, and hematite (Tang et al., 2008). The experimental setup is presented in Figure 2. The compacted sample is placed between two porous stones and filter papers. On

the top, a piston is fixed with a screw to prevent any axial displacement generated by soil swelling. During the test, the sample is saturated from the bottom with synthetic water having the same chemical composition as the ground water in the Bure underground research laboratory of ANDRA (see details in Table 1).

On the cell inner wall, a total pressure sensor is mounted to measure the radial swelling pressure. A force transducer is also used in order to measure the axial force generated by the soil swelling. All data are recorded by a data logger.

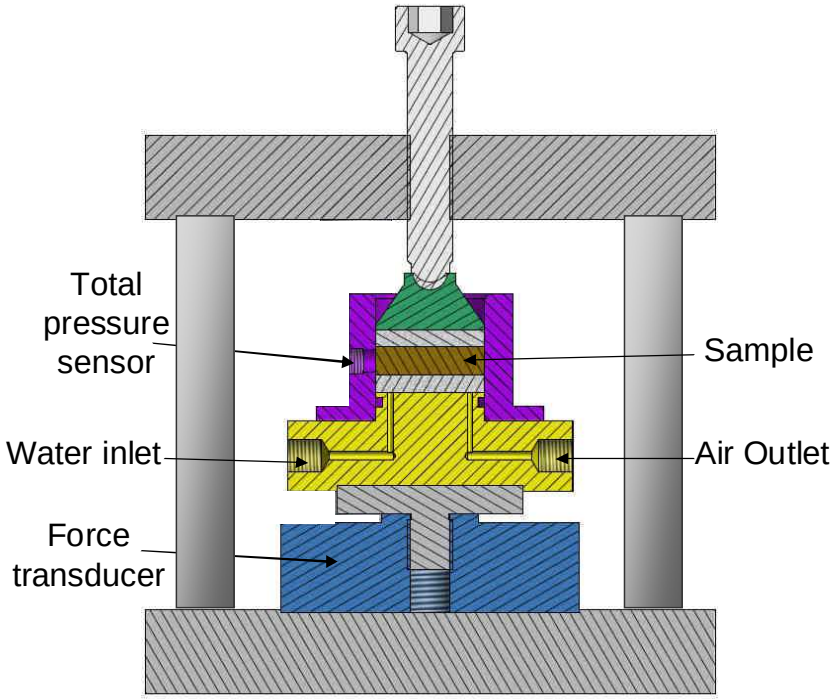


Figure 2. Layout of the cell for swelling pressure measurement

At the end of each test, the exact sand percentage in the samples (*S*) was determined as follows: samples were weighed after being oven dried and then, they were submerged in a large volume of water allowing the bentonite to be hydrated and swell until it became a suspension; then, all was washed on a 200 µm sieve to collect sand grains. The collected sand grains were then oven dried and weighed to determine the sand proportion in the mixture, defined as the mass of dry sand over the mass of the dry sample.

Table 1. Chemical composition of synthetic water (Wang et al., 2012)

Components	$NaHCO_3$	Na_2SO_4	NaCl	KCl	$CaCl_2.2H_2O$	$MgCl_2.6H_2O$	$SrCl_2.6H_2O$
Mass/Litter of solution (g)	0.28	2.216	0.615	0.075	1.082	1.356	0.053

A series of tests were carried out (see Table 2) using two cells on samples compacted either

inside (In-cell) or outside (Out-cell) the cell. Two tests were conducted by considering a 14% technological void corresponding to the volumetric one for the in situ SEALEX experiments (Barnichon et al., 2012). This void is the gap between the compacted disks and between the compacted plug and host rock, which is created during the construction. Other tests were carried out without technological void but at different dry densities ranging from 1.27 Mg/m^3 to 1.70 Mg/m^3. Different sand fractions (*S*) were also considered: from 32% to 40%. The dry density (ρ_d) was deduced from the measured global density and the initial water content (w = 10.2%). For each test with 14% technological void, two values of dry densities were indicated in Table 2; the first one refers to the initial one while the other is the final one after swelling and filling of the 14% technological void.

Table 2. Test program and results for all performed tests

ID	Preparation	Void	ρ_d (Mg/m^3)	S (%)	ρ_{db} (Mg/m^3)	P_h (MPa)	P_v (MPa)	C_a	S_r
CS01C1	Out-cell	-	1.65	35.00	1.37	1.43	1.72	0.83	-
CS03C1	Out-cell	-	1.65	38.13	1.35	1.52	1.64	0.93	-
CS05C1	Out-cell	-	1.67	35.80	1.39	1.33	1.52	0.88	-
CS06C1	Out-cell	-	1.68	39.60	1.36	1.26	1.61	0.78	-
CS07C1	Out-cell	-	1.67	38.60	1.36	1.32	1.73	0.76	1.07
CS09C1	In-cell	-	1.40	40.00	1.07	0.23	0.28	0.82	0.97
CS10C1	In-cell	-	1.43	34.16	1.16	0.42	0.43	0.98	0.94
CS12C1	Out-cell	-	1.55	38.96	1.22	0.66	0.68	0.97	1.03
CS13C1	Out-cell	-	1.60	38.17	1.28	0.87	0.86	1.01	1.09
CS14C1	In-cell	-	1.60	39.83	1.27	1.07	1.11	0.96	1.04
CS01C2	Out-cell	14%	1.95→1.66	35.56	1.38	1.10	1.30	0.85	-
CS02C2	Out-cell	14%	1.60→1.36	38.20	1.03	0.11	0.23	0.48	-
CS04C2	Out-cell	-	1.70	32.34	1.45	1.83	2.03	0.90	1.07
CS05C2	In-cell	-	1.60	37.25	1.29	0.97	1.00	0.97	1.08
CS07C2	In-cell	-	1.27	40.39	0.94	0.17	0.32	0.53	0.84

As the bentonite fraction is responsible for the swelling pressure development, in order to facilitate the analysis of test results, the bentonite dry density (ρ_{db}) was determined based on the dry density and the sand fraction while assuming that the mixture void ratio belongs to bentonite only (Dixon et al., 1985; Lee et al., 1999; Agus, 2005), as follows:

$$\rho_{db} = \frac{(B/100)\rho_m G_{ss}}{G_{ss}(1+w_m/100) - \rho_m(1-B/100)} \qquad (1)$$

where ρ_m (Mg/m^3) is the mixture density; B (%) is the bentonite content (in dry mass) in the mixture, and which is deduced from the sand fraction S (%); w_m is the water content of the mixture; G_{ss} is the specific gravity of sand (2.65).

For the samples used in different tests, the bentonite dry density (ρ_{db}) varied from 0.94 Mg/m^3 to 1.45 Mg/m^3.

Prior to swelling pressure measurement, the Out-cell samples were prepared at the desired dry density by static uni-axial compaction of the mixture powder in a cylindrical mould using a mechanical press at a loading rate of 0.1 mm/min. Samples were then removed from the mould and placed inside the test cell. This procedure was applied to obtain compacted soil specimens having a dry density higher than 1.5 Mg/m^3 (Out-cell, Table 2). For specimens of lower initial dry densities (i.e. lower than 1.5 Mg/m^3), this procedure was revealed to be not applicable due to the difficulties related to removing loose specimens from the mould. Thereby, for these specimens the soil was compacted directly inside the cell (In-cell, Table 2). The obtained sample was a disk having a diameter of 38 mm and a height of 10 mm at the target dry density. In the case of 14% radial technological void, the samples were compacted outside the cell (Out-cell) in a cylindrical mould having an internal diameter of 35 mm and then placed at the centre of the cell.

3 Experimental results

Figures 3 and 4 depict the swelling pressure evolution over time in the case of high and low bentonite dry densities, respectively. Figures 3a, 3c, 4a and 4c show the evolution of the vertical and horizontal swelling pressures (P_v and P_h) during the first 10 hours, while Figures 3b, 3d, 4b and 4d show the evolution for the whole test duration. Different kinetics of swelling pressure can be observed:

The swelling pressure starts with a fast increase, reaches a peak value, decreases a little, and then continues to increase slowly until stabilisation. This kinetics is identified for both radial and axial swelling pressure evolution for tests CS03C1, CS05C1, CS06C1, CS07C1 and CS04C2, which were performed on Out-cell samples having high bentonite dry densities (>1.3 Mg/m^3).

The swelling pressure starts with a fast increase, reaches a highly marked peak, decreases quickly and then slightly increases or stabilises at a value significantly lower that the peak value. This pattern of kinetics with more marked peaks is observed in tests CS12C1, CS13C1, CS14C1 and CS05C2 on In-cell and Out-cell samples having medium bentonite dry densities

(from 1.16 to 1.30 Mg/m^3). Some exceptions occur for the axial swelling pressure evolution in tests CS12C1 and CS13C1.

The swelling pressure increases, reaches a non-pronounced peak and then decreases and stabilises at a value lower than the peak value. This kinetics is identified for the tests CS09C1 and CS07C2 on In-cell samples having low bentonite dry densities (<1.10 Mg/m^3).

The swelling pressure increases and then stabilises without reaching a peak. This is observed for the vertical and horizontal swelling pressures in tests CS01C2 and CS02C2 where a 14% radial technological void is considered.

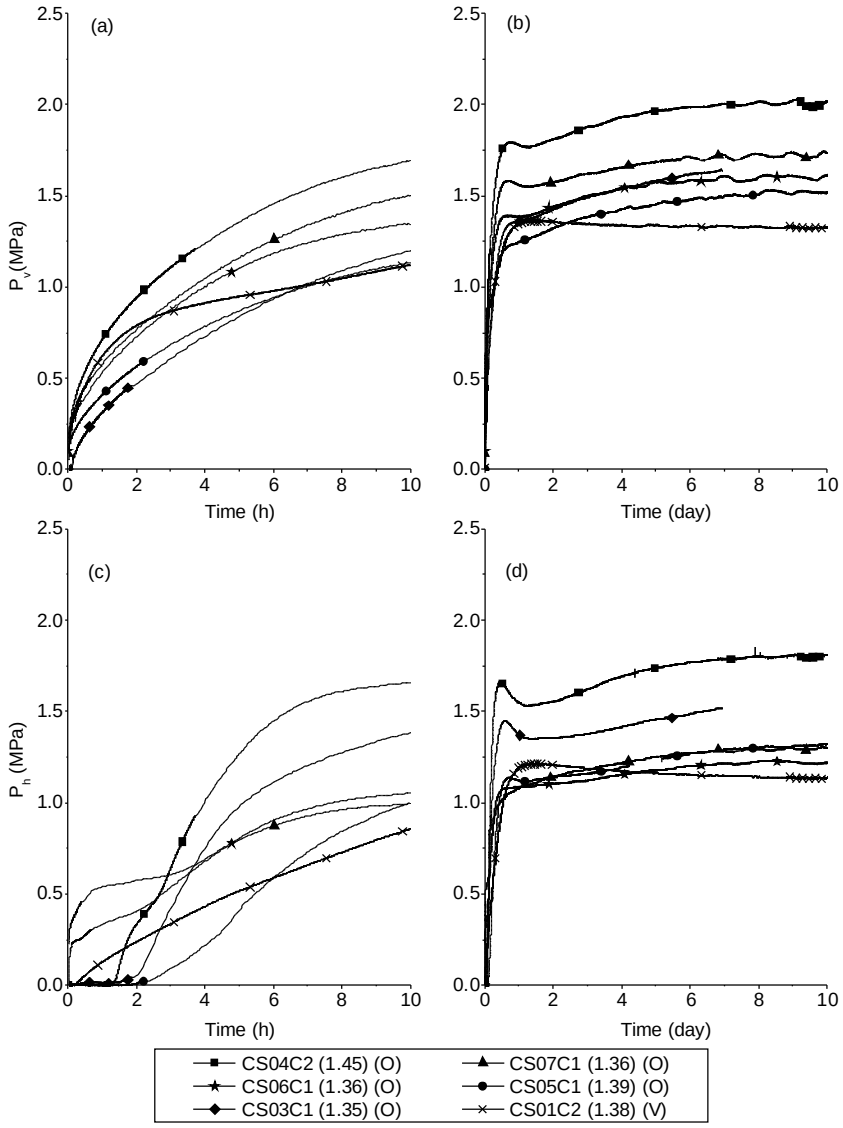


Figure 3. Kinetics of vertical and horizontal swelling pressure (a,c) at the fist 10 hours and (b,d) for the whole duration of test in the case of high bentonite dry densities; The letters O, I and V in the legend refer to the method of sample preparation: Out-cell, In-cell and with 14% Void, respectively.

On the whole, peaks are the most marked in the range of medium bentonite dry densities

(from 1.16 to 1.30 Mg/m^3). Outside this range, the peaks are less pronounced. The consideration of technological void is detriment to peak generation.

For the tests on Out-cell samples, all swelling pressures start from zero. On the contrary, in the case of In-cell samples, residual radial pressure is identified after compaction. The curves for radial swelling pressure in this case start thereby from a positive value. It can be however observed that this residual value does not affect the final value of swelling pressure because after the first increase and reaching the peak, the swelling pressure decreases and reaches an expected value close to the values from other tests on Out-cell samples.

Comparison between the evolutions of radial and axial swelling pressures shows that peaks are more marked for the horizontal pressures than for the vertical ones.

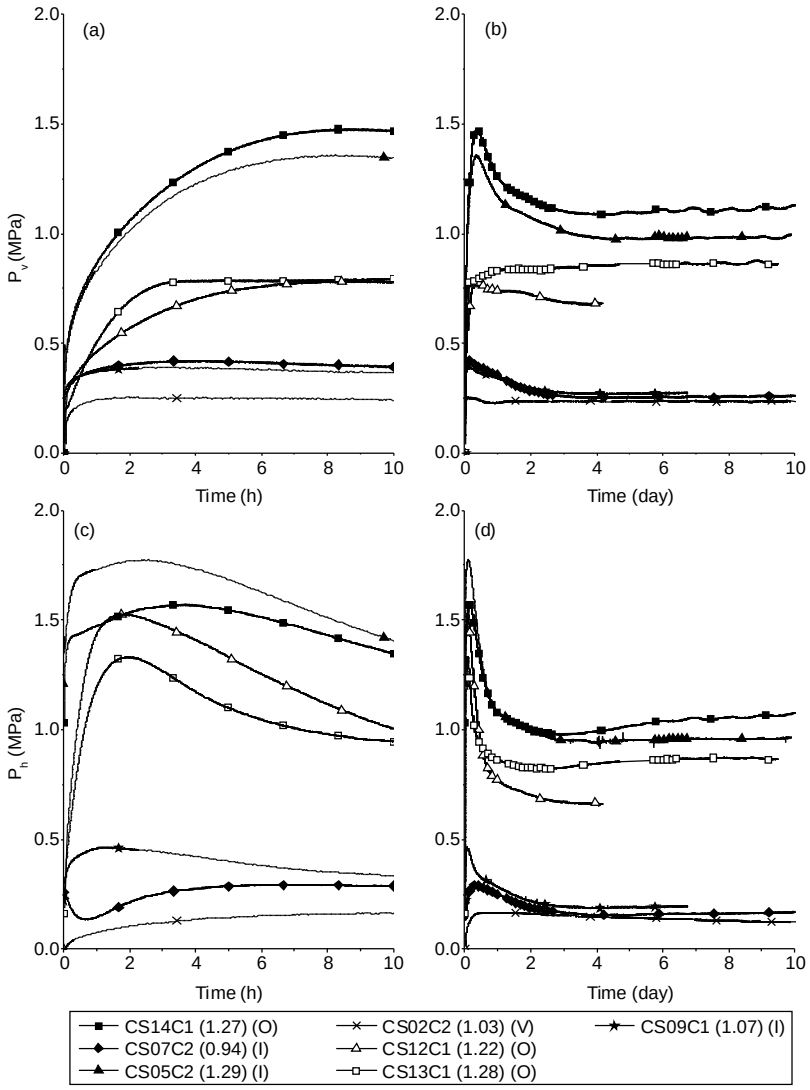


Figure 4. Kinetics of vertical and horizontal swelling pressure for low bentonite dry densities (a,c) at the fist 10 hours and (b,d) for the whole duration of test; The letters O, I and V in the legend refer to the method of sample preparation: Out-cell, In-cell and with 14% Void respectively.

The radial (horizontal) swelling pressure (P_h) and the axial (vertical) swelling pressure (P_v)

values presented in Table 2 are the stabilisation (final) values (see Figures 3 and 4). The variations of these values for different bentonite dry densities are presented in Figure 5. Note that stabilisation was considered as reached when the variation of swelling pressure was less than 0.05 MPa/day. An exponential increase of swelling pressure (vertical and horizontal) with increasing dry density of bentonite (ρ_{db}) is identified. This is in agreement with the results of Karnland et al. (2008) and Wang et al. (2012). The relationship (for both vertical and horizontal swelling pressures) follows the general expression established by Wang et al. (2012):

$$\sigma_s = \alpha \times \exp^{\beta \rho_{db}} \qquad (2)$$

where α and β are two constants mainly depending on the types of bentonite. Here, α = 0.0013 and β = 5.1053.

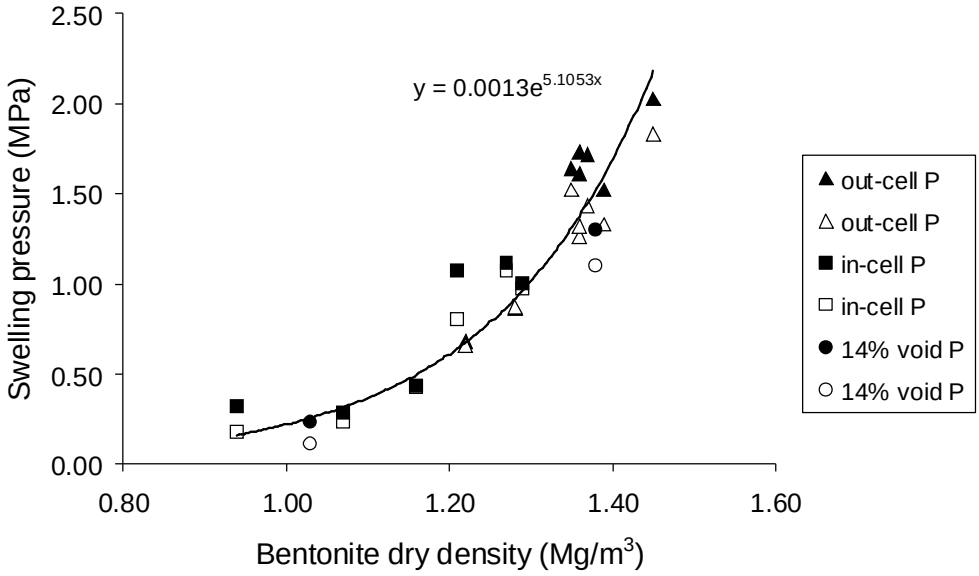


Figure 5. Variation of vertical and horizontal swelling pressures with bentonite dry density under different test conditions

The swelling pressure with 14% radial technological void follows the global trend of the results while considering the final dry density values. This confirms that the final dry density governs the swelling pressure.

From Figure 5 we can also observe that the final values of radial and axial swelling pressures are not the same, and the axial ones are mostly larger than the radial ones.

This can be explained by the effect of the uni-axial compaction which causes an anisotropic behaviour of the samples. In order to further analyse this anisotropic behaviour, an anisotropy coefficient (C_a) is defined as the ratio of P_h to P_v. This coefficient is presented versus the

bentonite dry density in Figure 6. It can be observed that, in the range of medium bentonite dry densities from 1.16 Mg/m^3 to 1.3 Mg/m^3, the soil swelling behaviour is mostly isotropic with values of C_a close to 1. At higher bentonite dry densities, the anisotropy coefficient becomes slightly smaller than 1, with values ranging from 0.76 to 0.90. When the bentonite dry density is lower than 1.1 Mg/m^3, the anisotropy becomes more significant with C_a ranging from 0.48 to 0.82. In addition, comparison between the results of In-cell and Out-cell samples shows that the sample preparation mode does not influence the anisotropy coefficient.

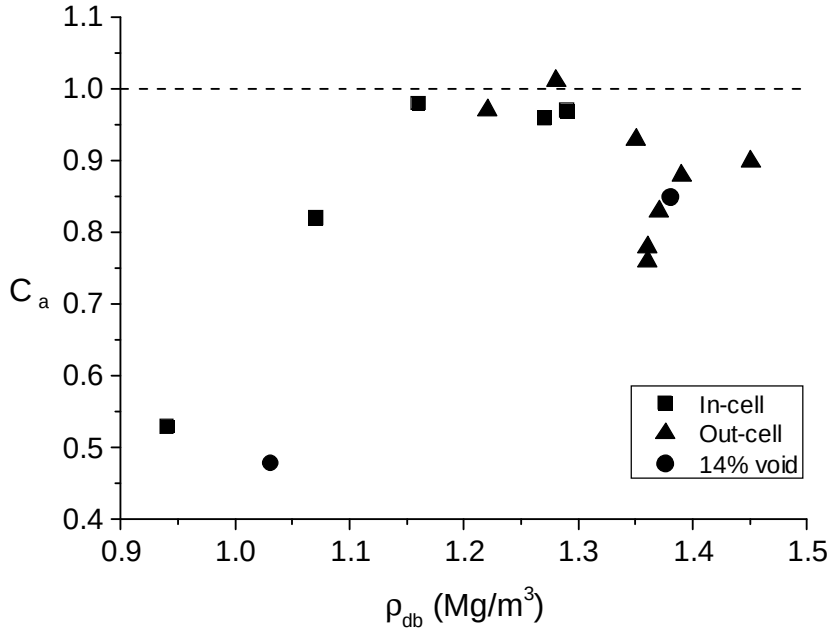


Figure 6. Anisotropy coefficient variation with bentonite dry density for different test conditions

4 Discussion

In order to better understand the results obtained, an investigation of the microstructure of the compacted mixture is needed because what happens at the microscopic scale is at the origin of the macroscopic behaviour. The microstructure of bentonite has been largely studied in the past (Pusch, 1982; Tessier, 1990; Mitchell, 1993) and it has been evidenced that at the microscopic scale, bentonite particles are formed by the superposition of platelets (or lamella). Particles have a plate shape (large surface compared to the thickness) that enables their superposition to form an anisotropic aggregate. The bentonite grains used in this study have a mean size of about 1.2 mm and are formed by crumbling the aggregates at given humidity. Comparable grain sizes were reported by Lloret and Villar (2007) for the Febex bentonite. The compacted samples include four pore populations: the interlayer pores (or intra-particle), the inter-particle pores (or intra-aggregate), the inter-aggregate pores (or intra-

grain) and the inter-grain pores (Kröhn, 2003; Lloret and Villar, 2007).

The evolution of swelling pressure over time evidenced different kinetics in different tests conducted. A first trend with a fast increase at the beginning followed by a decrease and a slow re-increase was identified in the tests on Out-cell samples with relatively high bentonite dry densities. This trend was observed also by Wang et al. (2012), Karnland et al. (2008) and Lee et al. (2012). The first increase in swelling pressure is related to the swelling of bentonite grains at microscopic scale. The peak occurrence followed by a decrease of swelling pressure corresponds to the reorganisation of the microstructure of the soil characterised by the collapse of macro-pores (inter-grain pores). Upon hydration, bentonite grains swell and split up, filling macro-pores. If the bentonite dry density is high enough, the grains can continue swelling after filling the macro-pores, resulting in a subsequent increase of swelling pressure. Basically, the larger the volume of macro-pores, the larger the pores collapse. Indeed, a more significant decrease of swelling pressure was observed at lower dry densities of bentonite, i.e. when more macro-pores can be expected. In addition, in the case of lower bentonite dry densities (though still in a medium range), a small increase of swelling pressure was noticed after the peak occurrence. On the contrary, for the tests at very low bentonite dry densities, the microstructure was so loose that only light peaks were identified followed by stabilisation. For the tests where 14% radial technological void was considered, no peaks were observed - the swelling pressure just increased quickly and then slowly before reaching stabilisation. Although the 14% technological void was only radial, this trend was observed for both radial and axial swelling pressures. The only difference is that the first increase was quicker in the axial direction because the void was annular. The absence of peak in both directions suggests that during radial swelling that allowed the 14% technological void to be filled progressively, there was not sudden collapse affecting the axial swelling pressure.

The difference in peaks magnitude between radial and axial swelling pressure suggests the presence of more macro-pores along the radial direction than along the axial one. This can be related to the sample preparation procedure, in particular the way the powder was poured into the mould and the friction against the mould during compaction.

When considering the stabilisation value of swelling pressure in the axial and radial directions and when plotting them versus bentonite dry density (Figure 5), it was observed that the axial and radial swelling pressures increased with increasing bentonite dry density, following an exponential function similar to that obtained by Karnland et al. (2008) and Wang et al. (2012). This confirms that the bentonite dry density is the key parameter in describing the soil

swelling behaviour.

In Figure 5 it was observed that the axial (P_v) and radial (P_h) swelling pressures are not identical, the axial one being larger than the radial one. This difference reveals an anisotropic behaviour of the compacted samples. This anisotropy is related to the microstructure of the sample as well as its evolution during hydration. Samples in this study were prepared by uni-axial compaction of the mixture powder which favours a more significant swelling reaction in the direction of the compaction force application (axial direction). Additionally, the bentonite grains used (see Figure 7a) mostly have an irregular shape with one dimension larger than the others. A zoom on a single grain is also presented in Figure 7 in two directions: the top view in Figure 7b shows a dimension of the grain that is at least 2.5 times larger than the thickness of the grain that can be seen in Figure 7c. This plate shape favours an anisotropic arrangement of the grains in the compacted sample, because when placing the powder of mixture in the cell the bentonite grains tend to find a stable position with larger face side in the vertical direction. The subsequent loading during compaction enhances this arrangement, thus the anisotropic behaviour. Upon hydration, the grains will swell and split up trying to fill the macro-pores. This process leads to a microstructure collapse, decreasing the initial anisotropy.

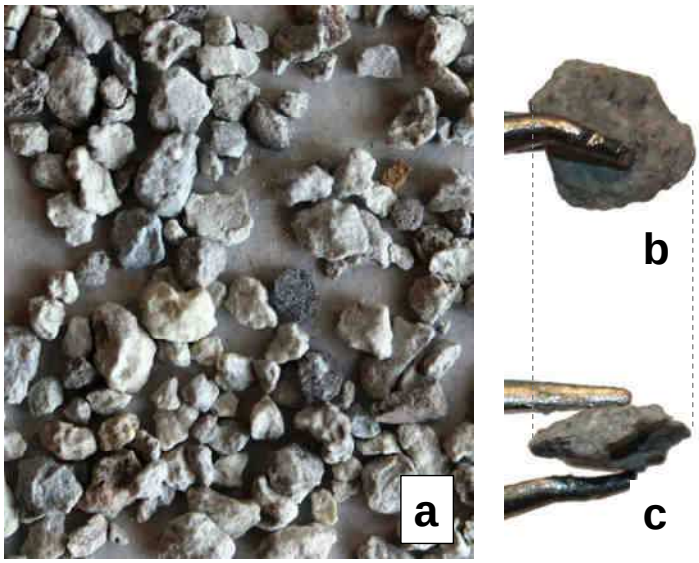


Figure 7. (a) A specimen of the bentonite powder grains used in this study. Zoom on a single bentonite grain rotated in two different directions: Top view (b) and side view (c).

The anisotropy coefficient C_a is defined as the ratio of radial (P_h) to axial (P_v) swelling pressure. The relationship between this coefficient and the bentonite dry density shows that in the range of medium bentonite dry densities, this coefficient is close to 1 indicating an isotropic behaviour. From Figures 3 and 4 it is noticed that the higher peaks of swelling pressure belong to the tests with medium bentonite dry densities. These marked peaks, as

noted previously, suggest a significant collapse of microstructure that favours the development of an isotropic microstructure. This explains the isotropic behaviour shown in Figure 6 for the samples at medium bentonite dry densities.

In the case of high bentonite dry densities, the curves shown in Figure 3 exhibit small peaks, suggesting a limited collapse of microstructure. Thus the microstructure remained anisotropic. This is explained by the fact that, at high bentonite dry densities, there was not enough space (macro-pores) allowing bentonite grains to swell. Thus, the microstructure collapse was limited. This leads to a high degree of anisotropy with C_a between 0.76 and 0.90.

In the case of very low bentonite dry densities (< 1.10 Mg/m^3), there was enough space for bentonite grains to swell but, at low density, the grains could not fill up all the voids and give rise to microstructure collapse. This is confirmed by the swelling curves in Figure 4 which show very limited peaks. The initial anisotropy is thus preserved with values of C_a ranging from 0.48 and 0.82.

The two tests with 14% technological void at different dry densities did not display any pronounced anisotropy response. Their results followed the global trend depending only on the bentonite dry density. This suggests that the technological void can be included in the soil macro-pores when analysing the soil swelling behaviour, as reported by Wang et al. (2013).

From a practical point of view, in the case of a sealing plug with compacted disks of bentonite/sand mixture, this is mainly the radial swelling pressure that should be considered to study the sealing performance. From the results obtained in this study, it is observed the radial swelling pressure is often lower than the axial one. This feature of anisotropy is important and should be accounted for in the design of sealing plugs.

5 Conclusion

The anisotropy of swelling pressure of compacted bentonite/sand mixture was investigated at the laboratory scale by performing different tests at different dry densities, including tests on samples with technological void. The results were analysed in terms of bentonite dry densities. Different trends of kinetics of swelling pressure evolution were identified for different bentonite dry densities and different directions. However, stabilisation was observed for all cases, indicating the full saturation of the samples. Some differences in kinetics at the beginning of tests were observed with different sample preparation techniques, though this did not affect the final stabilisation value. While presenting the final values versus the dry density of bentonite, an exponential relationship was found. However, a difference between the axial

and radial swelling pressures was noticed, suggesting an anisotropic swelling behaviour due to the uni-axial compaction mode and due to the anisotropic arrangement of the plate bentonite grains. Upon hydration, this anisotropy can decrease with the induced microstructure collapse. This was particularly observed for tests at medium bentonite dry densities from 1.15 Mg/m^3 to 1.30 Mg/m^3 with an anisotropy coefficient C_a close to 1 indicating an isotropic behaviour at stabilisation. This coefficient was found to decrease for higher bentonite dry densities, showing that the samples preserved their initial anisotropy after hydration because of the limited volume of macro-pores preventing the microstructure collapse. At lower bentonite dry densities, it was not possible for bentonite grains to fill the macro-pores - no microstructure collapse occurred. Therefore, anisotropy was also well preserved.

In practice, it is recommended to take into account not only the radial swelling pressure but also the anisotropic swelling behaviour while assessing the performance of sealing plugs.

References

Agus, S., Schanz, T. 2005. Swelling pressures and wetting-drying curves of a highly compacted bentonite-sand mixture. Unsaturated Soils: Experimental Studies, pages 241–256.

Barnichon, J.D., Dick, P. and Bauer C. 2012. The SEALEX in situ experiments: performance test of repository seals. Harmonising Rock Engineering and the Environment – Qian & Zhou (eds) Taylor & Francis Group, London. ISBN 978-0-415-80444-8, pages 1391-1394.

Börgesson, L., Karnland, O. and Johanneson, L.E. 1996. Modelling of the physical behaviour of clay barriers close to water saturation. Engineering Geology, 41 : 127-144.

Castellanos, E., Villar, M.V., Romero, E., Lloret, A. and Gens, A. 2008. Chemical impact on the hydro-mechanical behaviour of high-density febex bentonite. Physics and Chemistry of the Earth, Parts A/B/C, 33(Supplement 1):S516 – S526.

Cho, W. J., Lee, J. O. and Kang, C. H. 2000. Influence of temperature elevation on the sealing performance of a potential buffer material for a high-level radioactive waste repository, Ann. Nucl. Energy, 27, 1271–1284.

Dixon, D.A., Gray, M.N. and Graham, J. 1996. Swelling and hydraulic properties of bentonites from Japan, Canada and USA. In Proceedings of the second International Congress on Environmental Geotechnics, Osaka, Japan, pages 5–8.

Delage, P., Howat, M. D. and Cui, Y. J. 1998. The relationship between suction and swelling properties in a heavily compacted unsaturated clay. Engineering Geology 50**,** 31-48.

Imbert, C. and Villar, M.V. 2006. Hydro-mechanical response of a bentonite pellets-powder mixture upon infiltration. Applied Clay Science, 32(3-4):197–209.

Karnland, O., Muurinen, A. and Karlsson, F. 2005. Bentonite swelling pressure in NaCl solutions-Experimentally determined data and model calculations. Advances in

Understanding Engineering Clay Barriers. Page 241.

Karnland, O., Olsson, S. and Nilsson, U. 2006. Mineralogy and sealing properties of various bentonites and smectite-rich clay material. SKB.

Karnland, O., Nilsson, U., Weber, H. and Wersin, P. 2008. Sealing ability of Wyoming bentonite pellets foreseen as buffer material - Laboratory results. Physics and Chemistry of the Earth (33) S472-S475.

Komine, H. and Ogata, N. 1994. Experimental study on swelling characteristics of compacted bentonite. Canadian geotechnical journal, 31(4):478–490.

Komine, H. and Ogata, N. 2003. New equations for swelling characteristics of bentonite-based buffer materials. Canadian Geotechnical Journal. 40(2):460–475.

Komine, H. and Ogata, N. 2004. Predicting swelling characteristics of bentonites. Journal of Geotechnical and Geoenvironmental engineering, 130:818.

Komine, H., Yasuhara, K. and Murakami, S. 2009. Swelling characteristics of bentonites in artificial seawater. Canadian Geotechnical Journal. 46(2):177-189.

Kröhn, K.P. 2003. New conceptual models for the resaturation of bentonite. Applied clay science, 23(1-4):25–33.

Lee, J.O., Lim, J.G., Kang, I.M. and Kwon, S. 2012. Swelling pressures of compacted Ca-bentonite. Engineering Geology. doi: 10.1016/j.enggeo.2012.01.005

Lloret, A. and Villar, M.V. 2007. Advances on the knowledge of the thermo-hydro-mechanical behaviour of heavily compacted "FEBEX" bentonite. Physics and Chemistry of the Earth 32 701-715.

Madsen, FT. 1998. Clay mineralogical investigations related to nuclear waste disposal. Clay Minerals. 33(1):109–129.

Mitchell, JK. 1993. Fundamentals of soil behaviour. John Wiley and sons, inc., New York.

Pusch, R. 1979. Highly compacted sodium bentonite for isolating rock-deposited radioactive waste products. Nucl. Technol. United States. 45(2):153-157.

Pusch, R., 1982. Mineral-water interactions and their influence on the physical behavior of highly compacted Na bentonite. Canadian Geotechnical Journal, 19(3):381–387.

Siddiqua, S., Blatz, J. and Siemens, G. 2011. Evaluation of the impact of pore fluid chemistry on the hydromechanical behaviour of clay-based sealing materials. Canadian Geotechnical Journal, NRC Research Press, 48, 199-213.

Tang, A.M., Cui, Y.J. and Le, T.T. 2008. A study on the thermal conductivity of compacted bentonites. Applied Clay Science; 41:181-189.

Tang, C.S., Tang, A.M., Cui, Y.J., Delage, P., Schroeder, C. and De Laure, E. 2011. Investigating the Swelling Pressure of Compacted Crushed-Callovo-Oxfordian Argillite. Physics and Chemistry of the Earth 36 (17-18), 1857–1866.

Tessier, D. 1990. Organisation des matériaux argileux en relation avec leur comportement hydrique. Decarreau (Éd.): Matériaux argileux: structure, propriétés et applications.

Villar, M.V. 2002. Thermo-hydro-mechanical characterisation of a bentonite from Cabo de Gata. A study applied to the use of bentonite as sealing material in high level radioactive waste repositories. Publicación Técnica ENRESA 01/2002, Madrid, 258 pp.

Wang, Q., Tang, A.M., Cui, Y.J., Delage, P. and Gatmiri, B. 2012. Experimental study on the

swelling behaviour of bentonite/claystone mixture. Engineering Geology 124 : 59-66, doi : 10.1016/j.engeo.2011.10.003.

Wang, Q., Tang, A.M., Cui, Y.J., Barnichon, J.D. Delage, P., Ye, W.M. 2013. Voids effects on the hydro-mechanical behaviour of compacted bentonite-sand mixture. Soils and Foundations. Volume 53, Issue 2, Pages 232–245.

Yong. R.N., Boonsinsuk, P. and Wong, G. 1986. Formulation of backfill material for a nuclear fuel waste disposal vault. Canadian Geotechnical Journal, 23(2):216–228.

Microstructure and anisotropic swelling behaviour of compacted bentonite/sand mixture

Simona Saba[1,2], Jean-Dominique Barnichon[2], Yu-Jun Cui[1], Anh Minh Tang[1] and Pierre Delage[1]

Abstract: Pre-compacted elements (disks, torus) of bentonite/sand mixture are candidate materials for sealing plugs of radioactive waste disposals. Choice of this material is especially based on its swelling capacity allowing all gaps in the system to be sealed, and on its low permeability. When emplaced in the gallery, these elements will start to take water from the host rock and swell. Thereby, a swelling pressure will develop in the radial direction against the host rock and in the axial direction against the support structure. In this work, the swelling pressure of a small scale compacted disk of bentonite and sand was experimentally studied in both radial and axial directions. Different swelling kinetics were identified for different dry densities and along different directions. As a rule, the swelling pressure starts increasing quickly, reaches a peak value, decreases a little and finally stabilises. For some dry densities, higher peaks were observed in the radial direction than in the axial direction. The presence of peaks is related to the microstructure change and to the collapse of macro-pores. In parallel to the mechanical tests, microstructure investigation at the sample scale was conducted using microfocus X-ray computed tomography (µCT). Image observation showed a denser structure in the centre and a looser one in the border, which was also confirmed by image analysis. This structure heterogeneity in the radial direction and the occurrence of macro-pores close to the radial boundary of the sample can explain the large peaks observed in the radial swelling pressure evolution. Another interesting result is the higher anisotropy found at lower bentonite dry densities which was also analyzed by means of µCT observation of a sample at low bentonite dry density after the end of test. It was found that the macro-pores, especially that between sand grains, were not filled by swelled bentonite, which preserved the anisotropic microstructure caused by uni-axial compaction due to the absence of microstructure collapse.

Key words: Bentonite/sand mixture, nuclear waste disposal, anisotropy, swelling pressure, microstructure, microfocus X-ray computed tomography.

1 Introduction

In the concept of deep radioactive waste disposals in clayey host-rocks, sealing materials are used to limit water fluxes around the excavated galleries in the post-closure phase. Compacted bentonite/sand mixtures are often considered as possible sealing materials due to their low permeability, good radionuclides retention capacity and swelling ability (Pusch 1979; Yong et al. 1986). A possible configuration used in sealing plugs consists in a series of pre-compacted bentonite/sand disks inserted between two concrete confining components. Once the disposal galleries closed, plugs will be progressively infiltrated by the host rock pore water. They will swell and seal the so-called technological voids of the system (Wang et al. 2013), i.e. the voids remaining between blocks and at the interfaces with the rock after placement.

[1] Ecole des Ponts ParisTech, Laboratoire Navier, Marne La Vallée, France
[2] Institut de Radioprotection et de Sûreté Nucléaire (IRSN), Fontenay-aux-Roses, France

Afterwards, swelling pressure will progressively develop both radially along the host-rock and axially along the adjacent bentonite/sand disks and then on the mechanical confining components. In the design of sealing plugs, the swelling pressure is a key parameter to be controlled. Indeed, it must be high enough to ensure good sealing performance and at the same time it must be lower than the in situ minor stress in the host rock and the yield stress supported by the confinement elements.

Generally, a unique swelling pressure considered as isotropic is considered in the design of sealing plugs and/or engineered barriers and in the assessment of their swelling behaviour. Accordingly, laboratory measurements are concentrated on only one swelling pressure, usually the axial one. Number of studies on the swelling properties of compacted bentonite-based materials was reported (Pusch 1982; Komine and Ogata 1994, 2003, 2004; Delage et al. 1998; Agus and Schanz 2005; Komine et al. 2009; Wang et al. 2012). The swelling pressure can be determined in the laboratory by different methods: constant volume, swell-load, zero swell and adjusted constant volume method (Tang et al. 2011b). As mentioned above, the swelling pressure was measured in most cases in the axial direction. Some authors also tried to measure the radial swelling pressure, e.g. Börgesson et al. (1996), Cho et al. (2000) and Lee et al. (2012). Lee et al. (2012) measured both the radial and axial swelling pressures in a constant volume cell with pressure sensors mounted in the two directions. They found a difference between the radial and axial swelling pressures, the larger difference being observed at higher dry densities. This was explained by the anisotropic microstructure of compacted bentonite.

In order to better understand the macroscopic response of the compacted bentonite/sand mixture, especially in terms of swelling pressure, an investigation of the microstructure is needed. Various observations of the microstructure of compacted bentonites and sand bentonite mixture have been carried out by using mercury intrusion porosimetry -MIP - and scanning electron microscopy - SEM (Cui et al. 2002; Montes-H 2002; Lloret et al. 2003; Delage et al. 2006; Villar and Lloret 2001). These techniques require a cautious preliminary dehydration of the samples, most often by freeze-drying. They provide local observations on a small part of millimetric samples. For a larger scale, microfocus X-ray computed tomography (µCT) is needed. This technique allows a high-resolution non-destructive 3D observation without any sample pre-treatment. Moreover, further 3D information on the whole sample (including grain size distribution as well as pores distribution and inter-connectivity) can be obtained. µCT has been previously applied to monitor hydro-chemo-mechanical processes

(Comina et al. 2008), to detect dessication cracks (Gerbrenegus et al. 2006; Mukunoki et al. 2006) and to investigate the microstructure of compacted bentonite-based materials (Kozaki et al. 2001, Van Geet et al. 2005 and Kawaragi et al. 2009).

In this study, the swelling pressure of a small scale compacted disk of bentonite and sand was studied in both radial and axial directions. Different swelling kinetics were identified for different dry densities and along different directions. In parallel to the mechanical tests, microstructure investigation at the sample scale was conducted by using microfocus X-ray computed tomography (µCT).

2 Material and methods

2.1 Material

The material studied is a compacted mixture of Wyoming MX-80 bentonite (commercial name Gelclay WH2) and quartz sand (commercial name TH1000) with a proportion (in weight) of sand of 30%. The mixture was provided in boxes. Actually, examination of the sand proportion (*S*) in the samples tested showed that the real proportion varies from 32 to 40% (See Table 2). The initial water content (w_m) of the mixture was 10.2% corresponding to a suction of 73.3 MPa (measured using a chilled mirror dew point tensiometer). Note that this mixture is the same as that used in the in-situ experiments (SEALEX) carried out in the Tournemire underground laboratory (Barnichon et al., 2012) by IRSN (Institut de Radioprotection et de Sûreté Nucléaire, the French expert national organisation in nuclear safety).

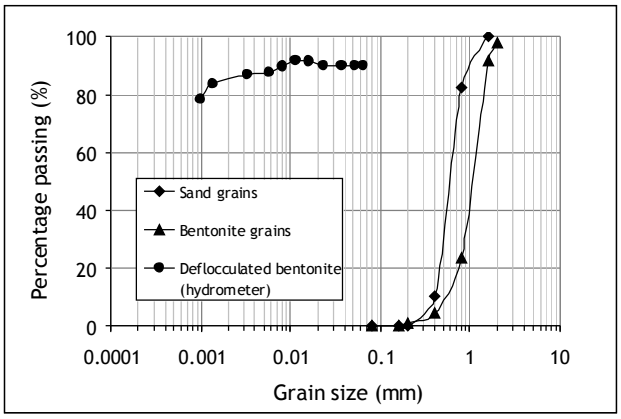


Figure 1. Grain size distribution curves of bentonite, sand and deflocculated bentonite.

The grain size distribution of the bentonite powder obtained by dry sieving is presented in Fig. 1 together with that of pure bentonite obtained using the conventional hydrometer method. The grain size distribution of the sand is also shown in Fig. 1. The curves show that

materials are well sorted with a mean grain diameter D_{50} of 1.2 mm and 0.6 mm for bentonite and sand, respectively. The unit mass of bentonite particles was measured and found equal to 2.77 Mg/m^3, in agreement with literature data (Karnland et al., 2006; Madsen, 1998). The unit mass of sand is 2.65 Mg/m^3. The main clay mineral of the MX80 bentonite is montmorillonite (92%), other minerals being quartz, alumina, and hematite (Tang et al. 2008).

2.2 Anisotropic swelling pressure experimental setup

The experimental setup is presented in Figure 2. The compacted sample is placed between two porous stones and filter papers. On top, a piston is fixed with a screw to prevent any axial displacement upon swelling. During the test, the sample is saturated from the bottom with synthetic water having the same chemical composition as the pore water from the Bure underground research laboratory (Andra, see details in Table 1). A total pressure sensor is mounted on the cell inner wall to measure the radial swelling pressure. A force transducer is mounted axially in order to measure the axial force generated by the soil swelling. All data are recorded by a data logger.

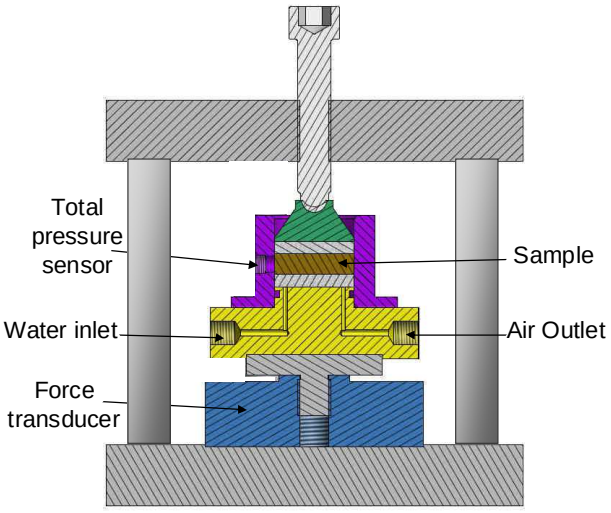


Figure 2. Layout of the constant volume cell for the swelling pressure tests.

Table 1 Composition of the synthetic water (Wang et al. 2012)

Components	$NaHCO_3$	Na_2SO_4	NaCl	KCl	$CaCl_2.2H_2O$	$MgCl_2.6H_2O$	$SrCl_2.6H_2O$
Mass/L (g)	0.28	2.22	0.62	0.08	1.08	1.36	0.05

A series of tests has been performed using two cells, with samples being compacted either inside (In-cell) or outside (Out-cell) the cell. Tests with different dry densities (ρ_d) ranging from 1.27 Mg/m^3 to 1.70 Mg/m^3 were carried out. Different sand fractions *(S)* were also

considered: from 32% to 40%. The dry density (ρ_d) was deduced from the measured global density and the initial water content (w = 10.2%). Two tests were conducted by considering a 14% technological void referring to the macro void volume existing in the in situ SEALEX experiments (Barnichon et al., 2012). Two values of dry densities were considered for each test with 14% technological void; the first one refers to the initial value while the other is the final value after swelling and the filling of the 14% technological void.

Table 2 Test program and results for all performed tests. (O), (I) and (V) refer to Out-cell, In-cell and with 14% void as sample preparation methods, respectively.

ID	ρ_d (Mg/m^3)	S (%)	ρ_{db} (Mg/m^3)	P_h (MPa)	P_v (MPa)	C_a
CS01C1(O)	1.65	35.00	1.37	1.43	1.72	0.83
CS03C1(O)	1.65	38.13	1.35	1.52	1.64	0.93
CS05C1(O)	1.67	35.80	1.39	1.33	1.52	0.88
CS06C1(O)	1.68	39.60	1.36	1.26	1.61	0.78
CS07C1(O)	1.67	38.60	1.36	1.32	1.73	0.76
CS09C1(I)	1.40	40.00	1.07	0.23	0.28	0.82
CS10C1(I)	1.43	34.16	1.16	0.42	0.43	0.98
CS12C1(O)	1.55	38.96	1.22	0.66	0.68	0.97
CS13C1(O)	1.60	38.17	1.28	0.87	0.86	1.01
CS14C1(I)	1.60	39.83	1.27	1.07	1.11	0.96
CS01C2(V)	1.95→1.66	35.56	1.38	1.10	1.30	0.85
CS02C2(V)	1.60→1.36	38.20	1.03	0.11	0.23	0.48
CS04C2(O)	1.70	32.34	1.45	1.83	2.03	0.90
CS05C2(I)	1.60	37.25	1.29	0.97	1.00	0.97
CS07C2(I)	1.27	40.39	0.94	0.17	0.32	0.53

As the bentonite fraction is responsible for the swelling pressure development, the bentonite dry density (ρ_{db}) was determined based on the dry density and on the sand fraction while assuming that the mixture void ratio belongs to bentonite only (Dixon et al. 1985; Lee et al. 1999; Agus 2005), as follows:

$$\rho_{db} = \frac{(B/100)\rho_m G_{ss}}{G_{ss}(1+w_m/100) - \rho_m(1-B/100)} \qquad (1)$$

where ρ_m (Mg/m^3) is the mixture density; B (%) is the bentonite content (in dry mass) in the mixture and is deduced from the sand proportion S (%); w_m is the water content of the mixture; G_{ss} is the specific gravity of sand (2.65).

For the samples used in different tests, the bentonite dry density (ρ_{db}) varied from 0.94 Mg/m^3 to 1.45 Mg/m^3.

Prior to swelling pressure measurement, the Out-cell samples were prepared at the desired dry density by static uniaxial compaction of the mixture powder in a cylindrical mould using a mechanical press, at a loading rate of 0.1 mm/min. Samples were then removed from the

mould and placed inside the test cell. This procedure was applied to obtain compacted soil specimens having a dry density higher than 1.5 Mg/m^3 (Out-cell, Table 2). For specimens with lower initial dry densities (i.e. lower than 1.5 Mg/m^3), this procedure was not applicable due to the difficulties related to removing loose specimens from the mould. For these specimens, the soil was then compacted directly inside the cell. The obtained sample was a disk having a diameter of 38 mm and a height of 10 mm at the target dry density. In the case of 14% radial technological void, the samples were prepared by compaction in a cylindrical mould having an internal diameter of 35 mm and then placed at the centre of the cell.

2.3 µCT and image analysis

Microfocus X-ray computed tomography (µCT) was used to examine in three dimensions the internal microstructure of the compacted bentonite/sand mixtures. µCT is a non-destructive observation technique that has proven to be useful in the investigation of various geological porous media including compacted bentonite (Kozaki et al. 2001), bentonite pellet/powder mixture (Van Geet et al. 2005) and compacted bentonite/quartz mixture (Kawaragi et al. 2009). It consists firstly in recording a set of two-dimensional X-ray radiographs of an object at several angles (typically at 180° or 360°) and secondly in reconstructing the 3D slices from the radiographs using a mathematical algorithm. The final 3D image of the internal structure is obtained by stacking the slices. The final measurement is the attenuation coefficient to X-rays which depends on the mass density and the atomic number of the object (Ketcham and Carlson 2001; Van Geet et al. 2005).

The scans presented here were carried out with the µCT of the Navier laboratory (Ecole des Ponts ParisTech), an "Ultratom" device specifically designed and manufactured by RXsolutions (France). Images were reconstructed using the software Xact-reconstruction developed by RXsolutions. The final 3D image is a 16 bit type with a size of 1840×1840×386 voxels. The image analysis and treatment was then carried out using ImageJ, a public domain Java image processing program (Rasband 1997-2012). Note that the image was first converted to 8 bits for size reasons.

Two scanned samples are shown in this paper. The first one is at the initial state, compacted like an Out-cell sample with a diameter of 50 mm and a height of 10 mm and with a sand content of 35%. Its dry density is 1.8 Mg/m^3 (bentonite dry density ρ_{db} of 1.54 Mg/m^3). The second one was scanned after four months of hydration in constant volume cell. It has a 38 mm diameter, 10 mm height, 30% sand fraction and a bentonite dry density (ρ_{db}) of 0.97 Mg/m^3.

3 Results and discussions

3.1 Comparison of swelling pressure kinetics (axial vs. radial)

Fig. 3 (a) and (b) depicts the evolution with respect to time of axial and radial swelling pressures for samples at different bentonite dry densities. The swelling pressure changes start with a quick increase followed by a peak value, a decrease and finally a slight increase or stabilisation.

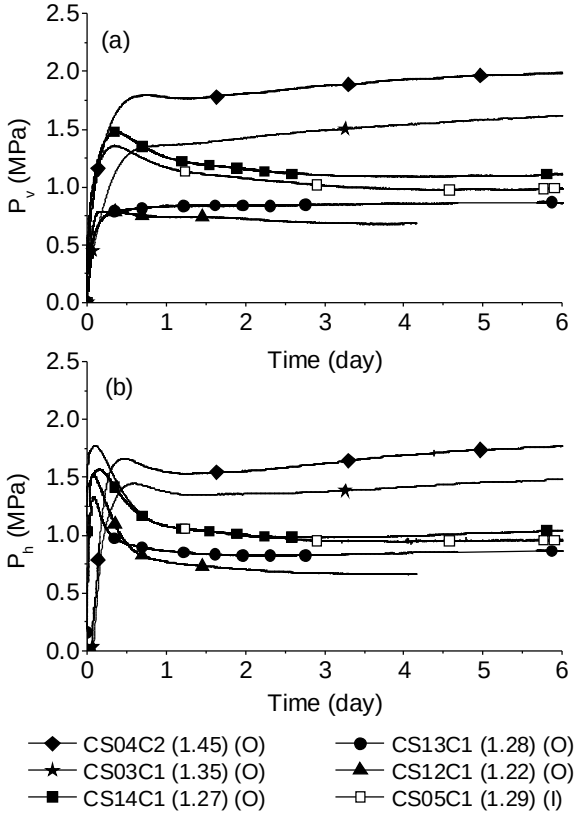


Figure 3. Kinetics of the axial (a) and radial (b) swelling pressure for different bentonite dry densities; The letters O and I in the legend refer to the method of sample preparation: Out-cell and In-cell, respectively.

For the tests on Out-cell samples, all swelling pressures start from zero. On the contrary, a residual radial stress is identified in the case of In-cell samples after compaction.

Therefore, the curve for radial swelling pressure starts from a positive value in the case of In-cell samples. It can however be observed from the curves that this residual value did not affect the final value of the swelling pressure. As after the first increase and reaching the peak, the swelling pressure decreases and reaches an expected value close to the other values obtained from other tests on Out-cell samples. Further examination of the peaks for radial and axial swelling pressures shows that the radial pressures exhibit more marked peaks than the axial pressures. The presence of peaks is related to microstructure changes and to the collapse that contributes to the filling of macro-pores. Here, macro-pores refer to the largest population of

pores found between bentonite grains and that can be seen in Fig. 4 and Fig. 5.

The bentonite grains have a mean size of 1.2 mm and are formed by the aggregation of bentonite aggregates. Comparable grain sizes were reported by Lloret and Villar (2007) in the Febex bentonite. The first increase in swelling pressure at the beginning is related to the swelling of bentonite grains at macroscopic scale. With time, grains will merge into aggregates with particles that fill up macro-pores and cause a decrease of the swelling pressure, corresponding to the microstructure collapse.

The difference in peaks magnitude between radial and axial swelling pressure suggests the presence of more macro-pores along the radial direction than along the axial one. A further look into the microstructure of the compacted mixture was then performed to clarify this point. µCT was used to examine the 3D microstructure of a compacted bentonite/sand sample having a bentonite dry density of 1.54 Mg/m^3 and a water content of 10.2%. Fig. 4 shows the radial cross-section at a position of 4 mm from the top of sample. The µCT technique is able to distinguish the various components according to their density and atomic composition (the grey level range goes from white representing high attenuating material to black representing void).

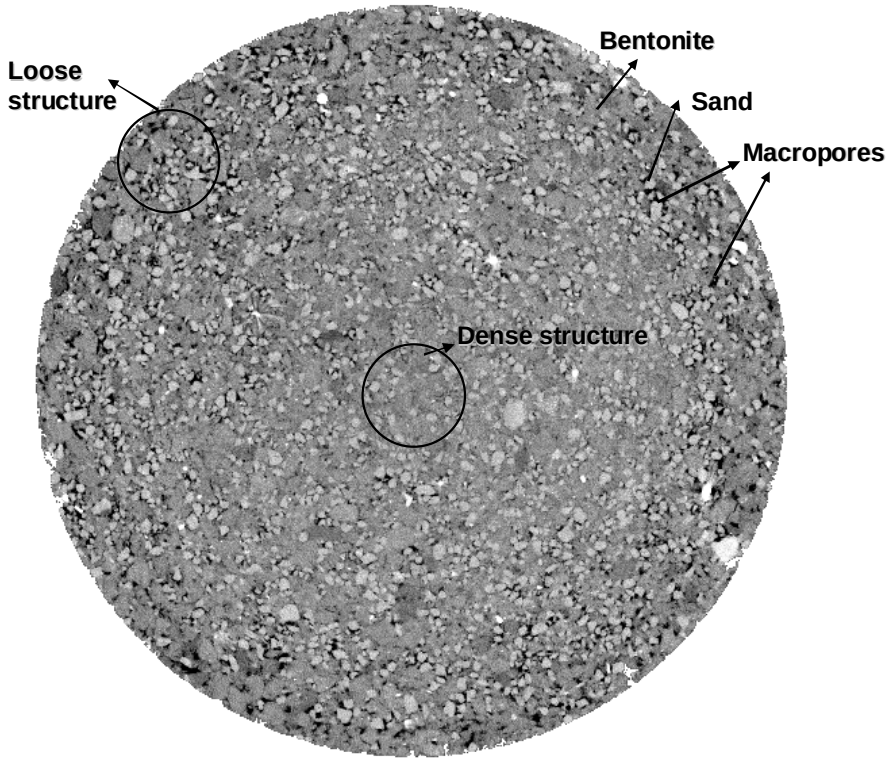


Figure 4. A typical radial µCT cross-section of the compacted bentonite/sand mixture sample.

A clear distinction can be made between the clearer sand grains and the slightly darker

bentonite powder grains, even though their respective densities are not very different (2.4 – 2.5 Mg/m^3 for the bentonite powder and 2.65 Mg/m^3 for the sand). One can also observe in Fig. 4 that the sample density is not strictly homogeneous, with more voids at the perimeter and a higher density with fewer voids in the centre. This could be due to the sample preparation procedure, in particular the way the powder was poured into the mould and also to the friction against the mould during compaction. Observation along the perimeter shows that the bentonite powder grains remain clearly apparent around the sample and that they are apparently more frequent than at the centre. At the centre, powder grains appear to be more compacted one against another, resulting in a denser microstructure.

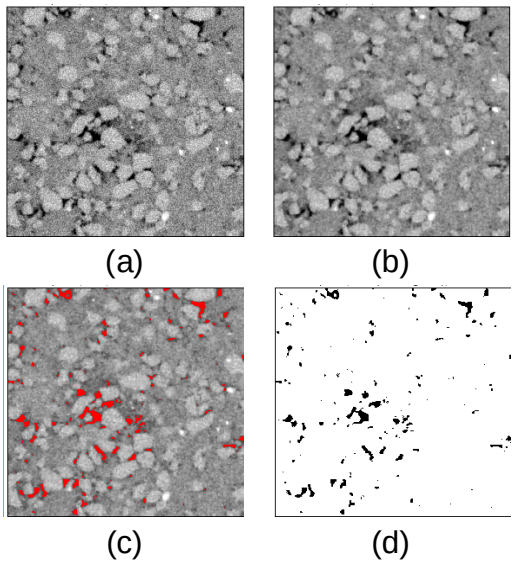


Figure 5. Images at different stages before segmentation: a) non-treated, b) after applying 3D median filter, c) during threshold and d) final segmented image.

Further investigation of the microstructure was carried out using the "ImageJ" image analysis software. The first step consisted in reducing the noise in the image by applying a 3D median filter with a 1 pixel radius. Then, a segmentation of the image was performed in order to isolate pores from the other phases. The grey threshold value used to segment the image was found after analysing the histogram and using the "mixture modelling" function that gave the value of 73 as the grey threshold value separating pores from the other phases.

Fig. 5 shows an image at different stages before segmentation: initial state, after applying a 3D median filter, while applying 73 as a threshold value and finally the segmented image. The porosity was calculated from the histogram of the segmented image by dividing the number of black voxels by the total number of voxels.

The spatial distribution of the porosity was investigated at different locations along the *x* and *y*

directions by using volumes with heights equal to 271 pixels. The locations of the volumes sections investigated are indicated in Fig. 6 (a). Fig. 6 (b) shows the variation of porosity with respect to x and y (volumes 1 to 12). A clear difference in porosity values is observed between the border (x, y = 160 and 1515) and the centre.

3.2 Larger anisotropy at lower bentonite dry densities

The radial swelling pressure (P_h) and the axial swelling pressure (P_v) values presented in Table 2 are the stabilized final values of the swelling pressure evolution (Fig. 3). The radial and axial values are not identical, the axial ones being mostly larger than the radial ones. This can be explained by the effect of the uni-axial compaction that favours the reaction in the direction of the compaction force. In order to analyse this anisotropic behaviour, an anisotropy coefficient (C_a) is defined as the ratio of P_h to P_v.

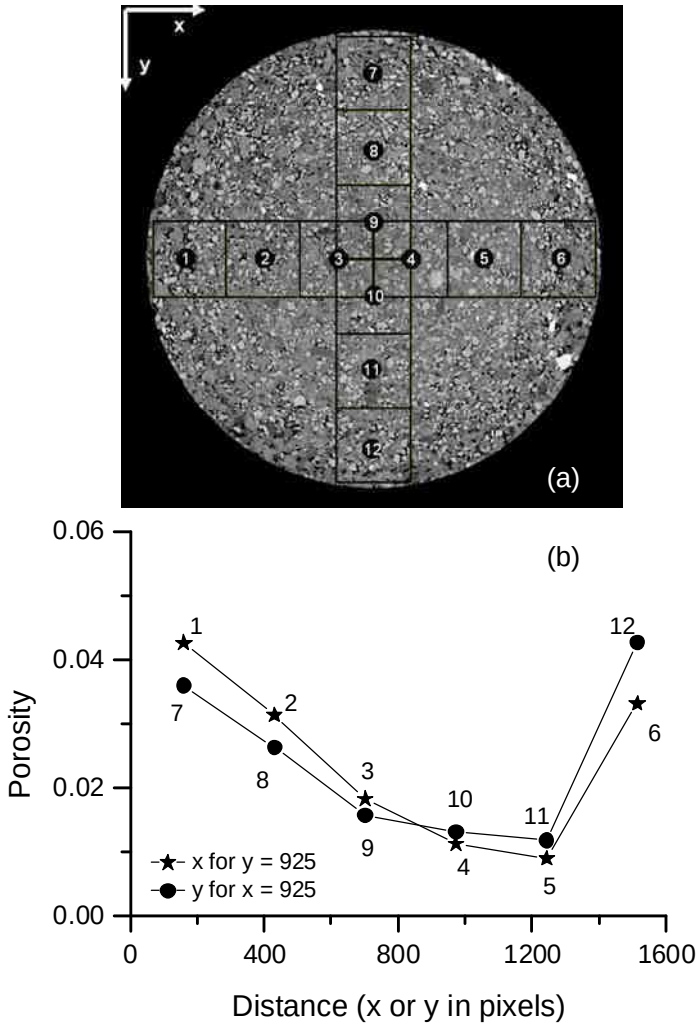


Figure 6. Sections of the volumes where the porosity was investigated in the sample (thickness 271 voxels) (a) and the corresponding results (b).

This coefficient is presented versus the bentonite dry density in Fig. 7. It can be observed that, in the range of medium bentonite dry densities, the swelling behaviour is mostly isotropic as

indicated by values of the anisotropy coefficient close to 1. These densities vary from 1.16 Mg/m^3 to 1.3 Mg/m^3. At higher bentonite dry densities, the anisotropy coefficient becomes slightly smaller than 1 with values ranging between 0.90 and 0.76. When the bentonite dry density is lower than 1.1 Mg/m^3, the anisotropy becomes higher with coefficients varying from 0.82 to 0.48. In addition, the sample preparation mode (In-cell or Out-cell) does not seem to influence the anisotropy coefficient.

The anisotropy behaviour is also related to the microstructure changes of the compacted mixture. After the uni-axial compaction of the grains-powder mixture, an initial structural anisotropy is induced by the compaction process that results in a larger swelling reaction in the compaction direction. On the other hand, upon hydration, bentonite grains will swell and split up, filling macro-pores. This process leads to a microstructure collapse, decreasing the initial anisotropy.

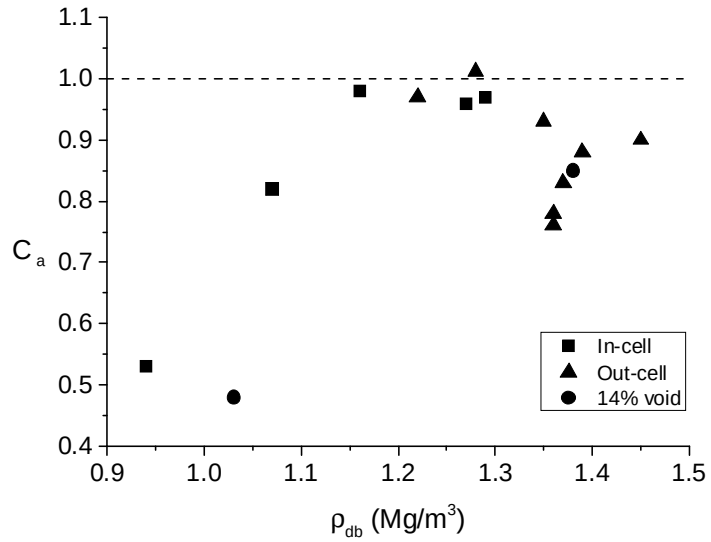


Figure 7. Anisotropy coefficient changes with respect to bentonite dry density for different test conditions.

From Fig. 3, the most marked peaks in the swelling pressure evolution are observed in the tests with medium range of bentonite dry densities. As explained previously, peaks indicate a collapse in the microstructure that favours the development of an isotropic microstructure. This explains the isotropic behaviour shown in Fig. 7 for the samples with medium bentonite dry densities and an anisotropy coefficient close to 1.

In the case of high bentonite dry densities, the kinetics in Fig. 3 exhibits small peaks, indicating a limited collapse of the microstructure that remained anisotropic. This is explained by the fact that, at high bentonite dry densities, there is not enough space (macro-pores) for bentonite grains to swell, preventing the microstructure collapse. This leads to a high degree of anisotropy with a coefficient of anisotropy ranging from 0.76 to 0.90.

In the case of very low bentonite dry densities (< 1.15 Mg/m^3), bentonite grains can swell but cannot fill up all the voids and give rise to microstructure collapse. The swelling kinetics curves also show small peaks in this range of bentonite dry densities, confirming the absence of microstructure collapse. The initial anisotropy is then preserved and it is represented by an anisotropy coefficient ranging from 0.48 to 0.82.

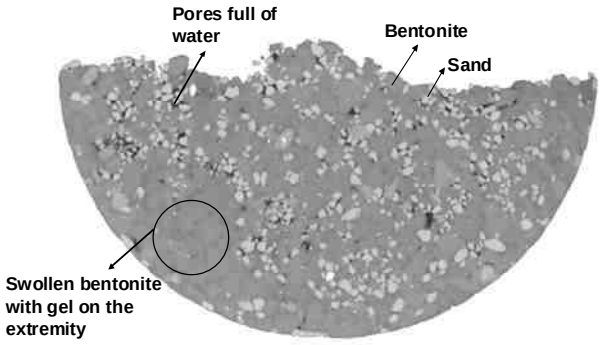


Figure 8. Radial cross-section at a depth of 5 mm of a part of the compacted sample after a four-month hydration under constant volume conditions.

To further investigate the anisotropy at low bentonite dry densities, a 3D microstructure observation has been performed by X-Ray µCT on a sample with a bentonite dry density of 0.97 Mg/m^3 after a four-month hydration under constant volume conditions. A radial cross-section at a distance of 5 mm from the sample surface is presented in Fig. 8. Different phases corresponding to different grey levels can be clearly distinguished: from the lightest to the darkest, sand grains, bentonite grains, the gel formed around the bentonite grains (after their swelling) and the pores. Pores are found to be almost saturated by water as their grey level is lighter from the one corresponding to air. Interestingly, some macro-pores can still be seen between the sand grains, confirming that the swelling of bentonite grains cannot fill all macro-pores. Also, it can be observed from the image that the bentonite closed the pores between bentonite grains more easily than between the sand grains. This contributes to preserve the initial anisotropy.

4 Conclusions

In the design of sealing plugs for deep radioactive waste disposal in clayey host-rocks, the swelling pressure is an important parameter to be studied. In this work, an experimental study on the anisotropy of swelling pressure of compacted bentonite/sand mixture was carried out. Two phenomena were identified and analyzed by µCT.

The first one concerns the difference in peaks magnitude between radial and axial swelling pressure kinetics with radial swelling pressure peaks larger than the axial ones. This reveals

that the sample may be looser in the radial direction than in the axial one, because peaks are related to the collapse of macro-pores, and this collapse is more pronounced if there are more micro-pores. A µCT image of a sample similar to the tested samples showed a concentration of macro-pores at the radial border of the sample. Image analysis confirmed this heterogeneity of porosity being related to the sample preparation method.

The second phenomenon concerns the anisotropic swelling of samples at low bentonite dry densities. It is known that, after hydration under constant volume conditions, the bentonite grains swell, fill up the macropores and result in a microstructure collapse. This leads to a decrease of the initial anisotropy induced by the axial compaction. On the contrary, higher anisotropy was observed at lower densities. The µCT image of a sample at a low bentonite dry density, after the end of a swelling pressure test showed that bentonite could not fill all the macro-pores. Consequently, bentonite at low density was not able to produce a collapse of macro-pores in the sample, which led to preservation of the initial sample anisotropy.

References

Agus, S. 2005. An Experimental study on hydro-mechanical characteristics of compacted bentonite-sand mixtures. PhD thesis, Weimar.

Agus, S S, Schanz, T. 2005. Effect of shrinking and swelling on microstructures and fabric of a compacted bentonite-sand mixture. Proceedings of the International Conference on Problematic Soils, Cyprus, 32, 543 – 550.

Barnichon, J D, Dick, P, Bauer, C. 2012. The SEALEX in situ experiments: performance test of repository seals. Harmonising Rock Engineering and the Environment – Qian & Zhou (eds) Taylor & Francis Group, London, ISBN 978-0-415-80444-8, pages 1391-1394.

Börgesson, L, Karnland, O, Johanneson, L E. 1996. Modelling of the physical behaviour of clay barriers close to water saturation. Engineering Geology, 41 : 127-144.

Castellanos, E, Villar, M V, Romero, E, Lloret, A, Gens, A. 2008. Chemical impact on the hydro-mechanical behaviour of high-density febex bentonite. Physics and Chemistry of the Earth, Parts A/B/C, 33(Supplement 1):S516 – S526.

Cho, W J, Lee, J O, Kang, C H. 2000. Influence of temperature elevation on the sealing performance of a potential buffer material for a high-level radioactive waste repository, Ann. Nucl. Energy, 27, 1271–1284.

Comina, C, Foti, S, Musso, G, Romero, E. 2008. EIT oedometer: an advanced cell to monitor spatial and time variability in soil. ASTM Geotechnical Testing Journal, 31 (5), 404–412.

Cui, Y J, Loiseau, C, Delage, P. 2002. Microstructure changes of a confined swelling soil due to suction controlled hydration. In Unsaturated soils: proceedings of the Third International Conference on Unsaturated Soils, UNSAT, Recife Brazil, volume 2, 593-598.

Delage, P, Marcial, D, Cui, Y J, Ruiz, X. 2006. Ageing effects in a compacted bentonite: a microstructure approach, Géotechnique, 56(5):291–304.

Delage, P, Howat, M D, Cui, Y J. 1998. The relationship between suction and swelling

properties in a heavily compacted unsaturated clay. Engineering Geology, 50 (1-2) **:**31-48.

Dixon, D A, Gray, M N, Thomas, A W. 1985. A study of the compaction properties of potential clay--sand buffer mixtures for use in nuclear fuel waste disposal. Engineering Geology, 21: 247—255.

Gebrenegus, T, Tuller, M, Muhuthan, B. 2006. The application of X-ray computed tomography for characterisation of surface crack networks in bentonite-sand mixtures. In: Desrues J, Viggiani G, Bésuelle P (eds) Advances in X-ray tomography for geomaterials, ISTE Ltd, London, UK: 207–212.

Karnland, O, Olsson, S, Nilsson, U. 2006. Mineralogy and sealing properties of various bentonites and smectite-rich clay material. SKB.

Kawaragi, C, Yoneda, T, Sato, T, Kaneko, K. 2009. Microstructure of saturated bentonites characterized by X-ray CT observations. Engineering Geology, 106, 51–57.

Ketcham, R A, Carlson, W D. 2001. Acquisition, optimization and interpretation of X-ray computed tomographic imagery: applications to the geosciences. Computers & Geosciences, Vol. 27, 381-400.

Komine, H, Ogata, N. 1994. Experimental study on swelling characteristics of compacted bentonite. Canadian geotechnical journal, 31(4):478–490.

Komine, H, Ogata, N. 2003. New equations for swelling characteristics of bentonite-based buffer materials. Canadian Geotechnical Journal, 2003, 40(2):460–475.

Komine, H, Ogata, N. 2004. Predicting swelling characteristics of bentonites. Journal of Geotechnical and Geoenvironmental engineering, 130:818.

Komine, H, Yasuhara, K, Murakami, S. 2009. Swelling characteristics of bentonites in artificial seawater. Canadian Geotechnical Journal, 46(2):177-189.

Kozaki, T, Suzuki, S, Kozai, N, Sato, S, Ohashi, H. 2001. Observation of microstructures of compacted bentonite by microfocus X-ray computerized tomography (Micro-CT). Journal of Nuclear Science Technology, 38 (8), pp. 697–699.

Lee, J O, Cho, W J, Chun, K S. 1999. Swelling Pressures of a Potential Buffer Material for High-Level Waste Repository. Journal of the Korean Nuclear Society, 31: 139-150.

Lee, J O, Lim, J G, Kang, I M, Kwon, S. 2012. Swelling pressures of compacted Ca-bentonite. Engineering Geology, doi: 10.1016/j.enggeo.2012.01.005

Lloret, A, Villar, M V. 2007. Advances on the knowledge of the thermo-hydro-mechanical behaviour of heavily compacted “FEBEX” bentonite. Physics and Chemistry of the Earth, 32 701-715.

Madsen, F T. 1998. Clay mineralogical investigations related to nuclear waste disposal. Clay Minerals, 33(1):109–129.

Montes-H G., 2002. Etude expérimentale de la sorption d’eau et du gonflement des argiles par microscopie électronique à balayage environnementale (ESEM) et analyse digitale d’images. PhD Thesis, Université Louis Pasteur, Strasbourg, France.

Mukunoki, T, Otani, J, Maekawa, A, Camp, S, Gourc, J P. 2006. Investigation of crack behaviour on cover soils at landfill using X-ray CT. In: Desrues J, Viggiani G, Bésuelle P(eds) Advances in X-ray tomography for geomaterials. ISTE Ltd, London, UK, 213–219.

Pusch, R. 1982. Mineral-water interactions and their influence on the physical behavior of highly compacted Na bentonite. Canadian Geotechnical Journal, 19(3):381–387.

Rasband, W S. 1997-2012. ImageJ, U. S. National Institutes of Health, Bethesda, Maryland, USA, http://imagej.nih.gov/ij/.

Saba, S, Delage, P, Cui, Y J, Tang, A M, Lenoir, N, Barnichon, J D. A further insight into the microstructure of compacted bentonite/sand mixture. Engineering Geology. Submitted – a.

Saba, S, Tang, A M, Cui, Y J, Tran, T P H, Barnichon, J D. Anisotropic swelling of compacted bentonite/sand mixture. Soils and Foundations. Submitted - b.

Tang, C S, Tang, A M, Cui, Y J, Delage, P, Schroeder, C, De Laure, E. 2011. Investigating the Swelling Pressure of Compacted Crushed-Callovo-Oxfordian Argillite. Physics and Chemistry of the Earth, 36 (17-18), 1857–1866.

Van Geet, M, Volckaert, G, Roels, S. 2005. The use of microfocus X-ray computed tomography in characterising the hydration of a clay pellet/powder mixture. Applied Clay Science, 29 (2):73–87.

Villar, M V, Lloret, A. 2001. Variation in the intrinsic permeability of expansive clays upon saturation. In: Adachi K., Fukue M. (eds) Clay Science for Engineering, A.A. Balkema, Rotterdam 259-266.

Wang, Q, Tang, A M, Cui, Y J, Delage, P, Gatmiri, B. 2012. Experimental study on the swelling behaviour of bentonite/claystone mixture. Engineering Geology, 124: 59-66, doi: 10.1016/j.engeo.2011.10.003.

Wang, Q., Tang, A M, Cui, Y J, Delage, P, Barnichon, J D, Ye, W M. 2013. The effects of technological voids on the hydro-mechanical behaviour of compacted bentonite-sand mixture. Soils and Foundations. Volume 53, Issue 2, Pages 232–245

Yong, R N, Boonsinsuk, P, Wong, G. 1986. Formulation of backfill material for a nuclear fuel waste disposal vault. Canadian Geotechnical Journal, 23(2):216–228.

Chapter 4

Hydro-mechanical response of mock-up tests

INTRODUCTION

The French institute IRSN is carrying out the SEALEX project aiming at identifying the key factors related to the long-term performance of bentonite-based sealing systems. This project consists of a series of in situ experiments performed in natural conditions at the Tournemire Underground Research Laboratory.

In parallel, laboratory mock-up tests were designed at a 1/10 scale of the SEALEX project and with similar boundary conditions in order to provide further and quicker information about the behaviour of the studied material. The test cell was specially designed with local measurements of radial swelling pressure and measurement of the global axial swelling pressure. The cell permitted saturation of the sample under confined conditions while monitoring the swelling pressure, the axial displacement and the volume of injected water. Two mock-up tests were performed; one with water injected from the bottom and the other with two side water injection. Results of the two tests are compared in terms of swelling kinetics as well as the potential effect of entrapped air. When full saturation was considered as reached, and also in a relation to IRSN requirements, the confinement failure was studied and the recovery capacity of the seal was investigated. This case was simulated in the test by the piston release creating an axial void of 20%. The progressive sealing of this void was ensured by the axial swelling of the seal accompanied by its density decrease. The void recovery was monitored by the radial swelling pressure sensors. The resulting density gradient was estimated from the radial swelling pressure measurements using an exponential relationship. The evolution of this gradient over time was monitored and a homogenisation can be expected at long-term. The dismantling of a previous similar test by Wang et al. (2013a) that lasted 350 days enabled the dry density at different heights to be determined. The density gradient was found smaller than that in the present test.

The first part of this chapter presents a detailed description of all parts of the mock-up test cell. A validation of the cell was done by comparing the obtained results with those from literature. This work was presented in a paper submitted to “Geotechnical Testing Journal”.

The second part of this chapter consists of a comparison of the two mock-up tests that were carried out with different saturation boundary conditions. It also presents a combination of suction measurements obtained from Wang et al. (2013b) and swelling pressure measurements at the same position for the similar material during infiltration. The hydro-mechanical behaviour of the material was thereby analysed. Finally, the failure of axial

confinement was simulated and the density gradient evolution was monitored. The results are presented in the form of a paper submitted to Canadian Geotechnical Journal.

Small scale infiltration column with local measurements of swelling pressure: cell validation

Simona Saba[12], Yu-Jun Cui[2], Jean-Dominique Barnichon[1] and Anh Minh Tang[2]

Abstract: This paper describes a small scale infiltration cell that was designed to study the behaviour of sealing materials used in the context of radioactive waste disposal. These sealing materials are supposed to swell upon contact with water and then ensure a good sealing of all gaps in the system. The cell is a small scale mock-up at a 1/10 scale of large scale in situ experiments conducted by the French Institute for Radiation Protection and Nuclear Safety (IRSN) in the framework of the SEALEX project. The cell consists in a rigid body ensuring mechanical confinement and a hydraulic part enabling saturation of the hosted sample. It is also equipped with three types of sensors: pressure sensors, force transducer and displacement transducer in order to monitor the swelling behaviour of the sample at different positions (axially and radially) and to check whether any axial displacement takes place. A detailed description of all the parts forming the cell is presented and the design is validated by carrying out a test on a compacted bentonite/sand mixture considered as a candidate sealing material. The test gives satisfactory results in terms of swelling pressure (kinetics and value) compared with those in literature.

Keywords: small scale infiltration cell; bentonite/sand mixture; SEALEX experiments; swelling pressure; constant volume conditions

1 Introduction

In the French concept of deep geological disposal of radioactive wastes, it is planned to emplace waste canisters in galleries excavated in deep low-permeability host rocks (claystone). After the installation of canisters, galleries are supposed to be sealed by the swelling of compacted clay-based materials, which should further limit fluxes of underground water around the galleries. Considering the complexity and the importance of the problems related to the seal of clay-based materials, both laboratory and field tests are needed. In this study, a Mock-up test was designed and carried out in the laboratory at a scale of 1/10 of the large scale in-situ experiments (SEALEX) performed by the French Institute for Radiation Protection and Nuclear Safety (IRSN) to investigate the long term behaviour of the compacted sealing materials. As the SEALEX in-situ experiments consider the case corresponding to failure of the retaining structures and follow the capacity of the sealing materials to recover the void created by this failure (see Barnichon et al., 2010 and 2012 for more details), the present laboratory experiment was then designed for a similar purpose: it reproduces the same boundary conditions and is capable to reproduce the same void created by the failure of the retaining structures. Also, it has similar measurements as the field experiments (swelling

[1] Institut de Radioprotection et de Sûreté Nucléaire (IRSN), Fontenay-aux-Roses, France
[2] Ecole des Ponts ParisTech, Laboratoire Navier/Cermes, Marne-La-Vallée, France

pressure, volume of injected water).

The laboratory experiment consists of a mechanical part, a hydraulic part and a measurement part. The mechanical part consists of a rigid stainless steel cylinder that hosts the soil sample and a fixing system that ensures the confined mechanical conditions in both radial and axial directions. For the saturation of soil sample, water inlets are designed in the base of the cell and in the upper piston, and they are connected to water tanks. Six pressure sensors, one force transducer and a displacement transducer are used to monitor the radial swelling pressure along the sample, the axial swelling and the displacement of the piston, respectively. This cell can be used to test different sealing materials: different types of bentonite, mixtures of bentonite with other materials like sand and crushed claystone. It can also be used for different test configurations: one-side or two-side saturation; confined or free swell conditions in the axial direction.

The mechanical behaviour of sealing materials has been largely studied in the past, especially in terms of swelling pressure. Pusch (1982), Komine and Ogata (1994), Agus and Schanz (2005) and Wang et al. (2012) studied the swelling behaviour of bentonite-based materials, but only in the axial direction. Some authors also tried to measure the radial swelling pressure (Cho et al., 2000; Lee et al., 2012; Saba et al., 2013), although this was achieved only in elementary tests and not in mock-up tests. In the cell developed in this study, the swelling pressure is measured radially along an infiltration column (at different positions along the sample). This is another particularity of this infiltration cell - it gives the mechanical measurements along the sample during the saturation process, while usually, infiltration columns are used to measure the hydraulic parameters like relative humidity, water content or suction (Loiseau et al., 2002; Cui et al., 2008; Wang et al., 2013b).

In this paper, a detailed description of the cell is presented with all its components and the sensors used. Validation of the design was done through testing a compacted bentonite/sand mixture that has been extensively studied in the context of nuclear waste disposal, and through comparing the results obtained with the results from literature.

2 Materials

The soil used to the cell validation is a mixture of bentonite and sand with a bentonite fraction of 70% in dry mass. The bentonite is an MX80 from Wyoming, USA, having a liquid limit of 575%, a plastic limit of 53% and a unit mass of 2.77 Mg/m^3. Its cation exchange capacity (CEC) is 76 meq/100g (83% of Na^+). This bentonite is known to be highly water absorbent

with a specific surface as large as 710 m^2/g. The swelling index was also measured, equal to 27 $cm^3/2g$. This large value also indicates its high swelling capacity. The sand (pure quartz) used in the mixture comes from Eure and Loire (France) with a unit mass of 2.65 Mg/m^3. It was sieved at 2 mm prior to being mixed with the bentonite grains that were previously equilibrated with a water content of 13%. The grain size distribution curves of the bentonite and sand were determined by dry sieving and are presented in Figure 1, along with the grain size distribution curve of the deflocculated bentonite determined by the hydrometer method.

The saturation water used in the test is synthetic water obtained by mixing the chemical components listed in Table 1 with distilled water using a magnetic stirrer until full dissolution. This composition is similar to that of the pore water present in the rock considered in the French program of geological radioactive waste disposal.

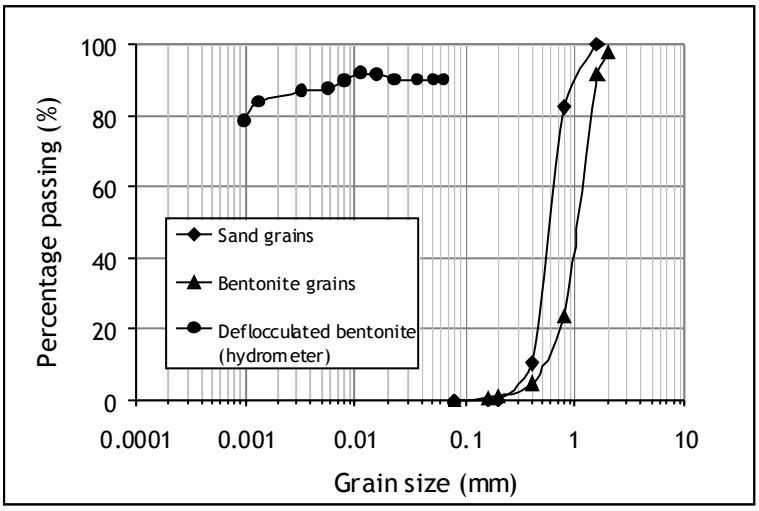


Figure 1. Grain size distribution curves.

Table 1. Chemical composition of synthetic water (Wang et al., 2012).

Component	$NaHCO_3$	Na_2SO_4	NaCl	KCl	$CaCl_2.2H_2O$	$MgCl_2.6H_2O$	$SrCl_2.6H_2O$
Mass/Litter of solution (g)	0.28	2.216	0.615	0.075	1.082	1.356	0.053

3 Experimental set-up

As mentioned before, the experiment conducted aims to study the swelling properties of sealing materials at a scale of 1/10 of the SEALEX in-situ tests and with the same boundary conditions. It consists in saturating the soil sample that represents the seal under confined conditions while monitoring different parameters such as swelling pressure, injected water volume and piston displacement over time. The designed experiment is presented in Figure 2 and consists of several parts: i) the mechanical part (in grey) that hosts the soil sample; ii) the

hydraulic part (in blue) that enables the saturation of the sample and which consists of the water tanks and water connexions; iii) the measurements part (in red) with all the sensors (total pressure, force transducer, displacement indicator) and the acquisition system (data logger and computer).

3.1 The mechanical part

The stainless steel cell was designed to mechanically ensure the confined conditions. A hollow cylinder of 11 mm thick is fixed by three screws to a thick base with water inlets. In the axial direction, a piston is placed on the top of the soil specimen and it is blocked by a screw that is fixed to a stiff structure (see Figure 2 and Figure 3). This stiff structure consists of two stainless steel disks respectively on the two sides of the cylinder, connected by three metallic rods.

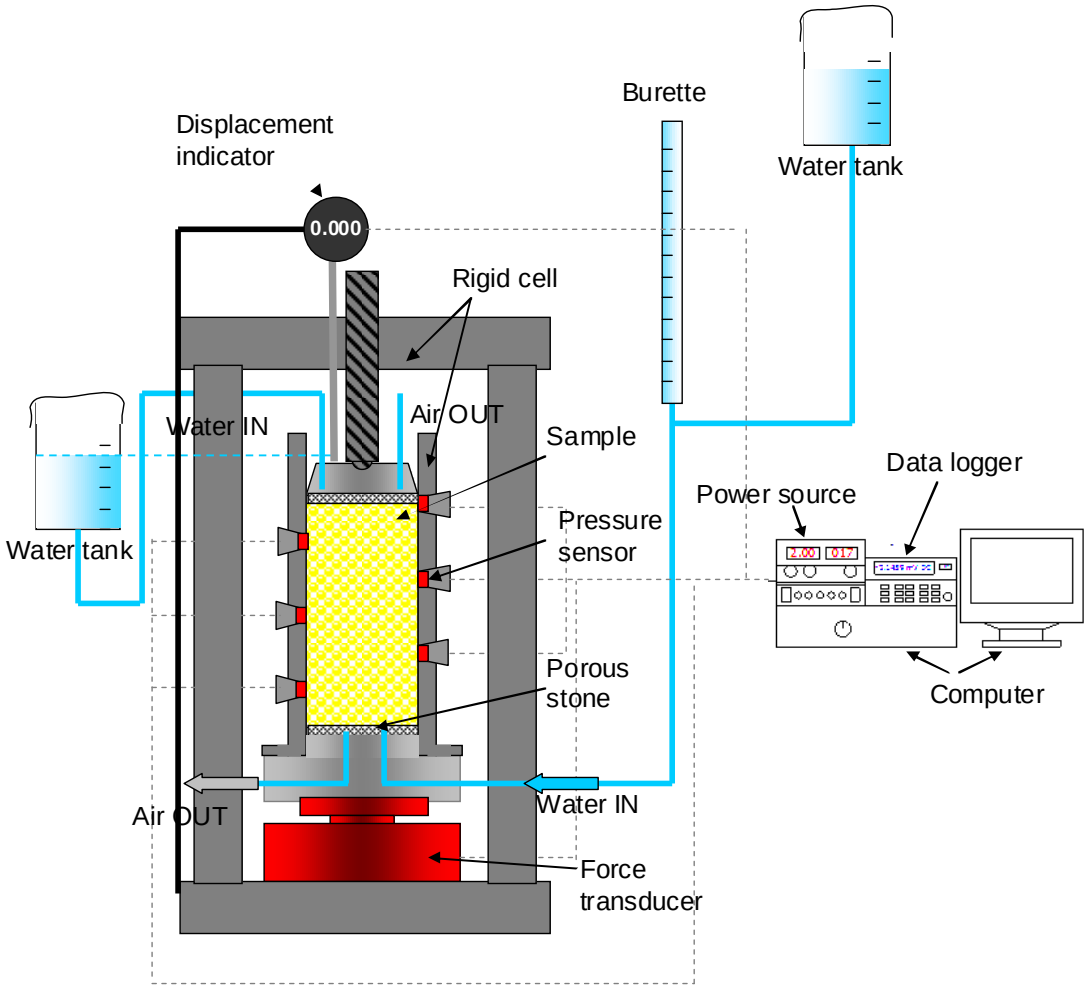


Figure 2. Outline of the experimental set-up with its mechanical part (in grey), hydraulic part (in blue) and measurement part (in red).

The cell was designed to stand high pressures exerted by the soil specimen under constant volume conditions. The force due to soil swelling is directly transmitted to the screw, and then

to the stiff structure (disks and rods). The transmission between the screw and the upper plate occurs at the centre of the plate; the force is then localised near the screw. The deformation of the plate at this specific location was measured by a displacement transducer when simulating a swelling pressure of 8 MPa. The simulation was done by substituting the soil specimen with a metallic piece and turning the central screw to apply the desired pressure that was measured by the force transducer (placed between the base and the bottom plate). The measured displacement was 6 µm, which can be considered as negligible in this pressure range.

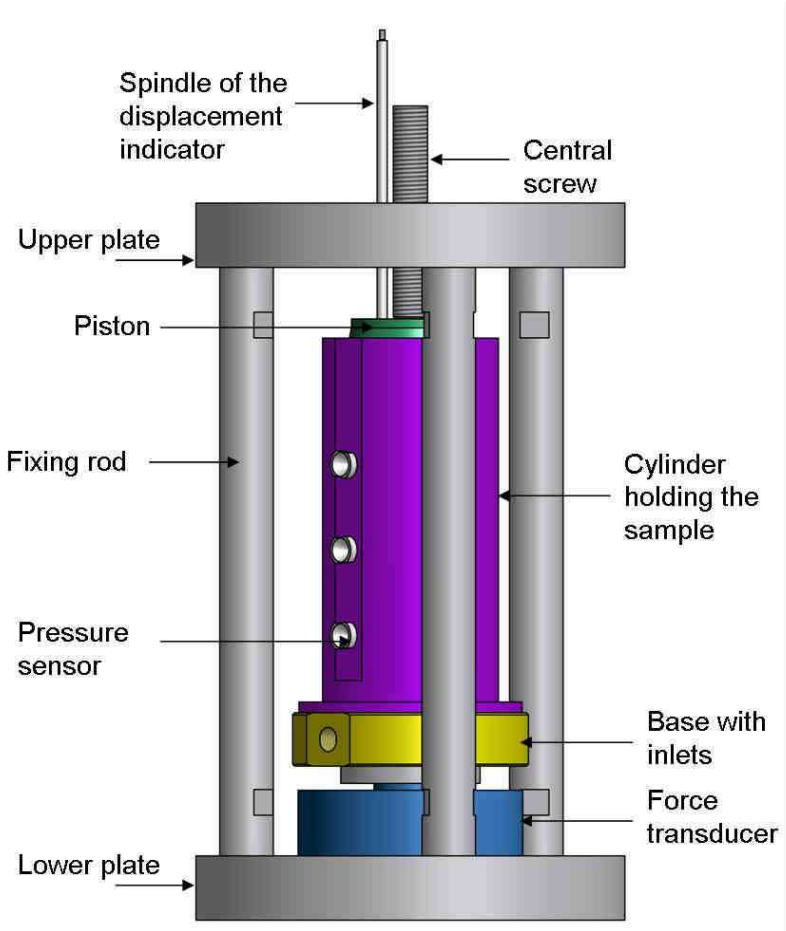


Figure 3. 3D view of the cell.

3.2 The hydraulic part

Depending on the test configurations, either one-side (generally from the bottom) or two-side (from the top and the bottom) saturation may be applied. For this purpose, the cell was designed in such a way that both one-side and two-side saturation are allowed.

The base of the cell on which the cylinder is mounted (see Figure 4) is equipped with a water inlet and an air outlet. The air outlet is needed to evacuate the air that is present in the base and in all the system near the inlets. At the faces of both inlets, mechanical valves are mounted and sealed, allowing the entrance of water and the evacuation of water or air to be

controlled. Flexible water hoses are connected to the valves; the side serving as a water inlet is connected to a burette and then to a water tank. The graduated burette helps in monitoring the volume of water entering the cell, and it is regularly supplied with water from the water tank. A valve is also added between the water tank and the burette, allowing the water flow between them to be controlled.

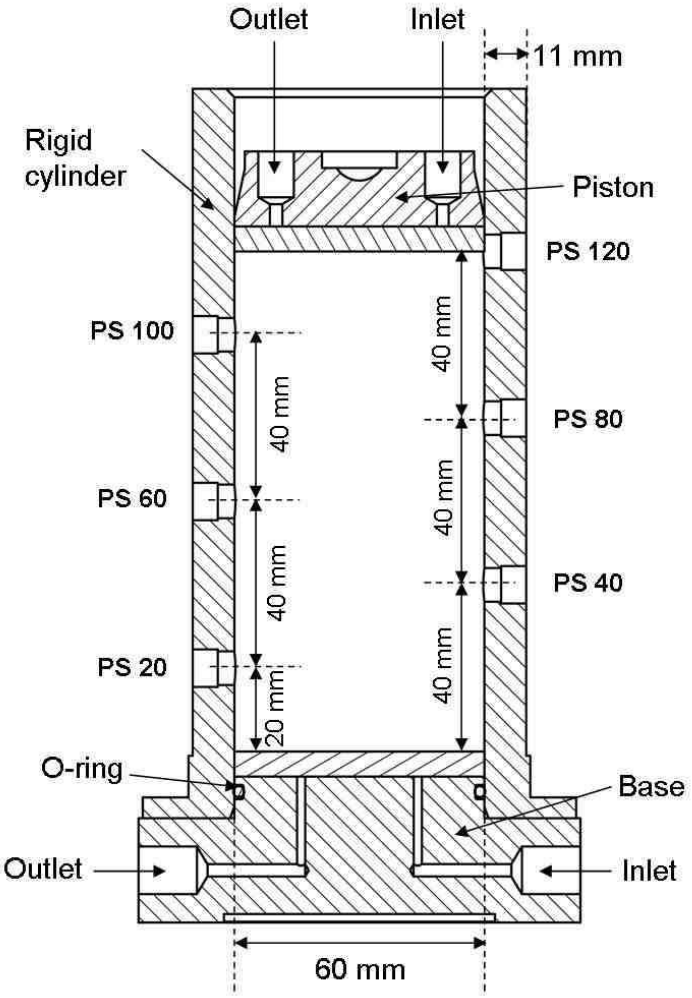


Figure 4. Cross section of the cell with the positions of the pressure sensors.

The piston is also equipped with a water inlet and an air outlet, allowing the saturation to be processed from the top if needed. A water tank is connected directly to the water inlet of the piston, and its position is adjusted so that water can enter the cell through the top of the piston. However, the water level should not exceed the top of the rigid cell as shown in Figure 2. No pressure is applied to water during the saturation process.

3.3 The measurements parts

a) Total pressure sensors

Six total pressure sensors are used to measure the radial swelling pressure along the sample at

different positions. Figure 4 shows the locations of the sensors. They are labelled according to the distance between them and the lower extremity of the sample, for instance, PS20, PS40, PS60, PS80, PS100 and PS120 are situated at 20, 40, 60, 80, 100 and 120 mm respectively from lower end of the sample. Owing to the limited size of the internal diameter of the cell (60 mm), miniature pressure sensors are used here. They have a diameter of 6 mm (see Figure 5) and a working range from zero to 5 MPa + 150% of safe overloading. For a proper installation of these sensors in the cylinder wall, an extra piece is needed due to their very small size: the fitting piece (Figure 5) that guarantees a good protection of the sensor during installation.

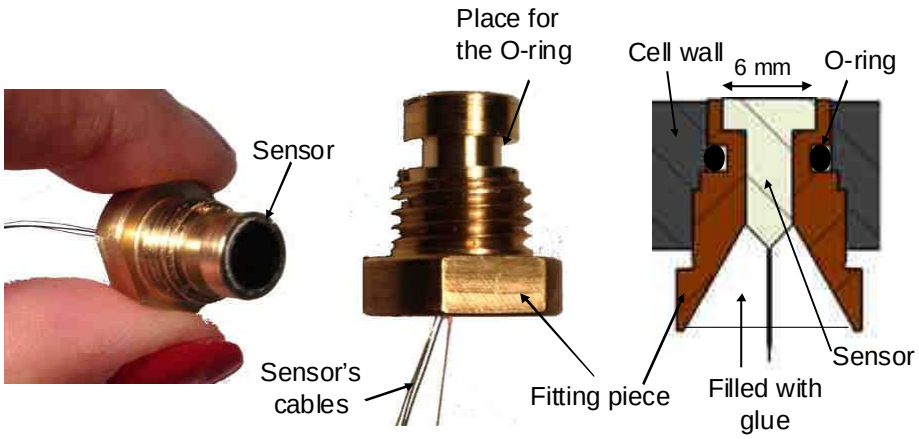


Figure 5. Total pressure sensor's fitting piece.

This fitting piece also enables an easier installation of the sensors in the cell wall by simply screwing them into their dedicated holes. The sensors are installed in the fitting pieces using adhesive (strong Araldite glue) as it is recommended by the manufacturer (see the assembly in Figure 5). The same glue is also used to fill the gap behind the sensor's end to cover the thin cables and rigidify the connexion between cables and sensor because this connexion can be easily damaged by the weight of the fitting piece. The four cables of the sensors are welded to longer cables and then two of them are connected to the data logger and the two others to the power source. The power source provides an excitation voltage of 2 V. Between the sensors and the data logger or the power source, connectors are installed in order to facilitate the insertion of the sensors to the cell wall.

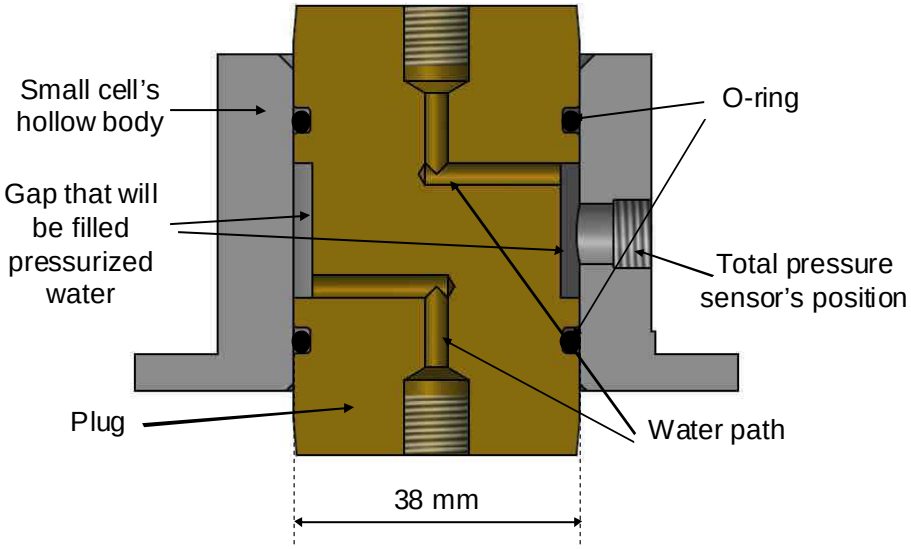


Figure 6. Calibration plug for total pressure sensors inserted in the small cell.

Prior to their use, the sensors are calibrated to verify their performance. To this end, a series of pressures is applied to the measuring face of the sensor and the responses are recorded. The pressure is imposed by means of a volume pressure controller. To apply a pressure to the sensor by injecting pressurized water, the best way is to insert the sensor in a smaller cell (reduced height (45 mm instead of 175 mm) and diameter (38 mm instead of 60 mm)) and to design a plug that enables water injection facing the sensor while ensuring a good sealing. The cross section of the plug inserted in the cell is presented in Figure 6. This figure also shows the water paths and the gap near the sensors position that will be filled with pressurized water. The plug has a water inlet connected to the pressure/volume controller and an air inlet that helps in evacuating air from the plug before being filled with water. Once filled, the extremity of outlet is closed and pressure can be imposed by the pressure/volume controller. A loading/unloading pressure path is applied with pressure values firstly increased from 200 kPa to 4500 kPa and then decreased. The output voltage of the sensor is recorded by the data logger.

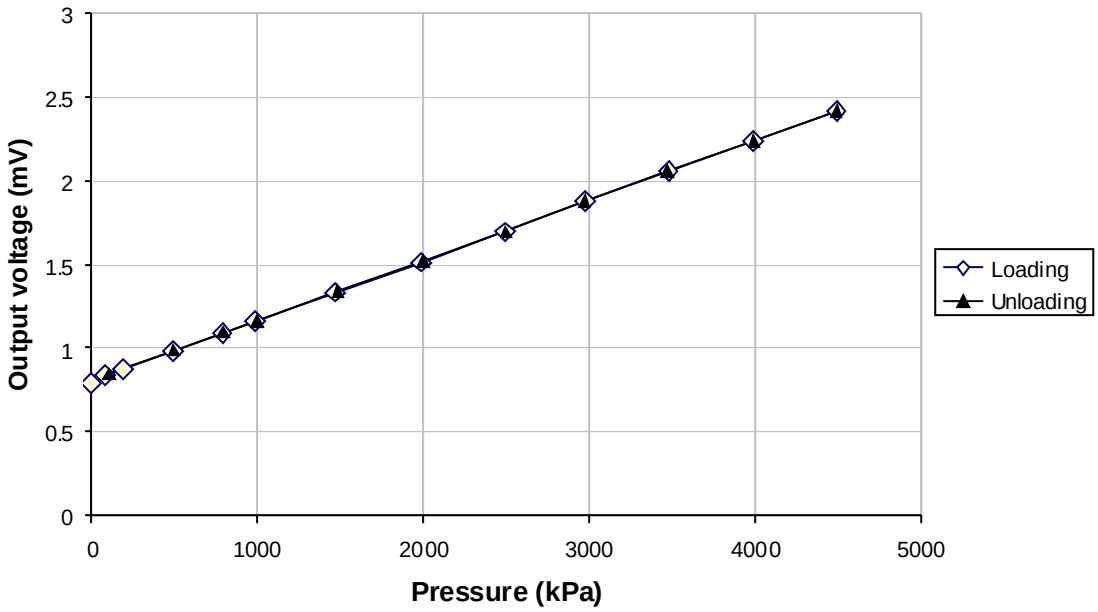


Figure 7. Calibration curve of the total pressure sensor PS40.

All the used total pressure sensors were calibrated and they all gave a linear relation between imposed pressure and output voltage. An example is shown in Figure 7, corresponding to sensor PS40 located at 40 mm height from the bottom. The calibration curve shows that the sensor's response at zero pressure is not zero and this value should be taken into account while converting the output voltage into pressure. The slope of the linear curve is a constant, equal to $\Delta V/\Delta P = 0.0003696$ mV/kPa for sensor PS40. To convert the reading given by the sensor to the corresponding pressure, the following equation is used:

$$P(t) = \frac{V(t) - V_0}{slope}$$

where:

V(t) is the sensor's output voltage at time t (in mV);

V_0 is the sensor's output voltage at zero pressure (in mV).

According to the manufacturer, the measured pressure is calculated using the following equation:

$$P = \left(\frac{V(t) - V_0}{V_{excitation}} \right) \frac{P_{\max}}{k}$$

where:

V(t) is the sensor's output voltage at time t (in mV),

V_0 is the sensor's output voltage at zero pressure (in mV);

$V_{excitation}$ is the excitation voltage fixed by the power source (in V)

P_{max} is the capacity of the sensor (in MPa);

k is the rated output voltage given by the manufacturer and depends on the class of the sensor (in mV/V).

In order to make a comparison of the two equations, the value of $\frac{V_{excitation} \times k}{P_{max}}$ is calculated with $V_{excitation}$ taken equal to 1.99 V, k taken equal to 0.928 mV/V (given by the manufacturer) and P_{max} taken equal to 5 MPa. The obtained result is 0.0003694, which is quite close to the calibration coefficient determined before (0.0003696).

b) Force transducer

The force transducer is placed under the cell base and measures the axial swelling pressure of the sample. It is powered by a conditioner that is directly connected to the data logger. The capacity of this transducer is 2.5 tons, corresponding to 8.8 MPa pressure given the sample dimensions. The calibration equation provided by the manufacturer was used for data treatment, as follows:

$$F = (V(t) - V_0) \times 5 - 25$$

where:

F is the compressive force (negative value in kN);

V(t) is the output voltage given by the sensor at time t (in V);

V_0 is the output voltage given by the sensor before hydration begins (before swelling pressure is applied on the sensor; it corresponds to the weight of the cell and the sample) (in V).

c) Displacement transducer

A digital displacement transducer is installed to measure the displacement of the piston. The displacement of the piston is measured mainly to verify that no axial deformation occurs in constant volume conditions. In case of other test configurations where axial swelling is allowed, this transducer allows the axial displacement to be monitored. The display module is fixed to a magnetic support that is in turn fixed to the bottom stainless steel plate. The spindle passes through a perforated hole in the upper stainless steel plate and it is adjusted so that the contact point touches the top of the piston. The used displacement transducer has an accuracy

of 1 µm and it is connected to the data logger for the recording displacement.

4 Test procedure

4.1 Sample preparation

For the sample preparation, the bentonite/sand mixture was compacted uni-axially using a mechanical press. The target dimensions of the sample are 120 mm in height and 60 mm in diameter, which corresponds to 1/10 of the in-situ SEALEX seals dimensions (120 cm and 60 cm). The target dry density of the sample is 1.67 Mg/m^3, which corresponds to the same final dry density as in the SEALEX tests: the initial dry density in SEALEX tests is 1.97 Mg/m^3, and after expansion (filling a 14.33% technological void) it becomes 1.67 Mg/m^3. In order to obtain a homogeneous sample, it was compacted in 3 layers of 40 mm height each. The sample was directly compacted in the cell after closing the holes in the cell's wall by screwing solid plugs having the same shape as the fitting pieces. The inner wall of the cylinder was coated with grease in order to minimize the friction between the soil and the cell. A porous stone and a filter paper having the same internal diameter as the cell were placed at the bottom of the cell. The mass of soil powder needed to prepare the first layer was placed in several steps while stirring the mixture each time and trying to flatten the surface each time by tapping it manually using the piston. Another filter paper was placed at the top. The piston of 60 mm diameter was put onto the filter paper, followed by a long piston with a diameter of 50 mm. A piece was needed to centre the longer piston in the cell; it was a hollow plastic adjustable cylinder (piston aligner) that fitted the space between the internal surface of the cell and the piston (see Figure 8 for more details). The cell was placed on the displacement shaft of the mechanical press and it was adjusted in order to connect the top of the piston to the force transducer as shown in Figure 8. A metallic ball was used to create a simple connexion between the piston and the force transducer. The compaction then started at a constant displacement rate of 0.1 mm/min till a given axial stress of 13 MPa in this case monitored by the force transducer. The target height was also monitored by making marks on the piston. After the axial stress reached the desired value (13 MPa) and the marks on the piston also confirmed the target height, the displacement shaft was fixed till the axial stress became stable (change in axial stress by relaxation was less than 0.05 MPa/hour).

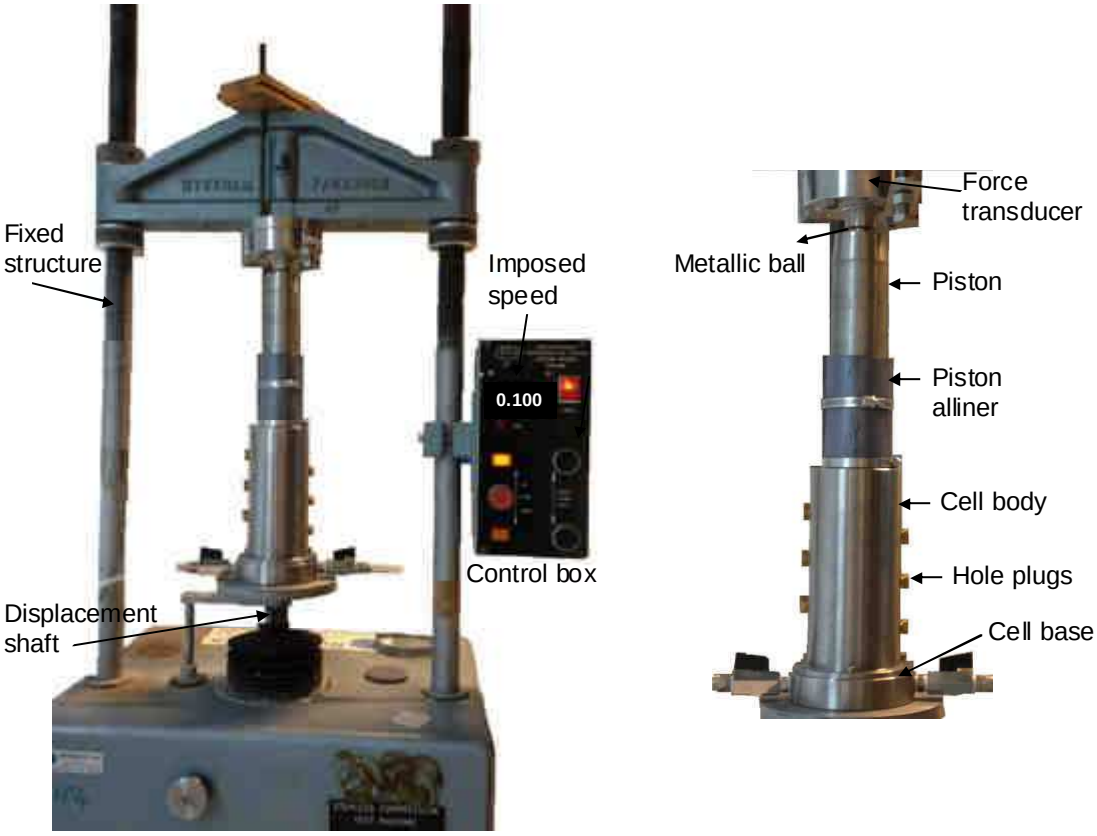


Figure 8. Sample compaction in the mechanical press.

This took about 20 hours. Afterwards, the cell was unloaded and moved out of the mechanical press; the height of the compacted sample was measured manually using a calliper. The same procedure was repeated for the two other layers, with the upper surface of the compacted layer being scarified each time before placing the new mixture powder in order to ensure a good junction of layers. The details of the three layers forming the sample after compaction are presented in Figure 9. The final mean density obtained was 1.69 Mg/m^3, close to the target density (1.67 Mg/m^3).

4.2 Test protocol

At the end of the compaction of the last layer, the cell was placed on the tray of the force transducer between the two stainless steel plates fixed with the three rods. The central screw was adjusted to touch the piston and apply an initial pressure of 100 kPa. This pressure allowed a good contact between the cell, the piston and the sample. The radial sensors are then screwed to the cell wall and adjusted so that an initial pressure of 100 kPa was also applied to ensure a good contact between the sensor and the sample. Note that the imposed values were approximately 100 kPa because it was difficult to impose exactly 100 kPa by just turning the fitting piece in the cell wall.

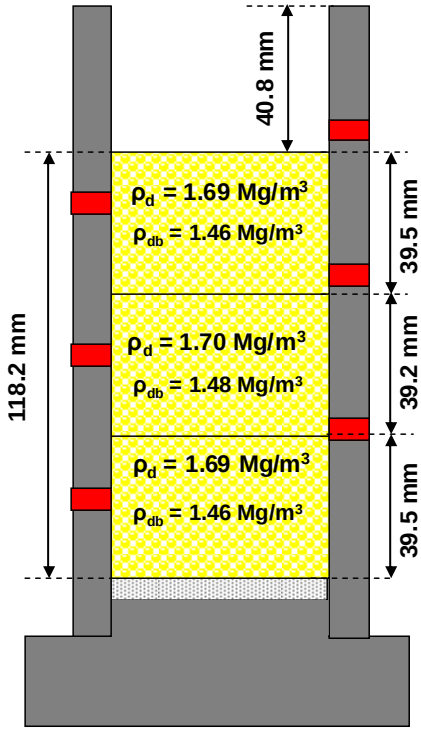


Figure 9. Dimensions and final dry densities of the layers of the compacted soil specimen.

The sample saturation in this test is only from the bottom. The water hoses that had been saturated previously were then connected to the inlets while keeping the valves closed. Note that the previous saturation of the water hoses before their connexion helps in avoiding a large water level drop in the burette at the initial stages of the test. The test started by setting on the data acquisition program to record all the initial values before the hydration started. The water level in the burette was also noted before opening the inlet valve (at the base). The air outlet was also opened in order to eliminate air in all the connexions and pieces. The water level in the burette was manually recorded after opening the valve. Note however that neither the valves nor the passages in the base were saturated before, thus, a quick drop in water level in the burette was inevitable. The evolutions of axial and radial swelling pressures were recorded during hydration as well as the displacement of the piston. The injected water was continuously monitored by noting the water level in the burette every day.

5 Results and discussion

5.1 Vertical displacement of the piston

Although the cell was designed to have constant volume conditions, deformation due to the non-perfect contacts between the base of the cell, the sample and the piston can however take place. Figure 10 shows the evolution of the recorded displacement over time, together with that reported by Wang et al. (2013a). The displacement increased over time and reached 0.32 mm that represents 0.25% of the sample height. The value obtained in this study is

slightly higher than that obtained by Wang et al. (2013a) - 0.15 mm; but is consistent with the higher axial swelling pressure reached in the present work (5 MPa) compared to Wang et al. (1.8 MPa). This displacement is small enough to be neglected in the analysis of results.

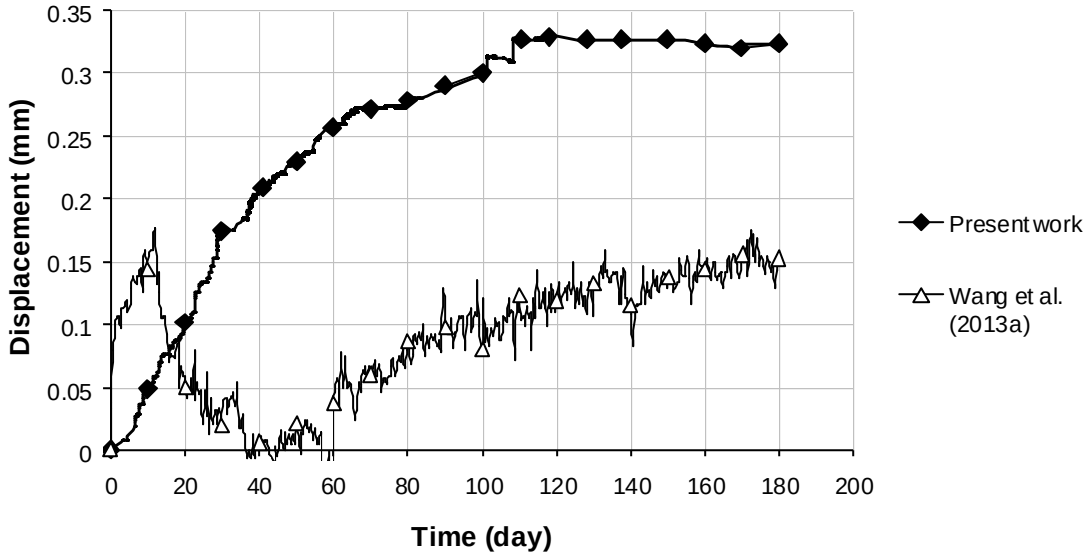


Figure 10. Evolution of the piston's displacement over time in the present work and in the work of Wang et al. (2013a).

5.2 Swelling pressure

The swelling pressure development over time is presented in Figure 11 with a zoom on the first 20 days. Examination of the starting point shows that all the first values are close to 100 kPa except for the sensor at 82 mm height that started from a higher value (595 kPa). In fact, as explained before, it was difficult to adjust the position of the sensor to have an exact initial pressure value of 100 kPa. On the whole, the swelling pressure increased over time except for the one corresponding to sensor PS120 at 120 mm height that gave an almost unchanged response of 70 kPa. It was suspected that this sensor was not in contact with the sample. This sensor was planned for another test configuration with release of the piston or with the axial swelling of the sample allowed. For the other sensors, the rate of increase was nevertheless different depending on their positions. A higher rate was found for the sensors that were closer to the wetting source, the highest rate being logically observed for sensor PS20 that was the closest to the bottom. The curve corresponding to this sensor exhibits a first quick increase, reaching a peak value followed by a slight decrease and then a very slow increase to reach a stabilisation around 3.5 MPa. The second high increase rate corresponds to sensor PS40. Its corresponding swelling pressure evolution was similar to that of PS20 except for the presence of peak. Indeed, compared to PS20, sensor PS40 showed a smoother change

between the very quick first increase and the stabilisation. The stabilisation also occurred at around 3.5 MPa. The curves relative to sensors PS60 and PS80 increased at similar initial rates in the beginning with a slightly higher rate for PS60. They reached a peak at around 5.0 MPa followed by a decrease.

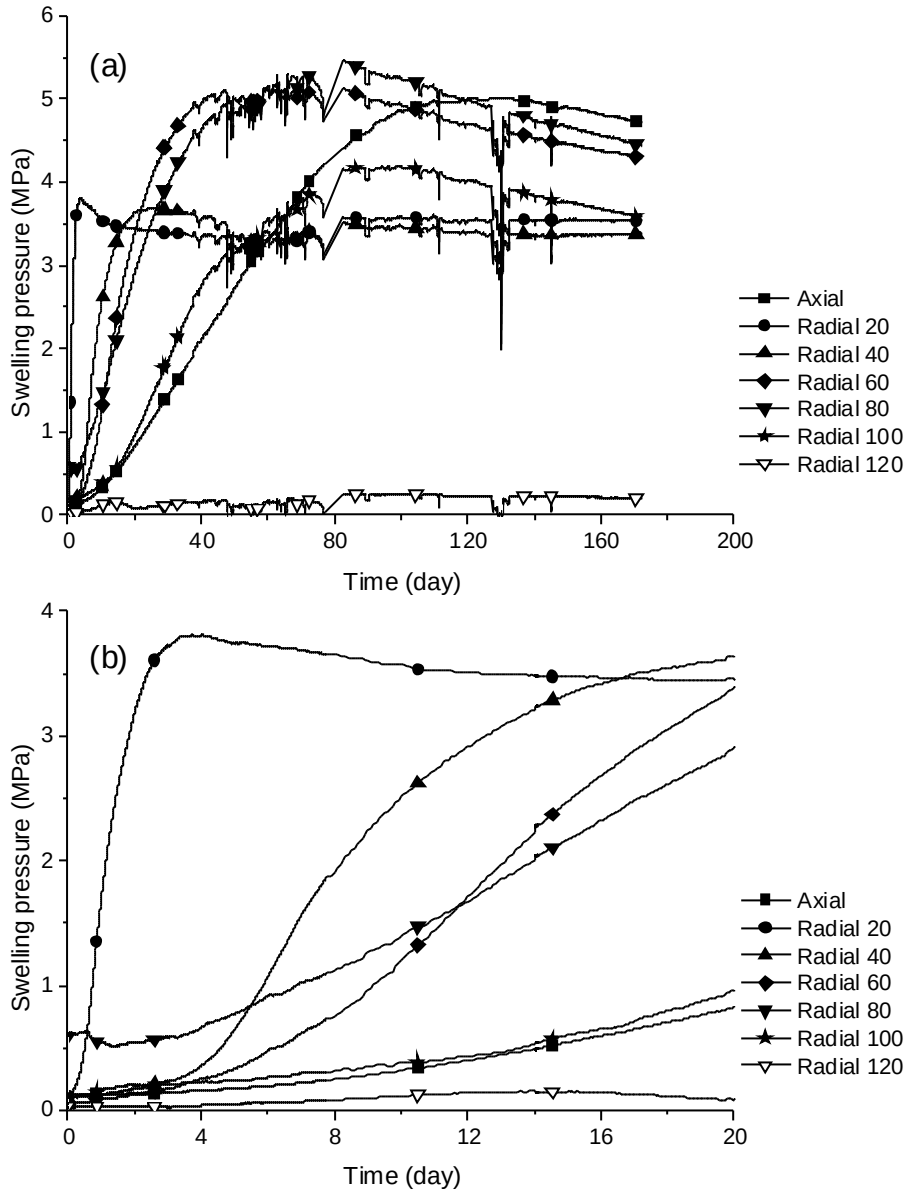


Figure 11. Swelling pressure development over time (a) with a zoom on the first 20 days (b).

The values at the end of the test were respectively 4.4 and 4.3 MPa. At 100 mm height, a lower increase rate was observed; a peak was reached at 4.2 MPa followed by a continuous decrease with a final value of 3.6 MPa. The axial swelling pressure curve presented the lowest initial increase rate; it reached a peak at around 5 MPa followed by a decrease at a rate similar to those for sensors PS60 and PS80. The axial swelling pressure measured by the force transducer then corresponds to that of the sample at the farthest position from the wetting

source; thus, its initial increase rate was found as expected to be the lowest. The swelling pressure values measured by the pressure sensors are compatible with those obtained by other authors on the same material: Karnland et al. (2008), Wang et al. (2012) also obtained a swelling pressure of 3.5 MPa for a bentonite/sand mixture compacted to 1.67 Mg/m^3 although they used different measurement techniques. Thereby, it can be concluded that the response of the used sensors is reliable regarding the final value (stabilisation value). As far as the kinetics of swelling pressure and more specifically the increase rate is concerned, it was expected that the initial increase was quicker when the measure was closer to the wetting face. In fact, during the infiltration test, water was progressively absorbed by the material and it took more time to reach the upper layers. This is similar to most infiltration tests where the recorded data is the relative humidity as in Wang et al. (2013b). The kinetics of relative humidity was found to be similar to the swelling pressure kinetics observed in the present work.

5.3 Volume of injected water

The volume of injected water that was monitored manually is presented versus time in Figure 12 together with the results reported by Wang et al. (2013a) in a similar test. A quick increase is observed at the beginning followed by a linear increase at a lower rate. The theoretical total volume corresponding to the fully saturated state of the sample is calculated as the volume of the total void in the sample: total volume – volume of solid – volume of existing water (w_b=13%). By considering a unit mass of 2.77 Mg/m^3 for bentonite and a unit mass of 2.65 Mg/m^3 for sand, it is found that this theoretical total volume is equal to 75 mL. Comparison between the curve obtained in this study and that reported by Wang et al. (2013a) shows that both curves are comparable except for the first increase that is higher in the case of Wang et al. (2013a). This can be explained by the presence of an annular technological void imposed in the test of Wang et al. (2013a).

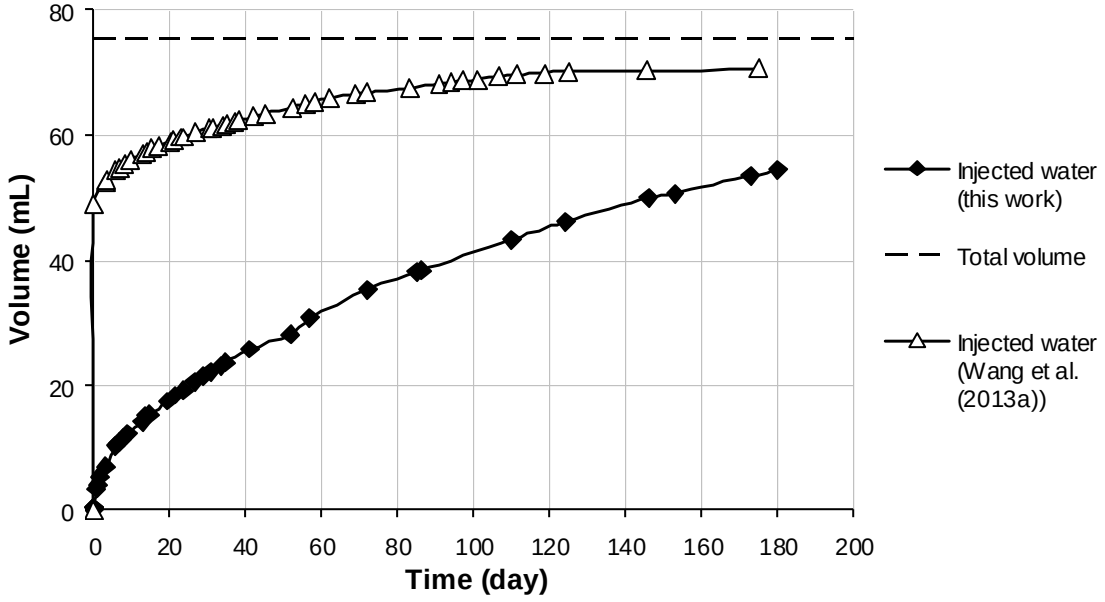


Figure 12. Evolution of the injected water volume over time in the present work and in Wang et al. (2013a).

6 Conclusion

This study describes an experimental setup designed to investigate the swelling behaviour of compacted sealing materials that could be used in the future French radioactive waste disposal. This setup is a Mock-up test at a 1/10 scale of the SEALEX in-situ experiments performed in the Tournemire underground research laboratory of the French Institute for Radiation Protection and Nuclear Safety (IRSN). The test consists in saturating the sample representing the seal under confined conditions and then, in monitoring the evolution of different parameters over time. The stainless steel rigid cell ensures the confined conditions in the radial direction, while the piston on the sample is blocked to ensure the confined conditions in the axial direction. The cell is equipped with three types of sensors: pressure sensors placed along the wall of the cell, allowing the radial swelling pressures at various heights to be monitored; a force transducer placed on the bottom of the cell, allowing the axial pressure to be monitored; a displacement transducer that measures the piston displacement. Validation of the cell was conducted through a test on a compacted MX80 bentonite/sand mixture. The sample was prepared by uni-axial compaction of the mixture powder at an initial dry density of 1.67 Mg/m^3. Sample saturation was processed from water inlets at the bottom and at the top of the sample. The volume of injected water was monitored manually by noting the level variation in the burettes. The results of swelling pressure shows a good correspondence with those reported in literature (Karnland et al., 2008; Wang et al., 2012; Saba et al., 2013). The injected water volume measured manually is compatible with that

reported by Wang et al. (2013a). The piston displacement recorded also falls in the range reported by Wang et al. (2013a). These observations show that the designed cell is suitable for testing compacted swelling materials with the monitoring of swelling pressures at different heights, both in radial and axial directions.

7 References

Agus, S., Schanz, T. 2005. Swelling pressures and wetting-drying curves of a highly compacted bentonite-sand mixture. Unsaturated Soils: Experimental Studies, pages 241–256.

Barnichon, J.D., Dick. P., & Deleruyelle, F. 2010. A sealing performance in situ experiments project (SEALEX): main objectives and expected outcomes, Clays in natural & Engineered Barriers for Radioactive Waste Confinement, 4th international meeting, march 2010, Nantes, France 261-262

Barnichon, J. D., Dick P. & Bauer C. 2012. The SEALEX in situ experiments: performance test of repository seals. Harmonising Rock Engineering and the Environment – Qian & Zhou (eds) Taylor & Francis Group, London, ISBN 978-0-415-80444-8, pages 1391-1394.

Cho, W. J., Lee, J. O. and Kang, C. H. 2000. Influence of temperature elevation on the sealing performance of a potential buffer material for a high-level radioactive waste repository, Ann. Nucl. Energy, 27, 1271–1284.

Cui, Y.J., Tang, A.M., Loiseau, C. & Delage, P. 2008. Determining the unsaturated hydraulic conductivity of a compacted sand-bentonite mixture under constant-volume and free-swell conditions. Physics and Chemistry of the Earth, Parts A/B/C, 33(Supplement 1):S462 – S471.

Delage, P., Howat, M.D., & Cui., Y.J. 1998. The relationship between suction and swelling properties in a heavily compacted unsaturated clay. Engineering Geology, 50(1-2), 31-48.

Karnland O., Nilsson U., Weber H. and Wersin P., 2008. Sealing ability of Wyoming bentonite pellets foreseen as buffer material - Laboratory results. Physics and Chemistry of the Earth (33) S472-S475.

Komine H. and Ogata N., 1994. Experimental study on swelling characteristics of compacted bentonite. Canadian geotechnical journal, 31(4):478–490.

Lee J.O., Lim J.G., Kang I.M. and Kwon S., 2012. Swelling pressures of compacted Ca-bentonite. Engineering Geology. doi: 10.1016/j.enggeo.2012.01.005

Loiseau, C., Cui, Y.J. & Delage, P. 2002. The gradient effect on the water flow through a compacted swelling soil. Proc. 3rd Int Conf Unsaturated Soils, UNSAT'2002 Recife, Brazil, Balkema, vol. 1, pp. 395-400.

Pusch, R., 1982. Mineral-water interactions and their influence on the physical behavior of highly compacted Na bentonite. Canadian Geotechnical Journal, 19(3):381–387.

Saba, S., Cui, Y.J., Tang, A.M., Barnichon, J.D. & Tran, T.P.H. submitted. Anisotropic swelling of compacted bentonite/sand mixture. Soils and Foundations.

Wang, Q., Tang, A. M., Cui, Y.J., Delage, P., & Gatmiri, B. 2012. Experimental study on the swelling behaviour of bentonite/claystone mixture, Engineering Geology, Vol. 124, 59–66.

Wang, Q., Tang, A. M., Cui, Y.J., Barnichon J.D. & Ye W.M. 2013a. A comparative study on

the hydro-mechanical behaviour of compacted bentonite/sand plug based on laboratory and field infiltration tests, Engineering Geology, Vol. 162, 79–87.

Wang, Q., Cui, Y.J., Tang, A. M., Barnichon, J. D., Saba, S. & Ye, W.M. 2013b. Hydraulic conductivity and microstructure changes of compacted bentonite/sand mixture during hydration. Engineering Geology, doi: 10.1016/j.enggeo.2013.06.013

Investigation of the swelling behaviour of compacted bentonite/sand mixture by mock-up tests

Simona Saba[1,2], Jean-Dominique Barnichon[2], Yu-Jun Cui[1] and Anh Minh Tang[1]

Abstract: The long-term behaviour of sealing plugs used in geological disposals of radioactive waste is investigated within the SEALEX project initiated by the French Institute for Radiation protection and Nuclear Safety (IRSN). Both in-situ large-scale and laboratory small-scale experiments were conducted for this purpose. This paper presents the laboratory results regarding the swelling behaviour of the sealing plug. The studied material is a compacted mixture of bentonite and sand. Two small-scale mock-up tests were carried out at a 1/10 scale of the in-situ experiments, one with saturation from the bottom only and the other with saturation from both top and bottom. Swelling pressure was monitored at different positions of the soil sample in both axial and radial directions. Results showed that the two-side saturation accelerates the swelling pressure kinetics by a time factor of 4. The radial swelling pressure kinetics depends on the infiltration lengths. Further analysis based on the relative humidity measurements conducted in an infiltration test performed previously showed that the variations of swelling pressure with suction are similar to those found in literature, and that threshold points exist indicating the initiation of soil collapse. These threshold points were found to appear at higher suction when the soil was farther from the wetting source. The failure of the axial confining elements in the storage galleries was also simulated in the mock-up test by releasing the piston and allowing a limited axial swelling of 20%. The radial swelling pressures were found to decrease sharply at the piston release and during the free axial swelling. A swelling pressure gradient was found from the bottom to the top with a higher value at the bottom. The density gradient was estimated based on the swelling pressure profile.

Keywords: bentonite/sand mixture; mock-up test; swelling pressure; threshold point; density profile; confinement failure.

1 Introduction

Highly compacted mixture with 70% bentonite and 30% sand in dry mass is one of the candidate materials for the sealing plugs used in deep radioactive waste disposal galleries. Upon contact with water, bentonite will swell, filling all voids in the storage system in particular the radial technological void between the sealing plug and the host-rock and the gaps between the blocks forming the plug. As a result, all possible fluxes around the galleries will be limited. After filling the voids, a swelling pressure should then develop radially against the host-rock and axially against the confinement elements that are placed at the back of the sealing plugs to prevent axial displacements.

The hydro-mechanical behaviour of different sealing materials has been studied in the past at both laboratory and field scales. The swelling behaviour of bentonite-based materials was

[1] Ecole des Ponts ParisTech, Laboratoire Navier, Marne La Vallée, France
[2] Institut de Radioprotection et de Sûreté Nucléaire, Fontenay-aux-Roses, France

studied in the laboratory by Komine and Ogata (1994), Agus and Schanz (2005), Karnland et al. (2008) and Wang et al. (2012, 2013a). It was found that the swelling pressure is governed by the dry density of bentonite. The hydraulic properties of these materials in unsaturated state were also studied and especially in terms of hydraulic conductivity (Loiseau et al., 2002; Cui et al., 2008; Ye et al., 2009; and Wang et al., 2013b). Very often, infiltration tests with relative humidity monitoring were carried out. It was observed that during infiltration in constant volume conditions, the unsaturated hydraulic conductivity decreases first and then increases after a certain suction threshold due to changes in microstructure.

Several studies on the hydro-mechanical behaviour of sealing materials have been conducted under field conditions in underground research laboratories (URLs) worldwide (FEBEX at Grimsel, Switzerland, RESEAL at Mol, Belgium, KEY at Bure, France, etc.). In parallel to the large-scale in situ tests, small-scale laboratory tests are often carried-out (small scale tests in CIEMAT laboratory linked to FEBEX, SB mock-up at GRS's Geotechnical Laboratory at Braunschweig, Ophelie mock-up by SCK.CEN/Euridice at Mol).

Recently, the French Institution for Radiation Protection and Nuclear Safety (IRSN) has launched in-situ tests within the SEALEX project in order to study the long-term performance of sealing plugs (Barnichon et al., 2010, 2012). In parallel to the SEALEX in situ experiments, small-scale laboratory tests have also been carried out aiming at providing useful information in terms of hydraulic and mechanical properties of the corresponding seals.

In this study, laboratory mock-up tests at a scale of 1/10 of the SEALEX experiments were performed with monitoring of swelling pressure at different positions of the soil sample. Two saturation processes were considered: saturation from the bottom side only was adopted in Mock-up 1 while saturation from both the top and bottom sides was adopted in Mock-up 2. The results obtained from both tests were compared in terms of swelling kinetics and possible effect of entrapped air. Moreover, the hydro-mechanical behaviour was further investigated by combining the swelling pressure from Mock-up 1 and the suction from an infiltration test performed by Wang et al. (2013b) on the same material.

Furthermore, in relation to the SEALEX experiments, the incidence of a failure of the confinement elements was also studied experimentally in terms of sealing capacity after the recovering of the void created by this failure. For this purpose, a 20% axial void was created in Mock-up 2 by releasing the piston. When this void was filled by soil swelling, development of the swelling pressure in the radial and axial directions was monitored. The profile of density was estimated from the swelling pressure measurements and then compared to the

density profile obtained after dismantling a previous similar mock-up test performed by Wang et al. (2013a).

2 Materials

The tests were performed on a compacted mixture of 70% (dry mass) Wyoming MX80 bentonite and 30% quartz sand from Eure and Loire (France). This MX80 bentonite has a liquid limit of 575%, a plastic limit of 53% and a unit mass of particles of 2.77 Mg/m^3. Its cation exchange capacity (CEC) is 76 meq/100g (83% of Na^+). The mixture was prepared by adding the sand grains (unit mass of 2.65 Mg/m^3) with the bentonite powder previously hydrated at a water content of 13%. The water used in the tests has the same chemical composition as the pore water of the Callovo-Oxfordian claystone from the ANDRA URL in Bure (see Wang et al., 2013b). It was prepared by mixing the corresponding chemical components with distilled water using a magnetic stirrer until full dissolution.

3 Experimental methods

3.1 Laboratory equipment

Figure 1 shows the layout of the small-scale infiltration cell (mock-up test cell) that is 1/10 of the in situ SEALEX experiments.

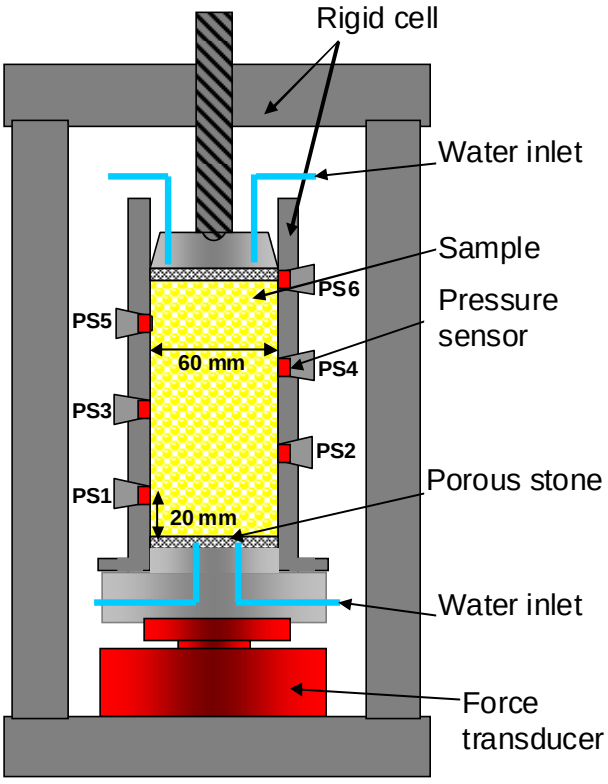


Figure 1. Layout of the mock-up test cell.

This cylindrical cell ensures confined saturation conditions for the material thanks to its rigid

structure that prevents any radial deformation and to a piston that is blocked by a screw preventing any axial displacement. The saturation of the material can be processed from the top (from the piston side) and/or from the bottom (the base) of the cell depending on the test configuration. The bottom base and the upper piston are each equipped by an inlet for water and an outlet for air. The body of the cell is equipped with six total pressure sensors (PS1 to PS6) measuring the radial swelling pressure at different heights of the sample (h = 20, 40, 60, 80, 100 and 120 mm from the bottom side) to be monitored. A force transducer is placed under the cell base that helps in monitoring the axial swelling pressure.

The suction values used for analysis were obtained by Wang et al. (2013b) using a relative humidity infiltration cell. This cell consists in a stainless steel cylinder that ensures the confined saturation conditions. The bottom base of the cell is equipped with a water inlet. Four relative humidity (RH) sensors (RH50, RH100, RH150 and RH200) are installed every 50 mm along the sample at 50, 100, 150 and 200 mm respectively from the wetting end (bottom).

3.2 Sample preparation and test procedure

All the soil specimens considered in this study (mock-up tests and relative humidity test by Wang et al., 2013b) were prepared by static uni-axial compaction at a rate of 0.1 mm/min to a maximum vertical stress of 13 MPa. This resulted in a mean dry density of 1.69 Mg/m^3 in Mock-up 1 and Mock-up 2 and 1.67 Mg/m^3 in the relative humidity infiltration test by Wang et al. (2013b). Specimens were compacted in 3 layers for the mock-up tests and in 5 layers for the relative humidity test in order to ensure the homogeneity of the specimens. During compaction, the surface of the compacted layer was scarified before the next layer was added in order to ensure a good junction between them. Compaction was done either in the test cell itself (case of the mock-up tests) or in a separate cylindrical mould having the same diameter as the testing cell (case of relative humidity test by Wang et al., 2013b).

To ensure a good contact between the sensors and the sample, an initial stress of 0.1 MPa was applied by screwing the sensors at a certain level in the cell. All the tests started from opening the water inlet valves. At the beginning of the tests, air in the base or in the piston was evacuated by opening the air outlet valve until no air bubble was observed in the tubes. Water was then injected either from the bottom only (Mock-up 1, relative humidity test) or from both the top and the bottom (Mock-up 2). The radial and axial pressures or the relative humidity were recorded automatically by a data logger.

In Mock-up 2, after the constant-volume saturation step, the piston was released by turning

the central screw up to 24 mm which corresponds to 20% of the initial height of the sample. The same procedure as in Wang et al. (2013a) was followed. The saturation process continued and the axial swelling and the radial swelling pressures were monitored until total filling of the void. Afterwards, the piston was blocked again by the central screw and the axial swelling pressure was monitored again. Figure 2 summarises all the three tests considered in this study with their respective configurations regarding saturation (one side or two side) and axial confinement (confined or released).

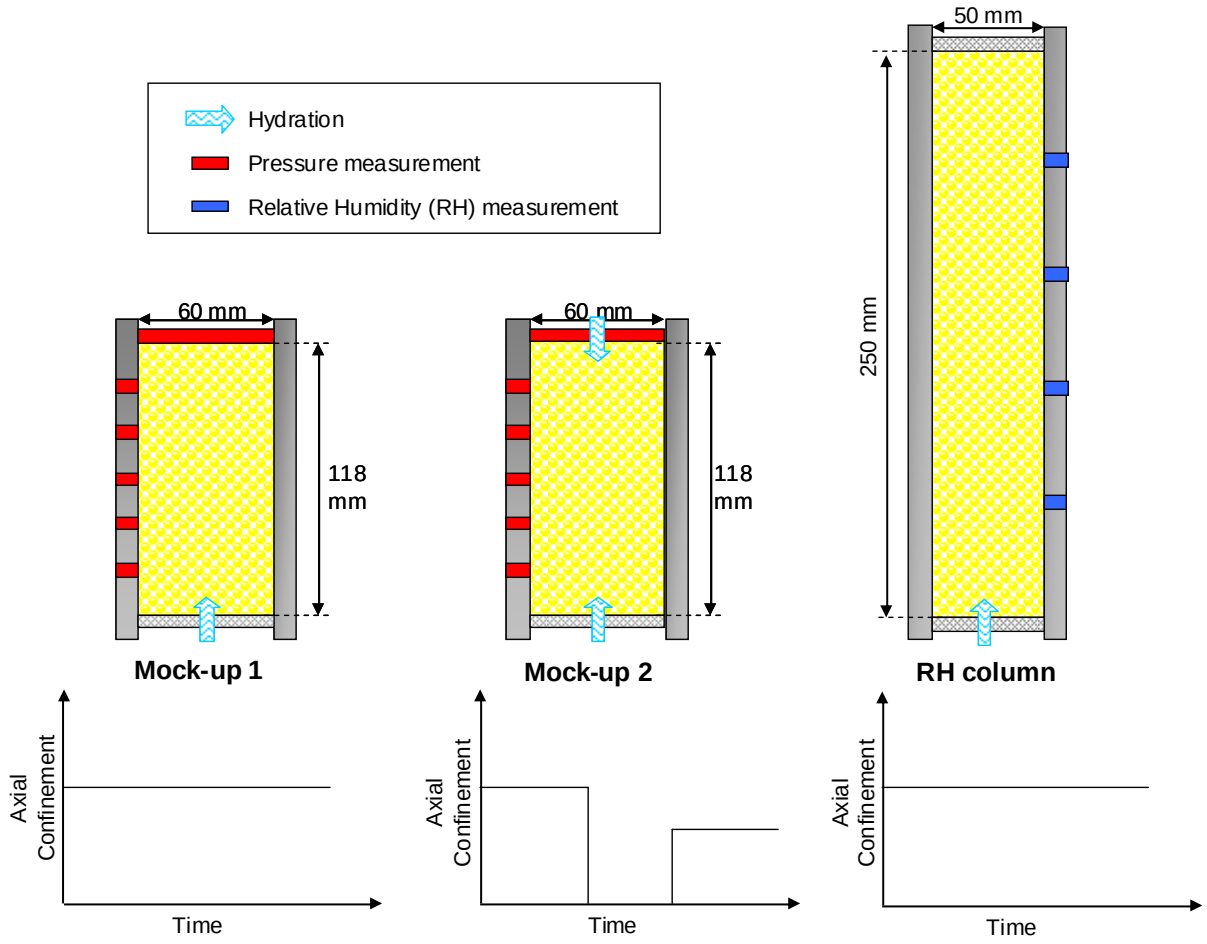


Figure 2. Schematic view of the three tests with their corresponding configurations regarding hydration and axial confinement

4 Mock-up tests

4.1 Mock-up 1

The evolution of swelling pressures is presented in Figure 3 with a zoom on the first 20 days. A first quick increase is observed for all curves. However, the rate of increase is different. A higher rate is found for the sensors located closer to the bottom of the sample, the highest rate being logically observed for sensor PS1 that is the closest to the wetting source. The curve corresponding to this sensor exhibits a first quick increase, reaching a peak value followed by a slight decrease and then a very slow increase to reach stabilisation at about 3.5 MPa. The

second highest increase rate corresponds to sensor PS2 with a swelling pressure evolution similar to that of PS1 except that it has a smoother peak. The curves relative to sensors PS3 and PS4 increase at similar initial rates in the beginning with a slightly higher rate for PS3. At 100 mm height, sensor PS5 records a lower increase rate.

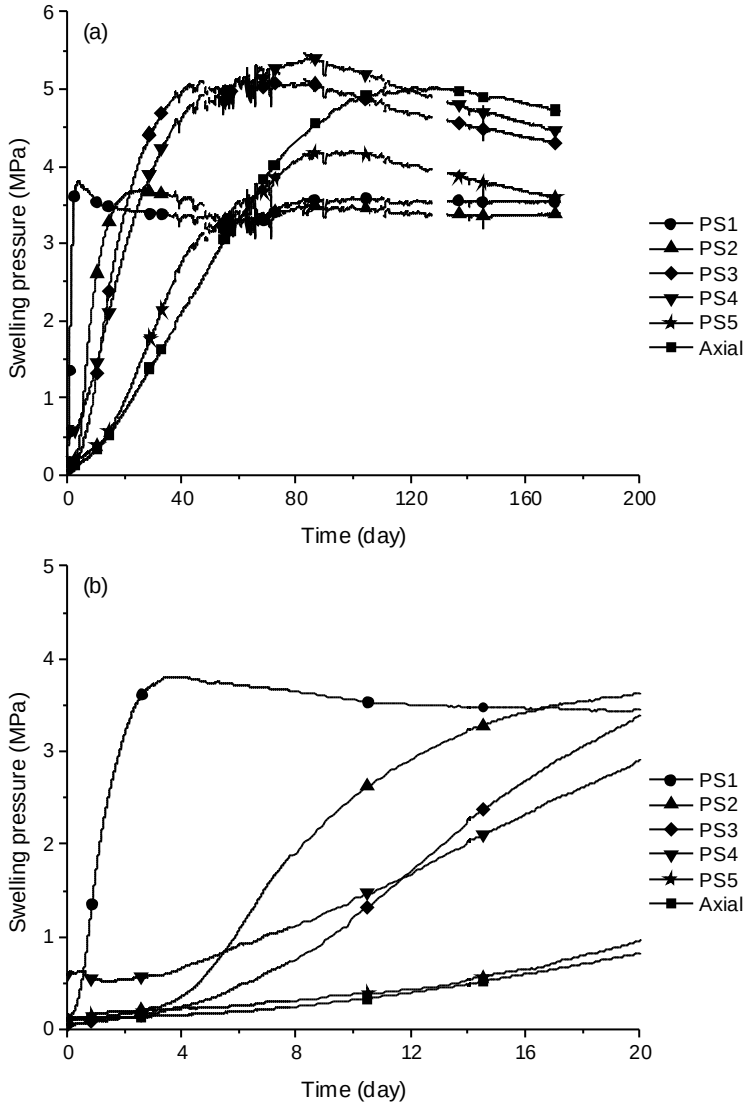


Figure 3. Swelling pressure evolution in Mock-up 1 (a) with a zoom on the first 20 days (b).

The axial swelling pressure curve shows the lowest initial increase rate. The axial swelling pressure measured by the force transducer corresponds to the global pressure transmitted to the piston. In fact, according to the cell design, and as shown in Figure 4, the swelling of the sample is transmitted to the blocked upper piston, and then the force is transmitted to the force transducer. When the sample is hydrated from the bottom (Mock-up 1), the lowest layers start swelling resulting in a friction with the cell's internal wall. The pressure being measured at the top, i.e. at the farthest position from the wetting source, its initial increase rate was found as expected to be the lowest. When the sample is also hydrated from the top (Mock-up 2), the

swelling of the upper layers is directly transmitted to the piston without the effect of friction (see Figure 4). When the sample is only hydrated from the bottom, as the measure is then done at the top, at the farthest position from the wetting source, its initial increase rate was found as expected to be the lowest. The peak occurrence order follows the same order as for the increase rate: the peak occurred later when the sensors were farther from the wetting end. The curves corresponding to sensors PS3, PS4, PS5 and the axial one exhibit smoother peaks with higher amplitude.

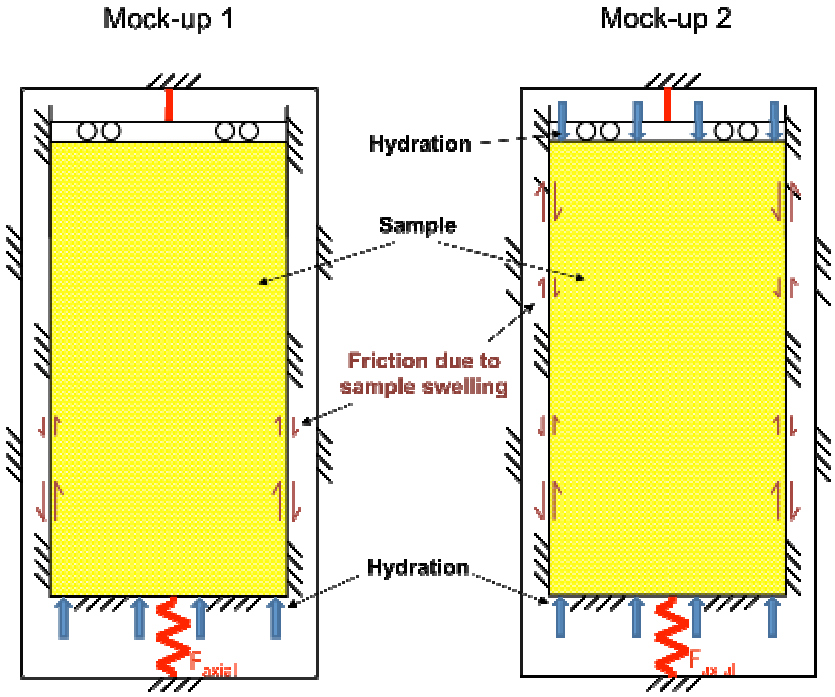


Figure 4 A simplified scheme of the mock-up tests with their hydration configuration, boundary conditions, and resulting frictions after swelling.

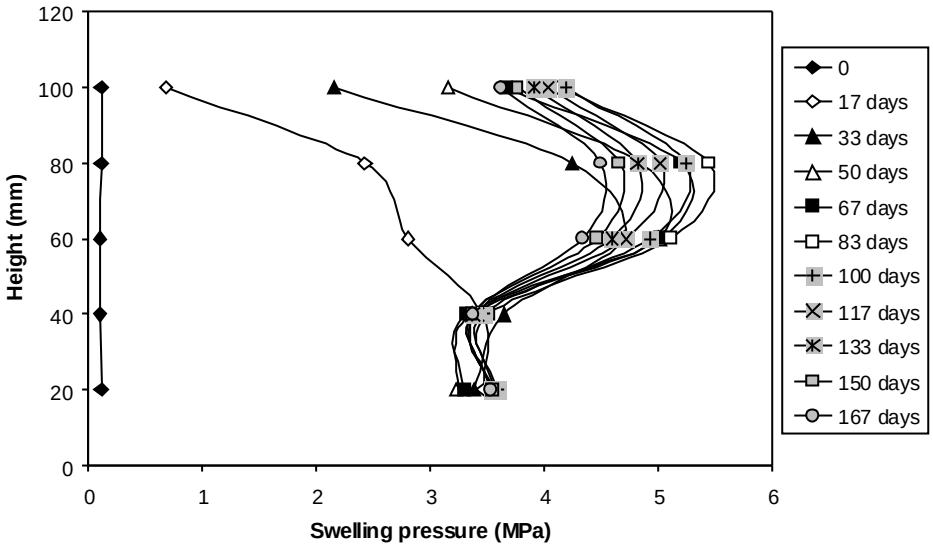


Figure 5 Swelling pressure profiles evolution at a time interval of 17 days from Mock-up 1.

Figure 5 presents the evolution of swelling pressure profiles in Mock-up 1 over 167 days,

with a time interval of 17 days. The initial swelling pressure profile is almost uniform, at a value around 100 kPa. It is observed again that the stabilisation of the swelling pressure is faster when the sensors positions are closer to the wetting source. Looking at the points located at 20 mm and 40 mm in Figure 5, from 17 days the points converge to a value between 3 and 4 MPa, while for the higher levels (60, 80 and 100 mm), the convergence is slower as indicated by the points of the 17-day curve which is not close to the other curves at 20 and 40 mm. We can also see that except for sensor PS5, the peak magnitudes are higher when the positions are farther from the wetting source.

4.2 Mock-up 2

Figure 6a shows the evolution curves of swelling pressure for different heights in the first step (confined saturation) of Mock-up 2. Note that the saturation was processed in this test from the two sides of the sample. On the whole, the swelling pressure presents a quick increase in the beginning and then reaches a peak followed by a stabilisation or a slight decrease.

Figure 6b shows the swelling pressure evolution during the first 6 days. It is observed that the initial swelling pressure values are around 100 kPa. As far as the first increase is concerned, Figure 6b shows that the initial increase rates are not the same and depend on the distance from the sensor to the closest wetting source (the infiltration length). In fact, the axial swelling pressure curve measured at the top of the sample (at 0 mm from the upper wetting source) has the highest increase rate, followed by the curves of sensors PS1 and PS5 situated respectively at 20 mm from the bottom wetting source and at 18 mm from the top wetting source (piston). Then comes the increase rates of the curves of sensors RS40 and RS80 situated respectively at 40 mm from the bottom wetting source and at 38 mm from the top wetting source (piston). The curve corresponding to sensor PS3 starts with a higher swelling pressure value but its increase rate is the lowest. This sensor (PS3) is situated almost in the middle of the sample: at 60 mm from the bottom end and 58 mm from the top end.

The occurrence order of peaks shown in Figure 6a also follows the same order as for the increase rates, with peaks occurring later when the measurements are taken farther from the wetting end. If we admit that the final state was reached at 60 days, the final swelling pressure stabilisation values range from 2.5 MPa to 3.8 MPa. The axial swelling pressure curve reaches the highest final value of 3.7 MPa; a lower final value is obtained for sensors PS1 and PS5 (3.3 MPa). A similar value is found for sensor PS3 but its corresponding curve shows a clear decreasing trend. Sensor PS2 shows a value of 2.9 MPa and sensor PS4 gives the lowest one: 2.5 MPa.

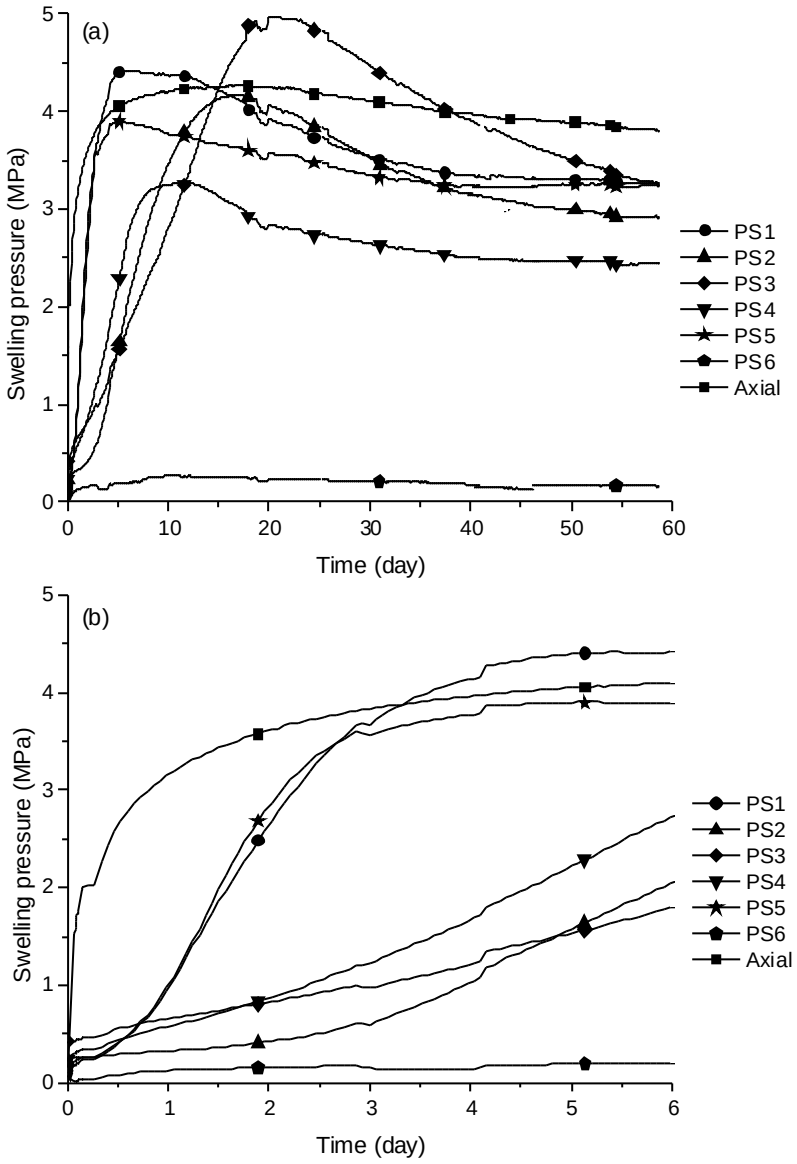


Figure 6. Swelling pressure evolution during the first step of Mock-up 2 (a) with a zoom on the first 6 days (b).

4.3 Comparative analysis and discussion

We can conclude from the two Mock-up tests that, at a position closer to the wetting source, the swelling pressure increases faster and reaches a peak earlier. Basically, the peak occurrence is linked to the collapse of macropores (inter-aggregates pores) of the compacted sample. Compacted bentonite has a complex microstructure (Pusch, 1982; Mitchell, 1993; Kröhn, 2003): parallel platelets form the bentonite particle that, combined with other particles can form the bentonite aggregate or the bentonite grain. These bentonite grains are compacted together with the sand grains to form the sample. Consequently, three types of pores exist in the sample: the pores between the platelets intra-particles, the pores between the bentonite particles (intra-aggregate) and the pores between the bentonite grains and the sand grains after

compaction (inter-aggregate). When the saturation starts, the parts closer to the wetting face undergo hydration in liquid phase resulting in swelling and exfoliation of the bentonite grains. More explicitly, the aggregates swell and at the same time exfoliate (get disaggregated), and the exfoliated parts fill the inter-aggregate macro-pores. If the swelling of aggregates gives rise to swelling pressure increase, it is not the case for the exfoliation. Indeed, exfoliation rather decreases the swelling pressure. At a macroscopic level, the exfoliation can be assimilated to collapse of macro-pores.

For the positions far from the wetting source, saturation will start by vapour phase. In this case, the phenomenon of exfoliation is expected to take place in a longer time and the overall swelling of bentonite grains prevails. This explains the different times for the occurrence of peaks, quicker for the positions closer to the wetting face. This also explains the magnitudes of peaks that are higher for the positions farther from the wetting source because the prevailing swelling of aggregates at short term and the later arrival of collapse (except for sensor PS5 that exhibits a low peak magnitude). As mentioned previously, the peak occurrence time corresponds to the water infiltration time, which depends on the infiltration length.

Figure 7 shows the swelling pressure evolution curves for sensors PS1 and PS2 in Mock-up 1 and sensors PS1, PS2, PS4 and PS5 in Mock-up 2, along with the axial swelling pressure curve from Mock-up 2. These curves correspond to infiltration lengths between 0 and 40 mm from the closest wetting end in both tests. The curve with the highest first increase rate corresponds to the axial swelling pressure curve at 0 mm distance from the upper wetting end. The stabilised value of this curve is also the highest, at about 4 MPa. The curves corresponding to infiltration lengths around 20 mm (PS1-1 in Mock-up 1, PS1-2 and PS5-2 in Mock-up 2) have very close initial increase rates with a slightly higher rate for sensor PS1-1. The peak occurrence times for these three curves are also close. Moreover, all the three curves stabilise at about 3.5 MPa. The next higher increase rate corresponds to the curve of sensor PS4-2 situated at 38 mm from the upper wetting end, and the curves of sensor PS2-2 and PS2-1 situated at 40 mm from the bottom of the sample. These three curves correspond to almost the same infiltration length and as a result, exhibit similar kinetics. Nevertheless, at the current stage their final values are different.

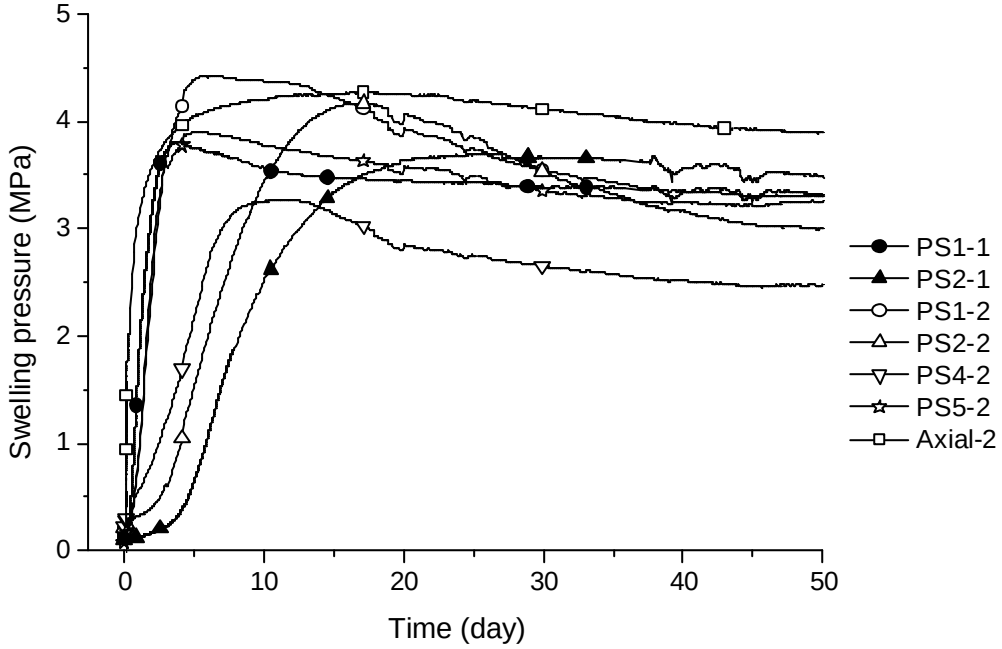


Figure 7. Swelling pressure evolution curves in Mock-up 1 and Mock-up 2 for infiltration lengths less than 40 mm.

Figure 8 shows the axial swelling pressure curve along with the curves corresponding to sensors PS3 and PS5 in Mock-up 1 and the axial swelling pressure curve as well as that corresponding to PS3 and PS-4 in Mock-up 2. If we compare the curves corresponding to sensor PS3 situated at the middle height of the sample from Mock-up 1 and Mock-up 2, we can conclude that the first increase is faster when the saturation is processed from two sides (Mock-up 2). Consequently, the peak occurrence time is shorter in the case of Mock-up 2 but the peak magnitudes are similar. The peak occurrence time ratio is equal to 3 as 60 divided by 20 (corresponding to curves PS3-1 and PS3-2 in Figure 8). Normally, with two-side saturation, the infiltration length is reduced by half which should divide the time ratio by 4 based on the theory of soil consolidation. The theoretical time ratio obtained is 4, to be compared with the value of 3 obtained in the test.

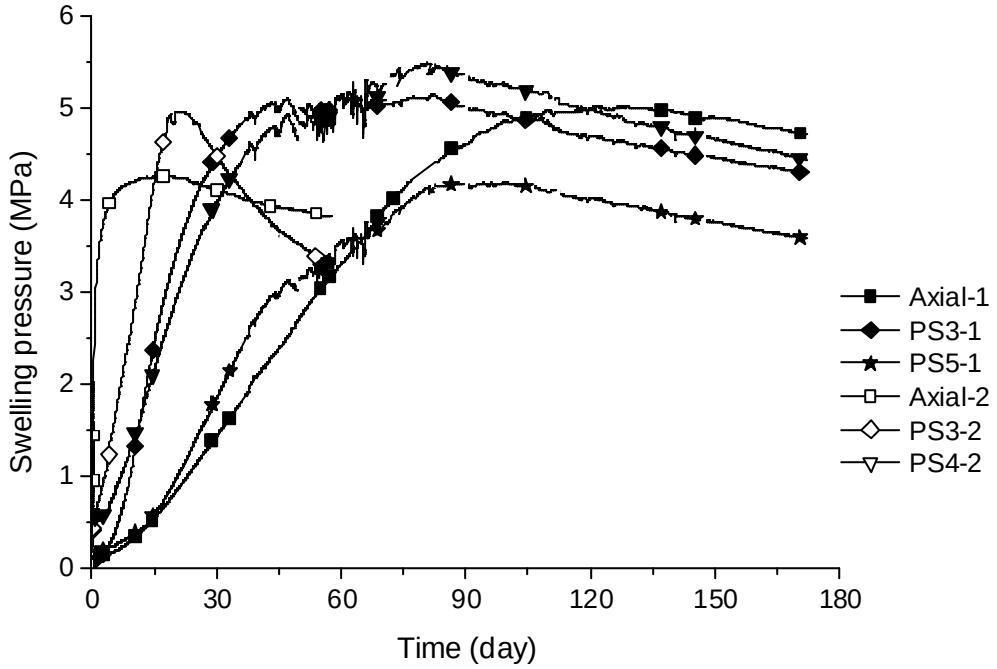


Figure 8. Swelling pressure evolution curves in Mock-up 1 and Mock-up2 for infiltration lengths larger than 60 mm, and with the axial swelling pressure development in both tests.

When comparing the development of the axial swelling pressure between Mock-up 1 and Mock-up 2, we can see that the first increase rate in Mock-up 2 is largely higher than in Mock-up 1 and consequently the peak occurrence time is smaller. In fact, the axial swelling pressure measurement corresponds to the swelling pressure in the upper end of the sample, thus, in Mock-up 1 it corresponds to an infiltration length of 100 mm while in Mock-up 2 it corresponds to 0 mm. This large difference in infiltration length results in a large difference in the first increase rate and in the peak occurrence time. In Mock-up 1, swelling started in the lower layers of the sample but was measured on the top of the sample; the resulting friction on the internal surface of the cell should then be taken into account when considering the axial swelling pressure measurement. On the contrary, in Mock-up 2, the axial swelling pressure measurement was done directly for the swelling upper layers being saturated from the top. The effect of friction was then negligible as compared to the case of Mock-up 1. Thus, when comparing the two axial swelling pressure curves, the effect of friction in Mock-up 1 should be taken into account at the beginning but this effect should decrease with hydration of upper layers that are close to the force sensor measuring axial swelling pressure. Thereby, theoretically the axial swelling pressures should be the same in the two tests after a long time when the samples are fully saturated.

In order to compare the swelling kinetics in Mock-up 1 and Mock-up 2, the same boundary

conditions should be considered. Figure 10 presents the sketches of Mock-up 1 and Mock-up 2 with their corresponding boundary conditions: in Mock-up 1 a water flow is permitted from the bottom and no water flow from the top. In Mock-up 2, water flow exists from the top and the bottom of the sample which reveals the existence of a symmetry plan in the middle of the sample, at 60 mm from both sides.

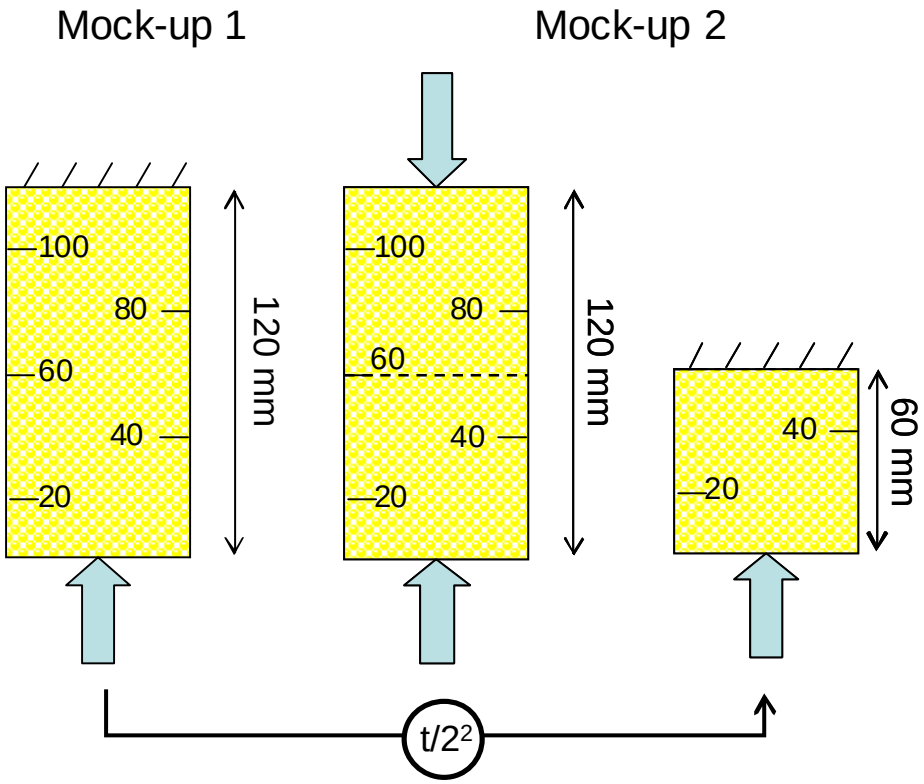


Figure 9. Sketch of the samples with their respective boundary conditions in both tests and after considering the symmetry plan in Mock-up 2.

At this symmetry plan, no water flow can take place. Thereby, if we only consider the lower middle part of the Mock-up 2 sample, we can say that it has the same boundary conditions as Mock-up 1. The comparison can now be done between Mock-up 1 with a length of 120 mm and Mock-up 2 having the same boundary conditions but a length of 60 mm. According to the theory of soil consolidation, the time ratio should be equal to the square of the infiltration length ratio: in this case, the time ratio should be equal to the square of 2 which is 4. To verify this point, let us first compare the measurements at the place with zero water flow: that consists in comparing the axial swelling pressure measurement in Mock-up 1 (at 120 mm) and the PS3 sensor in Mock-up 2 (at 60 mm). Figure 10 shows the comparison between these two curves while dividing the time scale in Mock-up 1 by 4. We can see that the first increase rates are similar; however, the peak occurrence times are slightly different.

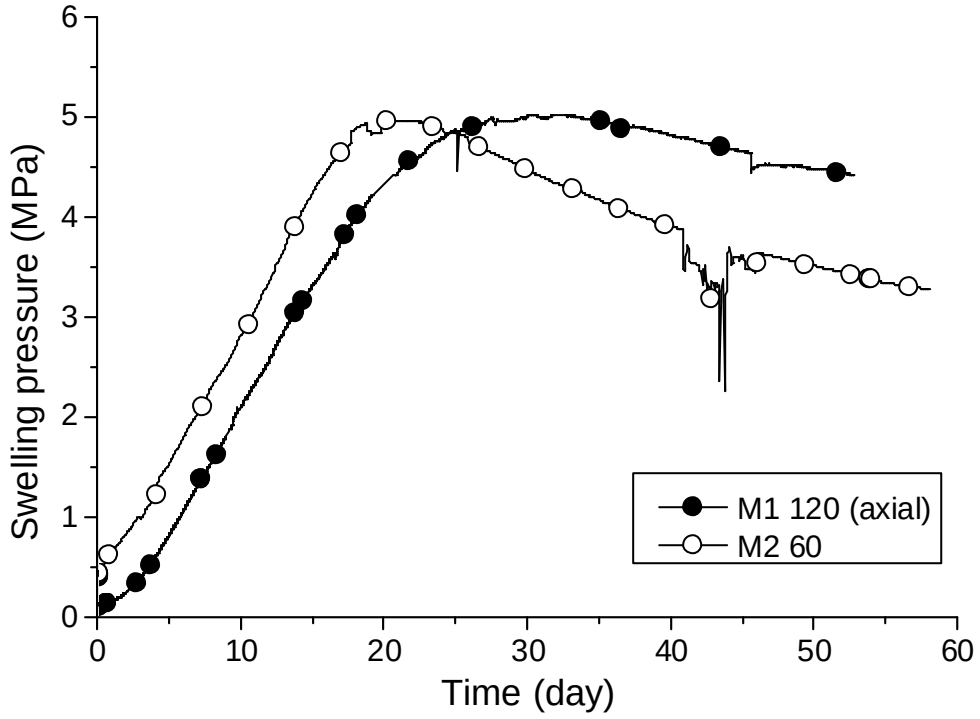


Figure 10. Comparison of the swelling pressure kinetics between Mock-up 1 and Mock-up 2 at the place with zero water flow: at 120 mm from the bottom in Mock-up 1 and at 60 mm in Mock-up 2.

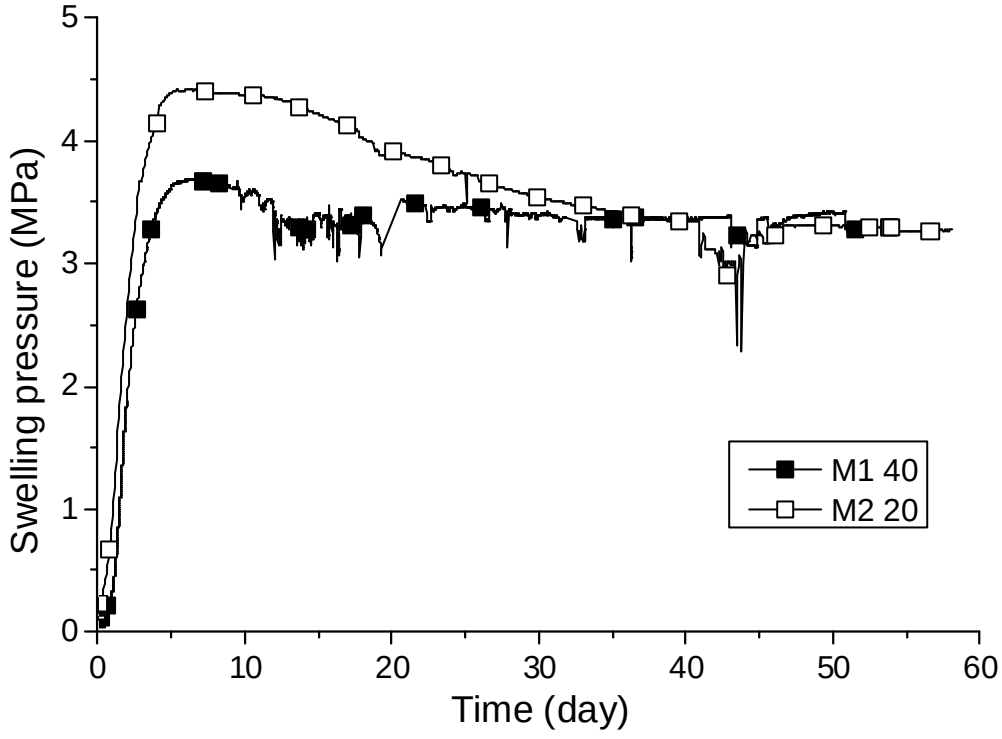


Figure 11. Comparison of the swelling pressure kinetics between Mock-up 1 and Mock-up 2 at 1/3 from the bottom of the sample: at 40 mm in Mock-up 1 and at 20 mm in Mock-up 2.

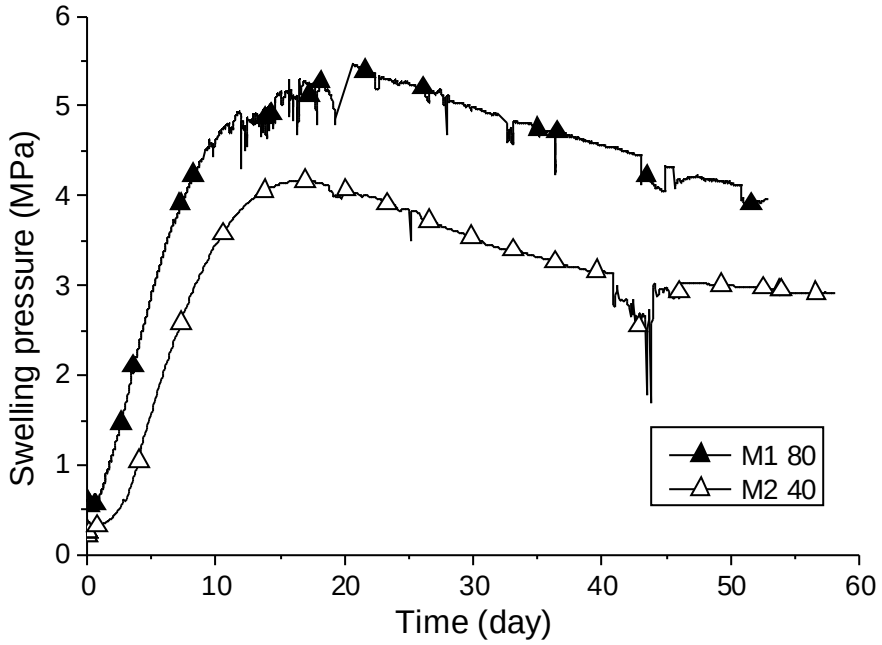


Figure 12. Comparison of the swelling pressure kinetics between Mock-up 1 and Mock-up 2 at 2/3 from the bottom of the sample: at 80 mm in Mock-up 1 and at 40 mm in Mock-up 2.

Another comparison is done for the same length ratio from the bottom (wetting source) of the sample in Mock-up 1 (total length = 120 mm) and Mock-up 2 (total length = 60 mm). This comparison involves sensor PS2 (at 1/3 of the length = 40 mm) in Mock-up 1 and sensor PS1 (at 1/3 of length = 20 mm) in Mock-up 2. The corresponding swelling pressure curves are presented in Figure 11. We can see that the curves are in good agreement with very similar first increase rates, similar peak occurrence times and also similar final swelling pressure values. Figure 12 shows the comparison between sensors PS4 in Mock-up 1 (at 2/3 of the sample's length = 80 mm) and PS2 in Mock-up 2 (at 2/3 of the sample's length = 40 mm). We can see that the curves have similar first increase rates, similar peak occurrence times but slightly different swelling pressure values.

One important concern in the test with saturation by two sides comes from the possible effect of entrapped air. This can be verified in the case of Mock-up 2 where two-side saturation was processed and air contained in the pores could be entrapped within the sample. If this happens, the entrapped air will prevent water to infiltrate further toward the centre of the sample. Consequently, the soil will remain unsaturated and there will not be a fast swelling pressure increase. However, we can see from Figures 10, 11 and 12 that a good correspondence is found between Mock-up 1 and Mock-up 2 while considering a factor of 4 which can confirm that air was not entrapped. Note that several days after the start of Mock-up 2, water was blocked in the hose from the burette as air was noticed in the hose. This indicated the presence of entrapped air in the bottom even though this part was saturated at

the beginning of the test by evacuating all air. When entrapped air was noticed, it was necessary to open the air outlet during the test to let air be evacuated. Afterwards, the valve was closed and water circulated again at the entrance hose. The same evacuation procedure was also done from the top (from the piston). This suggests that during the test, air was not entrapped in the sample, and instead, it went out of the sample by diffusion through the saturated part of sample.

5 Swelling pressure versus suction

In the work of Wang et al. (2013b), the same bentonite/sand mixture was tested and the sample was prepared by compaction to a similar dry density. Figure 13 shows the two tests with all their measurement points. The swelling pressure measurements in Mock-up 1 are given at the infiltration lengths of 20, 40, 60, 80 and 100 mm. In order to obtain the relationship between swelling pressure and suction, suction values at these same infiltration lengths should be estimated. For this purpose, the relative humidity at 20 and 40 mm are determined by linear interpolation between the value given by sensor RH50 and the value at the bottom (0 mm height) assumed to be 100%. In the same manner, the relative humidity at 60 and 80 mm are determined by linear interpolation of the measurements given by sensors RH50 and RH100; the relative humidity at 118 mm is determined from the measurements of RH100 and RH150. Note that the level of 118 mm corresponds to the level where the axial swelling pressure was measured. Knowing the relative humidity, the total suction can be calculated using Kelvin's law.

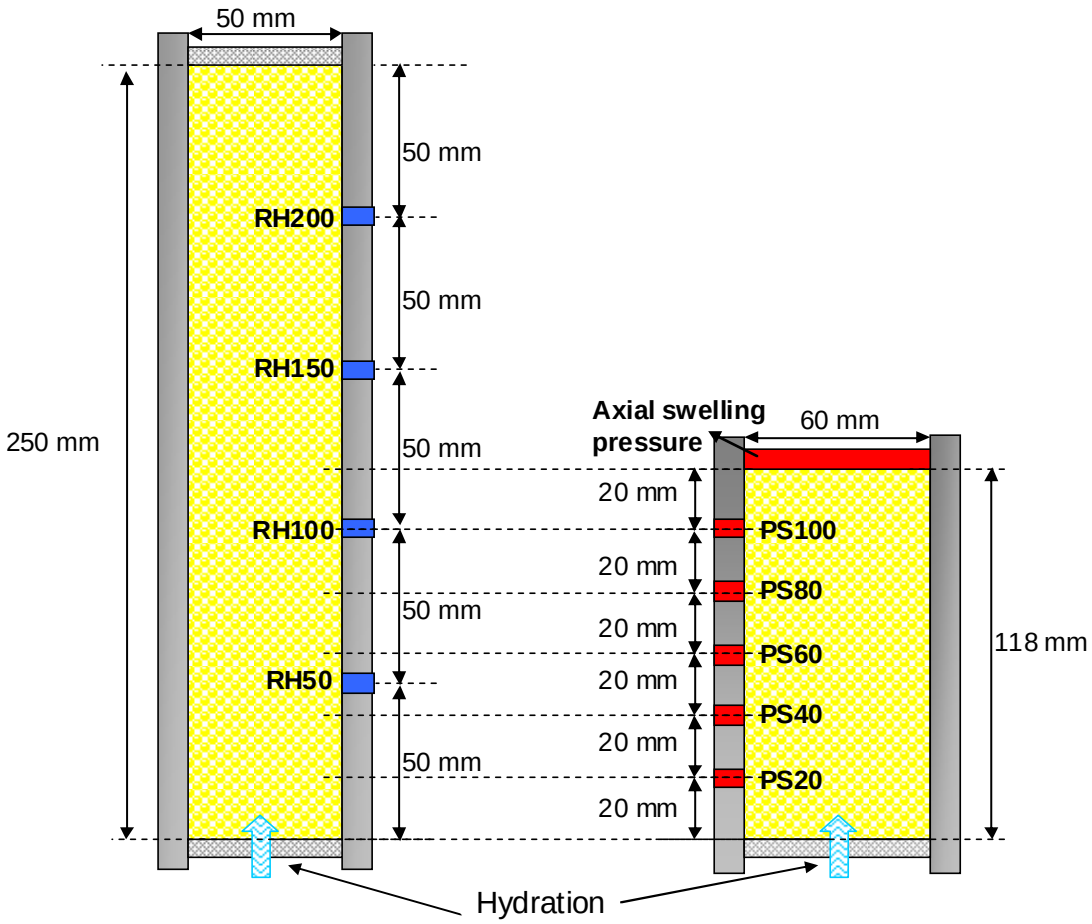


Figure 13. Positions for relative humidity and swelling pressure measurements in the relative humidity infiltration test and Mock-up1, respectively.

Figure 14 shows the suction profiles obtained by plotting the suction values corresponding to the same heights considered in Mock-up 1. It is observed that the initial suction is 64 MPa everywhere and as the test proceeds, suction decreases due to the saturation progress. The suction decreases faster at the bottom of the sample near the wetting source.

Figure 15 is obtained by plotting the corresponding values of swelling pressure (from Figure 5) and suction (Figure 10), the different curves corresponding to the different distances to the wetting source. The starting point is almost the same for all the curves and corresponds to the initial suction of 64 MPa and initial swelling pressure of 100 kPa. The overall evolution of the curves is similar to that obtained in a previous work by Lloret et al. (2003), with a suction decrease and an increase followed by a decrease of swelling pressure. The points where the slopes change or the swelling pressures start to decrease are referred to as the "yield point or pre-consolidation stress" in Lloret et al. (2003), and they correspond to the peaks identified in Mock-up 1.

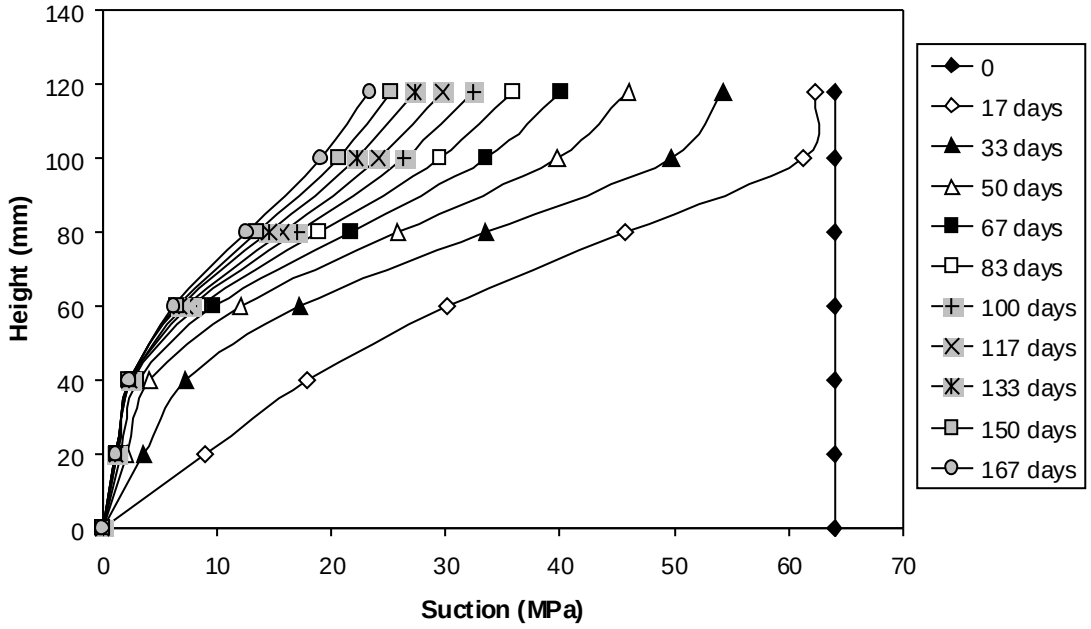


Figure 14. Suction profiles evolution at a time interval of 17 days from the relative humidity infiltration test (Wang et al., 2013b).

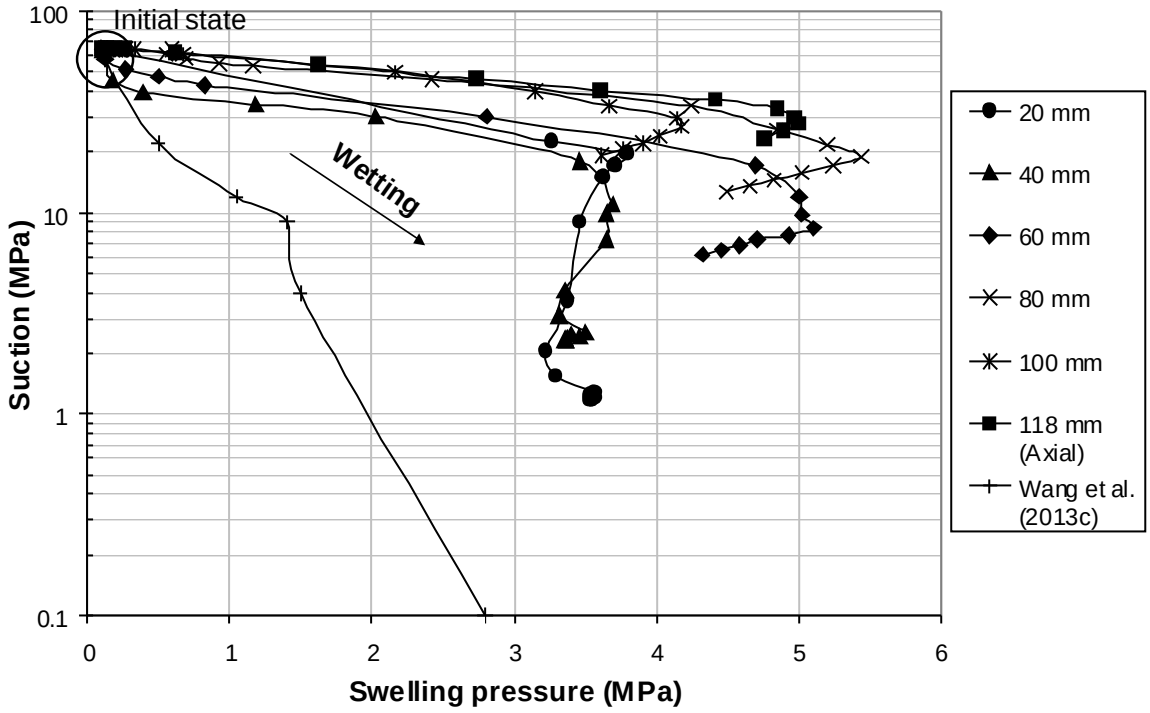


Figure 15. Suction versus swelling pressure for different infiltration lengths.

Some observations can be made from this figure:

1) Starting from the initial state, the suction decreases faster when closer to the wetting source. In other words, the first slope is higher near the wetting source. The swelling pressure increase takes place at higher suctions in the upper layers farther from the wetting source. This suggests that the upper layers are hydrated by vapour (high suctions) as opposed to the

bottom layers.

2) The point of slope change, "yield point or peak", is reached at higher suctions for higher heights (far from the wetting source). For instance, two groups are identified: one for 20, 40 and 60 mm height and the second for 80, 100 and 118 mm height, and with peaks reached at higher suctions for the second group. This may be explained as follows:

i) As it was stated in the previous paragraph, the upper layers were mainly hydrated by vapour phase and the peaks were then reached at higher suctions, suggesting that the peak was reached when the soil swelling is exceeded by soil exfoliation.

ii) If we consider the stress path that the soil was undergoing and the Loading-Collapse (LC) curve defined by Alonso et al. (2005) in the BExM model, the layers from the wetting source (the upper layers) were pre-stressed because of the earlier swelling of the bottom layers. As a result, when they are later saturated, they reached the LC curve at higher suctions than those corresponding to non-pre-stressed layers (the bottom layers).

Figure 15 also shows the results obtained by Wang et al. (2013c) from swelling pressure tests on different samples hydrated by vapour phase at different suctions. The curve obtained from results of Wang et al. (2013c) has an initial slope higher than the curve corresponding to 20 mm height. The corresponding yield point is present at low suction (around 9 MPa). This suggests that the results of Wang et al. (2013c) correspond better to those near the wetting source. This could be the effect of dimensions because the tests performed by Wang et al. (2013c) have a thickness of 10 mm (comparable with the first layer in the mock-up test at 20 mm). At this size, equilibrium was reached much faster. This is quite different from the situation for the top layers in Mock-up 1.

6 Simulation of confinement failure in Mock-up 2

In the second step of Mock-up 2, we tended to reproduce the failure of the confining elements in the axial direction. It consisted in releasing the piston by turning up the blocking screw. The swelling was not prevented anymore and a free axial swelling took place. A total of 20% axial gap was created for this purpose, as in the SEALEX in situ tests. Figure 16 shows the swelling pressure evolution before and after the piston release. A zoom around the piston release is presented in Figure 17. The sudden decrease in swelling pressure is clearly observed especially for the axial swelling pressure that dropped to zero. The radial swelling pressures exhibited a gradient with the maximum value for the lowest soil layer at 20 mm height (PS1), followed by those at 40 mm height (PS2), at 60 mm (PS3), at 80 mm (PS4) and finally at

100 mm (PS5).

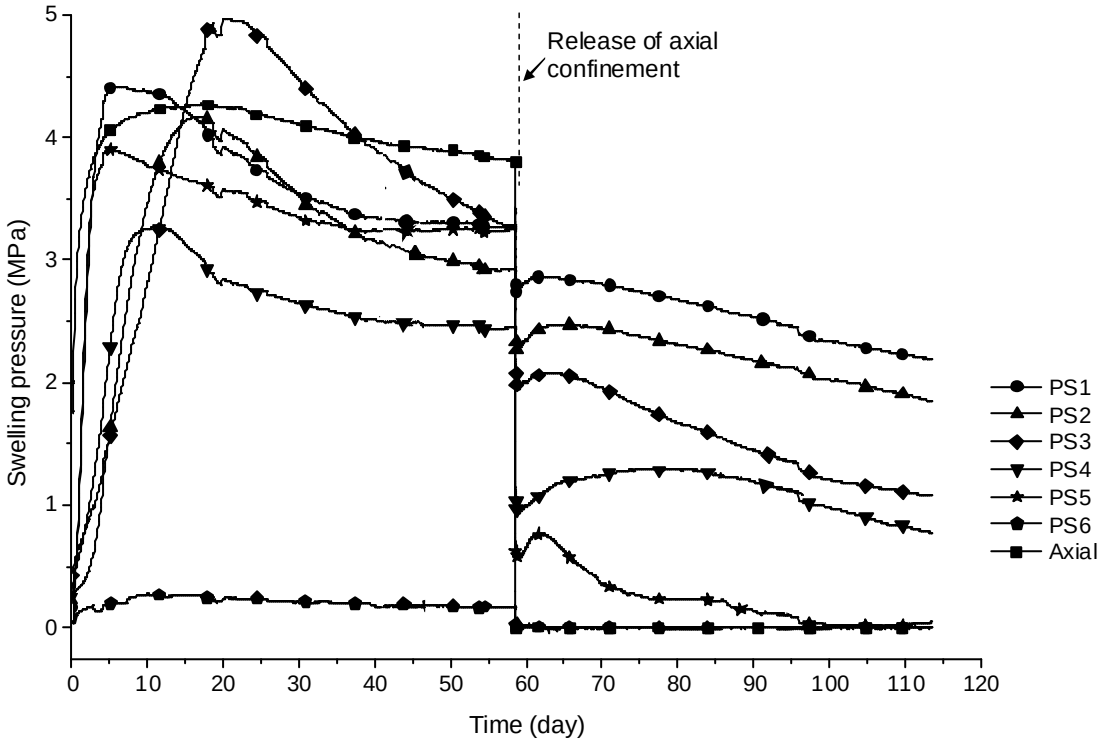


Figure 16. Overall evolution of swelling pressure during step 1 and the current stage of step 2 of Mock-up 2.

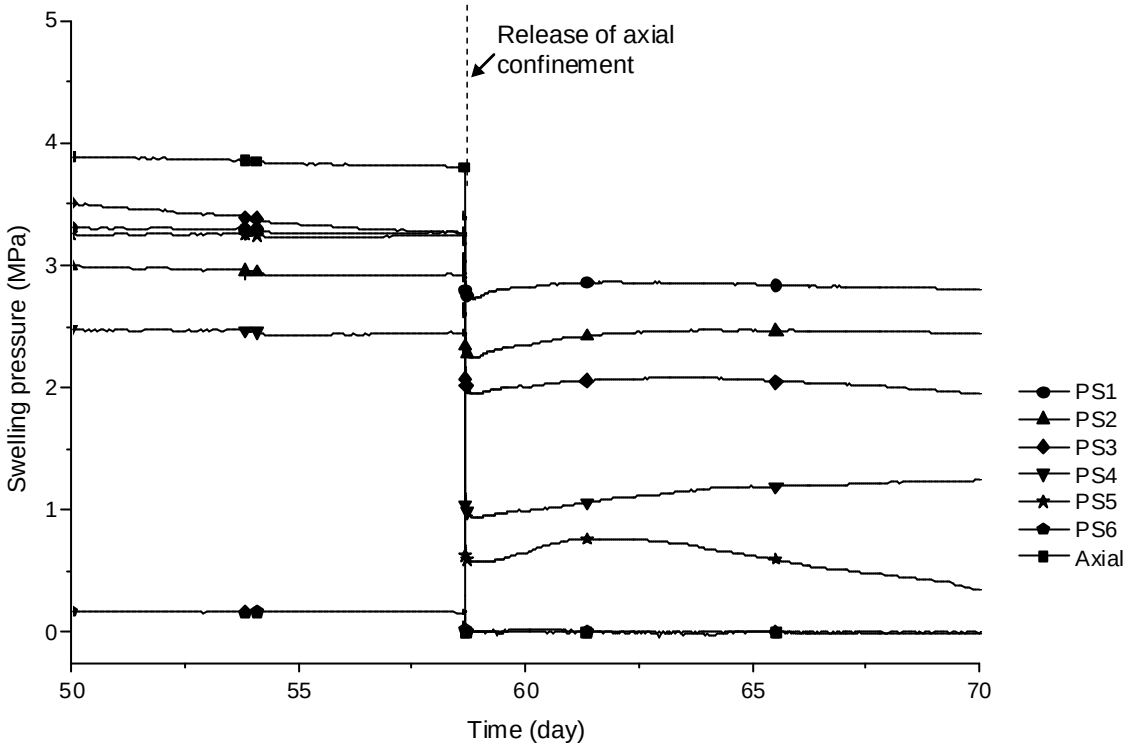


Figure 17. Zoom on the transition phase between step 1 and step 2 (axial confinement release) of Mock-up 2.

Zero swelling pressure was measured at 120 mm (PS6). Note that sensor PS6 was not in

contact with the sample in the first step of the test before the piston release. The piston release allowed axial swelling, thus the material started swelling and it progressively reached sensor PS6. From that moment, sensor PS6 started recording swelling pressure. Sensor PS5 showed a first drop in swelling pressure, followed by a slight increase and a decrease again to finally reach zero. The same kinetics is observed for sensors PS4, PS3, PS2 and PS1. In fact, when the confinement was released from the top, the top layers started swelling relatively freely resulting in a reduction in their density and a reduction in their swelling pressure. The small increase after the first drop may be due to the confinement release corresponding to an unloading process. The bottom layers could not swell freely due to the effects of the upper layers and the friction between the sample and the cell wall. A density gradient was then produced in the axial direction along the sample. Obviously, as saturation proceeded, this density gradient evolved and equilibrium can be expected at long-term, which should lead to a homogeneous sample.

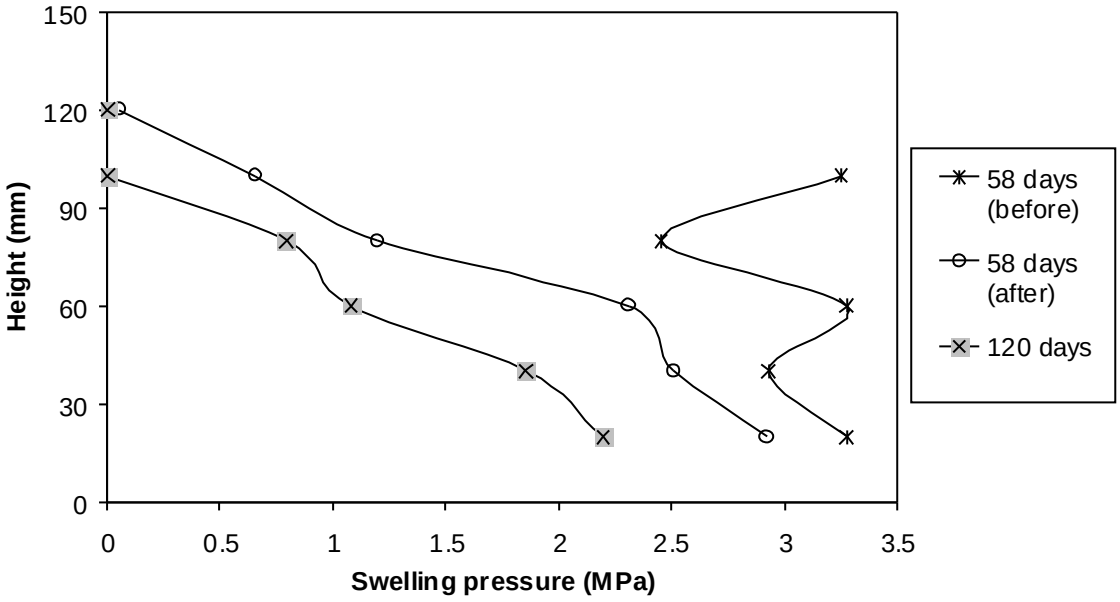


Figure 18. Swelling pressure profiles at the start of step 2 (at 58 days, just before and after the piston release) and at the current stage of test (at 120 days).

Figure 18 shows the swelling pressure profiles corresponding to the moments before and after piston release (at 58 days). The last available measurements after the piston release (120 days) are also shown in this figure. It is observed again that, after the release, the top layers exhibited zero swelling pressure after the free swelling, and the bottom layers exhibited a slight decrease.

Karnland et al. (2008) evidenced that an exponential relationship exists between the effective dry density of MX80 bentonite and the final swelling pressure, as follows:

$$\sigma_s = 0.0002 \exp(6.7486 \rho_{db}) \quad (1)$$

This relationship was confirmed by Saba et al. (2013) for the same bentonite but with slightly modified parameters:

$$\sigma_s = 0.0013 \exp(5.1053 \rho_{db}) \quad (2)$$

where σ_s is the swelling pressure in MPa and ρ_{db} is the effective dry density of bentonite in Mg/m^3. The relationship between the dry density and the effective dry density of bentonite is as follows.

$$\rho_d = \frac{\rho_{db}}{(\frac{(1-B)\times\rho_{db}}{G_{ss}}) + B} \quad (3)$$

where ρ_d is the dry density, ρ_{db} is the effective dry density of bentonite, B is the mass fraction of bentonite in the mixture (70% in this study) and G_{ss} is the specific gravity of sand.

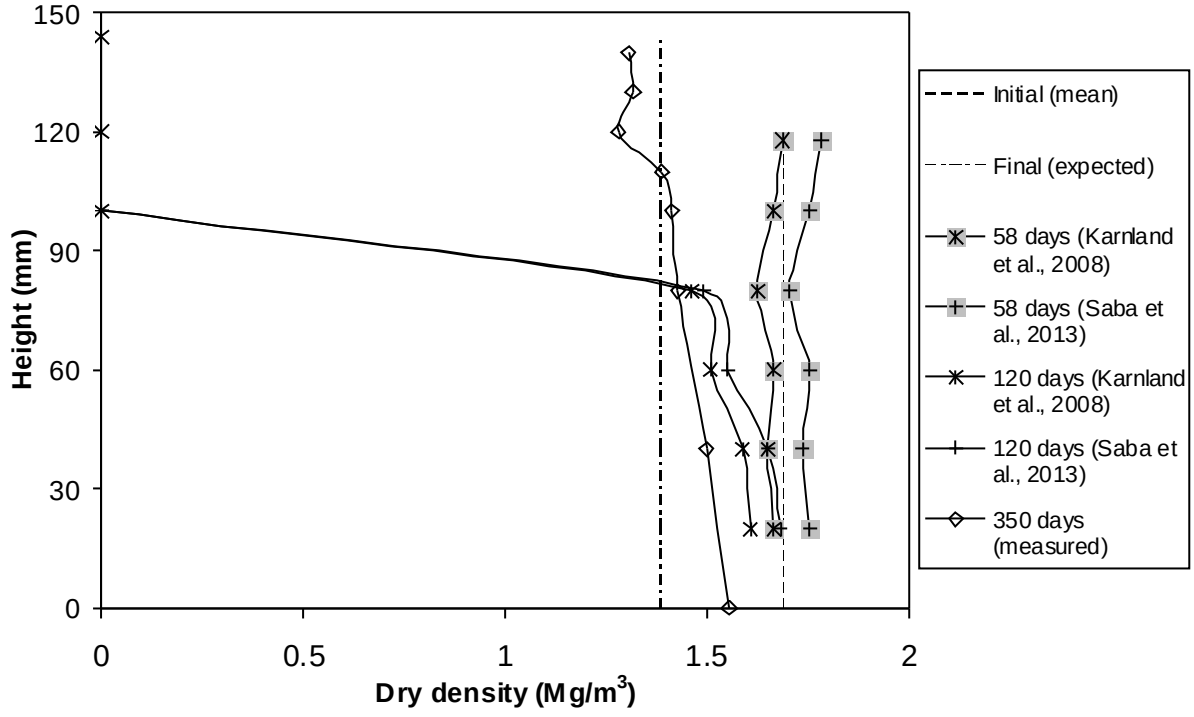


Figure 19. Dry density profiles deduced from the swelling pressure profiles.

Note that the relationship found by Karnland et al. (2008) was found by elementary tests and with axial swelling pressure measurements while the one obtained by Saba et al. (2013) was also by elementary tests but with axial and radial measurements. Bentonite dry density is the effective dry density of bentonite in the compacted mixture and is the most important factor affecting the swelling pressure values (Wang et al., 2012). By considering the swelling

pressure profile at 58 days before the piston release as the stabilisation values or final swelling pressures, and the values at 120 days as the final swelling pressures after the release, the bentonite dry density profile was then estimated using Eqs. 1 and 2. The calculated dry density profiles are then plotted in Figure 19. The mean initial bentonite dry density and the estimated final one after a swelling strain of 20% are also plotted in Figure 19. The mean initial dry density is the one measured after compaction (1.69 Mg/m^3). The final dry density is calculated by considering the final volume with a new height of 144 mm instead of 120 mm. We can see that at the initial state before the piston release, the density values estimated from the swelling pressure values are close to the measured ones. After the release, the estimated final value falls somewhere in the middle of the calculated dry densities. The calculated densities of the bottom layers are higher than the estimated final one and those of the upper layers are lower than the estimated final one. This indicates that the final state has not been reached yet.

A previous similar mock-up test was conducted by Wang et al. (2013a) on the same material with the similar dimensions. The test followed also the same procedure: first confined saturation followed by piston release and free axial swelling. The only difference with the present Mock-up 1 is the presence of 14% radial technological void in the mock-up test of Wang et al. (2013a) and the sample's initial dry density being 1.97 Mg/m^3. After filling the 14% radial technological void, this dry density became 1.67 Mg/m^3 as average value, the same as in the current test. After 9 months of free axial swelling (step 2), the test was dismantled and the sample was taken out from the cell by sawing it near the internal surface of the cell. Then sample was cut at different heights (0, 40, 80, 100, 110, 120, 130 and 140 mm). A total of eight disks were prepared by cutting, each having a thickness of 10 mm approximately. Each disk was then cut in pieces in order to make different measurements. The water content was measured by oven drying, while the dry density was determined based on the volume measurement by the fluid displacement technique (see Head, 1980, Geiser, 1999) using immiscible oil "Kerdane" that has a density of 0.791 at 20°C. The obtained dry density profile is presented in Figure 19. We can see that after almost 350 days after the piston release and the free swelling, the sample was still not homogeneous and a density gradient still existed along the sample. This clearly shows that the sample homogenisation is a long process.

7 Conclusion

The long-term behaviour of sealing plugs with different configurations is investigated within

the SEALEX project. Here, two mock-up tests at a 1/10 scale of the in-situ experiments were performed with radial and axial measurements of swelling pressure at different positions. In Mock-up 1 saturation was processed from the bottom side only, while in Mock-up 2 saturation was processed both from bottom and top sides. A comparison of the two tests was made in terms of swelling kinetics, final swelling pressure. The possible effect of entrapped air in Mock-up 2 was also examined. It was found that the swelling pressure kinetics depends on the infiltration length, with quicker increase for shorter infiltration length (closer to the wetting source). The two-side saturation process accelerated the swelling pressure kinetics by a time factor of 4 that was found when considering the symmetry plan in Mock-up 2 with zero water flow and then same boundary conditions as Mock-up 1 but with the half of the length. Air was found to be evacuated by diffusion in Mock-up 2, thus, there was no effect of trapped air induced by two-side saturation.

In order to estimate the suction changes in the mock-up tests, the mechanical results obtained from Mock-up 1 were combined with the hydraulic results obtained by Wang et al. (2013b) from an infiltration test carried out on the same material. The curves of suction versus swelling pressure were plotted for different infiltration lengths. Similar shapes were obtained when compared to the curves reported in the literature (Lloret et al., 2003 and Wang et al., 2013c). Yield points (or peaks) were found to take place at higher suction for the positions farther from the wetting source as they were mainly hydrated by vapour phase.

The failure of axial confining elements was also experimentally simulated by adopting an axial void through releasing the piston. The recovery of the void by the swelling sample was monitored. The swelling pressure profiles showed a sudden decrease after the piston release due to free swelling. A gradient was found along the sample, with higher swelling pressure values in the bottom. The density profile obtained from the exponential relationship between the bentonite dry density and the swelling pressure was also plotted, and a density gradient was found along the sample. Comparison with the dry density profile obtained after dismantling a similar mock-up test performed by Wang et al. (2013a) during 350 days showed that over time, the density gradient decreases, and a homogeneous density can be expected at long-term.

In order to complete the long-term behaviour study, Mock-up 1 will be continued. It is expected to obtain a unique final swelling pressure at all heights, reflecting of a homogeneous density within the sample. Similarly, the void recovery step of Mock-up 2 will also be continued and the final state of homogeneous dry density in the sample will be verified.

8 References

Agus S., Schanz T. 2005. Swelling pressures and wetting-drying curves of a highly compacted bentonite-sand mixture. Unsaturated Soils: Experimental Studies, pages 241–256.

Alonso, E. E., Alcoverro, J., Coste, F. 2005. The FEBEX benchmark test: case definition and comparison of modelling approaches. International Journal of Rock Mechanics & Mining Science 42(5-6): 611 – 638.

Barnichon, J.D., Dick. P., & Deleruyelle, F. 2010. A sealing performance in situ experiments project (SEALEX): main objectives and expected outcomes, Clays in natural & Engineered Barriers for Radioactive Waste Confinement, 4th international meeting, March 2010, Nantes, France 261-262.

Barnichon, J. D., Dick P. & Bauer C. 2012. The SEALEX in situ experiments: performance test of repository seals. Harmonising Rock Engineering and the Environment – Qian & Zhou (eds) Taylor & Francis Group, London, ISBN 978-0-415-80444-8, pages 1391-1394.

Cho W. J., Lee J. O. and Kang C. H., 2000. Influence of temperature elevation on the sealing performance of a potential buffer material for a high-level radioactive waste repository, Ann. Nucl. Energy, 27, 1271–1284.

Cui, Y.J., Tang, A.M., Loiseau, C. and Delage, P. 2008. Determining the unsaturated hydraulic conductivity of a compacted sand-bentonite mixture under constant-volume and free-swell conditions. Physics and Chemistry of the Earth, Parts A/B/C, 33(Supplement 1):S462 – S471.

Cui, Y.J., Yahia-Aissa M. and Delage P. 2002. A model for the volume change behaviour of heavily compacted swelling clays. Engineering Geology 64 (2-3), 233-250.

Delage, P., Howat, M.D., & Cui., Y.J. 1998. The relationship between suction and swelling properties in a heavily compacted unsaturated clay. Engineering Geology, 50(1-2), 31-48.

Geiser, F. 1999. Comportement mécanique d'un limon non saturé : étude expérimentale et modélisation constitutive. Switzerland: Thesis, Ecole Polytechnique Fédérale deLausanne, EPFL.

Gens, A. and Alonso, E. E. 1992. A framework for the behaviour of unsaturated expansive clays. Can.Geotech. J. 29(6): 1013 – 1032.

Head, K H. 1980, Manual of soil laboratory testing, volume 1: soil classification and compaction tests [M]. London: Pentech Press.

Karnland O., Nilsson U., Weber H. and Wersin P., 2008. Sealing ability of Wyoming bentonite pellets foreseen as buffer material - Laboratory results. Physics and Chemistry of the Earth (33) S472-S475.

Komine H. and Ogata N., 1994. Experimental study on swelling characteristics of compacted bentonite. Canadian geotechnical journal, 31(4):478–490.

Kröhn K.P., 2003. New conceptual models for the resaturation of bentonite. Applied clay science, 23(1-4):25–33.

Lee J.O., Lim J.G., Kang I.M. and Kwon S., 2012. Swelling pressures of compacted Ca-bentonite. Engineering Geology. doi: 10.1016/j.enggeo.2012.01.005

Lloret, A., Villar, M. V., Sanchez, M., Gens, A., Pintado, X. and Alonso, E. E., 2003. Mechanical behaviour of heavily compacted bentonite under high suction changes.

Géotechnique 53, No. 1, 27-40.

Loiseau, C., Cui, Y.J. & Delage, P. 2002. The gradient effect on the water flow through a compacted swelling soil. Proc. 3rd Int Conf Unsaturated Soils, UNSAT'2002 Recife, Brazil, Balkema, vol. 1, pp. 395-400.

Mitchell JK. 1993. Fundamentals of soil behaviour. John Wiley and sons, inc., New York.

Pusch, R., 1982. Mineral-water interactions and their influence on the physical behavior of highly compacted Na bentonite. Canadian Geotechnical Journal, 19(3):381–387.

Saba, S., Cui, Y.J., Tang, A.M., Barnichon, J.D. & Tran, T.P.H. submitted. Anisotropic swelling of compacted bentonite/sand mixture. Soils and Foundations.

Wang, Q., Tang, A. M., Cui, Y.J., Delage, P., & Gatmiri, B. 2012. Experimental study on the swelling behaviour of bentonite/claystone mixture, Engineering Geology, Vol. 124, 59–66.

Wang, Q., Tang, A. M., Cui, Y.J., Barnichon J.D. & Ye W.M. 2013a. A comparative study on the hydro-mechanical behaviour of compacted bentonite/sand plug based on laboratory and field infiltration tests, Engineering Geology, Vol. 162, 79–87.

Wang, Q., Cui, Y.J., Tang, A. M., Barnichon, J. D., Saba, S. & Ye, W.M. 2013b. Hydraulic conductivity and microstructure changes of compacted bentonite/sand mixture during hydration. Engineering Geology 164, 67-76.

Wang Q., Tang A.M., Cui Y.J., Barnichon J.D. & Ye W.M. 2013c. Investigation of the hydro-mechanical behaviour of compacted bentonite/sand mixture based on the BExM model. Computer and Geotechnics 54, 46-52.

Ye W.M., Cui Y.J., Qian L.X. & Chen B. 2009. An experimental study of the water transfer through compacted GMZ bentonite. Engineering Geology 108, 169 – 176.

Chapter 5

Link between laboratory experiments and in situ tests

INTRODUCTION

As mentioned in the previous chapter, two mock-up tests were designed at a 1/10 scale of the in situ SEALEX experiments run by IRSN. These mock-up tests provided local radial swelling pressure measurements at different positions in the sample and global axial swelling pressure. Beyond the scale effect and the difference in test procedure, it appears interesting to compare the results of mock-up and in situ tests. To this end, the second SEALEX test PT-N1 was selected where the same material was tested with measurements of swelling pressure and relative humidity at different positions in the seal.

A comparison of swelling pressure measurements was done between the the mock-up and the in situ tests. Another comparison was undertaken in terms of relative humidity between the results obtained from the infiltration column of Wang et al. (2013b) and those from the in situ tests.

The comparative study was subjected to a paper submitted to “Engineering Geology” and is presented in this chapter.

On the hydro-mechanical behaviour of compacted bentonite/sand mixture: comparison between laboratory and in situ experiments

Simona Saba[1,2], Jean-Dominique Barnichon[1], Yu-Jun Cui[2], and Anh Minh Tang[2]

Abstract: This paper compares the laboratory small scale infiltration tests and the in situ SEALEX experiments taking place at the Tournemire Underground Laboratory of IRSN - the French Institute for Radiation Protection and Nuclear safety. The main objective of SEALEX is to identify the key factors affecting the long-term performance of bentonite-based sealing systems when considering an initial technological void. In this project, several tests have been conducted while varying each time one parameter related to the seal composition, geometry or test conditions. Meanwhile, small scale laboratory infiltration tests were carried out in controlled conditions, aiming at providing useful measurements in terms of hydraulic and mechanical properties of the seal. The results obtained showed a good correspondence in terms of relative humidity measurements between the laboratory and the in situ tests when considering the saturation effect due to the existence of technological void in situ. The comparison factor was the distance to the closest wetting source. When comparing the swelling pressures, a time scale factor of 100 was found between the in situ experiment and the laboratory test. At the current stage of both tests, the in situ results are still at the beginning of the expected evolution and the prediction of this evolution can be done based on the laboratory results.

Keywords: laboratory small scale tests; SEALEX experiments; bentonite/sand mixture; relative humidity; swelling pressure; anisotropic swelling behaviour.

1 Introduction:

Compacted mixtures of bentonite and sand are often considered as candidate sealing materials in radioactive waste disposal concepts. These materials can swell upon contact with water, which thus closes all the initial gaps in the disposal system, in particular, the technological void between the seal and the host-rock, between the compacted blocks of bentonite/sand mixture etc. The hydraulic behaviour of this compacted mixture as well as its swelling properties have been widely studied at small scale in the laboratory and at large scale in underground research laboratories (URLs). At the laboratory scale, Pusch (1979), Delage et al. (1998), Lloret et al. (2003), Romero et al. (2005), Lloret &Villar (2007), Wang et al. (2012, 2013a, 2013b) studied amongst other the behaviour of sealing materials in laboratory conditions. In underground research laboratories (URL), various experiments have also been performed in the past: TSX at Manitoba, Canada; FEBEX at Grimsel, Switzerland, RESEAL at Mol, Belgium, KEY at Bure, France, etc. In 2010, the French Institute for Radiation Protection and Nuclear Safety (IRSN) launched the SEALEX project aiming at identifying the key factors controlling the long-term performance of bentonite-based sealing systems.

[1] Institut de Radioprotection et de Sûreté Nucléaire (IRSN), Fontenay-aux-Roses, France
[2] Ecole des Ponts ParisTech, Laboratoire Navier/Cermes, Marne La Vallée, France

This project consists in a series of in situ sealing experiments emplaced in a claystone formation (Toarcian argillite) at the Tournemire URL located in the South of France. Various technical parameters that may influence the overall hydraulic and mechanical performance of the seals are investigated, allowing progress in the knowledge on the key parameters that the implementer should specify and control in situ (Barnichon and Deleruyelle, 2009). In order to explore precisely the effect of the technical specifications, the test series were designed by changing one parameter at a time (see Barnichon and Deleruyelle, 2009; Barnichon et al., 2010, 2012) among which the intra-core geometry (jointed vs. monolithic disks), the core composition (MX80/sand ratio) and the core conditions (pre-compacted vs. in situ compacted). The second test of this series, denoted as "performance test PT-N1", is based on a clay core made of pre-compacted monolithic disks of MX80 bentonite/sand mixture (70/30 ratio in dry mass). The clay core is 120 cm long and 60 cm in diameter. A seal of such size normally needs several years to be fully saturated due to the very low permeability of the compacted bentonite based materials. In this test, the injected water volume, total pressure and relative humidity changes upon saturation are monitored at several positions within the plug or seal. After full saturation, the overall hydraulic properties (inherent permeability, occurrence of leakage) of the sealing system will be determined.

In parallel, two small scale laboratory tests were performed on samples prepared with the same material as for PT-N1 test (MX80 bentonite/sand mixture). The first test consisted in measuring the relative humidity at different heights of a soil column (H = 250 mm, D = 50 mm). The second test was designed at a scale of 1/10 of the in situ test (height = 120 mm and diameter = 60 mm) and consisted in measuring the radial and axial swelling pressures at different heights of the sample. In both tests, a rigid stainless steel cell was used to simulate the confined boundary conditions (zero volume change conditions).

In a previous work by Wang et al. (2013c), the same in situ PT-N1 test was compared with a simpler laboratory 1/10 Mock-up test. Between the laboratory and in situ conditions, an up-scaling ratio of 2.5 was obtained by comparing the injected water volume and the axial swelling pressure evolution during the saturation process. In comparison with this previous work, the present study is more local as it provides a comparison of the relative humidity and the radial swelling pressure at different positions of the samples between the laboratory and in situ tests. Note that the link between the small scale laboratory tests and the in situ experiments can provide useful information for predicting the saturation duration, the kinetics of some key parameters as well as their maximum values.

2 Materials studied

The soil studied is a compacted mixture of bentonite and sand, with a bentonite fraction of 70% in dry mass. The bentonite is a MX80 bentonite from Wyoming, USA, having a liquid limit of 575%, a plastic limit of 53% and a unit mass of 2.77 Mg/m^3. The cation exchange capacity (CEC) is 76 meq/100g (83% of Na^+). The sand pure quartz used in the mixture comes from Eure and Loire (France) with a unit mass of 2.65 Mg/m^3. It was sieved at 2 mm before being mixed with the bentonite grains previously hydrated to a water content of 13%. The saturation water used in the tests has a similar chemical composition as the pore water of the Callovo-Oxfordian claystone from the Andra's URL in Bure (France). It was obtained by mixing the corresponding chemical components (see Table 1) with distilled water using a magnetic stirrer until full dissolution.

Table 1. Chemical composition of the used synthetic water; similar to the pore water composition of claystone in Bure site (ANDRA) (Wang et al., 2012).

Component	$NaHCO_3$	Na_2SO_4	NaCl	KCl	$CaCl_2.2H_2O$	$MgCl_2.6H_2O$	$SrCl_2.6H_2O$
Mass (g)/Liter of solution	0.28	2.216	0.615	0.075	1.082	1.356	0.053

3 SEALEX in situ test

As mentioned before, the in situ experiment (PT-N1) was selected among SEALEX tests to make the comparison with the laboratory tests because it corresponds better to the laboratory tests conditions. The prefabricated seal was inserted in a horizontal borehole of 60 cm diameter that was air-drilled for this purpose within the Toarcian claystone from the Tournemire URL. The seal is made of a succession of 8 monolithic pre-compacted disks, each having 56 cm diameter and 15 cm thickness. The total length of the seal is then 120 cm. The diameter of the seal is slightly smaller than the borehole's diameter for the technical reasons related to the emplacement operation of the seal; in its initial state, a radial technological void (equivalent to 2 cm on radius) is then existing, representing 14.33% of the total volume (volume of void / volume of borehole considering the seal length of 120 cm). The disks were prepared by static uni-axial compaction of MX80/sand to an initial dry density of 1.97 Mg/m^3. At this dry density and after hydration, swelling and filling of the 14.33% technological void, the final dry density should reach an average of 1.67 Mg/m^3. The expected final swelling pressure at this final dry density should then fall between 3 and 4 MPa, which is high enough for fulfilling the seal specification and which remains lower than the minor in situ stress to avoid mechanical damage to claystone.

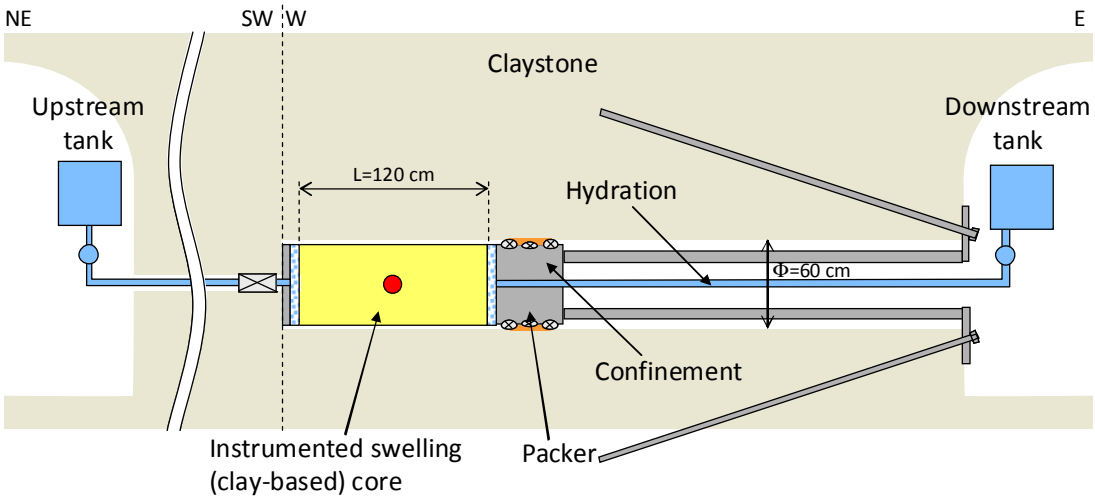


Figure 1. Layout of the PT-N1 in situ test.

Figure 1 shows the general layout of the test with the seal sandwiched between two porous plates, allowing water flow from two injection lines (i.e. upstream and downstream). Mechanically, the upstream plate lies in direct contact with the host-rock while the downstream one is fixed by a confining system maintaining a constant volume condition. A packer-like device for water tightness is used to prevent water leakage from the interface between the confining plug and rock. Three types of sensors are installed within the compacted blocks to provide data in terms of swelling pressure, pore water pressure and relative humidity. For the clarity of comparison, only the distribution of relative humidity and swelling pressure sensors is shown in Figure 2 in a more detailed layout. Eight relative humidity sensors (22-1,2; 52-1,2; 38-1,2; 8-1,2) are installed in pairs in the compacted blocks at a distance of 8, 22, 38 and 52 cm from the porous filters as shown in Figure 2. Their distribution in the blocks is shown in Figure 3 – sections A and B; they are positioned at 15 cm from the seal surface.

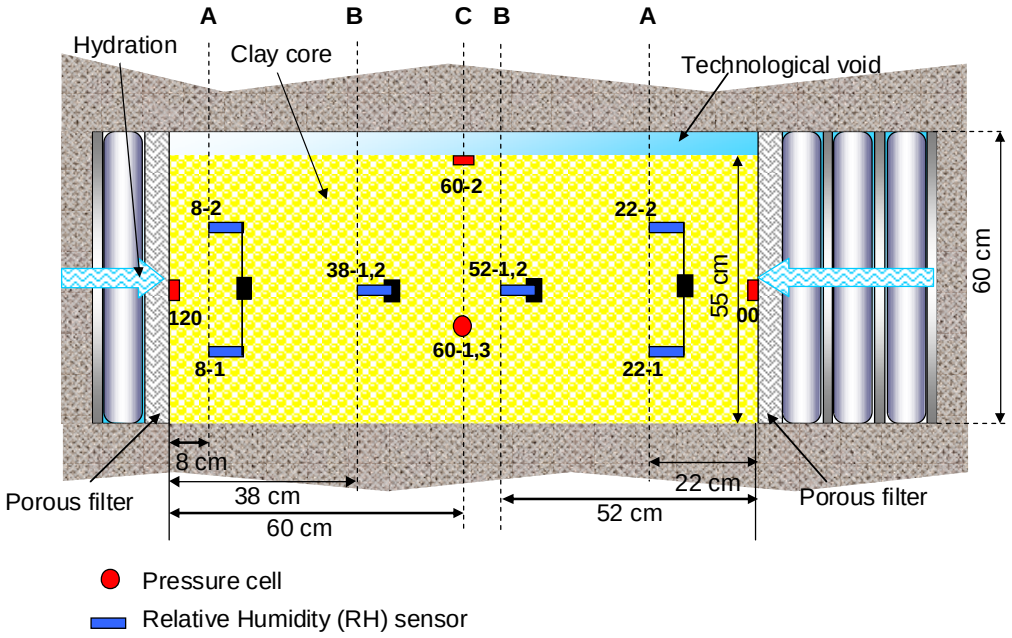


Figure 2. Distribution of the relative humidity and swelling pressure sensors in the seal.

Some of these sensors did not work properly, hence, only the working sensors (22-1,2; 52-2; 38-2; 8-2) are considered in this study. The seal is being hydrated from its two ends (extremity or upstream and downstream sources). However, due to the presence of radial technological void that will be firstly flooded by water, another hydration source exists around the seal (denoted here as the surface wetting source).

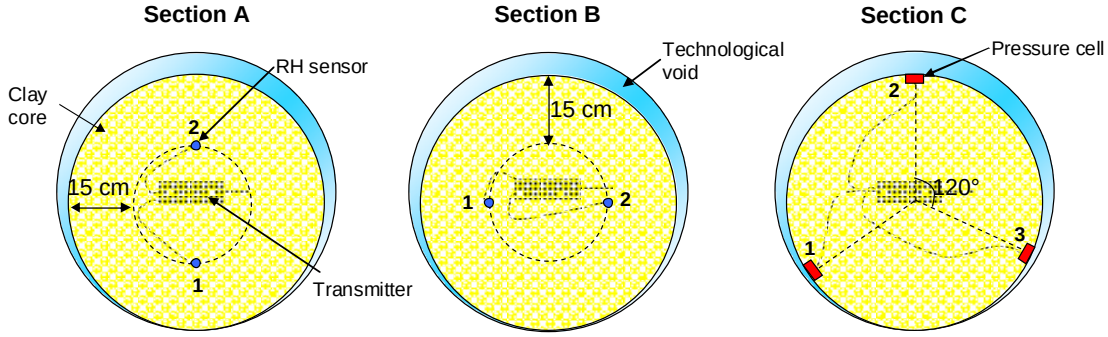


Figure 3. Different cross-sections with positions of the relative humidity and swelling pressure sensors.

Note that the technological void is not uniformly distributed around the seal: is the largest at the top of the seal and is zero on the bottom as shown in Figure 3. Sensor 22-1 (see Figure 2) measures the relative humidity in the seal axially 22 cm from the downstream wetting source and radially 15 cm from the bottom surface of the seal (see Figure 3 – section A). This bottom surface is in contact with the host-rock which makes it difficult for water to infiltrate at exactly 15 cm from the bottom but possibly from more depending on how exactly the seal is placed in the bottom (see Figure 4 – section A).

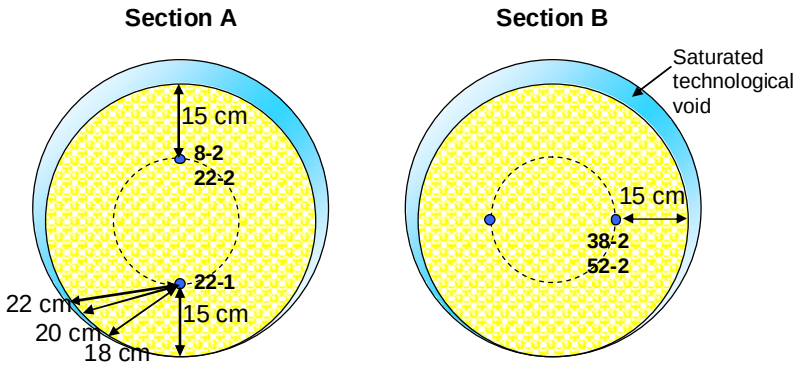


Figure 4. Detailed description of the positions of the used relative humidity sensors in the cross-sections of the seal.

The distance to the closest wetting source will be considered in the analysis of the results measured by the sensors. Therefore, for sensor 22-1, the shortest path is between 15 cm and 22 cm as shown in Figure 4. Sensors 22-2, 52-2 and 38-2 are located at 15 cm from the surface of the seal in contact with the water filling the technological void (the surface wetting source) as shown in Figure 4. They are also located at 22, 52 and 38 cm respectively from the porous filters. The closest wetting source is then at 15 cm (i.e. the minimum value between 15 cm and 22 cm). Sensor 8-2 measures the relative humidity at 8 cm from the upstream wetting source (Figure 2) and at 15 cm from the surface wetting source (Figure 4). The shortest hydration path is then 8 cm.

Five total pressure sensors (00; 60-1,2,3; 120) are installed in the seal. Three of them (60-1,2,3) are installed at the surface of the seal at 60 cm from the extremity wetting sources to measure the radial swelling pressure. As shown in Figure 3 – section C, these three sensors are emplaced at an angle of 120° between them. The other two sensors (00 and 120) are installed at the two extremities of the seal (in contact with the porous filters) and in the centre of the sections to measure the axial swelling pressure. However, one of them (sensor 120) did not work properly.

Prior to the assemblage of blocks, the sensors were placed in the holes specially prepared in the disks with their shapes and at their pre-assigned positions. Wireless sensors were used to limit preferential flow along cables, and a wireless transmitter was installed at each measurement section. Since then, sensors data are collected by a receiver located outside the seal, and they are recorded by a data logger.

As far as the test procedure is concerned, a water volume of 49 L was first injected, which corresponds to the volume of the estimated technological void. This operation was completed in one hour. Afterwards, water injection was stopped due to a leak at the side packer. Once

fixed, water injection restarted 20 days later, with a water pressure of 0.01 MPa (Wang et al. 2013c). As the saturation proceeds, the injected water volumes at both upstream and downstream chambers are also recorded.

4 Laboratory tests

Three laboratory tests have been carried out and are compared with the PT-N1 in situ test: one relative humidity infiltration test where relative humidity is monitored at different positions, and two small scale tests (Mock-up 1 and Mock-up 2) designed at the 1/10 scale of the in situ test, and where the swelling pressures in both radial and axial directions are monitored at different positions. The difference between the two mock-ups comes from the water infiltration process: only from the bottom side in Mock-up 1 and from two sides (top and bottom) in Mock-up 2. Note that all laboratory tests were conducted in the vertical direction (see Figure 5 and Figure 6) which is different from the in situ test that is performed in a horizontal borehole (see Figure 1 and Figure 2).

4.1 Test in relative humidity infiltration cell

a) Experimental setup

The cell is a stainless steel cylinder containing the specimen with a rigid structure preventing any volume changes (radial and axial). Four relative humidity (RH) sensors (RH50, RH100, RH150 and RH200) are installed every 50 mm along the sample at a distance of 50, 100, 150 and 200 mm from the wetting end. They are fixed in dedicated ports in the wall of the cell. The two ends of the cell are covered by porous stones to ensure uniform boundary conditions especially in terms of water distribution. The bottom base is equipped by water inlets and the top base contains an outlet allowing for air outflow.

b) Sample preparation

The soil specimen used during this test is 250 mm long and 50 mm in diameter. It is statically compacted in a cylindrical mould having 50 mm inner diameter at a rate of 0.1 mm/min to a maximum vertical stress of 13 MPa. It is compacted in 5 layers of 50 mm thickness each. Before adding a new layer, the surface of the compacted layer is carefully scarified before the next layer is added in order to ensure a good junction between both layers (see Wang et al. 2013b for more details). The dry density after compaction is 1.67 Mg/m^3, the same value as the final dry density for the in situ test after expansion and filling of the technological void.

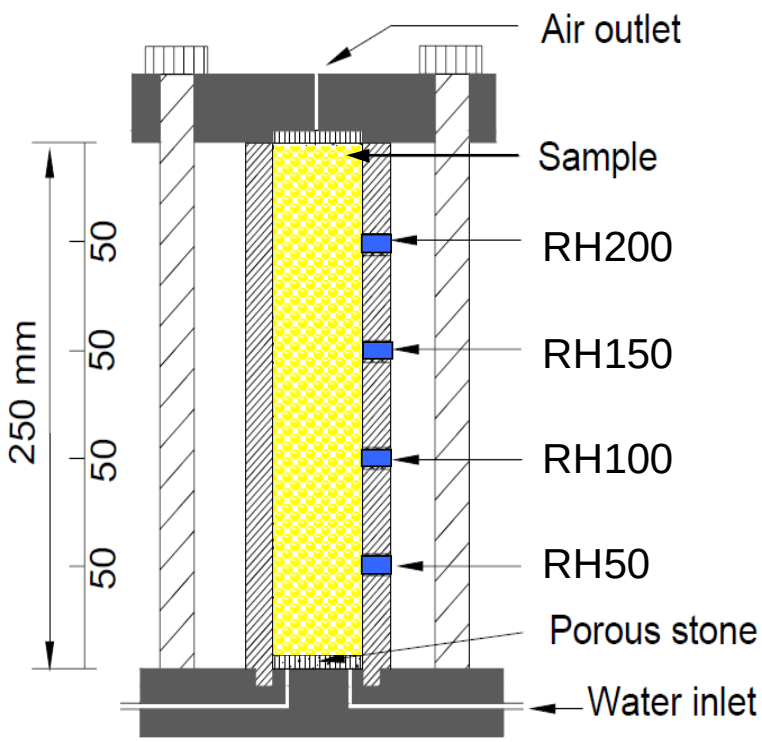


Figure 5. Layout of the relative humidity laboratory test cell with positions of the relative humidity sensors.

c) Test procedure

After compaction, the specimen is carefully introduced into the testing cell shown in Figure 5 (having the same diameter as the compaction cell) by connecting the ends of the two cells. Water supply is done through the water inlets at the cell base. The relative humidity measurements are recorded via a data logger. The water volume injected into the sample is monitored during the test by manually noting the decreasing volume in a burette connected to the water inlets.

4.2 Small scale tests (mock-up tests)

a) Experimental setup

Figure 6 shows the layout of the small scale hydration cell containing the soil specimen having 60 mm diameter and 120 mm height (1/10 of PT-N1 seal dimensions). Porous stones are placed at the two sides of the sample to ensure uniform saturation through the sample section. A piston of 60 mm diameter is placed on top of the upper porous stone and it is in contact with a screw connected to a rigid structure that prevents any axial displacement. This test configuration simulates the condition of the in situ test where the confining structure does not allow displacements.

The bottom and the upper piston are each equipped with a water inlet and an outlet for air expulsion. Six total pressure sensors are fixed on the wall of the cell, enabling the radial swelling pressures at different heights of the sample (h = 20, 40, 60, 80, 100 and 120 mm from the wetting side) to be monitored. A force transducer is placed under the cell base and monitors the axial swelling pressure.

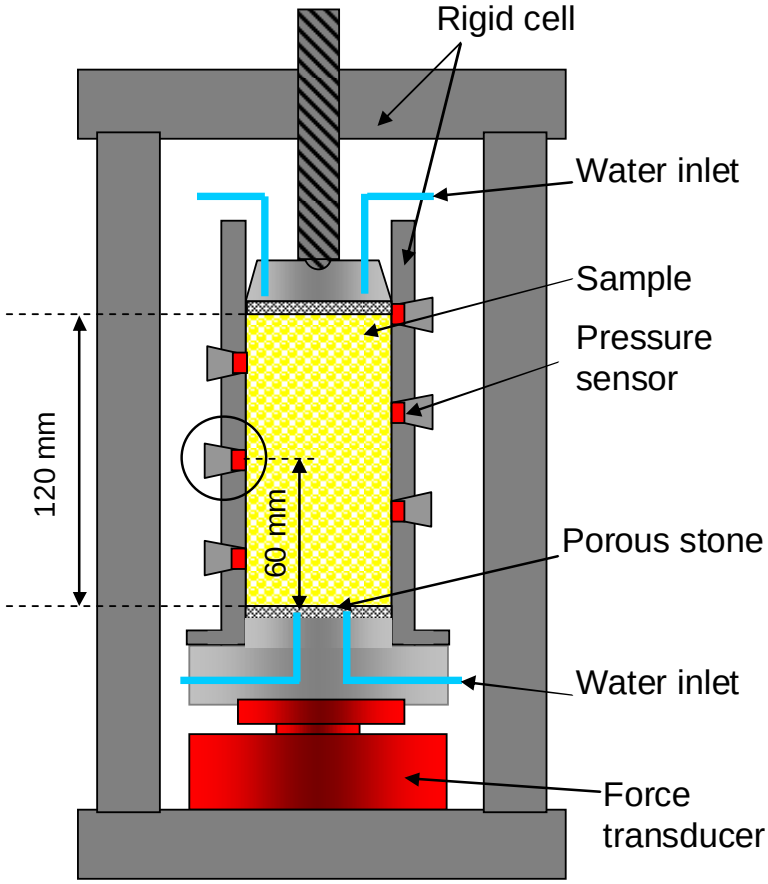


Figure 6. Layout of the swelling pressure laboratory test cell with positions of the sensors.

b) Sample preparation

The soil specimen studied in this test is statically compacted in the test cell itself at a strain rate of 0.1 mm/min and to a maximum vertical stress of 13 MPa. In order to ensure the homogeneity of the specimen, the compaction is carried out in 3 layers of 40 mm each. As in the relative humidity test, the surface of the compacted layer is carefully scarified before the next layer is added. The obtained dry density is the same as in the relative humidity test (1.67 Mg/m^3), which corresponds to the final dry density of the seal for the in situ test after expansion and filling the 14.33% technological void.

c) Test procedure

Two small scale tests have been conducted, with the only difference in the saturation process. To ensure a good contact between the load cell and the piston, between the piston and the sample and between the sample and the bottom part, an initial stress of 0.1 MPa is applied on the specimen by turning the screw before water infiltration. Similarly, to have a better contact between the total pressure sensors and the soil specimen, the total pressure sensors are slightly pushed in the cell. The synthetic water is then injected either from the bottom only (Mock-up 1) or from both the top and the bottom sides (Mock-up 2). The radial and axial pressures are recorded automatically by a data logger, while the injected water volume is followed manually by noting the water level changes in the burettes.

5 Experimental results and comparison

5.1 Relative humidity

Figure 7 shows the evolution of the relative humidity over time obtained by sensors RH50, RH100, RH150 and RH200 in the laboratory and 22-1,2; 52-2; 38-2; 8-2 in situ. As explained in section 3, to have meaningful comparison, the distance to the closest wetting source must be considered for the in situ test while considering the surface hydration source resulting from the saturated technological void. The considered distances are then 8 cm for sensor 8-2, 15 cm for sensors 38-2; 52-2 and 22-2 and 20 cm for sensor 22-1. Figure 8 shows the results of sensor 22-1, which are compared with the laboratory relative humidity curves obtained at 15, 18, 20 and 22 cm (between 15 and 22 cm as shown in Figure 8) from the surface wetting source. The plot shows that the curve obtained by sensor 22-1 fits best with the laboratory curve obtained at 20 cm from the surface wetting source. Note that the laboratory relative humidity curves at 15 and 20 cm from the wetting source are obtained by directly plotting the results given by sensors RH150 and RH200 respectively, while those at 8, 18 and 22 cm are obtained by linear interpolation between the curves of sensors RH50 and RH100 (for 8 cm), RH150 and RH200 (for 18 cm) and by linear extrapolation of the curve of sensor RH200 (for 22 cm).

For the comparative study with the laboratory test, only the relative humidity measurements corresponding to the positions at 8, 15 and 20 cm in the infiltration cell are used. They are presented in Figure 7. Several observations can be made:

- All the relative humidity values for the in situ test and the small scale test started from 60 ± 2% (around 58% in situ and 62% in the laboratory). This value corresponds to the

hydric state of the material at its initial state, after compaction at initial water content of 11%.

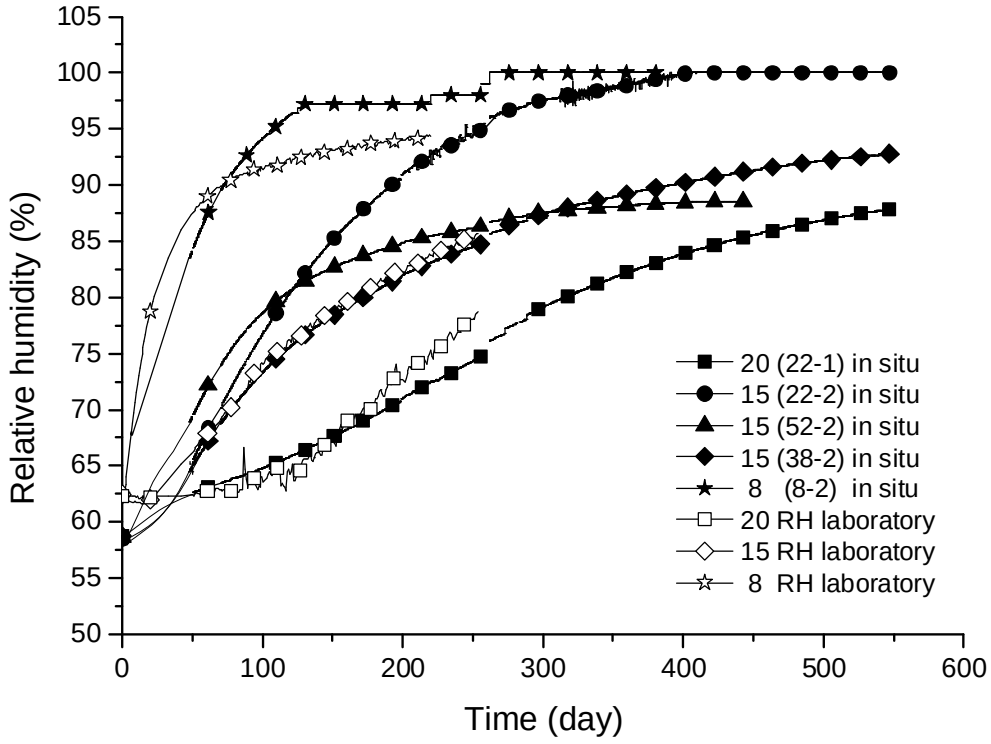


Figure 7. Evolution of the relative humidity at different hydration distances for the small scale and in situ tests.

- There is a good agreement between laboratory and in situ test results for the corresponding positions. For the curves corresponding to 8 cm from the wetting end, both (in situ and laboratory curves) start with a fast increase followed by a quick stabilisation. The slight difference between the two curves can be related to the hydration path that is not well defined for the in situ test and also to the adopted linear interpolation. The laboratory curve given by the sensor at 15 cm fits the best with the in situ curve of sensor 38-2 but less satisfactorily with sensors 22-2 and 52-2. It is difficult to explain this difference as in such large scale in situ test, the test conditions are not easy to control locally. On the whole, the four curves exhibit an increase of relative humidity over time at a lower initial rate than the curves at 8 cm. The in situ curve corresponding to sensor 22-1 fits well with the laboratory curve at 20 cm from the wetting end. This sensor (22-1) is located at the bottom of the seal where the seal is in contact with the rock; thus, the shortest hydration path through the technological void should be larger than 15 cm and less than 22 cm. It is observed that the laboratory

curve corresponding to 20 cm fits better than that corresponding to 22 cm with the in situ curve of sensor 22-1 as shown in Figure 8. The soil around the sensor is then more hydrated by the water infiltrating from the technological void than from the downstream extremity source (at 22 cm).

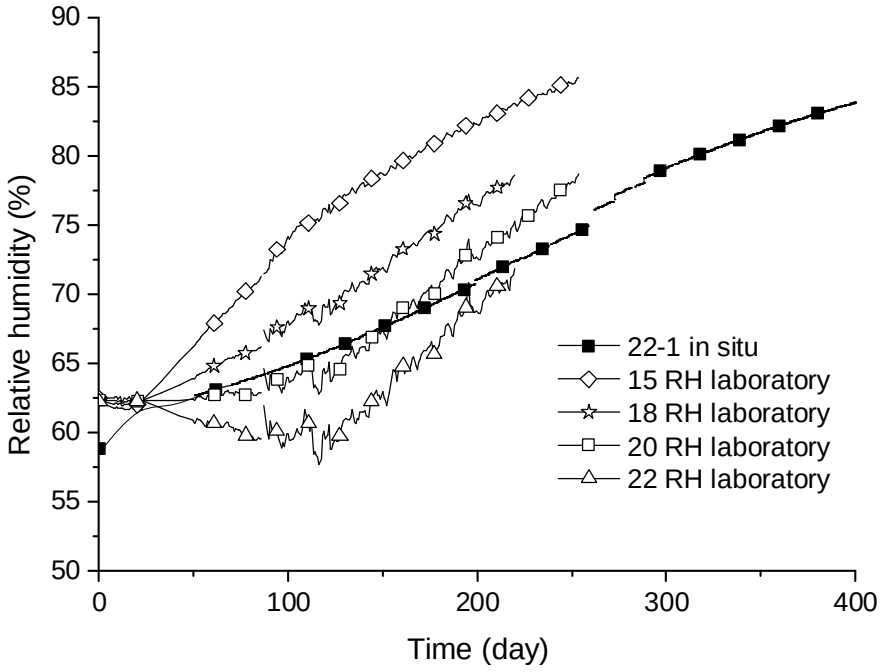


Figure 8. Comparison of the relative humidity curve given by in situ sensor 22-1 with the curves given by the laboratory test at 15, 18, 20 and 22 cm from the wetting end.

- As far as the relative humidity evolution kinetics is concerned, both in situ and laboratory measurements show a quick increase at short distance from the wetting source. As sensor 8-2 is the closest to the hydration source, the in situ and laboratory curves exhibit the quickest increase at the beginning and a stabilisation afterwards to a value close to 100%, while the curves of 20 cm from the wetting source start increasing slowly and then get faster before stabilisation. The increase rate decreases as the distance from the wetting source increases. This was also observed by Loiseau et al. (2002) and Cui et al. (2008) on small scale infiltration tests performed on bentonite/sand mixture.

5.2 Swelling pressure

In order to compare the in situ swelling pressure results to Mock-up 1 and Mock-up 2 results, the boundary conditions should be first discussed. Figure 9 represents a sketch for Mock-up 1, Mock-up 2 and the in situ experiments. In Mock-up 1, water infiltration is only from the bottom side and is zero from the top while in Mock-up 2 and in situ, water infiltration is from the two sides of the seal. With a two side infiltration, a symmetry plan exists in the middle of

the seal; at 60 mm in Mock-up 2 and 600 mm in situ.

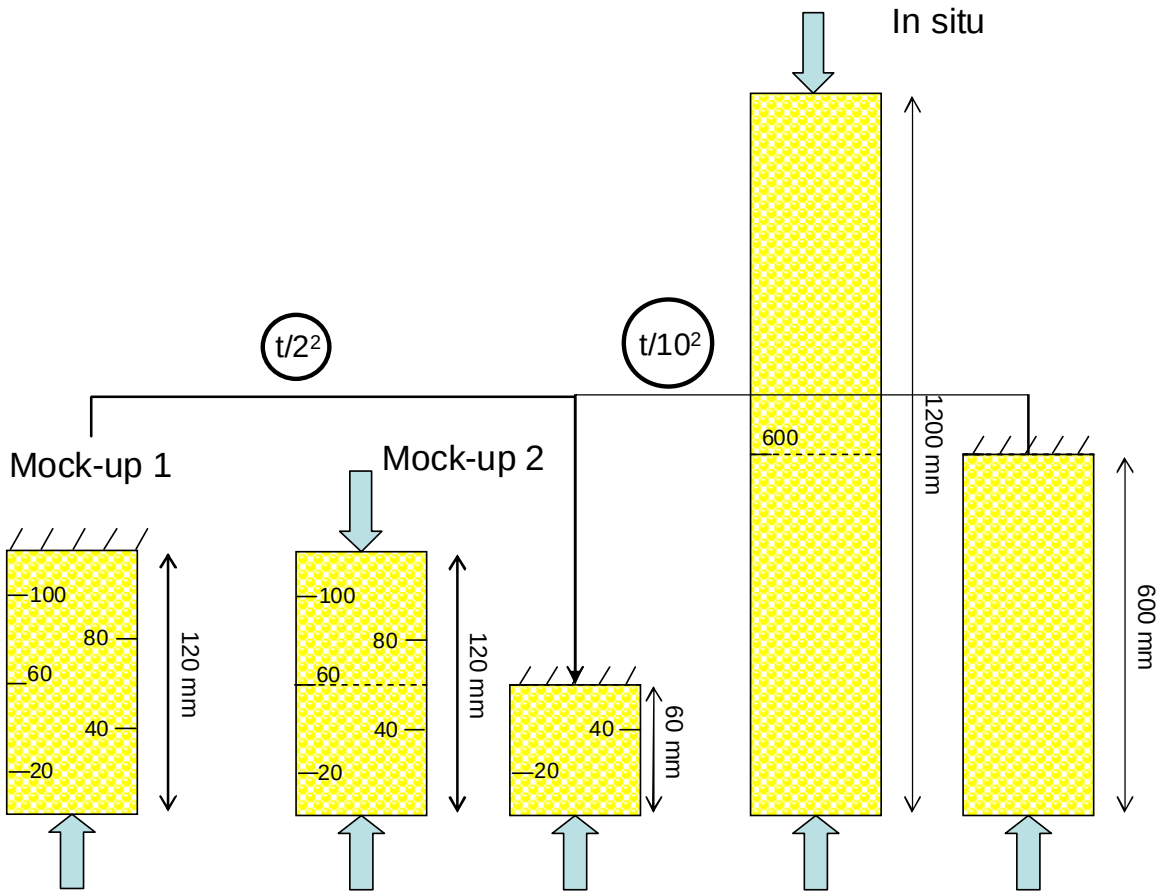


Figure 9. The sketch of the samples with their respective boundary conditions in Mock-up 1, Mock-up 2 and in situ tests as well as the comparison factors between them.

At this symmetry plan, there is no water flow; we can then only consider one half of the Mock-up 2 and the in situ test and compare them with Mock-up 1. The respective infiltration lengths in Mock-up 1, Mock-up 2 and in situ test are 120 mm, 60 mm and 600 mm. The comparable measurements will be the ones corresponding to the side without water flow and that with water flow. This corresponds to comparing the axial measurement in Mock-up 1 (at the top) to the radial measurement in Mock-up 2 (at 60 mm) and the radial measurement in situ (at 600 mm). On the other hand, we can compare the measurements at the water infiltration side which will correspond to the axial measurement in Mock-up 2 (at 0 mm from the top wetting source) and the axial measurement in situ (at 0 mm from wetting source).

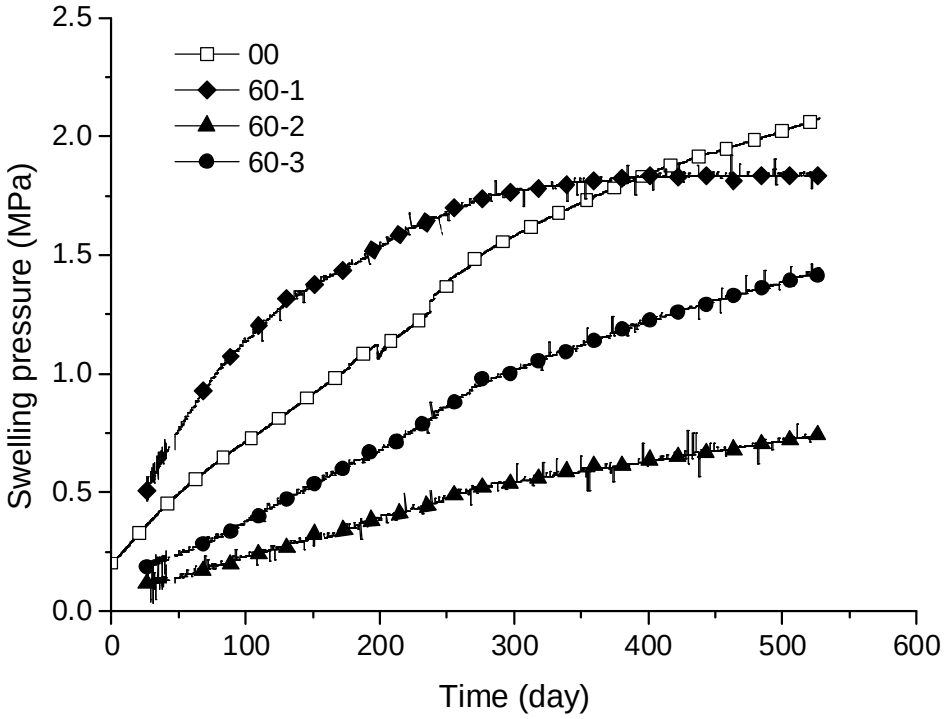


Figure 10. Evolution of the in situ radial and axial swelling pressures over time.

Figure 10 shows the evolution of swelling pressure from the in situ test for both the radial and axial directions. The radial pressure sensors at section 60 cm started giving measurements after 26 days of hydration because of a technical problem. Considering their initial values at 26 days, sensor 60-1 starts from 0.50 MPa while 60-2 starts from 0.12 MPa and 60-3 from 0.19 MPa. The axial pressure sensor 00 starts from 0.20 MPa at the very beginning and it reaches 0.37 MPa after 26 days. On the whole, the swelling pressures increase over time at different rates, depending on the sensors position. The curve of sensor 60-1 exhibits the fastest increase at the beginning and then stabilises after 300 days. The curves of sensors 60-2 and 60-3 exhibit an almost linear increase, with the smaller increase rate corresponding to sensor 60-2. As mentioned before, the technological void is not uniform; it is the largest at the top of the seal near sensor 60-2 (see Figure 3 – Section C), and it is smaller near sensors 60-1 and 60-3. As a result, the minimum swelling pressure is expected to be given by sensor 60-2 as the seal can swell freely more in the zone of sensor 60-2 than in the zones of sensors 60-1 and 60-3. As sensors 60-1 and 60-3 are symmetrical with respect to the borehole axis, they should measure the same swelling pressure. However, sensor 60-1 gives higher swelling pressures, which may be explained by the fact that the compacted disks may not be perfectly centred in the borehole, causing one sensor to be closer to the rock than the other. The axial swelling pressure also increases in an almost linear way, and at almost 400 days it started reaching higher values than the curve of 60-1.

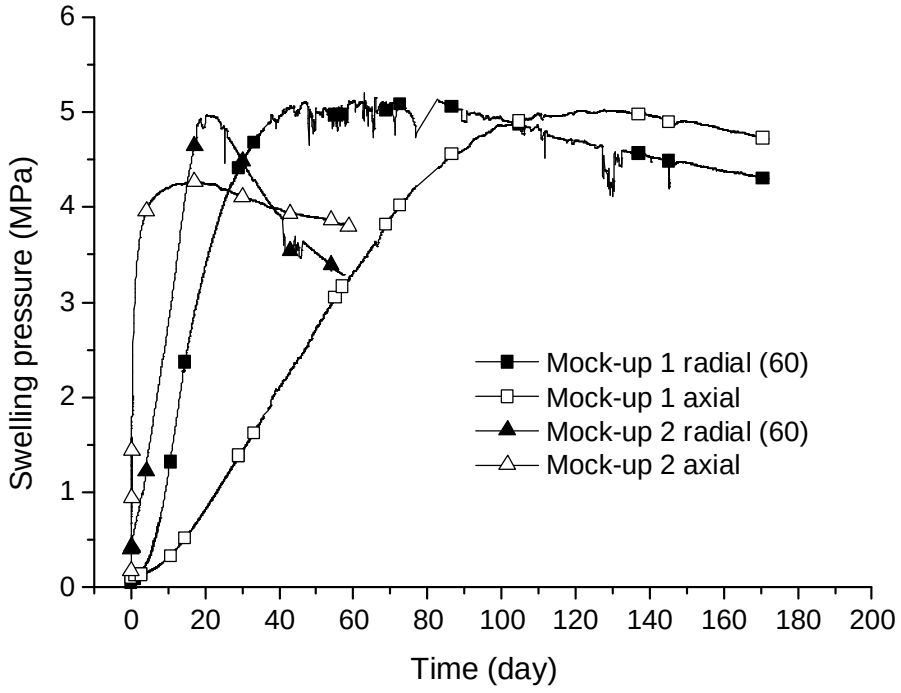


Figure 11. Evolution of the small scale radial and axial swelling pressures in Mock-up 1 and Mock-up 2 tests.

The laboratory results for radial (at 60 mm) and axial swelling pressure evolution are presented in Figure 11 for the two tests. On the whole, the swelling pressure increases quickly in the beginning, reaches a peak and then starts decreasing slowly. The peaks are reached at about 4 to 5 MPa. The swelling pressures did not stabilise yet; the expected stabilisation values is estimated around 3.5 MPa from the results of Karnland et al. (2008) and Wang et al. (2012) for a compacted MX80 bentonite/sand mixture with a dry density of 1.67 Mg/m^3. As far as the hydration path is concerned, we can see that the increase rate is higher in Mock-up 2 with two-side hydration. This is normal as the saturation is faster when the infiltration length is shorter. The axial swelling pressure is a little higher than the radial one, 4.6 MPa against 4.3 MPa in Mock-up 1 and 3.7 MPa against 3.4 MPa in Mock-up 2.

To be able to compare these measurements with different infiltration lengths, we should consider the consolidation theory that considers that time is inversely proportional to the square of the infiltration length. As a consequence and when considering Mock-up 2 as a reference, a scale factor of 4 (2^2) should be considered to compare Mock-up 1 to Mock-up 2 and of 100 (10^2) when comparing the in situ test to Mock-up 2. Figure 12 shows the axial swelling pressure results in Mock-up 2 and in the in situ test after dividing the time scale by 100. We can see that at this stage of the in situ experiment the kinetics are different which could be explained by the fact that the measurements techniques are different. It is a local

measurement in situ (the total pressure cell located at the centre of the seal section) while the force transducer in the mock-up tests records the force on the whole cross section. The axial swelling pressure in the present mock-up tests was applied indirectly by the force transducer placed on the bottom of the cell while in the in situ PT-N1 test, the force transducer was directly in contact with the cell piston. The deformability of the cell should also be considered in the present mock-up tests.

The time scale in Figure was kept at 60 days (actual time for Mock-up 2) in order to be able to project the in situ results in time. The time scale factor of 100 seems promising to be able to predict the in situ axial swelling pressure values.

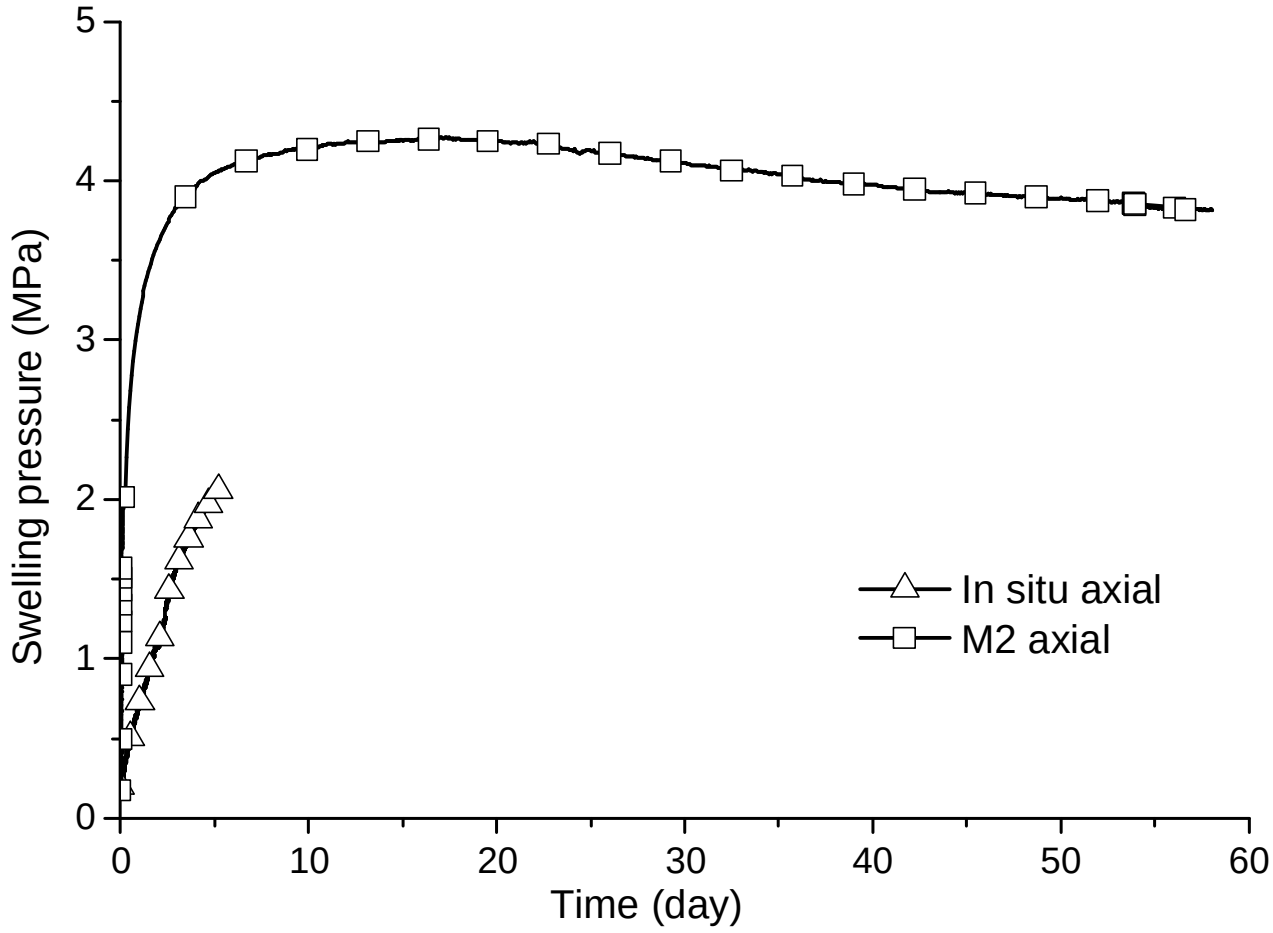


Figure 12. Comparison of the axial swelling pressure measurement at 0 mm distance to the wetting source between the in situ test and Mock-up 2.

Figure 13 shows the comparison in swelling pressure kinetics for the sample's side where no water flow exists, with the axial swelling pressure at 120 mm in Mock-up to the radial swelling pressure at 60 mm in Mock-up 2 and to the radial swelling pressure at 600 mm in the in situ test. The time scales for the Mock-up 1 curve as divided by 4 and the one for in situ divided by 100.

A first look on the figure reveals a promising comparison between the in situ and the Mock-up tests. The in situ radial swelling pressure curves fit well with the start of the Mock-up curves. The curve corresponding to the sensor 60-3 in the in situ tests fits the best with the Mock-up 2 curve. This comparison helps in predicting the swelling pressure kinetics in situ based on the results from the Mock-up tests.

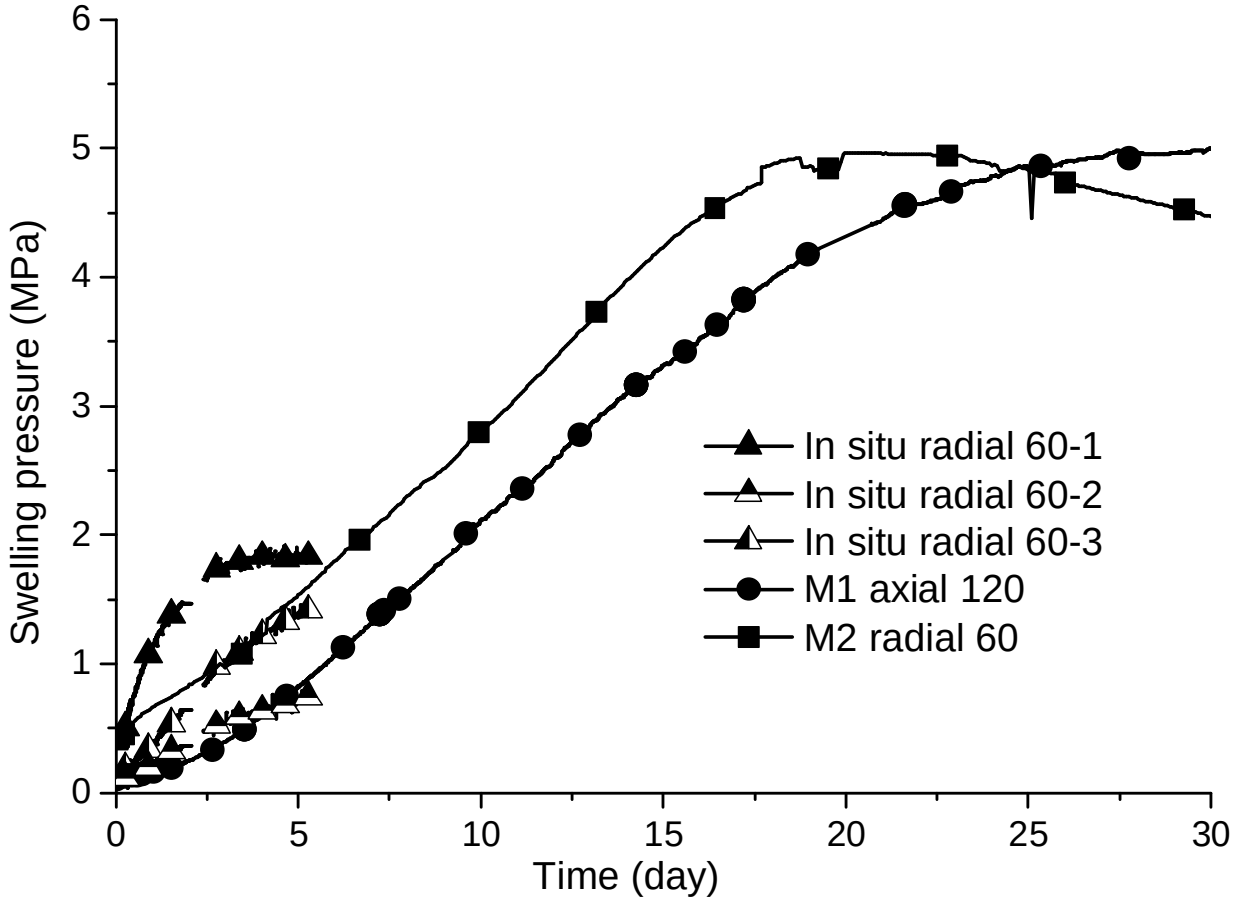


Figure 13. Comparison of the swelling pressure kinetics at the side of the sample with no water flow between Mock-up 1, Mock-up 2 and in situ tests while dividing the time scale by 4 in Mock-up 1 and by 100 in the in situ test.

The radial swelling pressure recorded by sensor PS60 in the mock-up tests should be more comparable with those of sensors 60-1 and 60-3 and not 60-2. In fact, as it stated before, the technological void is not a uniform ring around the seal: it is the largest at the top of the seal (near sensor 60-2) and it is significantly smaller at the bottom (near the sensors 60-1 and 60-3); the configuration of the mock-up tests (without technological void) is then closer to that of the in situ test in the zone near sensors 60-1 and 60-3.

6 Conclusion

In the framework of SEALEX project initiated by IRSN, the performance test PT-N1 was conducted to investigate the performance of sealing materials. In this test, the relative

humidity, swelling pressure in both radial and axial directions and injected water volume were monitored. A comparison was made in terms of swelling pressures and relative humidity measurements. Two types of laboratory experiments were performed: the first one provided the relative humidity at different positions in the sample and the other corresponds to a 1/10 mock-up test with respect to the PT-N1 test and provided the radial and axial swelling pressures. During the saturation process, the evolutions of the relative humidity for the in situ and laboratory tests fitted well for a given hydration distance while considering the effect of the saturation due to existence of the technological void. When comparing the evolution kinetics of radial or axial swelling pressures between the small scale tests and the in situ test, the boundary conditions in the three tests were analysed to be the same while considering the symmetry plan. The three tests models, with the same boundary conditions having a water flow from one side and not from the other, had different infiltration lengths. Time scale factors were found between the in situ and the mock-up tests based on the consolidation theory. Considering Mock-up 2 as a reference, a factor of 100 was found with the in situ test and a factor of 4 with Mock-up 1. The time scale factor between the in situ and the mock-up tests is very important because it helps in predicting the in situ results in the future years based on the mock-up results.

References

Barnichon, J.D. & Deleruyelle, F. 2009. Sealing Experiments at the Tournemire URL. EUROSAFE.

Barnichon, J.D., Dick. P., & Deleruyelle, F. 2010. A sealing performance in situ experiments project (SEALEX): main objectives and expected outcomes, Clays in natural & Engineered Barriers for Radioactive Waste Confinement, 4th international meeting, March 2010, Nantes, France, 261–262.

Barnichon, J.D., Dick P. & Bauer C. 2012. The SEALEX in situ experiments: performance test of repository seals. Harmonising Rock Engineering and the Environment – Qian & Zhou (eds) Taylor & Francis Group, London, ISBN 978-0-415-80444-8, pages 1391–1394.

Cui, Y.J., Tang, A.M., Loiseau, C. & Delage, P. 2008. Determining the unsaturated hydraulic conductivity of a compacted sand-bentonite mixture under constant-volume and free-swell conditions. Physics and Chemistry of the Earth, Parts A/B/C, 33(Supplement 1):S462–S471.

Delage,P., Howat, M.D., & Cui., Y.J. 1998. The relationship between suction and swelling properties in a heavily compacted unsaturated clay. Engineering Geology, 50(1-2), 31–48.

Karnland O., Nilsson U., Weber H. and Wersin P., 2008. Sealing ability of Wyoming bentonite pellets foreseen as buffer material - Laboratory results. Physics and Chemistry of the Earth (33) S472–S475.

Lloret, A., Villar, M.V., Sánchez, M., Gens, A., Pintado, X. & Alonso, E. E. 2003. Mechanical behaviour of heavily compacted bentonite under high suction changes. Géotechnique 53, No. 1, 27–40.

Lloret, A., & Villar, M. 2007. Advances on the knowledge of the thermo-hydro-mechanical behaviour of heavily compacted FEBEX bentonite. Physics and Chemistry of the Earth, 32, 701–715.

Loiseau, C., Cui, Y.J. & Delage, P. 2002. The gradient effect on the water flow through a compacted swelling soil. Proc. 3rd Int Conf Unsaturated Soils, UNSAT'2002 Recife, Brazil, Balkema, vol. 1, pp. 395–400.

Romero, E., Villar, M. V. & Lloret, A. 2005. Thermo-hydro-mechanical behaviour of heavily overconsolidated clays. Engng Geol. 81(3): 255–268.

Pusch, R. 1979. Highly compacted sodium bentonite for isolating rock-deposited radioactive waste products. Nucl. Technol. United States. 45(2):153–157.

Saba, S., Cui, Y.J., Tang, A.M., Barnichon, J.D. & Tran, T.P.H. submitted. Anisotropic swelling of compacted bentonite/sand mixture. Soils and Foundations.

Wang, Q., Tang, A. M., Cui, Y.J., Delage, P., & Gatmiri, B. 2012. Experimental study on the swelling behaviour of bentonite/claystone mixture, Engineering Geology, Vol. 124, 59–66.

Wang Q., Tang A.M., Cui Y.J., Barnichon J.D. Delage P., Ye W.M. 2013a. Voids effects on the hydro-mechanical behaviour of compacted bentonite-sand mixture. *Soils and Foundations* 53(2), 232–245.

Wang, Q., Cui, Y.J., Tang, A. M., Barnichon, J. D., Saba, S. & Ye, W.M. 2013b. Hydraulic conductivity and microstructure changes of compacted bentonite/sand mixture during hydration. Engineering Geology, doi: 10.1016/j.enggeo.2013.06.013

Wang, Q., Tang, A. M., Cui, Y.J., Barnichon J.D. & Ye W.M. 2013c. A comparative study on the hydro-mechanical behaviour of compacted bentonite/sand plug based on laboratory and field infiltration tests, Engineering Geology, Vol. 162, 79–87.

Conclusions and Outlook

CONCLUSIONS and OUTLOOK

A study on the hydro-mechanical behaviour of compacted bentonite/sand mixture used as sealing materials in geological nuclear waste disposal was presented. The overall study focused on the swelling of this material upon hydration in case of presence of the radial technological void between the seal and host rock. This technological void is inevitable for the installation of the seal in the borehole. The key point of this study is the heterogeneity created at the seal/ host rock interface between the loose gel formed by the swelling of bentonite and the compacted bentonite behind the gel. After the sealing of the void, the gel will be consolidated between the host rock and the continuously swelling centre. The free swelling then becomes confined and a swelling pressure will be generated radially on the host rock and axially on the adjacent compacted disks and then on the confining elements.

Various experimental tests were carried out in this study: microstructure observation of the initial state of samples by microfocus X-ray Computed Tomography (µCT) and by Mercury Intrusion Porosimetry (MIP); swelling, gel formation and density gradient evolution observation by time lapse photography and µCT; swelling pressure anisotropy in constant volume conditions with swelling pressure measurements in two directions and the hydro-mechanical behaviour investigation by 1/10 mock-up tests with local swelling pressure measurements. The mock-up tests also helped in studying the accidental failure of the confining elements and the capacity of the material to seal the resulting void. The created density gradient after void filling was again monitored by considering the relationship between the measured swelling pressure and the dry density. Finally, the results were used for interpreting the in-situ observations in a SEALEX experiment.

As compacted microstructure

The microstructure of compacted bentonite/sand mixture samples was studied by µCT that provided interesting complementary features that could not be identified by the MIP technique. µCT also allowed further observation of the mutual arrangement of bentonite and sand grains. The commonly admitted hypothesis of the existence of isolated sand grains among a clay matrix was not confirmed. Conversely, sand grains appeared to be connected forming a loose granular skeleton with inter-grains large pores that were also detected by MIP. Porosity heterogeneity was observed along the sample with a larger porosity on the periphery. This was confirmed quantitatively after carrying out a 3D estimation of porosity using image analysis. The interconnection of pores identified could have some effects on the initial permeability of the sample since it could facilitate the propagation of vapour within the

mixture. In order to further explore the pore's connectivity and pore's dimensions, a full image analysis should be done in the future. This will also permit exploring the pores network orientation as well as the grains orientation.

Another 3D image was analysed on a sample after a confined saturation (swelling pressure) test at a relatively lower initial dry density. It was found that some inter-sand-grains macro pores remained unclogged.

Limited swelling and homogenisation

Thanks to the observations and the digital image processing of the photos obtained by time-lapse photography it revealed possible to identify the swelling mechanism of compacted bentonite/sand sample. Swelling was not homogeneous but occurred by exfoliation of bentonite grains in contact with water. The image analysis allowed the swelling kinetic curves to be defined. It was found that swelling started rapidly and then continued at a lower rate. The sand grains were found to be pushed outwards in the direction of bentonite swelling until they dropped down by gravity when the swelled bentonite became as loose as a bentonite suspension.

A similar test was performed to study the 3D limited swelling and homogenisation of compacted MX80 bentonite/sand mixture by µCT. The scans at different hydration times also showed that swelling took place at the scale of the grains and it started quickly at the beginning and became slower over time. The self sealing capacity of the mixture was confirmed as some initial fractures disappeared after hydration. Swelling continued with the increase in gel production and the decrease in the volume of the unsaturated central part. From day 3 to day 52, the swelled sample touched the border of the cell and swelling became prevented. Visually, the material became more homogeneous, with sand grains uniformly dispersed in the bentonite gel matrix. This homogenisation was further studied by image analysis by plotting grey level profiles along the same diameter of the sample at different hydration times. During the first days, a grey level gradient was found between the dense centre and the loose border of sample. This gradient became smoother over time as the density of the central part decreased and that of the border increased. To be able to see the homogenisation in a clearer fashion, it is necessary to wait longer time and continue the monitoring of the experiment. For more precise quantitative density homogenisation results, a proper calibration is needed between the grey level and the corresponding density. To this end, several samples having the same initial conditions but different densities should be

scanned under the same conditions; that will allow having a proper relationship between the measured grey level and the density.

Swelling pressure

Laboratory elementary tests with swelling pressure measurements in two different directions (axial and radial) were performed at different sample's dry densities. Different trends of kinetics of swelling pressure evolution were identified for different bentonite dry densities, different measurement directions and different sample's preparation methods. However, stabilisation was observed for all cases, indicating the full saturation of the samples. An exponential relationship was found between the final swelling pressure values and the effective dry density of bentonite. A difference between the axial and radial swelling pressures was noticed, suggesting an anisotropic swelling behaviour. Upon hydration, this anisotropy can be expected to decrease because of the induced microstructure collapse. This was particularly observed for tests at medium bentonite dry densities from 1.15 Mg/m^3 to 1.30 Mg/m^3. This coefficient was found to decrease for higher bentonite dry densities, indicating that the initial anisotropy was preserved after hydration because of the limited volume of macro-pores preventing the microstructure collapse. At lower bentonite dry densities, anisotropy was also preserved because it was not possible for bentonite grains to fill the macro-pores creating a microstructure collapse. An elaborated microstructure investigation is needed to confirm the internal mechanism influencing this anisotropic behaviour at different densities before and after the swelling pressure tests. It would also be interesting to study the effect of sand fraction and initial powder wetting on this behaviour.

Mock up tests

A mock-up test was designed at a 1/10 scale of the SEALEX in-situ experiments. The test allowed a confined saturation of the sample representing the seal and monitoring the evolution of different parameters over time. The specially designed cell is equipped with local radial swelling pressure measurements at various heights and a global axial swelling pressure measurement. Validation of the cell was verified by the good correspondence between the results obtained and those from literature on compacted MX80 bentonite/sand mixture. The results of swelling pressure showed a good correspondence with those reported by Karnland et al., 2008; Wang et al., 2012 and Saba et al., 2013. The injected water volume measured manually was found compatible with that reported by Wang et al. (2013a). The designed cell was thereby suitable for testing compacted swelling materials with the monitoring of swelling pressures at different heights, in both radial and axial directions.

Two Mock-up tests were performed with bottom side saturation in Mock-up 1 and two side saturation in Mock-up 2. It was found that the swelling pressure kinetics depended on the infiltration length, with quicker increase for shorter infiltration length (closer to the wetting source). The two-side saturation process accelerated the swelling pressure kinetics by a time factor of 4 which was found by considering the consolidation theory and supposing the infiltration length is reduced to the half with two side saturation.

The hydraulic results obtained by Wang et al. (2013b) from an infiltration test on the same material and the present swelling pressure measurements were used to plot the curves of suction versus swelling pressure for different infiltration lengths. Similar shapes were obtained when compared to the curves reported in the literature (Lloret et al., 2003 and Wang et al., 2013c). Yield points (or peaks) were found to take place at higher suction for the positions farther from the wetting source as they were mainly hydrated by water vapour.

The failure of axial confinement was also experimentally studied by adopting an axial void through releasing the piston after full saturation. The swelling pressure profiles showed a sudden decrease after the piston release due to free swelling. A swelling pressure gradient was found along the sample with higher values in the bottom. This gradient was also represented in terms of density using the exponential relationship between the effective bentonite dry density and the swelling pressure. Comparison with the dry density profile obtained after dismantling a similar 350-day mock-up test performed by Wang et al. (2013a) showed that the density gradient was decreasing over time, and a homogeneous density can be expected in long term. It would be interesting to perform similar mock-up tests with simultaneous µCT scans and a proper calibration between the grey level and the density. That will permit to monitor the density gradient evolution over time and to confirm the achievement of homogenisation.

Link between laboratory and in situ tests

A comparison was made between the results of laboratory tests and in-situ experiments in terms of swelling pressures, relative humidity and swelling pressure anisotropy. The relative humidity measurements were obtained from a previous infiltration test by Wang et al. (2013b). The evolutions of the relative humidity for the in situ and laboratory tests agreed well for a given hydration distance while considering the effect of the saturation due to the existence of the technological void. For the comparison of the evolution kinetics of radial or axial swelling pressures between the small scale test and the in situ test, the consolidation theory was also considered and a time factor of 100 was found between Mock-up 2 with a

length 10 times smaller than that of the in situ test. The comparison while considering this time factor was promising as it permits to predict the in situ results in the future based on the laboratory results.

References

REFERENCES

Agus, S.S. and Schanz, T. 2005. Effect of shrinking and swelling on microstructures and fabric of a compacted bentonite-sand mixture. Proceedings of the International Conference on Problematic Soils, Cyprus, 32, 543 – 550.

Ahmed, S., Lovell, C. W. and Diamond, S. 1974. Pore sizes and strength of compacted clay. J. Geotech. Eng. Div. Am. Soc. Civ. Eng., GT4, 407– 425.

Alonso, E. E., Alcoverro, J., Coste, F. 2005. The FEBEX benchmark test: case definition and comparison of modelling approaches. International Journal of Rock Mechanics & Mining Science 42(5-6): 611 – 638.

Barnichon, J.D. & Deleruyelle, F. 2009. Sealing Experiments at the Tournemire URL. EUROSAFE.

Barnichon, J.D., Dick. P., & Deleruyelle, F. 2010. A sealing performance in situ experiments project (SEALEX): main objectives and expected outcomes, Clays in natural & Engineered Barriers for Radioactive Waste Confinement, 4th international meeting, march 2010, Nantes, France 261-262

Barnichon, J. D., Dick P. & Bauer C. 2012. The SEALEX in situ experiments: performance test of repository seals. Harmonising Rock Engineering and the Environment – Qian & Zhou (eds) Taylor & Francis Group, London, ISBN 978-0-415-80444-8, pages 1391-1394.

Börgesson L., Karnland O. and Johanneson L.E., 1996. Modelling of the physical behaviour of clay barriers close to water saturation. Engineering Geology, 41 : 127-144.

Carminati A., Kaestner A., Hassanein R. and Koliji A. 2006. Hydraulic properties of aggregate-aggregate contacts. In: Desrues J, Viggiani G, Bésuelle P (eds.) Advances in Xray tomography for geomaterials. ISTE Ltd, London, UK, 325–331

Castellanos E., Villar M.V., Romero E., Lloret A. and Gens A., 2008. Chemical impact on the hydro-mechanical behaviour of high-density febex bentonite. Physics and Chemistry of the Earth, Parts A/B/C, 33(Supplement 1):S516 – S526.

Cho W. J., Lee J. O. and Kang C. H., 2000. Influence of temperature elevation on the sealing performance of a potential buffer material for a high-level radioactive waste repository, Ann. Nucl. Energy, 27, 1271–1284.

Comina C., Foti S., Musso G. and Romero E. 2008. EIT oedometer: an advanced cell to monitor spatial and time variability in soil. Geotech Test J. ASTM 31, No. 5, 404–412.

Cui Y.J., Loiseau C. and Delage P. 2002. Microstructure changes of a confined swelling soil due to suction controlled hydration. In Unsaturated soils: proceedings of the Third International Conference on Unsaturated Soils, UNSAT 2002, 10-13 March 2002, Recife, Brazil, volume 2, 593-598.

Cui, Y.J., Yahia-Aissa M. and Delage P. 2002. A model for the volume change behaviour of heavily compacted swelling clays. Engineering Geology 64 (2-3), 233-250.

Cui, Y.J., Tang, A.M., Loiseau, C. & Delage, P. 2008. Determining the unsaturated hydraulic conductivity of a compacted sand-bentonite mixture under constant-volume and free-swell conditions. Physics and Chemistry of the Earth, Parts A/B/C, 33(Supplement 1):S462 – S471.

Delage P., Audiguier M., Cui Y.J., and Howat M. 1996. The microstructure of a compacted silt. Canadian Geotechnical Journal, 33: 150-158.

Delage P., Howat M. D. and Cui Y. J., 1998. The relationship between suction and swelling properties in a heavily compacted unsaturated clay. Engineering Geology 50**,** 31-48.

Delage P., Marcial D., Cui Y.J. and Ruiz X. 2006. Ageing effects in a compacted bentonite: a microstructure approach, Géotechnique 56(5):291–304.

Delage P. 2009. Compaction behaviour of clay: discussion. Géotechnique 59 (1), 75-76.

Dixon D.A., Gray M.N. and Graham J., 1996. Swelling and hydraulic properties of bentonites from Japan, Canada and USA. In Proceedings of the second International Congress on Environmental Geotechnics, Osaka, Japan, pages 5–8.

Dixon D., Chandler N., Graham J. and Gray M. 2002. Two large-scale sealing tests conducted at Atomic Energy of Canada's underground research laboratory: the buffer container experiment and the isothermal test. Canadian Geotechnical Journal 39 (3): 503-518.

Dueck, A., Goudarzi, R. and Börgesson, L. 2012. Buffer homogenisation, status report. SKB technical report TR-12-02.

Dvinskikh, S.V., Szutkowski, K. and Furó, I. 2009. MRI profiles over very wide concentration ranges: Application to swelling of a bentonite clay. Journal of Magnetic Resonance 198 (2009) 146–150.

Gens A., Alonso E.E., Suriol J. and Lloret A. 1995. Effect of structure on the volumetric behaviour of a compacted soil. Proc. 1st Int. Conf on Unsaturated Soils UNSAT' 95 1, 83-88.

Gebrenegus T., Tuller M. and Muhuthan B. 2006. The application of X-ray computed tomography for characterisation of surface crack networks in bentonite-sand mixtures. In: Desrues J, Viggiani G, Bésuelle P (eds) Advances in X-ray tomography for geomaterials. ISTE Ltd, London, UK: 207–212

Geiser, F. 1999. Comportement mécanique d'un limon non saturé : étude expérimentale et modélisation constitutive [D]. Switzerland: Thesis, Ecole Polytechnique Fédérale deLausanne, EPFL.

Gens, A. and Alonso, E. E. 1992. A framework for the behaviour of unsaturated expansive clays. Can.Geotech. J. 29(6): 1013 – 1032.

Head, K H. 1980, Manual of soil laboratory testing, volume 1: soil classification and compaction tests. London: Pentech Press.

Imbert C. and Villar M.V., 2006. Hydro-mechanical response of a bentonite pellets-powder mixture upon infiltration. Applied Clay Science, 32(3-4):197–209

Jansson, M. 2009. Bentonite erosion, laboratory studies. SKB technical report TR-09-33.

Karnland O., Muurinen A. and Karlsson F., 2005. Bentonite swelling pressure in NaCl solutions-Experimentally determined data and model calculations. Advances in Understanding Engineering Clay Barriers. Page 241.

Karnland O., Olsson S. and Nilsson U. 2006. Mineralogy and sealing properties of various bentonites and smectite-rich clay material. SKB.

Karnland O., Nilsson U., Weber H. and Wersin P., 2008. Sealing ability of Wyoming bentonite pellets foreseen as buffer material - Laboratory results. Physics and Chemistry of the Earth (33) S472-S475.

Kawaragi C., Yoneda T., Sato T. and Kaneko K. 2009. Microstructure of saturated bentonites characterized by X-ray CT observations. Engineering. Geology., 106, 51–57

Ketcham R. A. and Carlson W. D. 2001. Acquisition, optimization and interpretation of X-ray computed tomographic imagery : applications to the geosciences. Computers&Geosciences Vol. 27, 381-400.

Koliji A., Carminati A., Kaestner A., Vulliet L., Laloui L., Fluehler H., Vontobel P. and Hassanein R. 2006. Experimental study of flow and deformation in aggregated soils using neutron tomography. In: Desrues J, Viggiani G, Bésuelle P (eds). Advances in X-ray tomography for geomaterials. ISTE Ltd, London, UK: 341–348

Komine H. and Ogata N., 1994. Experimental study on swelling characteristics of compacted bentonite. Canadian geotechnical journal, 31(4):478–490.

Komine H. and Ogata N. 1999. Experimental study on swelling characteristics of sand-bentonite mixture for nuclear waste disposal. Soils and Foundations 39(2): 83-97.

Komine H. and Ogata N., 2003. New equations for swelling characteristics of bentonite-based buffer materials. Canadian Geotechnical Journal. 40(2):460–475.

Komine H. and Ogata N., 2004. Predicting swelling characteristics of bentonites. Journal of Geotechnical and Geoenvironmental engineering, 130:818.

Komine H., Yasuhara K. and Murakami S., 2009. Swelling characteristics of bentonites in artificial seawater. Canadian Geotechnical Journal. 46(2):177-189.

Kozaki T., Suzuki S., Kozai N., Sato S. and Ohashi H. 2001. Observation of microstructures of compacted bentonite by microfocus X-ray computerized tomography (Micro-CT). J. Nucl. Sci. Technol., 38 (8), pp. 697–699

Kröhn K.P., 2003. New conceptual models for the resaturation of bentonite. Applied clay science, 23(1-4):25–33.

Lee J O, Cho W J, Chun K S. 1999. Swelling Pressures of a Potential Buffer Material for High-Level Waste Repository. Journal of the Korean Nuclear Society, 31: 139-150.

Lee J.O., Lim J.G., Kang I.M. and Kwon S., 2012. Swelling pressures of compacted Ca-bentonite. Engineering Geology. doi: 10.1016/j.enggeo.2012.01.005

Li Z.M. 1995. Compressibility and collapsibility of compacted unsaturated loessial soils. Proc. 1st Int. Conf on Unsaturated Soils UNSAT' 95 1, 139-144, Paris, Balkema, Rotterdam.

Liu, L., Moreno, L. and Neretnieks, I. 2009. A Dynamic Force Balance Model for Colloidal Expansion and Its DLVO-Based Application. Langmuir 25, 679-687.

Lloret, A., Villar, M.V., Sanchez, M., Gens, A., Pintado, X. and Alonso, E.E. 2003. Mechanical behaviour of heavily compacted bentonite under high suction changes. Géotechnique 53, No. 1, 27-40.

Lloret A. and Villar M.V. 2007. Advances on the knowledge of the thermo-hydro-mechanical behaviour of heavily compacted "FEBEX" bentonite. Physics and Chemistry of the Earth 32 701-715.

Loiseau, C., Cui, Y.J. & Delage, P. 2002. The gradient effect on the water flow through a compacted swelling soil. Proc. 3rd Int Conf Unsaturated Soils, UNSAT'2002 Recife, Brazil, Balkema, vol. 1, pp. 395-400.

Madsen FT. 1998. Clay mineralogical investigations related to nuclear waste disposal. Clay Minerals, 33(1):109–129.

Mitchell J K. 1993. Fundamentals of soil behaviour. John Wiley and Sons, Inc., New York, ISBN: 0-471-85640-1

Montes-H G. 2002. Etude expérimentale de la sorption d'eau et du gonflement des argiles par microscopie électronique à balayage environnementale (ESEM) et analyse digitale d'images. PhD Thesis. Louis Pasteur University, Strasbourg I, France.

Moreno, L., Neretnieks, I. and Liu, L. 2010. Modelling of erosion of bentonite gel by gel/sol flow. SKB Technical report TR-10-64.

Mukunoki T., Otani J., Maekawa A., Camp S., Gourc J.P. 2006. Investigation of crack behaviour on cover soils at landfill using X-ray CT. In: Desrues J, Viggiani G, Bésuelle P(eds) Advances in X-ray tomography for geomaterials. ISTE Ltd, London, UK: 213–219.

Neretnieks, I., Liu, L. and Moreno, L. 2009. Mechanisms and models for bentonite erosion. SKB technical report TR-09-35.

Pusch, R. 1979. Highly compacted sodium bentonite for isolating rock-deposited radioactive waste products. Nucl. Technol, United States. 45(2):153-157.

Pusch, R. 1980. Swelling pressure of highly compacted bentonite. SKB technical report TR-80-13.

Pusch, R., 1982. Mineral-water interactions and their influence on the physical behavior of highly compacted Na bentonite. Canadian Geotechnical Journal, 19(3):381–387.

Pusch, R. 1999. Clay colloid formation and release from MX-80 buffer. SKB technical report TR-99-31.

Rasband W.S. 1997-2012. ImageJ, U. S. National Institutes of Health, Bethesda, Maryland, USA, http://imagej.nih.gov/ij/.

Razavi M.R., Muhunthan B. and Al Hattamleh O. 2007 Representative elementary volume analysis using X-ray computed tomography, Geotechnical Testing Journal 30 (3) doi:10.1520/GTJ100164.

Rolland S., Stemmelen D., Moyne C. and Masrouri F. 2003. Transfert hydrique dans un sol argileux gonflant non sature´: influence du confinement. Revue Française Géotech 104:21–35

Rolland S., Stemmelen D., Moyne C. and Masrouri F. 2005. Experimental hydraulic measurements in an unsaturated swelling soil using the dual-energy gamma-ray technique. Proceedings of International Symposium on Advanced Experimental Unsaturated Soil Mechanics, Trento, Italy. In: Tarantino A, Romero E, Cui YJ (eds) Advanced experimental unsaturated soil mechanics. Taylor, Francis Group, London, 305–310.

Romero E., Gens A., and Lloret A. 1999. Water permeability, water retention and microstructure of unsaturated compacted Boom clay. Engineering Geology, 54: 117-127.

Romero, E., Villar, M. V. & Lloret, A. 2005. Thermo-hydro-mechanical behaviour of heavily overconsolidated clays. Engng Geol. 81(3): 255–268.

Siddiqua S., Blatz J. and Siemens G. 2011. Evaluation of the impact of pore fluid chemistry on the hydromechanical behaviour of clay-based sealing materials. Canadian Geotechnical Journal, NRC Research Press, 48, 199-213.

Tang A.M., Cui Y.J. and Le T.T. 2008. A study on the thermal conductivity of compacted bentonites. Appl Clay Sci; 41:181-189.

Tang C.S., Tang A.M., Cui Y.J., Delage P., Schroeder C. and De Laure E., 2011. Investigating the Swelling Pressure of Compacted Crushed-Callovo-Oxfordian Argillite. Physics and Chemistry of the Earth 36 (17-18), 1857–1866.

Tarantino A. and De Col E. 2008. Compaction behaviour of clay. Géotechnique 58(3): 199-213.

Tessier D., 1990. Organisation des matériaux argileux en relation avec leur comportement hydrique. Decarreau (Éd.): Matériaux argileux: structure, propriétés et applications.

Van Geet M., Volckaert G. and Roels S. 2005. The use of microfocus x-ray computed tomography in characterising the hydration of a clay pellet/powder mixture. Applied Clay Science, 29(2):73–87, 2005.

Villar M.V. and Lloret A. 2001. Variation in the intrinsic permeability of expansive clays upon saturation. In: Adachi K., Fukue M. (eds) Clay Science for Engineering. A.A. Balkema, Rotterdam, 259-266.

Villar M.V., 2002. Thermo-hydro-mechanical characterisation of a bentonite from Cabo de Gata. A study applied to the use of bentonite as sealing material in high level radioactive waste repositories. Publicación Técnica ENRESA 01/2002, Madrid, 258 pp.

Wang Q., Tang A.M., Cui Y.J., Delage P. and Gatmiri B., 2012. Experimental study on the swelling behaviour of bentonite/claystone mixture. Engineering Geology 124 : 59-66, doi : 10.1016/j.engeo.2011.10.003.

Wang Q., Tang A M, Cui Y J, Delage P, Barnichon J D, Ye W M. 2013. The effects of technological voids on the hydro-mechanical behaviour of compacted bentonite-sand mixture. International Journal of Soils and Foundations.

Wang, Q., Tang, A. M., Cui, Y.J., Barnichon J.D. & Ye W.M. 2013. A comparative study on the hydro-mechanical behaviour of compacted bentonite/sand plug based on laboratory and field infiltration tests, Engineering Geology, Vol. 162, 79–87.

Wang, Q., Cui, Y.J., Tang, A. M., Barnichon, J. D., Saba, S. & Ye, W.M. 2013. Hydraulic conductivity and microstructure changes of compacted bentonite/sand mixture during hydration. Engineering Geology, doi: 10.1016/j.enggeo.2013.06.013

Wang Q., Tang A.M., Cui Y.J., Barnichon J.D. & Ye W.M. 2013. Investigation of the hydro-mechanical behaviour of compacted bentonite/sand mixture based on the BExM model. Computer and Geotechnics 54, 46-52.

Ye W.M., Cui Y.J., Qian L.X., Chen B. 2009. An experimental study of the water transfer through compacted GMZ bentonite. Engineering Geology 108, 169 – 176.

Yong R.N., Boonsinsuk P. and Wong G. 1986. Formulation of backfill material for a nuclear fuel waste disposal vault. Canadian Geotechnical Journal, 23(2):216–228.